UNIVERSIDAD DE MÁLAGA
Facultad de Ciencias
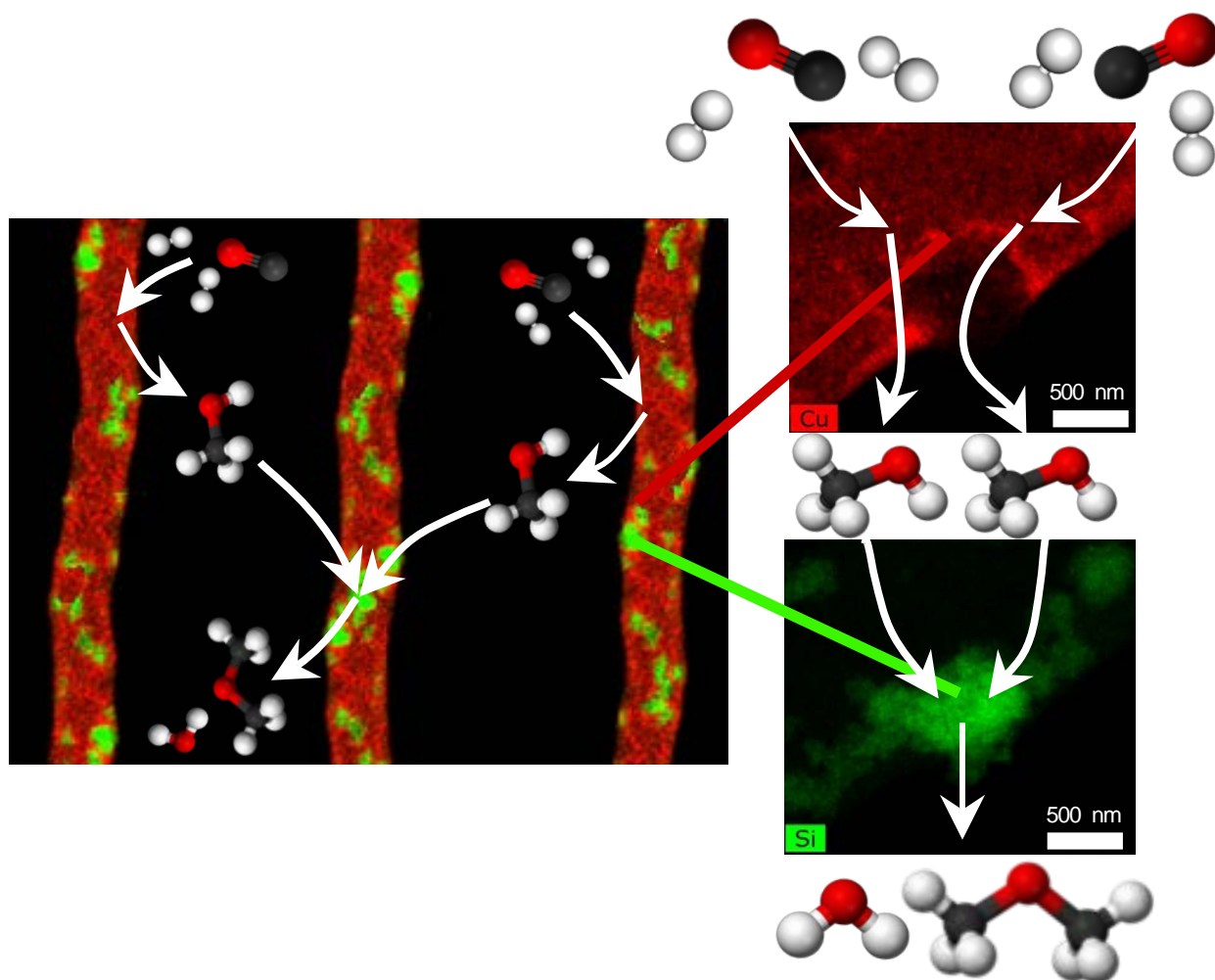## Departamento de Ingeniería Química

TESIS DOCTORAL

CATALIZADORES AVANZADOS PARA LA SÍNTESIS DIRECTA DE DIMETIL ÉTER

Programa de Doctorado:
Química y Tecnologías Químicas. Materiales y Nanotecnología.

Directores:

Dr. D. Tomás Cordero Alcántara

Dr. D. José Rodríguez Mirasol

José Palomo Jiménez

Málaga, 2019

UNIVERSIDAD DE MÁLAGA

Facultad de Ciencias

Departamento de Ingeniería Química

TESIS DOCTORAL

Para optar al Título de:

Doctor en Ingeniería Química con Mención Internacional

Catalizadores avanzados para la síntesis directa de dimetil éter

Autor: José Palomo Jiménez

Directores: Dr. D. Tomás Cordero Alcántara

                    Dr. D. José Rodríguez Mirasol

Programa de doctorado: Química y Tecnologías Químicas.

Materiales y Nanotecnología

Málaga, 2019

UNIVERSIDAD
DE MÁLAGA

AUTOR: José Palomo Jiménez

http://orcid.org/0000-0002-8169-5320

UNIVERSIDAD
DE MÁLAGA

D. TOMÁS CORDERO ALCÁNTARA, Catedrático de Ingeniería Química de la Universidad de Málaga,

D. JOSÉ RODRÍGUEZ MIRASOL, Catedrático de Ingeniería Química de la Universidad de Málaga,

CERTIFICAN: Que el trabajo de investigación recogido en la presente Memoria ha sido realizado bajo su dirección en el Departamento de Ingeniería Química de la Universidad de Málaga por el Ingeniero D. JOSÉ PALOMO JIMÉNEZ, y reúne, a su juicio, contenido científico suficiente y las condiciones necesarias para ser presentado y defendido ante el Tribunal correspondiente para optar al Grado de Doctor con Mención Internacional.

Málaga, noviembre de 2019

Fdo.: Dr. D. Tomás Cordero Alcántara   Fdo.: Dr. D. José Rodríguez Mirasol

UNIVERSIDAD
DE MÁLAGA

A mi familia

Contents

UNIVERSIDAD
DE MÁLAGA

This Thesis is motivated by the awareness that fossil fuels will finally come to an end. It could be said that we currently are in a transition period, moving from a petroleum oil-based economy to a more sustainable scenario, in which fuel will be produced via syngas-to-chemical processes, such as the syngas to dimethyl ether (DME) process. In this line, the main purpose of this Thesis is the preparation of alternative efficient catalysts for the direct DME synthesis from syngas.

For the preparation of the catalysts presented in this work, two different methodologies have been followed. On the one hand, activated carbon-based catalysts, presenting a granular morphology, were prepared by chemical and physical activation of a lignocellulosic waste followed by the impregnation with different metal salts. On the other hand, fibrillary structured inorganic catalysts were prepared by using the electrospinning technique.

This Thesis is divided into 7 chapters. Chapter 1 is a general introduction, covering the current state of art of the matter studied in this thesis. The experimental procedures followed in this Thesis are reported in Chapter 2. Chapters 3-7 conform the Results and Discussion block of this Thesis. The results of this Thesis are divided in two main parts, which are related to the two different methodologies followed for the preparation of the catalysts. On the one hand, in Chapters 3-5, the use of activated carbons as catalysts and catalyst supports was investigated. Chapter 3 addresses the preparation and characterization of activated carbon catalysts for the efficient methanol dehydration to DME. In this work, two kinds of activated carbons were prepared by chemical (with phosphoric acid) and physical (by CO2 partial gasification) activation of olive stone, an agri-food industry waste, and afterwards, they were loaded with different amounts of Zr (0 – 7.5 (w/w)). Chapter 4 presents a kinetic study of methanol dehydration to DME on the activated carbon catalyst that exhibited the best catalytic performance in Chapter 3. Chapter 5 is focused on

the direct synthesis of DME from syngas using activated carbons-based catalysts.

On the other hand, in Chapters 6 and 7, the preparation of inorganic-based fibrillar structured catalysts was addressed by using the electrospinning technique. Chapter 6 reports a straightforward method for the one-step preparation of nanostructured zirconia-zeolite fibrillar materials in the form of core-shell like structures, by using the electrospinning technique, and the use of these materials as efficient catalysts for methanol dehydration to dimethyl ether and for the direct synthesis of dimethyl ether from syngas. Chapter 7 addresses the preparation, characterization and application of one-dimensional structured bifunctional catalyst, presenting two well-defined catalytic phases, metallic and acid. The catalytic activity obtained for the different catalysts was correlated with the textural, structural and surface chemistry of the fibrillar catalysts studied. Finally, a detailed parametric study of the direct synthesis of DME from syngas on these bifunctional fibrillar catalysts has been carried out in a continuous fixed-bed reactor.

Each chapter has their own abstract and conclusions. A final chapter provide the general conclusions derived from this thesis and give a small insight in the remaining and future work coming as a result of this thesis.

Chapter 1

Introduction

1.1.- Global energy scenario and prospects.

From the beginning, human social development has been closely related to energy consumption. The way energy is obtained changes with the passing of the years, and alternative renewable technologies will be needed in order to meet the demands of a growing society.

The world population has grown drastically over the last decades, and recent estimations indicate that this trend will continue. In this scenario, the current world population, 7.5 billion in 2017, is expected to increase up to 9.7 billion in 2050 [1]. It has also to be taken into account that societies are prone to a continuous technological development, which will make necessary a huge amount of resource and energy in order to satisfy people's needs. In 2017, the total world energy demand was estimated as 13,551 Mtoe [2], and according to the International Energy Agency´s prospects, this figure will reach a value of 17,715 Mtoe by the end of 2040 [3]. Furthermore, as can be observed in Figure 1.1, most of this energy is obtained from fossil fuels (carbon, natural gas and petroleum oil), all composed of hydrocarbons with varying ratios of carbon and hydrogen.
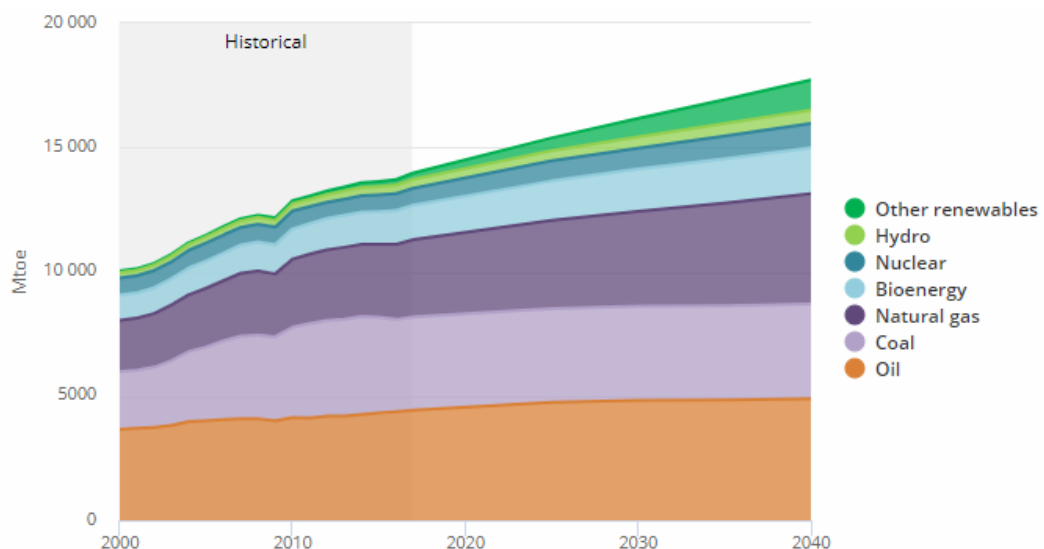
Figure 1.1. World total primary energy demand (TPED), under the new policies scenario [3].

These hydrocarbons, mainly coming from petroleum oil, are mostly used as automotive fuels, electrical power generation and heating. However, there are also many industries depending on these chemical compounds as raw materials, such as plastic, chemical, dyes and agriculture industries. The world oil demand growth an average of 1.7 (mb/d) per year during the last 10 years, and it is now estimated in 99.7 (mb/d) [4]. This global demand is expected to keep on growing as a consequence of the increasing world population and technological development. Regarding the worldwide oil proven reserves, they seem to have leveled off in the last 10 years, and the reserves-to-production ratio (the length of time that those remaining reserves would last if production were to continue at that rate) are now estimated in 52 years [2]. This fact indicates that the predictions of a rapid depletion of oil reserves carried out in the past were not very accurate, however, there is no doubt that these reserves will finally come to an end. It is true that oil reserves will not be exhausted from one day to the next, but supply and demand will provoke a far more spectacular rise in prices than might be expected [5].

In this scenario, synthetic routes for hydrocarbon production, by using alternative natural resources, will be more and more needed in order to meet the increasing world demand. Although these alternative processes are feasible, they are nowadays more costly. Nevertheless, the variations in the crude oil barrel price, from 40 to 110 $/bbl [2], in the last 10 years, are making these new synthetic routes more and more economically viable.

Synthetic oil production routes are feasible. These processes use synthesis gas (a mixture of carbon monoxide and hydrogen) as raw material. The synthesis gas can be produced by partial oxidation or reforming of natural gas or by gasification of coal or biomass. The coal gasification process was first used in 1850 to provide for street lighting. Then, during World War II it was used for the production of liquid synthetic fuels in Germany, yielding the development of the Coal-to-liquids (CTL) processes [6]. On the other hand, Natural gas can be used for synthesis gas obtention, via reforming processes, after which the generated synthesis gas can be used in turn for synthetic fuel production, constituting the so-called gas-to-liquid (GTL) processes.

The composition of the generated synthesis gas is highly influenced by the raw material and the gasification agent used in the process. In this sense, coal gasification leads to the obtention of a synthesis gas presenting an H_2/CO ratio of 0.8-1, whereas, natural gas reforming allows for obtaining an H_2/CO ratio of 2-2.5. The H_2/CO ratio can be modified through the Water Gas Shift Reaction (WGSR), Eq. 1.1.

$$H_2O + CO \leftrightarrow H_2 + CO_2 \quad (\Delta H_r^0 = -41.1 \text{ kJ·mol}^{-1}) \quad \text{(Eq. 1.1)}$$
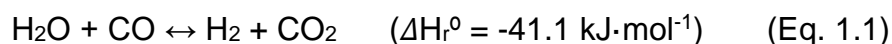
As for the natural gas and coal proven world reserves and the reserves-to-production ratio, it is estimated that they will last for 53 and 134 years [2], respectively. In this sense, the use of these natural resources could supply the hydrocarbon demand in a middle term, but in the end, they will also become exhausted, thus, they can only be considered as a transitional solution. These natural resources are located in specific zones on the Earth thus making some countries energetically dependent on others. Furthermore, the natural resources need to be transported to the consumption points, which is an additional cost to the process.

In contrast to coal and natural gas, biomass represents a renewable carbon source, which would lead to a considerable reduction of greenhouse gas emissions in these processes, promoting the transition to an energy system that reduces dependence on fossil fuels in a scenario that contemplates, on the one hand, the scarcity of fossil fuels, and on the other hand the growth of global demand and the impact of emissions on the environment. The production of synthetic fuel from biomass, mainly ethanol (via fermentation process) and biodiesel (via trans-esterification process), has been widely investigated [7,8]. However, these synthetic routes have demonstrated some drawbacks, such as the use of food crops for fuel production in underdeveloped countries, which increases food prices in these countries [9]. Therefore, fuel production through these routes could not be considered as an ideal solution. Apart from the aforementioned fermentation and trans-esterification processes, biomass can also be gasified to obtain synthesis gas for fuel production. For this process, any lignocellulosic material can work, even waste material, and thus, there is no competition between food and fuel production. The use of biomass waste as raw

material for gasification processes would result not only in an economic but also in an environmental profit. Synthesis gas generated from this process presents an H_2/CO ratio of 1-1.5, which could be increased by the catalytic Water Gas Shift Reaction (WGSR) (Eq. 1.1).

To sum up, it could be said that we are in a transition period, moving from a petroleum oil-based economy to a more sustainable scenario, in which fuel will be produced via syngas-to-chemical processes. In order to make feasible this transition, a great effort is still necessary in order to develop more efficient synthesis routes capable of supplying the future fuel demand.

Among the synthetic routes for fuel production, syngas-to-methanol and the derived dimethyl ether (DME) process is receiving a great deal of attention [5,10]. This process exhibits remarkable advantages when compared to other synthesis routes such as the Fischer-Tropsch process. For example, the syngas-to-methanol and the one-step syngas-to-DME processes, produce less CO_2 as a by-product as compared with the Fischer-Tropsch process [5]. Moreover, it has been reported that the former processes allow for operating under different H_2/CO ratios, being feasible the use of biomass derived synthesis gas [11,12]. Furthermore, the co-feeding of CO_2 to this process has also been studied, showing the possibility of synthesizing methanol and DME from CO_2 [13–15]. Then DME can be further converted into olefins by the well-stablished methanol to olefins (MTO) / dimethyl ether to olefins (DTO) processes [16–19], constituting a route for CO_2 valorization.

1.2.- Dimethyl ether (DME).

Historically, dimethyl ether (DME), the simplest aliphatic ether (CH_3-O-CH_3), has been used in several applications such as aerosol propellant (as a substitute to CFC), anesthetic and coolant.

Thanks to its physical and chemical properties, similar to liquified petroleum gases (LPG) and conventional diesel, plus the clean combustion achieved when used as fuel, this compound is considered as one of the most promising alternatives to petroleum derived fuel, and thus, its production is the

object of much research [20]. The interest for DME came up in the beginning of the 1990s, when it was postulated as a promising fuel and as an intermediate building block for many value-added chemicals, such as lower olefins, methyl acetate and dimethyl sulphate [21,22]. The interest for DME has increased with the passing of the years, and nowadays is considered as a key compound for human development in the XXI century [5].

1.2.1.- Properties and applications.

Dimethyl ether (DME) is a chemically stable colorless, non-toxic, non-carcinogenic, and environmentally friendly compound presenting a characteristic odor. Under normal pressure and temperature conditions, it is presented in gas phase. However, this gas can be easily liquified, cooling it down to its boiling point (-24.9 ºC) or compressing it up to 6.1 bar at 25 ºC [23], obtaining a colorless liquid, presenting properties similar to liquified petroleum gases (LPG). When compared to other higher ethers, this compound does not form an explosive peroxide, making it safe for storage and use. Table 1.1 shows the physical and chemical properties of DME, along with other chemical compounds presenting similar properties.

Table 1.1. Properties of DME, methanol, petroleum liquified gas and diesel.

	DME	Methanol	LPG	Diesel
Density (g/cm^3)	0,661*	0,792	0,54	0,856
Boiling point (ºC)	-24,9	64	-30	125-400
LHV (MJ/kg)	28,43	19,5	46,3	43.1
Cetane number (CN)	55-60	5	-	40-55
C content (% w/w)	52,2	52,2	82	87
S content (ppm)	0	0	10-50	250

*liquid phase density.

DME shows a high cetane number (CN=55-60) when compared to refinery diesel (CN=40-55), making this compound a suitable alternative to diesel fuel for compression-ignition engines. Moreover, DME presents a similar boiling point, and density as comparing with GLP (mostly C_3 and C_4). These handling characteristics are similar to LPG, making its supply and storage feasible by using the same infrastructure and equipment as those used for LPG with minor

modifications, reducing in this way the investment costs [24]. Regarding its environmental behavior, the absence of sulfur in its composition results in no SO_2 emissions when used as fuel. Moreover, its average lifetime in the atmosphere (about 5.1 days), and its global warming potential, is considerably lower than that presented by other gases, such as CO_2, CH_4 and N_2O [25]. This lower effect on global warming, together with its low toxicity, makes this chemical compound also suitable as a propellant in spray cans, replacing banned CFC gases.

1.2.2.- DME as fuel for compression-ignition engines.

Since the mid 1990s, DME has been widely investigated as a diesel substitute [26,27], and since then many studies have been carried out to make it feasible [28–30]. Along this line, Volvo group is currently running tests on DME-powered trucks [31].

Apart from its high cetane number, it presents a high oxygen content (34.8 %) and the absence of C-C bonds, resulting in a smokeless combustion and low particle emission [28]. In addition, CO and NO_x emissions have been demonstrated to be also very low [20,29]. Moreover, the use of DME in compression-ignition engines not only significantly reduces pollutant emissions, but also the noise of the motor to the level of a gasoline spark-ignited engine, keeping the fuel consumption close to diesel on an energy basis [28].

Besides the already presented advantages when using DME as a diesel substitute, it has to be pointed out that the lower energy density of DME when compared to diesel fuel makes it necessary to double the fuel storage tank size in order to achieve an equivalent driving range for a diesel vehicle. In addition, the lower viscosity DME presents, similar to LPG, could lead to leakages and lubricity problems in engines [5]. However, given that millions of engines are currently running on LPG, and the experience being acquired with this technology, problems related to the use of DME can be easily solved through the adequate selection of components and the use of additives.

1.2.3.- DME as household gas.

Liquified petroleum gas (LPG) is mainly used as a residential fuel for heating ang cooking purposes, and there is a huge demand for this fuel especially in Asian countries, such as India, Indonesia and China [32]. Realizing that LPG supplies will not meet the demand in the near future, DME has also started to be used as household gas. Along these lines, there are some studies dealing with the use of pure DME for these purposes [23]. However, with the aim of using the existing LPG infrastructure, LPG + DME mixtures are also being investigated, and some studies have pointed out that mixtures containing up to 20 % DME can be used with no or very little modification to existing equipment [32,33]. Moreover, the characteristic DME odor makes it unnecessary the addition of odorant additives.

1.2.4.- DME for electricity generation.

There are several studies dealing with the use of DME as fuel for gas turbines for power generation purposes, where it has demonstrated to be an excellent fuel [34,35]. General Electric reported performances and emissions comparable to gas natural when using DME as fuel [5]. Hitachi developed a 25 MW scale DME burner [36]. Tokyo Electric Power Company studied the use of DME in LPG-microturbine and reported that equivalent or superior performances were achieved using DME instead of LPG [37].

It is also interesting to mention that the use of DME as fuel for gas turbines allows the use of low purified DME (although all components must be in the same phase). In this sense, Amoco have carried out combustion tests with pure and fuel-grade DME, containing about 8 % methanol and 3 % water [35].

1.2.5.- DME as hydrogen source.

Another application for DME, derived from its high hydrogen content (13 %$_{w/w}$) and the lack of C-C bonds, that is currently being investigated is its use as hydrogen source for proton exchange membrane (PEM) fuel cells [38]. Made possible because DME can be reformed with water vapor at low temperature

(<300 ºC) [39]. This reforming process makes use of a bifunctional catalyst, in which DME hydrolysis (Eq. 1.2) and methanol steam reforming take place (Eq. 1.3). At the same time, the Water Gas Shift Reaction (WGSR) (Eq. 1.1) and the undesired DME partial decomposition (Eq. 1.4) also take place in this process.

$$CH_3OCH_3 + H_2O \leftrightarrow 2CH_3OH \qquad \text{(Eq. 1.2)}$$

$$CH_3OH + H_2O \leftrightarrow CO_2 + 3H_2 \qquad \text{(Eq. 1.3)}$$

$$H_2O + CO \leftrightarrow H_2 + CO_2 \qquad \text{(Eq. 1.1)}$$

$$CH_3OCH_3 \leftrightarrow CH_4 + H_2 + CO \qquad \text{(Eq. 1.4)}$$
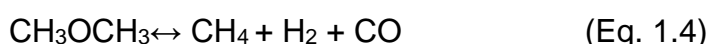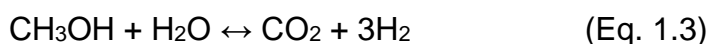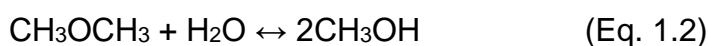
The proper selection of both metallic and acid phases of the bifunctional catalyst [40,41] allows the obtaining of a high H_2 yield and minimizing the CO formation (which is considered a poison for the PEM anode).

The lack of toxicity together with the availability of transport and storage infrastructures for DME, allows the use of PEM fuel cells avoiding the problems related to hydrogen transport and storage.

1.2.6.- DME for lower olefins production.

DME chemical structure, presenting an oxygen atom bonded to two methyl groups, confers this compound a high versatility for being used as an intermediate raw material. In this line, the use of DME instead of methanol in the well-established methanol-to-olefins (MTO) process has been studied, being developed the dimethyl ether-to-olefins process (DTO) [17,42,43]. The kinetic scheme for DME conversion to olefins is similar to that for methanol but avoiding the fast and highly exothermic methanol dehydration step. However, some differences in the process have been reported when using DME instead of methanol [44]. These differences can be attributed to the higher reactivity of DME and to the lower presence of water in the reaction media, which results in the faster deactivation of the catalyst [42]. To avoid this fast deactivation process, the use of mesoporous zeolites (mainly HZSM-5) is receiving great attention [45]. The use of modified HZSM-5 zeolite allows for controlling the selectivity to the reaction products [46], making it possible to achieve a high selectivity to

propylene (Dimethyl ether-to-propylene (DTP) process) [47]. A demonstration plant is currently being constructed for studying the feasibility of the DTP process in Mitsubishi Chemical's Mizushima plant (Japan) [48].

It is also important to mention that a non-purified DME can be used for DTO process, and thus, DME production stream (containing methanol) can be used without a further purification stage.

1.3.- DME synthesis processes.

Two alternative processes can be used for DME production: (i) a two-step process (the so-called indirect process), which consists of one stage of methanol production from synthesis gas [49–51], followed by a second stage of methanol dehydration on a solid acid catalyst [52–55]; (ii) a direct process, in which synthesis gas is fed to a reactor containing a bifunctional catalyst where the two aforementioned reactions take place [56–59].

1.3.1.- Indirect process.

Nowadays, DME is mostly produced by the so-called indirect process, using synthesis gas (H_2 + CO/CO_2) as raw material. As aforesaid, this process accounts on two catalytic stages. In the first, methanol is produced form synthesis gas, and then in the second, the generated methanol is dehydrated to DME. This process allows for optimizing both stages independently.

1.3.1.1.- Methanol synthesis.

Methanol was obtained for the first time in 1661 by Sir Robert Boyle through a rectification process of crude wood vinegar over milk of lime [60]. From 1830 to 1923, the so-called "alcohol of wood" was mainly obtained by wood dry distillation processes.

The first industrial process for methanol synthesis was introduced by *BASF* company in 1920. This process was feasible thanks to the development of zinc oxide-chromium oxide (ZnO-Cr_2O_3)-based catalysts, which presented a high resistance to sulfur compounds present in synthesis gas, usually obtained from

coal. By the end of 1923, this process was used at the *BASF Leuna Works*. This initial process was carried out under severe operating conditions (250 - 350 bar y 320 - 450 ºC) and was the one used for the methanol production for more than 40 years. In 1960, *Imperial Chemical Industries* (*ICI*) developed a synthesis route for methanol production using Cu/ZnO-based catalysts, using a sulfur-free synthesis gas as feedstock. The high activity these catalysts demonstrated allowed more favorable operating conditions (50 - 100 bar, 200 - 300 ºC). This new low-pressure process substituted the high-pressure one, and today's industrial production is based on this synthesis route, achieving a methanol production higher than 5,000 t/day [60].

Methanol synthesis from synthesis gas containing both carbon monoxide and carbon dioxide can be described by the equilibrium reactions represented in Eq. 1.5 and 1.6.

$$CO + 2H_2 \leftrightarrow CH_3OH \qquad (\Delta H_r^0 = -90.8 \ kJ \cdot mol^{-1}) \qquad (Eq. \ 1.5)$$

$$CO_2 + 3H_2 \leftrightarrow CH_3OH + H_2O \qquad (\Delta H_r^0 = -49.5 \ kJ \cdot mol^{-1}) \qquad (Eq. \ 1.6)$$
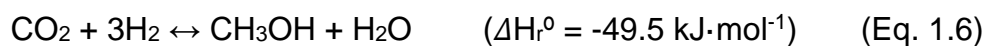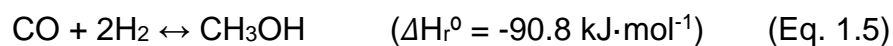
Methanol formation reactions (Eq. 1.5 and 1.6) are exothermic and proceed by reducing the mole number of the reactant. Therefore, according to Le Chatelier's principle, these chemical reactions are favored when working at low temperature and high pressure. In addition, WGSR (Eq. 1.1) also takes place, modifying the reactant gas composition.
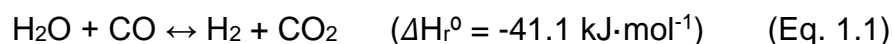
$$H_2O + CO \leftrightarrow H_2 + CO_2 \qquad (\Delta H_r^0 = -41.1 \ kJ \cdot mol^{-1}) \qquad (Eq. \ 1.1)$$

Chemical reactions involved in methanol synthesis are reversible, and thus they are limited by thermodynamic equilibrium, which is a function of the temperature, pressure and the synthesis gas composition. This thermodynamic limitation results in a low synthesis gas conversion per-pass, increasing the operating costs related to methanol separation and synthesis gas recirculation [5].

Methanol synthesis can be achieved from both CO and CO_2, and mixtures of them. It has been reported that the presence of CO_2 in the synthesis gas improves the reaction rate [61], thus CO and CO_2 mixtures are commonly used

in the industry. Synthesis gas composition is usually characterized by the stoichiometric number S (Eq. 1.7). Synthesis gas used in the industry usually presents a composition S>2:

$$S = \frac{mol\ H_2 - mol\ CO_2}{mol\ CO + mol\ CO_2} \qquad \text{(Eq. 1.7)}$$

As commented above, the synthesis gas needed for this process can be produced by partial oxidation or reforming of natural gas, or by gasification of coal or biomass. In this sense, biomass is presented as a renewable carbon source, which would lead to a considerable reduction of greenhouse gas emissions in this process, promoting the transition to an energy system that reduces dependence on fossil fuels in a scenario that contemplates, simultaneously, the scarcity of them, the growth of global demand and the impact of emissions on the environment. The composition of a synthesis gas generated from biomass gasification has been reported to be H_2 (39.2%), CO (38.1%), CO_2 (19.1%), CH_4 (1.4%) and H_2S (1.9%) [62]. As can be observed, this gas presents an H_2/CO close to 1 (S = 0.35), and the presence of sulfur compounds. However, after a conditioning unit for H_2S removal, and a WGSR stage, the composition of the gas can achieve the desired value H_2/CO close to 2 (S = 2, after removing part of the CO_2) [62,63].

It has to be noted that the industrial synthesis of methanol is highly optimized, producing a methanol purity higher than 95 % (on carbon basis). Only traces of methane, DME, methyl formate, or higher alcohols are found depending on the operating conditions and synthesis gas composition. Higher methanol purity can be achieved through a product stream rectification process.

Nowadays, industrial methanol production is carried out on Cu/ZnO-based catalysts [49,64–66]. Al_2O_3 is usually added to the Cu/ZnO metallic function due to its role as structural promoter, improving the mechanical stability and long-term stability of the catalyst. It has been reported that the Cu particle size, the metallic surface area, and the composition of the catalyst play an important role in the catalytic process [67]. Along this line, Chinchen et al. have observed a linear relationship between the catalytic activity and the metallic copper surface area [68]. When preparing these catalysts, a high Cu surface area and an intimate

contact between the Cu phase and the surrounding matrix is desired. These properties are highly influenced by the preparation methodology followed during the synthesis of the catalyst [66,69].

The most commonly used catalyst is the $Cu/ZnO/Al_2O_3$ ternary system (CZA), presenting a metal atomic ratio of Cu/Zn/Al = 6/3/1, prepared by their corresponding nitrates coprecipitation [49]. Nevertheless, there are other metallic functions, which have been also studied, such as $Cu/ZnO/ZrO_2$ [70,71]. The presence of ZrO_2 has demonstrated to improve the stability of Cu active sites in the CuO-ZnO function [72,73]. Moreover, it has been reported that the presence of ZrO_2 promotes Cu dispersion on the catalysts [11,74].

It is important to mention that Cu-based catalysts need to be in-situ reduced under H_2 flow, at a temperature of about 300 ºC, to achieve Cu reduced metal phases, which are the active sites for methanol synthesis. The presence of ZrO_2 has also demonstrated to lower this temperature due to a favorable CuO-ZrO_2 interaction [75].

Methanol synthesis is mostly carried out in fixed-bed reactors with quench or multitubular cooling [60]. As mentioned above, methanol synthesis is a highly exothermic reaction, and thus, the control of the bed temperature is important for avoiding overheating and the generation of hotspots, which may damage the catalyst. In addition, in order to avoid high pressure drops in the reactor, catalysts particles are pelletized to a particle size in the range of 4 - 6 mm [76,77]. However, the use of such particle size is translated into intraparticle diffuse limitations [78,79]. In order to overcome high pressure drops and enhance transport phenomena, the use of structured catalysts, such as monoliths, has also been studied [80].

Another catalyst morphology that can solve the aforesaid problems could be the use of fibrillar catalysts. In this sense, electrospinning is a simple and straightforward technique that has been successfully applied for the preparation of carbon and polymeric fibers in the submicro and nanoscale [81,82]. In this process, a viscous polymer solution held by its surface tension at the end of a capillary tube is subjected to a high voltage electric field, inducing the ejection of a charged liquid jet. As a result of the electrostatic repulsions between the surface

charges, a whipping phenomenon occurs in the space between the tip of the spinneret and the collector, causing the solvent evaporation, stretching the polymeric filament, and leading the deposition of the polymer fibers on the collector [83]. The use of the electrospinning technique for the preparation of different catalysts has also been recently reported [84–86]. The use of fibrillary structured catalysts in the submicrometric scale, could be very efficient in terms of intraparticle mass and heat transfer, avoiding, at the same time, the problems related to pressure drops of fixed-bed reactors working with such a reduced particle size.

1.3.1.2.- Methanol dehydration.

The second step in the indirect DME synthesis is methanol dehydration on a solid acid catalyst, yielding DME and water (Eq. 1.8).

$$2CH_3OH \leftrightarrow CH_3OCH_3 + H_2O \qquad (\Delta H_r^0 = -21.3 \text{ kJ·mol}^{-1}) \qquad \text{(Eq. 1.8)}$$
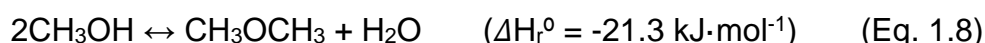
This exothermic reaction is usually carried out in a fixed bed reactor, at atmospheric pressure, in the temperature range of 250 - 400 ºC, depending on the solid acid catalyst used. This process achieves a methanol conversion per-pass about 80 %, DME being separated from the liquid phase by cooling it down. Unreacted methanol is separated from water by a distillation process and is recycled [87].

Catalytic dehydration of methanol is currently the main source of DME production. Along this line, many studies have been carried out in order to obtain catalysts with a high activity and selectivity towards DME [88–94]. Among the studied catalysts, γ-Al$_2$O$_3$ and zeolites have been widely investigated. On one hand, γ-Al$_2$O$_3$ is considered as the most efficient, owing to its high mechanical resistance, excellent lifetime and high selectivity towards DME [95]. However, there are some unsolved drawbacks, such as, the preferential adsorption of water produced during the methanol dehydration reaction on the Lewis acid sites, reducing its catalytic activity in this way. On the other hand, Zeolites (most often H-ZSM-5) are also commonly employed as catalysts for methanol dehydration [96]. These materials show a high hydrothermal stability and high catalytic activity. Yet, the presence of strong acid sites yields the production of undesirable

by-products and coke deposition, lowering the productivity of DME. To avoid coke deposition and increase the selectivity towards DME, the acid strength of these materials must be reduced [97].

Activated carbons used as catalysts and catalyst supports have received much attention in the recent decades owing to some great advantages, such as their high specific surface area, high thermal and chemical stability and the possibility to modify their surface chemistry, tuning their acidity that way. These materials can be obtained from several kinds of lignocellulosic waste [98–100], producing economic as well as environmental advantages. However, despite their potential, the use of activated carbons as catalysts for methanol dehydration has scarcely been studied to date. On this issue, Zawadzki et al. reported that the non-oxidized carbon surface is not active for this reaction, only observing certain activity after an oxidation treatment in oxygen [101]. In this sense, some attempts have been made in order to modify the carbon surface by oxidation with chemical reagents, such as $(NH_4)_2S_2O_8$, H_2SO_4 and HNO_3 [102,103]. However, the acid groups created by these means have a low thermal stability, resulting in a fast deactivation when the reaction temperature is increased.

It has been also reported that the use of phosphoric acid as activating reagent, under certain conditions of temperature and impregnation ratio, leads to the preparation of carbon materials showing a particular surface chemistry, consequence of the presence of phosphorus surface complexes, mainly in form of $C-PO_3$ and $C-O-PO_3$ groups [104]. These surface phosphorus groups provide the activated carbon with a surface acidity and a high oxidation resistance, making them suitable for catalysis applications, such as alcohol dehydration reactions [105,106]. In this line, methanol dehydration has been achieved on these materials, obtaining a selectivity towards DME higher than 95 %, when air is used as a reaction atmosphere [107]. However, when they are applied as catalysts in a non-oxidizing atmosphere, they suffer from fast deactivation due to coke deposition, exhibiting only a residual methanol conversion lower than 10%. Therefore, these materials cannot be applied to industrial DME production.

In the light of the aforementioned statements, the use of activated carbons as feasible catalysts for this application is still a pending issue, and more research

has to be carried out in order to prepare efficient carbon-based catalysts for this process.

1.3.2.- Direct process (Syngas-to-DME process).

Recently, a one-step process for the direct synthesis of DME has been intensively studied [57,58,108–110]. In this process, synthesis gas is fed to a reactor containing a bifunctional catalyst, where both methanol synthesis (on a Cu-based sites of the bifunctional catalyst), (Eq. 1.5 and 1.6), in parallel with the WGSR (Eq. 1.1), and methanol dehydration (on the acid sites of the catalyst) (Eq. 1.8), take place.

$$CO + 2H_2 \leftrightarrow CH_3OH \qquad (\Delta H_r^0 = -90.8 \ kJ \cdot mol^{-1}) \qquad (Eq. \ 1.5)$$

$$CO_2 + 3H_2 \leftrightarrow CH_3OH + H_2O \qquad (\Delta H_r^0 = -49.5 \ kJ \cdot mol^{-1}) \qquad (Eq. \ 1.6)$$

$$H_2O + CO \leftrightarrow H_2 + CO_2 \qquad (\Delta H_r^0 = -41.1 \ kJ \cdot mol^{-1}) \qquad (Eq. \ 1.1)$$

$$2CH_3OH \leftrightarrow CH_3OCH_3 + H_2O \qquad (\Delta H_r^0 = -21.3 \ kJ \cdot mol^{-1}) \qquad (Eq. \ 1.8)$$
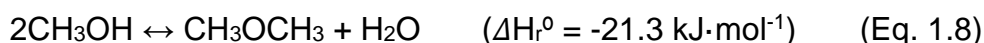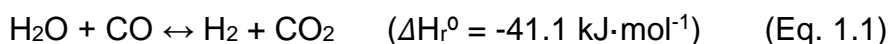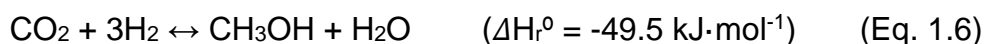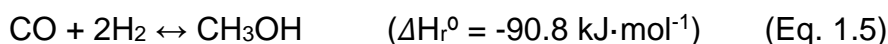
In addition, the undesired paraffin formation (mainly methane) (Eq. 1.9) also takes place in the process:
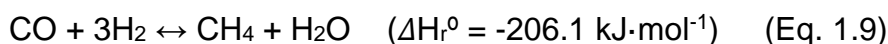
$$CO + 3H_2 \leftrightarrow CH_4 + H_2O \quad (\Delta H_r^0 = -206.1 \ kJ \cdot mol^{-1}) \quad (Eq. \ 1.9)$$

The use of this direct route presents two main advantages when compared to the indirect route. On the one hand, since both methanol synthesis and dehydration occur in only one reactor, there is a reduction in the investment costs related to equipment and infrastructures. On the other hand, as the generated methanol is in-situ consumed, equilibrium constraints related to methanol synthesis are reduced. This thermodynamic advantage makes it possible to work at lower pressure and/or higher temperature achieving a higher synthesis gas conversion per pass [58,111]. In the same way, water generated in methanol dehydration (Eq. 1.8) can be removed through the WGSR (Eq. 1.1), also favoring the methanol dehydration reaction and yielding more H_2, which is of high interest when using a synthesis gas presenting a low H_2/CO ratio, such as biomass derived syngas [12].

Syngas-to-DME process is highly exothermic, and thus chemical reactors must be designed to overcome the problems related to temperature control and heat transfer. The most commonly used chemical reactors for the direct DME synthesis are the fluidized bed reactor [12], the slurry reactors [112,113], and the fixed-bed reactors [114]. From a heat transfer viewpoint, fluidized bed reactors seem to be suitable, however, its use has not been highly investigated. The use of slurry reactors allows to operate under isothermal conditions due to the excellent heat transfer, avoiding the intraparticle diffuse limitations. Moreover, the catalyst can be added or removed during the reaction. However, problems related to catalyst abrasion and separation are common in this reactor. Fixed-bed reactors present several advantages; they are easy to scale-up and do not require an additional unit for the catalyst-products separation, catalyst abrasion does not occur, and higher catalyst loads per reactor volume can be used. Nevertheless, fixed-bed reactors present issues related to pressure drop and intraparticle diffuse limitations. In addition to the aforementioned reactors, the use of microchannel reactors, which improve heat and mass transfer and allow for a greater process intensification, has been also studied [115,116].

Catalysts used in the direct DME synthesis must present two well-defined catalytic active phases, one accounting for methanol synthesis and the other for methanol dehydration. As a component for methanol synthesis, the most commonly used catalytic phase is the $Cu/ZnO/Al_2O_3$ ternary system (CZA), presenting a metal atomic ratio of Cu/Zn/Al = 6/3/1, prepared by their corresponding nitrates coprecipitation [49]. However, as commented for methanol synthesis catalysts, it has been reported the use of metallic catalysts based on $Cu/ZnO/ZrO_2$ [71,74], $Cu/ZnO/MnO$ [108] and $Cu/Zn/Cr_2O_3$ [117]. The acid function involved in this catalyst must present a moderate acid strength, being enough so as to promote methanol dehydration, but not too high, so as to avoid further DME dehydration to olefins and higher hydrocarbons (which are related to coke formation). The most commonly studied acid functions for bifunctional catalysts are γ-Al_2O_3 and HZSM-5 zeolite [110,118,119]. In addition to them, other zeolites such as HMCM-22 [120], ferrierite [121], and Na modifies zeolites [57], and other acid solid such as SAPOs [122] have also been investigated.

When preparing bifunctional catalysts, it has to be noted that an adequate balance between the metal and acid sites must be achieved, keeping a close proximity among them [118]. The most suitable composition for a bifunctional catalyst is one that presents an excess of acid function. Under these conditions, the direct syngas-to-DME process is kinetically controlled by the methanol synthesis reaction, given that methanol dehydration is a fast step [123]. The preparation of bifunctional catalysts for this process is usually accomplished by physical mixing of their individual components [110,124–126]. Although this preparation procedure is simple and easy to scale-up, the catalysts prepared by this procedure present too great a distance between the two active sites involved in the syngas-to-DME process, thus lowering the performance of the catalyst.

As an alternative to these physical mixtures, the use of supported catalysts, in which the solid acid acts as support for the metallic phase, has been studied. In this way, the tandem process from synthesis gas to DME is achieved on the surface of one particle of the catalyst [95]. Conventional supported catalysts have been prepared by coprecipitation [127,128], impregnation [129] and sol-gel [130] methods. In addition to these methods, other preparation procedures have been reported for the preparation of supported bifunctional catalysts. Along this line, Gentzen et al. prepared them by supporting pre-synthesized Cu and ZnO nanoparticles on the acid support [131]. Zeng et al. used a physical sputtering technique for the preparation of the supported catalysts [132].

The advantages of using supported catalysts reside in the higher metallic surface area, the higher metal dispersion and a higher number of acid sites, allowing a better catalytic activity and selectivity to DME [132–134]. However, these catalysts lack uniformity for the metallic phase given that this phase is randomly distributed on the support, forming aggregates that can sinterize in the catalyst calcination stage [95]. In addition, metal deposition on the support results in a strong metal-support interaction, resulting in problems for the reducibility of the metallic phase, and thus, partially deactivating the catalyst [135]. Moreover, the random distribution of both hydrogenation and dehydration active sites on the catalyst provides an open and non-restrictive environment for the reactants, lowering the selectivity to DME.

In the last years, the use of bifunctional capsule catalysts, co-called core-shell catalysts, has been proposed for different catalytic processes [136–138]. In these catalysts, the metallic component is conforming the core of the catalyst, and it is confined by a lower thickness acid phase. The use of these catalysts for the syngas-to-DME process has been reported. Along this line, Yang et al. prepared $CuO-ZnO-Al_2O_3$ particles which were encapsulated by a HZSM-5 shell through a hydrothermal procedure [139]. Phienluphon et al. used a physical coating method to prepare $CuO/ZnO/Al_2O_3$-SAPO11 core-shell catalysts [140]. Wang et al. used commercial methanol synthesis catalyst particles ($CuO/ZnO/Al_2O_3$), which were confined by amorphous $SiO_2–Al_2O_3$ shell through a hydrothermal method [141]. Sanchez-Contador et al. reported the preparation of a core-shell catalyst by physical coating, using $CuOZnO-ZrO_2$ as core metallic function and SAPO-11 as shell acid function [142]. All these catalysts have demonstrated a higher selectivity to DME when compared to that the obtained with a catalyst prepared by physical mixing.

The use of these core-shell catalyst particles for the direct syngas-to-DME process has a huge interest. By using these catalysts, the synthesis gas reaches the Cu-based core of the catalyst particle, where it is converted to methanol. Then, when methanol leaves the core of the catalyst particle, it unavoidably needs to pass through the acid shell, due to the perfect spatial confinement, and thus it has more probability to be converted to DME. In addition, by controlling the thickness of the acid shell, the further conversion of DME to hydrocarbons can be avoided.

1.4.- Prospects and demand of DME

As aforementioned, DME presents a considerable industrial and market potential, for both electric energy generation and for being used as domestic fuel. Moreover, it presents some advantages when compared with liquified petroleum gases (LPG) and conventional diesel [95]. In fact, there is a great development regarding DME production industries all around the world, especially in Asia. For this reason, companies such as Haldor Topsoe, JFE Holdings, Air products & Chemical, and Korea Gas Corporation (KOGAS) have built several chemical

plants for the one-step DME production, using synthesis gas (a mixture of carbon monoxide and hydrogen) as feedstock. KOGAS has a chemical plant producing DME from natural gas. This plant is based on two units, in the first one natural gas is reformed to produce synthesis gas, which is used in the second unit for the one-step DME production. Toyo Engineering Co. has developed a two-step technology for the industrial production of DME, capable of producing 3,500 t/d [143]. In Japan, several companies, such as, Mitsubishi Gas Chemical, Mitsubishi Heavy Industries, and Mitsubishi Chemical Company, have developed an 80,000 t/year DME production industrial plant.

In 2011 DME world demand was estimated as 3 million tons per year. However, according to the current rate of increase this demand will reach a value of 80 million tons per year in 2020. As a consequence, the number of DME production plants, along with the number of projects related to its production, will increase in the next decade. However, despite the progress achieved to date, there are still pending issues, most of them related to the catalysts used in the process.

1.5.- References.

[1]   Population | United Nations, (n.d.). http://www.un.org/en/sections/issues-depth/population/ (accessed February 18, 2019).

[2]   BP Statistical Review of World Energy, 2018. https://www.bp.com/content/dam/bp/business-sites/en/global/corporate/pdfs/energy-economics/statistical-review/bp-stats-review-2018-full-report.pdf (accessed February 18, 2019).

[3]   World Energy Outlook, (n.d.). https://www.iea.org/weo/ (accessed February 18, 2019).

[4]   Oil Market Report- IEA, (n.d.). https://www.iea.org/oilmarketreport/omrpublic/ (accessed February 18, 2019).

[5]   G.A. Olah, A. Goeppert, G.K.S. Prakash, Beyond oil and gas : the methanol economy, Wiley-VCH, 2009.

[6]   A. Vian Ortuño, Introducción a la química industrial, Reverté, 1994.

[7]   Y. Sun, J. Cheng, Hydrolysis of lignocellulosic materials for ethanol production: a review, Bioresour. Technol. 83 (2002) 1–11. doi:10.1016/S0960-8524(01)00212-7.

[8]   F. Ma, M.A. Hanna, Biodiesel production: a review, Bioresour. Technol. 70 (1999) 1–15. doi:10.1016/S0960-8524(99)00025-5.

[9]   High-Level Conference on World Food Security: the Challenges of Climate Change and Bioenergy, (n.d.). http://www.fao.org/foodclimate/hlc-home/en/ (accessed February 18, 2019).

[10]   G.A. Olah, Beyond Oil and Gas: The Methanol Economy, Angew. Chemie Int. Ed. 44 (2005) 2636–2639. doi:10.1002/anie.200462121.

[11]   Y. Hua, X. Guo, D. Mao, G. Lu, G.L. Rempel, F.T.T. Ng, Single-step synthesis of dimethyl ether from biomass-derived syngas over CuO-ZnO-MOx(M = Zr, Al, Cr, Ti)/HZSM-5 hybrid catalyst: Effects of MOx, Appl. Catal. A Gen. 540 (2017) 68–74. doi:10.1016/j.apcata.2017.04.015.

[12]   W. Lu, L. Teng, W. Xiao, Simulation and experiment study of dimethyl ether synthesis from syngas in a fluidized-bed reactor, Chem. Eng. Sci. 59 (2004) 5455–5464. doi:10.1016/j.ces.2004.07.031.

[13]   T. Witoon, J. Chalorngtham, P. Dumrongbunditkul, M. Chareonpanich, J. Limtrakul, CO_2 hydrogenation to methanol over Cu/ZrO_2 catalysts: Effects of zirconia phases, Chem. Eng. J. 293 (2016) 327–336. doi:10.1016/j.cej.2016.02.069.

[14]   X. Dong, F. Li, N. Zhao, F. Xiao, J. Wang, Y. Tan, CO_2 hydrogenation to methanol over $Cu/ZnO/ZrO_2$ catalysts prepared by precipitation-reduction method, Appl. Catal. B Environ. 191 (2016) 8–17. doi:10.1016/j.apcatb.2016.03.014.

[15]   J. Xiao, D. Mao, X. Guo, J. Yu, Effect of TiO_2, ZrO_2, and TiO_2-ZrO_2 on the performance of CuO-ZnO catalyst for CO_2 hydrogenation to methanol, Appl. Surf. Sci. 338 (2015) 146–153. doi:10.1016/j.apsusc.2015.02.122.

[16]   I. Yarulina, S. Bailleul, A. Pustovarenko, J.R. Martinez, K. De Wispelaere, J. Hajek, B.M. Weckhuysen, K. Houben, M. Baldus, V. Van Speybroeck, F. Kapteijn, J. Gascon, Suppression of the Aromatic Cycle in Methanol-to-Olefins Reaction over ZSM-5 by Post-Synthetic Modification Using Calcium, ChemCatChem. 8 (2016) 3005. doi:10.1002/cctc.201601164.

[17]   P. Tian, Y. Wei, M. Ye, Z. Liu, Methanol to olefins (MTO): From fundamentals to commercialization, ACS Catal. 5 (2015) 1922–1938. doi:10.1021/acscatal.5b00007.

[18]   P. Pérez-Uriarte, A. Ateka, A.G. Gayubo, T. Cordero-Lanzac, A.T. Aguayo, J. Bilbao, Deactivation kinetics for the conversion of dimethyl ether to olefins over a HZSM-5 zeolite catalyst, Chem. Eng. J. 311 (2017) 367–377. doi:10.1016/J.CEJ.2016.11.104.

[19]   P. Losch, A.B. Pinar, M.G. Willinger, K. Soukup, S. Chavan, B. Vincent, P. Pale, B. Louis, H-ZSM-5 zeolite model crystals : Structure-diffusion-activity relationship in methanol-to-olefins catalysis, J. Catal. 345 (2017) 11–23. doi:10.1016/j.jcat.2016.11.005.

[20]   Z. Azizi, M. Rezaeimanesh, T. Tohidian, M.R. Rahimpour, Dimethyl ether:

A review of technologies and production challenges, Chem. Eng. Process. Process Intensif. 82 (2014) 150–172. doi:10.1016/j.cep.2014.06.007.

[21] G. Cai, Z. Liu, R. Shi, H. Changqing, L. Yang, C. Sun, Y. Chang, Light alkenes from syngas via dimethyl ether, Appl. Catal. A, Gen. 125 (1995) 29–38. doi:10.1016/0926-860X(94)00291-6.

[22] T. Shikada, K. Fujimoto, M. Miyauchi, H. o. Tominaga, Vapor phase carbonylation of dimethyl ether and methyl acetate with nickel-active carbon catalysts, Appl. Catal. 7 (1983) 361–368. doi:10.1016/0166-9834(83)80035-9.

[23] R. Matsumoto, I. Ishihara, M. Ozawa, K. Imahori, Development of Low-NOx Emission DME (Dimethyl Ether) Combustor, JSME Int. J. Ser. B. 47 (2004) 214–220. doi:10.1299/jsmeb.47.214.

[24] T.A. Semelsberger, R.L. Borup, H.L. Greene, Dimethyl ether (DME) as an alternative fuel, J. Power Sources. 156 (2006) 497–511. doi:10.1016/j.jpowsour.2005.05.082.

[25] D.A. Good, J.S. Francisco, Atmospheric Chemistry of Alternative Fuels and Alternative Chlorofluorocarbons, Chem. Rev. 103 (2003) 4999–5024. doi:10.1021/CR020654L.

[26] T.H. Fleisch, A. Basu, M.J. Gradassi, J.G. Masin, Dimethyl ether: A fuel for the 21st century, Stud. Surf. Sci. Catal. 107 (1997) 117–125. doi:10.1016/S0167-2991(97)80323-0.

[27] S.C. Sorenson, Dimethyl Ether in Diesel Engines: Progress and Perspectives, J. Eng. Gas Turbines Power. 123 (2001) 652–658. doi:10.1115/1.1370373.

[28] C. Arcoumanis, C. Bae, R. Crookes, E. Kinoshita, The potential of di-methyl ether (DME) as an alternative fuel for compression-ignition engines : A review, Fuel. 87 (2008) 1014–1030. doi:10.1016/j.fuel.2007.06.007.

[29] M. Yoon, S. Hyun, B. Woo, C. Sik, Combustion and emission characteristics of DME as an alternative fuel for compression ignition engines with a high pressure injection system, Fuel. 87 (2008) 2779–2786.

doi:10.1016/j.fuel.2008.01.032.

[30] Volvo Group, AB Volvo to develop third-generation DME engines for heavy vehicles, (n.d.). https://www.volvogroup.com/en-en/news/2006/jun/news-6928.html (accessed February 18, 2019).

[31] Volvo Group, Mack Trucks tests alternative fuel DME | Volvo Group, (n.d.). https://www.volvogroup.com/en-en/news/2017/jan/mack-trucks-tests-alternative-fuel-dme.html (accessed February 18, 2019).

[32] P.K. Arya, S. Tupkari, S. K., G.D. Thakre, B.M. Shukla, DME blended LPG as a cooking fuel option for Indian household: A review, Renew. Sustain. Energy Rev. 53 (2016) 1591–1601. doi:10.1016/J.RSER.2015.09.007.

[33] M. Marchionna, R. Patrini, D. Sanfilippo, G. Migliavacca, Fundamental investigations on di-methyl ether (DME) as LPG substitute or make-up for domestic uses, Fuel Process. Technol. 89 (2008) 1255–1261. doi:10.1016/J.FUPROC.2008.07.013.

[34] M.C. Lee, S. Bin Seo, J.H. Chung, Y.J. Joo, D.H. Ahn, Industrial gas turbine combustion performance test of DME to use as an alternative fuel for power generation, Fuel. 88 (2009) 657–662. doi:10.1016/j.fuel.2008.10.027.

[35] T.H. Fleisch, A. Basu, R.A. Sills, Introduction and advancement of a new clean global fuel : The status of DME developments in China and beyond, J. Nat. Gas Sci. Eng. 9 (2012) 94–107. doi:10.1016/j.jngse.2012.05.012.

[36] N. Kobayashi, H. Inoue, H. Koizumi, T. Watanabe, Robust Design of the Coaxial Jet Cluster Nozzle Burner for DME (Dimethyl Ether) Fuel, in: Vol. 2 Turbo Expo 2003, ASME, 2003: pp. 333–338. doi:10.1115/GT2003-38410.

[37] T. Tsuchiya, O. Masanori, Evaluation and demonstration of DME as an alternative fuel for micro-gas turbines, in: Proc Asian Cong Gas Turbine, 2005: p. 66.

[38] T. Zhang, K. Ou, S. Jung, B. Choi, Y.-B. Kim, Dynamic analysis of a PEM fuel cell hybrid system with an on-board dimethyl ether (DME) steam reformer (SR), Int. J. Hydrogen Energy. 43 (2018) 13521–13531.

doi:10.1016/J.IJHYDENE.2018.05.098.

[39]   S. Hočevar, W. Summers, Hydrogen Production, in: Hydrog. Technol., Springer Berlin Heidelberg, Berlin, Heidelberg, 2008: pp. 15–79. doi:10.1007/978-3-540-69925-5_2.

[40]   J. Ereña, J. Vicente, A.T. Aguayo, A.G. Gayubo, M. Olazar, J. Bilbao, Effect of combining metallic and acid functions in CZA/HZSM-5 desilicated zeolite catalysts on the DME steam reforming in a fluidized bed, Int. J. Hydrogen Energy. 38 (2013) 10019–10028. doi:10.1016/J.IJHYDENE.2013.05.134.

[41]   J. Ereña, J. Vicente, A.T. Aguayo, M. Olazar, J. Bilbao, A.G. Gayubo, Kinetic behaviour of catalysts with different CuO-ZnO-Al_2O_3 metallic function compositions in DME steam reforming in a fluidized bed, Appl. Catal.   B   Environ.   142–143   (2013)   315–322. doi:10.1016/J.APCATB.2013.05.034.

[42]   S.-G. Lee, H.-S. Kim, Y.-H. Kim, E.-J. Kang, D.-H. Lee, C.-S. Park, Dimethyl ether conversion to light olefins over the $SAPO$-34/ZrO_2 composite catalysts with high lifetime, J. Ind. Eng. Chem. 20 (2014) 61–67. doi:10.1016/J.JIEC.2013.04.026.

[43]   Y. Chen, H. Zhou, J. Zhu, Q. Zhang, Y. Wang, D. Wang, F. Wei, Direct Synthesis of a Fluidizable SAPO-34 Catalyst for a Fluidized Dimethyl Ether-to-Olefins   Process,   Catal.   Letters.   124   (2008)   297–303. doi:10.1007/s10562-008-9454-0.

[44]   Z. Liu, C. Sun, G. Wang, Q. Wang, G. Cai, New progress in R&D of lower olefin   synthesis,   Fuel   Process.   Technol.   62   (2000)   161–172. doi:10.1016/S0378-3820(99)00117-4.

[45]   T. Cordero-Lanzac, A. Ateka, P. Pérez-Uriarte, P. Castaño, A.T. Aguayo, J. Bilbao, Insight into the Deactivation and Regeneration of HZSM-5 Zeolite Catalysts in the Conversion of Dimethyl Ether to Olefins, Ind. Eng. Chem. Res. 57 (2018) 13689–13702. doi:10.1021/acs.iecr.8b03308.

[46]   I.A. Bakare, O. Muraza, M.A. Sanhoob, K. Miyake, Y. Hirota, Z.H. Yamani, N. Nishiyama, Dimethyl ether-to-olefins over aluminum rich ZSM-5: The role   of   Ca   and   La   as   modifiers,   Fuel.   211   (2018)   18–26.

doi:10.1016/J.FUEL.2017.08.117.

[47] T.-S. Zhao, T. Takemoto, N. Tsubaki, Direct synthesis of propylene and light olefins from dimethyl ether catalyzed by modified H-ZSM-5, Catal. Commun. 7 (2006) 647–650. doi:10.1016/J.CATCOM.2005.11.009.

[48] S. Bhattacharya, K.B. Kabir, K. Hein, Dimethyl ether synthesis from Victorian brown coal through gasification - Current status , and research and development needs, Prog. Energy Combust. Sci. 39 (2013) 577–605. doi:10.1016/j.pecs.2013.06.003.

[49] C. Baltes, S. Vukojević, F. Schüth, Correlations between synthesis, precursor, and catalyst structure and activity of a large set of $CuO/ZnO/Al_2O_3$ catalysts for methanol synthesis, J. Catal. 258 (2008) 334–344. doi:10.1016/j.jcat.2008.07.004.

[50] J.D. Grunwaldt, A.M. Molenbroek, N.Y. Topsoe, H. Topsoe, B.S. Clausen, In situ investigations of structural changes in Cu/ZnO catalysts, J. Catal. 194 (2000) 452–460. doi:DOI 10.1006/jcat.2000.2930.

[51] G.C. Chinchen, P.J. Denny, J.R. Jennings, M.S. Spencer, K.C. Waugh, Synthesis of Methanol. Part 1. Catalysts and Kinetics, Appl. Catal. 36 (1988) 1–65. doi:10.1016/S0166-9834(00)80103-7.

[52] M. Xu, J.H. Lunsford, D.W. Goodman, A. Bhattacharyya, Synthesis of dimethyl ether (DME) from methanol over solid-acid catalysts, Appl. Catal. A Gen. 149 (1997) 289–301. doi:10.1016/S0926-860X(96)00275-X.

[53] C.W. Seo, K.D. Jung, K.Y. Lee, K.S. Yoo, Dehydration of methanol over Nordstrandite based catalysts for dimethyl ether synthesis, J. Ind. Eng. Chem. 15 (2009) 649–652. doi:10.1016/J.JIEC.2009.09.037.

[54] G. Bercic, J. Levec, Catalytic dehydration of methanol to dimethyl ether. Kinetic investigation and reactor simulation, Ind. Eng. Chem. Res. 32 (1993) 2478–2484. doi:10.1021/ie00023a006.

[55] F. Yaripour, F. Baghaei, I. Schmidt, J. Perregaard, Catalytic dehydration of methanol to dimethyl ether (DME) over solid-acid catalysts, Catal. Commun. 6 (2005) 147–152. doi:10.1016/J.CATCOM.2004.11.012.

[56] M. Sánchez-Contador, A. Ateka, A.T. Aguayo, J. Bilbao, Behavior of SAPO-11 as acid function in the direct synthesis of dimethyl ether from syngas and CO_2, J. Ind. Eng. Chem. 63 (2018) 245–254. doi:10.1016/J.JIEC.2018.02.022.

[57] J. Ereña, R. Garoña, J.M. Arandes, A.T. Aguayo, J. Bilbao, Effect of operating conditions on the synthesis of dimethyl ether over a CuO-ZnO-Al_2O_3/NaHZSM-5 bifunctional catalyst, Catal. Today. 107–108 (2005) 467–473. doi:10.1016/j.cattod.2005.07.116.

[58] A.T. Aguayo, J. Ereña, D. Mier, J.M. Arandes, M. Olazar, J. Bilbao, Kinetic Modeling of Dimethyl Ether Synthesis in a Single Step on a CuO−ZnO−Al_2O_3/γ-Al_2O_3 Catalyst, Ind. Eng. Chem. Res. 46 (2007) 5522–5530. doi:10.1021/IE070269S.

[59] A.C. Sofianos, M.S. Scurrell, Conversion of synthesis gas to dimethyl ether over bifunctional catalytic systems, Ind. Eng. Chem. Res. 30 (1991) 2372–2378. doi:10.1021/ie00059a002.

[60] J. Ott, V. Gronemann, F. Pontzen, E. Fiedler, G. Grossmann, Methanol, in: Ullmann's Encycl. Ind. Chem., Wiley-VCH Verlag GmbH & Co. KGaA, Weinheim, Germany, 2012. doi:10.1002/14356007.a16_465.pub3.

[61] J.S. Lee, K.H. Lee, S.Y. Lee, Y.G. Kim, A Comparative Study of Methanol Synthesis from CO_2/H_2 and CO/H_2 over a Cu/ZnO/Al_2O_3 Catalyst, J. Catal. 144 (1993) 414–424. doi:10.1006/JCAT.1993.1342.

[62] M.C. Gutiérrez, J.M. Rosas, M.A. Rodríguez-Cano, I. López-Luque, J. Rodríguez-Mirasol, T. Cordero, Strategic situation, design and simulation of a biorefinery in Andalusia, Energy Convers. Manag. 182 (2019) 201–214. doi:10.1016/j.enconman.2018.12.038.

[63] S. Yang, B. Li, J. Zheng, R. Kumar, Biomass-to-Methanol by dual-stage entrained flow gasification : Design and techno-economic analysis based on system modeling, J. Clean. Prod. 205 (2018) 364–374. doi:10.1016/j.jclepro.2018.09.043.

[64] G.D. Sizgek, H.E. Curry-Hyde, M.S. Wainwright, Methanol synthesis over copper and ZnO promoted copper surfaces, Appl. Catal. A Gen. 115 (1994)

15–28. doi:10.1016/0926-860X(94)80375-7.

[65] K.M.V. Bussche, G.F. Froment, A steady-state kinetic model for methanol synthesis and the water gas shift reaction on a commercial Cu/ZnO/Al$_2$O$_3$ catalyst, J. Catal. 161 (1996) 1–10. doi:10.1006/JCAT.1996.0156.

[66] J. Bao, Z. Liu, Y. Zhang, N. Tsubaki, Preparation of mesoporous Cu/ZnO catalyst and its application in low-temperature methanol synthesis, Catal. Commun. 9 (2008) 913–918. doi:10.1016/J.CATCOM.2007.09.034.

[67] Y. Zhang, Q. Sun, J. Deng, D. Wu, S. Chen, A high activity Cu/ZnO/Al$_2$O$_3$ catalyst for methanol synthesis: Preparation and catalytic properties, Appl. Catal. A Gen. 158 (1997) 105–120. doi:10.1016/S0926-860X(96)00362-6.

[68] G.C. Chinchen, K.C. Waugh, D.A. Whan, The activity and state of the copper surface in methanol synthesis catalysts, Appl. Catal. 25 (1986) 101–107. doi:10.1016/S0166-9834(00)81226-9.

[69] F. Huber, H. Venvik, M. Rønning, J. Walmsley, A. Holmen, Preparation and characterization of nanocrystalline , high-surface area Cu-Ce-Zr mixed oxide catalysts from homogeneous co-precipitation, Chem. Eng. J. 137 (2008) 686–702. doi:10.1016/j.cej.2007.07.025.

[70] G. Bonura, M. Cordaro, C. Cannilla, F. Arena, F. Frusteri, The changing nature of the active site of Cu-Zn-Zr catalysts for the CO$_2$ hydrogenation reaction to methanol, Appl. Catal. B Environ. 152–153 (2014) 152–161. doi:10.1016/J.APCATB.2014.01.035.

[71] T. Witoon, N. Kachaban, W. Donphai, P. Kidkhunthod, K. Faungnawakij, M. Chareonpanich, J. Limtrakul, Tuning of catalytic CO$_2$ hydrogenation by changing composition of CuO–ZnO–ZrO$_2$ catalysts, Energy Convers. Manag. 118 (2016) 21–31. doi:10.1016/J.ENCONMAN.2016.03.075.

[72] L. Li, D. Mao, J. Yu, X. Guo, Highly selective hydrogenation of CO$_2$ to methanol over CuO–ZnO–ZrO$_2$ catalysts prepared by a surfactant-assisted co-precipitation method, J. Power Sources. 279 (2015) 394–404. doi:10.1016/J.JPOWSOUR.2014.12.142.

[73] F. Frusteri, G. Bonura, C. Cannilla, G. Drago Ferrante, A. Aloise, E.

Catizzone, M. Migliori, G. Giordano, Stepwise tuning of metal-oxide and acid sites of CuZnZr-MFI hybrid catalysts for the direct DME synthesis by CO_2 hydrogenation, Appl. Catal. B Environ. 176–177 (2015) 522–531. doi:10.1016/J.APCATB.2015.04.032.

[74]   M. Sánchez-Contador, A. Ateka, P. Rodriguez-Vega, J. Bilbao, A.T. Aguayo, Optimization of the Zr Content in the CuO-ZnO-ZrO_2/SAPO-11 Catalyst for the Selective Hydrogenation of CO+CO_2 Mixtures in the Direct Synthesis of Dimethyl Ether, Ind. Eng. Chem. Res. 57 (2018) 1169–1178. doi:10.1021/acs.iecr.7b04345.

[75]   J. Agrell, H. Birgersson, M. Boutonnet, I. Melián-Cabrera, R.M. Navarro, J.L.G. Fierro, Production of hydrogen from methanol over Cu/ZnO catalysts promoted by ZrO_2 and Al_2O_3, J. Catal. 219 (2003) 389–403. doi:10.1016/S0021-9517(03)00221-5.

[76]   K. Klier, Methanol Synthesis, Adv. Catal. 31 (1982) 243–313. doi:10.1016/S0360-0564(08)60455-1.

[77]   J.C.J. Bart, R.P.A. Sneeden, Copper-zinc oxide-alumina methanol catalysts revisited, Catal. Today. 2 (1987) 1–124. doi:10.1016/0920-5861(87)80001-9.

[78]   G.H. Graaf, H. Scholtens, E.J. Stamhuis, A.A.C.M. Beenackers, Intra-particle diffusion limitations in low-pressure methanol synthesis, Chem. Eng. Sci. 45 (1990) 773–783. doi:10.1016/0009-2509(90)85001-T.

[79]   G.H. Graaf, E.J. Stamhuis, A.A.C.M. Beenackers, Kinetics of low-pressure methanol synthesis, Chem. Eng. Sci. 43 (1988) 3185–3195. doi:10.1016/0009-2509(88)85127-3.

[80]   X.K. Phan, H. Bakhtiary-Davijany, R. Myrstad, P. Pfeifer, H.J. Venvik, A. Holmen, Preparation and performance of Cu-based monoliths for methanol synthesis, Appl. Catal. A Gen. 405 (2011) 1–7. doi:10.1016/j.apcata.2011.07.005.

[81]   G. Larsen, R. Velarde-Ortiz, K. Minchow, A. Barrero, I.G. Loscertales, A Method for Making Inorganic and Hybrid (Organic/Inorganic) Fibers and Vesicles with Diameters in the Submicrometer and Micrometer Range via

Sol−Gel Chemistry and Electrically Forced Liquid Jets, J. Am. Chem. Soc. 125 (2003) 1154–1155. doi:10.1021/JA028983I.

[82] R. Ruiz-Rosas, J. Bedia, M. Lallave, I.G. Loscertales, A. Barrero, J. Rodríguez-Mirasol, T. Cordero, The production of submicron diameter carbon fibers by the electrospinning of lignin, Carbon N. Y. 48 (2010) 696–705. doi:10.1016/J.CARBON.2009.10.014.

[83] I.G. Loscertales, A. Barrero, M. Márquez, R. Spretz, R. Velarde-Ortiz, G. Larsen, Electrically Forced Coaxial Nanojets for One-Step Hollow Nanofiber Design, J. Am. Chem. Soc. 126 (2004) 5376–5377. doi:10.1021/JA049443J.

[84] K. Huang, X. Chu, W. Feng, C. Zhou, W. Si, X. Wu, L. Yuan, S. Feng, Catalytic behavior of electrospinning synthesized $La_{0.75}Sr_{0.25}MnO_3$ nanofibers in the oxidation of CO and CH_4, Chem. Eng. J. 244 (2014) 27–32. doi:10.1016/J.CEJ.2014.01.056.

[85] R. Ruiz-Rosas, J.M. Rosas, I.G. Loscertales, J. Rodríguez-Mirasol, T. Cordero, Electrospinning of silica sub-microtubes mats with platinum nanoparticles for NO catalytic reduction, Appl. Catal. B Environ. 156–157 (2014) 15–24. doi:10.1016/J.APCATB.2014.02.047.

[86] R. Ruiz-Rosas, J. Bedia, J.M. Rosas, M. Lallave, I.G. Loscertales, J. Rodríguez-Mirasol, T. Cordero, Methanol decomposition on electrospun zirconia nanofibers, Catal. Today. 187 (2012) 77–87. doi:10.1016/j.cattod.2011.10.031.

[87] M. Müller, U. Hübsch, Dimethyl Ether, in: Ullmann's Encycl. Ind. Chem., Wiley-VCH Verlag GmbH & Co. KGaA, Weinheim, Germany, 2000. doi:10.1002/14356007.a08_541.

[88] S.S. Akarmazyan, P. Panagiotopoulou, A. Kambolis, C. Papadopoulou, D.I. Kondarides, Methanol dehydration to dimethylether over Al_2O_3 catalysts, Appl. Catal. B Environ. 145 (2014) 136–148. doi:10.1016/J.APCATB.2012.11.043.

[89] G. Laugel, X. Nitsch, F. Ocampo, B. Louis, Methanol dehydration into dimethylether over ZSM-5 type zeolites: Raise in the operational

temperature range, Appl. Catal. A Gen. 402 (2011) 139–145. doi:10.1016/j.apcata.2011.05.039.

[90] G. Pop, G. Bozga, R. Ganea, N. Natu, Methanol Conversion to Dimethyl Ether over H-SAPO-34 Catalyst, Ind. Eng. Chem. Res. 48 (2009) 7065–7071.

[91] S. Cheng, G.Z. Peng, A. Clearfield, Decomposition of Alcohols over Zirconium and Titanium Phosphates, Ind. Eng. Chem. Prod. Res. Dev. 23 (1984) 219–225. doi:10.1021/i300014a008.

[92] W. Alharbi, E.F. Kozhevnikova, I. V. Kozhevnikov, Dehydration of Methanol to Dimethyl Ether over Heteropoly Acid Catalysts: The Relationship between Reaction Rate and Catalyst Acid Strength, ACS Catal. 5 (2015) 7186–7193. doi:10.1021/acscatal.5b01911.

[93] S.Y. Hosseini, M.R. Khosravi Nikou, Investigation of different precipitating agents effects on performance of γ-Al$_2$O$_3$ nanocatalysts for methanol dehydration to dimethyl ether, J. Ind. Eng. Chem. 20 (2014) 4421–4428. doi:10.1016/J.JIEC.2014.02.010.

[94] B. Sabour, M.H. Peyrovi, T. Hamoule, M. Rashidzadeh, Catalytic dehydration of methanol to dimethyl ether (DME) over Al-HMS catalysts, J. Ind. Eng. Chem. 20 (2014) 222–227. doi:10.1016/j.jiec.2013.03.044.

[95] J. Sun, G. Yang, Y. Yoneyama, N. Tsubaki, Catalysis Chemistry of Dimethyl Ether Synthesis, ACS Catal. 4 (2014) 3346–3356. doi:10.1021/cs500967j.

[96] S. Jiang, J.-S. Hwang, T. Jin, T. Cai, W. Cho, Y.-S. Baek, S.-E. Park, Dehydration of Methanol to Dimethyl Ether over ZSM-5 Zeolite, Bull. Korean Chem. Soc. 25 (2004) 185–189. doi:10.5012/bkcs.2004.25.2.185.

[97] V. Vishwanathan, K.W. Jun, J.W. Kim, H.S. Roh, Vapour phase dehydration of crude methanol to dimethyl ether over Na-modified H-ZSM-5 catalysts, Appl. Catal. A Gen. 276 (2004) 251–255. doi:10.1016/j.apcata.2004.08.011.

[98] J. Rodríguez-Mirasol, T. Cordero, J.J. Rodríguez, Preparation and

characterization of activated carbons from eucalyptus kraft lignin, Carbon N. Y. 31 (1993) 87–95. doi:10.1016/0008-6223(93)90160-C.

[99] J.M. Rosas, J. Bedia, J. Rodríguez-Mirasol, T. Cordero, HEMP-derived activated carbon fibers by chemical activation with phosphoric acid, Fuel. 88 (2009) 19–26. doi:10.1016/J.FUEL.2008.08.004.

[100] J.M. Rosas, J. Bedia, J. Rodríguez-Mirasol, T. Cordero, On the preparation and characterization of chars and activated carbons from orange skin, Fuel Process. Technol. 91 (2010) 1345–1354. doi:10.1016/J.FUPROC.2010.05.006.

[101] J. Zawadzki, B. Azambre, O. Heintz, A. Krztoń, J. Weber, IR study of the adsorption and decomposition of methanol on carbon surfaces and carbon-supported catalysts, Carbon N. Y. 38 (2000) 509–515. doi:10.1016/S0008-6223(99)00130-X.

[102] J. Jasińska, B. Krzyżyńska, M. Kozłowski, Influence of activated carbon modifications on their catalytic activity in methanol and ethanol conversion reactions, Cent. Eur. J. Chem. 9 (2011) 925–931. doi:10.2478/s11532-011-0078-7.

[103] C. Moreno-Castilla, F. Carrasco-Marín, C. Parejo-Pérez, M. V. López Ramón, Dehydration of methanol to dimethyl ether catalyzed by oxidized activated carbons with varying surface acidic character, Carbon N. Y. 39 (2001) 869–875. doi:10.1016/S0008-6223(00)00192-5.

[104] M.J. Valero-Romero, F.J. García-Mateos, J. Rodríguez-Mirasol, T. Cordero, Role of surface phosphorus complexes on the oxidation of porous carbons, Fuel Process. Technol. 157 (2017) 116–126. doi:10.1016/J.FUPROC.2016.11.014.

[105] J. Bedia, R. Barrionuevo, J. Rodríguez-Mirasol, T. Cordero, Ethanol dehydration to ethylene on acid carbon catalysts, Appl. Catal. B Environ. 103 (2011) 302–310. doi:10.1016/J.APCATB.2011.01.032.

[106] J. Bedia, R. Ruiz-Rosas, J. Rodríguez-Mirasol, T. Cordero, Kinetic study of the decomposition of 2-butanol on carbon-based acid catalyst, AIChE J. 56 (2010) 1557–1568. doi:10.1002/aic.12056.

[107] M.J. Valero Romero, E.M. Calvo Muñoz, R. Ruíz Rosas, J. Rodríguez-Mirasol, T. Cordero, Phosphorus-containing mesoporous carbon acid catalyst for methanol dehydration to dimethyl ether, Ind. Eng. Chem. Res. (2019) acs.iecr.8b05897. doi:10.1021/acs.iecr.8b05897.

[108] A. Ateka, I. Sierra, J. Ereña, J. Bilbao, A.T. Aguayo, Performance of CuO-ZnO-ZrO$_2$ and CuO-ZnO-MnO as metallic functions and SAPO-18 as acid function of the catalyst for the synthesis of DME co-feeding CO$_2$, Fuel Process. Technol. 152 (2016) 34–45. doi:10.1016/j.fuproc.2016.05.041.

[109] F. Dadgar, R. Myrstad, P. Pfeifer, A. Holmen, H.J. Venvik, Direct dimethyl ether synthesis from synthesis gas: The influence of methanol dehydration on methanol synthesis reaction, Catal. Today. 270 (2016) 76–84. doi:10.1016/j.cattod.2015.09.024.

[110] A. García-Trenco, A. Martínez, Direct synthesis of DME from syngas on hybrid CuZnAl/ZSM-5 catalysts: New insights into the role of zeolite acidity, Appl. Catal. A Gen. 411–412 (2012) 170–179. doi:10.1016/j.apcata.2011.10.036.

[111] W.-J. Shen, K.-W. Jun, H.-S. Choi, K.-W. Lee, Thermodynamic investigation of methanol and dimethyl ether synthesis from CO$_2$ Hydrogenation, Korean J. Chem. Eng. 17 (2000) 210–216. doi:10.1007/BF02707145.

[112] Z. Gao, W. Huang, L. Yin, K. Xie, Liquid-phase preparation of catalysts used in slurry reactors to synthesize dimethyl ether from syngas : Effect of heat-treatment atmosphere, Fuel Process. Technol. 90 (2009) 1442–1446. doi:10.1016/j.fuproc.2009.06.022.

[113] Y. Ohno, H. Yagi, N. Inoue, K. Okuyama, S. Aoki, Slurry phase DME direct synthesis technology -100 tons/day demonstration plant operation and scale up study-, Stud. Surf. Sci. Catal. 167 (2007) 403–408.

[114] K. Omata, M. Hashimoto, M. Yamada, Artificial neural network and grid search aided optimization of temperature profile of temperature gradient reactor for dimethyl ether synthesis from syngas, Ind. Eng. Chem. Res. 48 (2009) 844–849.

[115] F. Hayer, H. Bakhtiary-Davijany, R. Myrstad, A. Holmen, P. Pfeifer, H.J. Venvik, Synthesis of dimethyl ether from syngas in a microchannel reactor-Simulation and experimental study, Chem. Eng. J. 167 (2011) 610–615. doi:10.1016/j.cej.2010.09.080.

[116] J. Hu, Y. Wang, C. Cao, D.C. Elliott, D.J. Stevens, J.F. White, Conversion of biomass syngas to DME using a microchannel reactor, Ind. Eng. Chem. Res. 44 (2005) 1722–1727. doi:10.1021/ie0492707.

[117] A. Venugopal, J. Palgunadi, K.D. Jung, O.-S. Joo, C.-H. Shin, Cu–Zn–Cr$_2$O$_3$ Catalysts for Dimethyl Ether Synthesis: Structure and Activity Relationship, Catal. Letters. 123 (2008) 142–149. doi:10.1007/s10562-008-9408-6.

[118] Q. Ge, Y. Huang, F. Qiu, S. Li, Bifunctional catalysts for conversion of synthesis gas to dimethyl ether, Appl. Catal. A Gen. 167 (1998) 23–30.

[119] J. Ereña, I. Sierra, M. Olazar, A.G. Gayubo, A.T. Aguayo, Deactivation of a CuO-ZnO-Al$_2$O$_3$/γ-Al$_2$O$_3$ catalyst in the synthesis of dimethyl ether, Ind. Eng. Chem. Res. 47 (2008) 2238–2247.

[120] J. Xia, D. Mao, W. Tao, Q. Chen, Y. Zhang, Y. Tang, Dealumination of HMCM-22 by various methods and its application in one-step synthesis of dimethyl ether from syngas, Microporous Mesoporous Mater. 91 (2006) 33–39. doi:10.1016/J.MICROMESO.2005.11.014.

[121] G. Bonura, C. Cannilla, L. Frusteri, A. Mezzapica, F. Frusteri, DME production by CO$_2$ hydrogenation: Key factors affecting the behaviour of CuZnZr/ferrierite catalysts, Catal. Today. 281 (2017) 337–344. doi:10.1016/J.CATTOD.2016.05.057.

[122] A. Ateka, P. Pérez-Uriarte, M. Sánchez-Contador, J. Ereña, A.T. Aguayo, J. Bilbao, Direct synthesis of dimethyl ether from syngas on CuO-ZnO-MnO/SAPO-18 bifunctional catalyst, Int. J. Hydrogen Energy. 41 (2016) 18015–18026. doi:10.1016/j.ijhydene.2016.07.195.

[123] A. García-Trenco, S. Valencia, A. Martínez, The impact of zeolite pore structure on the catalytic behavior of CuZnAl/zeolite hybrid catalysts for the direct DME synthesis, Appl. Catal. A Gen. 468 (2013) 102–111.

doi:10.1016/J.APCATA.2013.08.038.

[124] M. Stiefel, R. Ahmad, U. Arnold, M. Döring, Direct synthesis of dimethyl ether from carbon-monoxide-rich synthesis gas: Influence of dehydration catalysts and operating conditions, Fuel Process. Technol. 92 (2011) 1466–1474. doi:10.1016/J.FUPROC.2011.03.007.

[125] D. Mao, W. Yang, J. Xia, B. Zhang, Q. Song, Q. Chen, Highly effective hybrid catalyst for the direct synthesis of dimethyl ether from syngas with magnesium oxide-modified HZSM-5 as a dehydration component, J. Catal. 230 (2005) 140–149. doi:10.1016/J.JCAT.2004.12.007.

[126] G. Bonura, M. Cordaro, L. Spadaro, C. Cannilla, F. Arena, F. Frusteri, Hybrid Cu–ZnO–ZrO$_2$/H-ZSM5 system for the direct synthesis of DME by CO$_2$ hydrogenation, Appl. Catal. B Environ. 140–141 (2013) 16–24. doi:10.1016/J.APCATB.2013.03.048.

[127] P.S.S. Prasad, J.W. Bae, S. Kang, Y. Lee, K. Jun, Single-step synthesis of DME from syngas on Cu – ZnO – Al$_2$O$_3$/zeolite bifunctional catalysts : The superiority of ferrierite over the other zeolites, Fuel Process. Technol. 89 (2008) 1281–1286. doi:10.1016/j.fuproc.2008.07.014.

[128] S.-H. Kang, J.W. Bae, H.-S. Kim, G.M. Dhar, K.-W. Jun, Enhanced catalytic performance for dimethyl ether synthesis from syngas with the addition of Zr or Ga on a Cu−ZnO−Al$_2$O$_3$/γ-Al$_2$O$_3$ bifunctional catalyst, Energy & Fuels. 24 (2010) 804–810. doi:10.1021/ef901133z.

[129] R. Ahmad, D. Schrempp, S. Behrens, J. Sauer, M. Döring, U. Arnold, Zeolite-based bifunctional catalysts for the single step synthesis of dimethyl ether from CO-rich synthesis gas, Fuel Process. Technol. 121 (2014) 38–46. doi:10.1016/J.FUPROC.2014.01.006.

[130] G.R. Moradi, S. Nosrati, F. Yaripor, Effect of the hybrid catalysts preparation method upon direct synthesis of dimethyl ether from synthesis gas, Catal. Commun. 8 (2007) 598–606. doi:10.1016/J.CATCOM.2006.08.023.

[131] M. Gentzen, W. Habicht, D.E. Doronkin, J.-D. Grunwaldt, J. Sauer, S. Behrens, Bifunctional hybrid catalysts derived from Cu/Zn-based

nanoparticles for single-step dimethyl ether synthesis, Catal. Sci. Technol. 6 (2016) 1054–1063. doi:10.1039/C5CY01043H.

[132] C. Zeng, J. Sun, G. Yang, I. Ooki, K. Hayashi, Y. Yoneyama, A. Taguchi, T. Abe, N. Tsubaki, Highly selective and multifunctional Cu/ZnO/Zeolite catalyst for one-step dimethyl ether synthesis: Preparing catalyst by bimetallic physical sputtering, Fuel. 112 (2013) 140–144. doi:10.1016/J.FUEL.2013.05.026.

[133] S.-C. Baek, S.-H. Kang, J.W. Bae, Y.-J. Lee, D.-H. Lee, K.-Y. Lee, Effect of copper precursors to the activity for dimethyl ether synthesis from syngas over Cu-ZnO/γ-Al$_2$O$_3$ bifunctional catalysts, Energy & Fuels. 25 (2011) 2438–2443. doi:10.1021/ef200504p.

[134] J.W. Jung, Y.J. Lee, S.H. Um, P.J. Yoo, D.H. Lee, K.-W. Jun, J.W. Bae, Effect of copper surface area and acidic sites to intrinsic catalytic activity for dimethyl ether synthesis from biomass-derived syngas, Appl. Catal. B Environ. 126 (2012) 1–8. doi:10.1016/J.APCATB.2012.06.026.

[135] X. Liu, M.-H. Liu, Y.-C. Luo, C.-Y. Mou, S.D. Lin, H. Cheng, J.-M. Chen, J.-F. Lee, T.-S. Lin, Strong metal-support interactions between gold nanoparticles and ZnO nanorods in CO oxidation, J. Am. Chem. Soc. 134 (2012) 10251–10258. doi:10.1021/ja3033235.

[136] G. Yang, J. He, Y. Yoneyama, Y. Tan, Y. Han, N. Tsubaki, Preparation, characterization and reaction performance of H-ZSM-5/cobalt/silica capsule catalysts with different sizes for direct synthesis of isoparaffins, Appl. Catal. A Gen. 329 (2007) 99–105. doi:10.1016/J.APCATA.2007.06.028.

[137] J. Bao, G. Yang, C. Okada, Y. Yoneyama, N. Tsubaki, H-type zeolite coated iron-based multiple-functional catalyst for direct synthesis of middle isoparaffins from syngas, Appl. Catal. A Gen. 394 (2011) 195–200. doi:10.1016/J.APCATA.2010.12.041.

[138] N. Nishiyama, M. Miyamoto, Y. Egashira, K. Ueyama, Zeolite membrane on catalyst particles for selective formation of p-xylene in the disproportionation of toluene, Chem. Commun. 1 (2001) 1746–1747.

doi:10.1039/b105256j.

[139] G. Yang, N. Tsubaki, J. Shamoto, Y. Yoneyama, Y. Zhang, Confinement effect and synergistic function of H-ZSM-5/Cu-ZnO-Al$_2$O$_3$ capsule catalyst for one-step controlled synthesis, J. Am. Chem. Soc. 132 (2010) 8129–8136. doi:10.1021/ja101882a.

[140] R. Phienluphon, K. Pinkaew, G. Yang, J. Li, Q. Wei, Y. Yoneyama, T. Vitidsant, N. Tsubaki, Designing core (Cu/ZnO/Al$_2$O$_3$)–shell (SAPO-11) zeolite capsule catalyst with a facile physical way for dimethyl ether direct synthesis from syngas, Chem. Eng. J. 270 (2015) 605–611. doi:10.1016/J.CEJ.2015.02.071.

[141] Y. Wang, W. Wang, Y. Chen, J. Ma, R. Li, Synthesis of dimethyl ether from syngas over core–shell structure catalyst CuO–ZnO–Al$_2$O$_3$@SiO$_2$–Al$_2$O$_3$, Chem. Eng. J. 250 (2014) 248–256. doi:10.1016/j.cej.2014.04.018.

[142] M. Sánchez-Contador, A. Ateka, A.T. Aguayo, J. Bilbao, Direct synthesis of dimethyl ether from CO and CO$_2$ over a core-shell structured CuO-ZnO-ZrO$_2$@SAPO-11 catalyst, Fuel Process. Technol. 179 (2018) 258–268. doi:10.1016/J.FUPROC.2018.07.009.

[143] E.S. Yoon, C. Han, A Review of Sustainable Energy – Recent Development and Future Prospects of Dimethyl Ether (DME), Comput. Aided Chem. Eng. 27 (2009) 169–175. doi:10.1016/S1570-7946(09)70249-4.

Chapter 2

Experimental Methods

2.0.- Abstract

This section presents the general experimental methodology followed in this Thesis. It describes the most relevant aspects dealing with the preparation and characterization of the investigated materials and with the catalytic experiments and the experimental set up used to evaluate them. More detailed information and descriptions about the methodology followed in each section can be found in its corresponding chapter.

2.1.- Materials preparation.

In this Thesis, two different methodologies have been followed for preparing catalysts. On the one hand, activated carbon-based catalysts, presenting a granular morphology, were prepared by chemical and physical activation of a lignocellulosic waste followed by the impregnation with different metal salts. On the other hand, fibrillary structured inorganic catalysts were prepared by using the electrospinning technique.

2.1.1- Activated carbon-based catalysts preparation.

2.1.1.1.- Preparation of the activated carbons.

Two kinds of activated carbons were prepared. On the one hand, activated carbons were prepared by chemical activation of olive stone, an agri-food industry waste product, with phosphoric acid. In this process, the biomass precursor, supplied by Sociedad Cooperativa Andaluza Olivarera y Frutera San Isidro, Periana (Malaga, Spain), were impregnated with H_3PO_4 85% (w/w) aqueous solution, at room temperature and dried for 24 h at 60 °C, in a vacuum dryer. The impregnation ratio value (H_3PO_4/olive stone mass ratio) used in this case was 2. Once impregnated and dried, the substrate was activated in a conventional tubular furnace under continuous N_2 flow (150 cm^3/min STP) at 800 ºC for 2h. The activated sample was cooled inside the furnace under the same N_2 flow and then washed with distilled water at 60 ºC until showing a neutral pH and a negative phosphate analysis in the eluate [24].

On the other hand, an activated carbon was prepared by physical activation. This process consisted of the carbonization of 15 g of the same carbon precursor, followed by a partial gasification step. Both stages were carried out in a conventional tubular furnace at a heating rate of 10 ºC/min until reaching the desired temperature. Carbonization was carried out at 800 °C for 2 h in a nitrogen atmosphere (N_2; 99.999% purity purchased from Air Liquide) flow (150 cm^3/min STP). Then, the carbonized precursor was activated at the same temperature in a CO_2 flow (150 cm^3/min STP) for 7 h.

2.1.1.2.- Metal loading on the activated carbons.

To prepare the carbon-based catalysts for the different chemical reaction used in this Thesis, the activated carbons were loaded with Cu, Zn and Zr salts.

Zr loading was carried out over the different activated carbons by pore-volume impregnation of the dried samples. An appropriate amount of $ZrO(NO_3)_2$ solution was added to a known quantity of activated carbon to prepare catalysts with a Zr load ranging from 0.75 to 7.5 % (w/w). The impregnated carbons were dried overnight at 120 ºC and finally calcined at 250ºC for 2h in air.

Cu/Zn loading was carried out on the different activated carbons by pore-volume impregnation of the dried samples. An appropriate amount of $Cu(NO_3)_2 \cdot XH_2O$ and $Zn(NO_3)_2 \cdot XH_2O$ was added to a known quantity of activated carbon to prepare catalysts with a Cu and Zn loading of 10.5 and 5.5 %(w/w), respectively. The impregnated carbons were dried at 120 ºC for 24h and finally calcined at 300 ºC for 4h under continuous N_2 flow (150 150 cm^3/min STP).

2.1.2- Fibrillary structured catalysts preparation.

The experimental procedure followed for the preparation of the fibers presented in this Thesis involves the preparation of a polymer solution, the electrospinning of the resulting solution and the calcination of the prepared fibers.

2.1.2.1.- Preparation of the polymeric solutions.

Two different polymeric solutions, based on different oxide precursors, were used for the preparation of the fibrillar materials. The selection of each group of oxide precursors was based on the possibility of their being dissolved together to form a homogeneous solution. On the one hand, polymeric solutions based on zirconium (IV) propoxide (70 wt % in 1-propanol), polyvinylpyrrolidone (PVP), 1-propanol, zinc acetate and copper acetate were prepared. On the other hand, polymeric solutions based on zirconium acetate (16 %(w/w) in acetic acid), polyvinylpyrrolidone (PVP) and 1-propanol, zinc nitrate and copper nitrate were prepared.

These polymeric solutions contained the appropriate amount of copper and zinc salts to obtain a final CuO+ZnO concentration of 0, 25 and 35 %(w/w), keeping a molar Cu/Zn ratio of 2, in the final calcined fiber. Prior to the electrospinning process, the aforementioned polymeric solutions were vigorously stirred for 12 h at room temperature.

For the preparation of acid and bifunctional catalysts, different amounts of ZSM-5 zeolite (Zeolyst international, CBV 5524G, Si/Al 50, with mean crystal size of 120 nm) were also added to the aforesaid polymeric solutions, to obtain a final fiber with a zeolite mass concentration ranging from 5 to 50 %(w/w). The addition of zeolite to the polymeric solutions resulted in the preparation of different polymeric suspensions, which were vigorously stirred for 8 h at room temperature, before to the electrospinning process.

2.1.2.2.- Electrospinning of the polymer-based solutions/suspensions.

The electrospinning set-up used for the electrospun process consisted of a syringe pump, a needle or spinneret, a plate collector and two high voltage power suppliers. A typical problem when electrospinning containing rather volatile solvents solutions is the eventual solidification of the Taylor cone (or part of it) [45]. In this Thesis, we used a co-axial spinneret to overcome this problem, pumping 2-propanol through the outermost capillary needle, when it was necessary.

2.1.2.3.- Calcination of the electrospun fibers.

Finally, the electrospun fibers were recovered in form of non-woven cloth and then calcined in a muffle furnace at 500 ºC for 4 h under air atmosphere, to eliminate the remaining solvent and the polymer, stabilize the fibers and to transform the zeolite from the ammonium to the hydrogen form.

2.2.- Materials characterization.

2.2.1.- Porous texture.

The porous texture of the prepared catalysts was characterized by N_2 adsorption–desorption at -196 ºC and by CO_2 adsorption at 0 ºC, carried out in an ASAP 2020 equipment (Micromeritics). Samples were previously outgassed for at least 8 h at 150 ºC.

2.2.2.- Surface morphology.

The surface morphology of the samples was studied by scanning electron microscopy (SEM) using a Jeol JSM-6490LV micro-scope working at 25 kV voltage and by transmission electron microscopy (TEM) in a FEI Talos F200X microscope at an accelerating voltage of 200 kV and in a high annular dark field (HAADF).

2.2.3.- Surface chemistry.

2.2.3.1.- X-ray photoelectron spectroscopy (XPS).

XPS analyses of the samples were obtained by a VersaProbe II ESCA 5701 model Physical Electronics apparatus, with Al Kα radiation (1486.6 eV). For the analysis of the XPS peaks, the maximum of the C1s peak was set at 284.5 eV and used as a reference for the other peaks [31,32].

2.2.3.2.- Temperature programmed desorption (TPD).

TPD profiles were obtained in a custom fixed bed reactor placed inside an electrical furnace equipped with temperature control. The samples were heated from room temperature to 1600 °C at a heating rate of 10 °C/min in a N_2 flow (200 cm^3 STP/min). The amounts of CO and CO_2 desorbed from the samples were monitored by nondispersive infrared (NDIR) gas analyzers (Siemens ULTRAMAT 22).

2.2.4.- Crystal phases identification by X-ray diffraction.

X-ray diffraction patterns (XRD) of the calcined fibers were recorded in the region $2\theta=5-90°$ on an EMPYREAN PANalytical diffractometer using CuKα monochromatic radiation (operation value 45 kV and 40 mA), using a PIXcel detector and Soller slits (incident and diffracted beam) of 0.04 rad. The average crystallite size of the identified crystal phases was calculated by applying the Williamson-Hall method.

2.2.5.- Reducibility of the metallic species.

The reducibility of the metallic functions present on the catalysts were studied by temperature programmed reduction (H_2-TPR). For these analyses, the sample was loaded in a quartz fixed-bed microreactor and dried under helium flow at 100 °C. Then helium flow was switched to a 10 %(v/v) H_2 in helium stream, and kept for 15 min. Finally, the sample was heated up to 400 °C, at a heating rate of 5 °C/min, under the H_2 stream. H_2 consumption was monitored by mass spectroscopy (Pfeiffer Omnistar GCD-301), registering the signal m/z 2.

2.2.6.- Copper dispersion and metallic surface area.

The Cu dispersion and the Cu metallic surface area of the bifunctional catalysts were determined by N_2O selective chemisorption. For this analysis, the sample was firstly reduced under H_2 flow at a temperature of 270 °C for 2 hours. Thereafter, the sample was cooled to 60 °C, and the H_2 stream was switched to a N_2O diluted in He stream for the oxidation of the Cu^0 species [50]. N_2O

consumption was registered using an ECD-detector, enabling the determination of the copper dispersion and the active copper area.

2.2.7.- Surface acidity.

The total acidity and acid strength distribution of the prepared catalysts was determined by temperature programmed desorption of ammonia (NH_3-TPD). The NH_3-TPD was carried out using 100 mg of dried material, which was saturated with NH_3 (20 %(v/v) in helium) for 15 minutes at 100 ºC. After saturation, the weakly adsorbed NH_3 was desorbed in a helium flow at 100 ºC until no NH_3 was detected in the outlet stream. The NH_3-TPD was performed by raising the temperature up to 500 ºC at a heating rate of 10 ºC/min. The outlet NH_3 concentration was monitored by mass spectroscopy (Pfeiffer Omnistar GSD-301), registering the signal m/z 17, and using a TCD detector.

2.3.- Catalytic experiments.

2.3.1.- Methanol dehydration experiments.

Gas phase methanol dehydration experiments were carried at atmospheric pressure in a fixed-bed microreactor (i.d. 4 mm) place inside a vertical furnace with temperature control. Methanol was fed to the system by using a syringe pump (Cole-Parmer® 74900-00-05 model), using helium as carrier gas, which ensured a constant controlled methanol flow. To avoid condensation of any compound, all lines were heated up to 120 ºC.

The conversion was defined as the ratio of the amount of methanol converted to the amount of methanol supplied to the reactor. The selectivity (in mol%) was defined as the ratio of carbon moles in a specific product divided by the moles of converted methanol.

2.3.2.- Syngas to methanol/dimethyl ether experiments.

The methanol synthesis and the direct dimethyl ether synthesis from syngas experiments were carried out in a PID Eng. & Tech. Microactivity equipment, which is provided with a stainless steel fixed-bed reactor and allows

for operating at high temperature and pressures. Before starting the reaction, the catalyst was in-situ reduced at 270 ºC under H_2 flow (50 mL/min) for 2 h. After the reduction stage, the temperature was set to the reaction value and then the pressure was slowly increased up to the desired value. Finally, the syngas was introduced.

The conversion was defined as the ratio of the amount of CO converted to the amount of CO supplied to the reactor. The selectivity (in mol%) was defined as the ratio of carbon moles in a specific product divided by the moles of converted CO.

2.3.3.- Analysis of the reaction products.

The outlet gas concentrations were quantified by on-line gas chromatography (Perkin-Elmer Clarus 500 GC equipped with TCD and FID detectors). The used columns were a Permanent gases active carbon 80/100 mesh for CO and CO_2 separation and a 1.9m x 1/8" x 2.1mm Porapak N 80/100 + 0.5m x 1/8" x 2.1mm Porapak Q 80/100 column for methanol, DME and light hydrocarbons separation. N_2 was used as internal standard for GC analyses.

2.4.- Experimental units.

2.4.1.- Carbonization/activation/partial gasification with CO_2/calcination.

The different thermal treatments carried out under continuous gas flow were carried out in the same experimental unit, which is schemed in Figure 2.1. The system is composed by:

-Synthetic air, N_2 or CO_2 gas cylinders, depending on the thermal treatment.

-Mass flow meters (BROOKS, 5850 TR model).

-Mass flow controllers (GOOSEN, 5878 model).

-Horizontal tubular furnace (CARBOLITE FURNACES, CFT model; 12/75, 75 mm inner diameter, 750 mm heated length)

For the carbonization and chemical activation processes, the samples were introduced in the tubular furnace and the system was purged under N_2 flow (150 cm^3/min STP, 99.999 %, Air liquide) for 30 minutes. Once purged, the temperature was risen to 800 ºC at a heating rate of 10 ºC/min, and it was kept for 2 h. Finally, the samples were cooled to room temperature inside the tubular furnace keeping the N_2 flow. For the partial gasification with CO_2, the system was also purged under N_2 flow and heated to 800 ºC at a heating rate of 10 ºC/min. Once reached the target temperature, the gas fed was switched to CO_2 (150 cm^3/min STP, 99.998 %, Air liquide). After 7 h, the N_2 flow was restored to cool down the sample. Thermal treatments for nitrates decomposition were carried out in the same experimental unit schemed in Figure 2.1. In these cases, the system was purged under the corresponding gas flow (N_2 or synthetic air) for 30 minutes, and then it was heated to the desired temperature, at a heating rate of 10 ºC/min. Once reached the target temperature, the system was kept at this temperature for the corresponding time and then it was cooled to room temperature, keeping the same continuous gas flow.
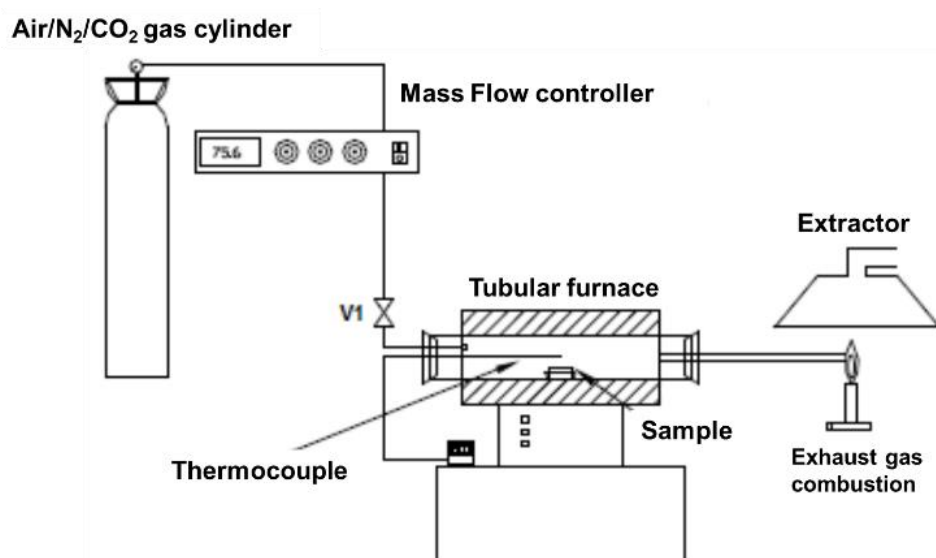

Figure 2.1. Experimental set up used for carbonization/activation/partial gasification with CO_2/calcination.

2.4.2.- Electrospinning set-up for the preparation of the fibers.

The electrospinning device used for the preparation of the fibers is schemed in Figure 2.2. It consists of the following elements:

-Two syringe pumps (Cole-Parmer® 74900-00-05 model).

-Two high voltage power suppliers.

-Spinneret made of two metallic coaxial needles.
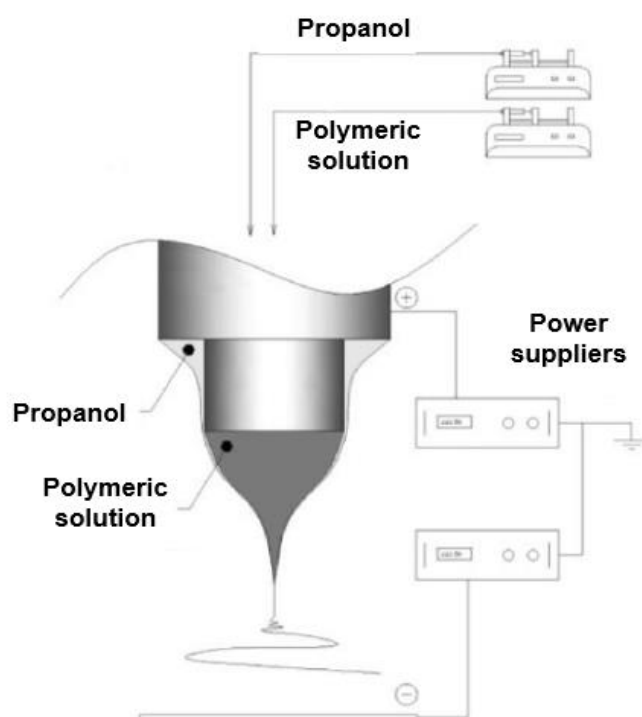
-Metallic plate collector.

Figure 2.2. Coaxial needle spinneret unit used for the preparation of the fibers.

2.4.3.- Methanol dehydration set-up.

The experimental set-up used to perform the methanol dehydration experiments is shown in Figure 2.3. The system consists of:

-Helium gas cylinder.

-Mass flow controller (Bronkhorst High-Tech).

-Syringe pump (Cole-Parmer® 74900-00-05 model).

-Custom quartz tubular reactor (internal diameter = 4 mm; length = 40 cm).

-Electrical furnace (HOBERSAL, ST18VO-0A PAD P DS PAD).

-K type thermocouple.

-Flexible heating cable.

-Gas chromatograph (Perkin-Elmer Clarus 500 GC equipped with TCD and FID detectors). The used columns were a Permanent gases active carbon 80/100 mesh for CO and CO_2 separation and a 1.9m x 1/8" x 2.1mm Porapak N 80/100 + 0.5m x 1/8" x 2.1mm Porapak Q 80/100 column for methanol, DME and light hydrocarbons separation.
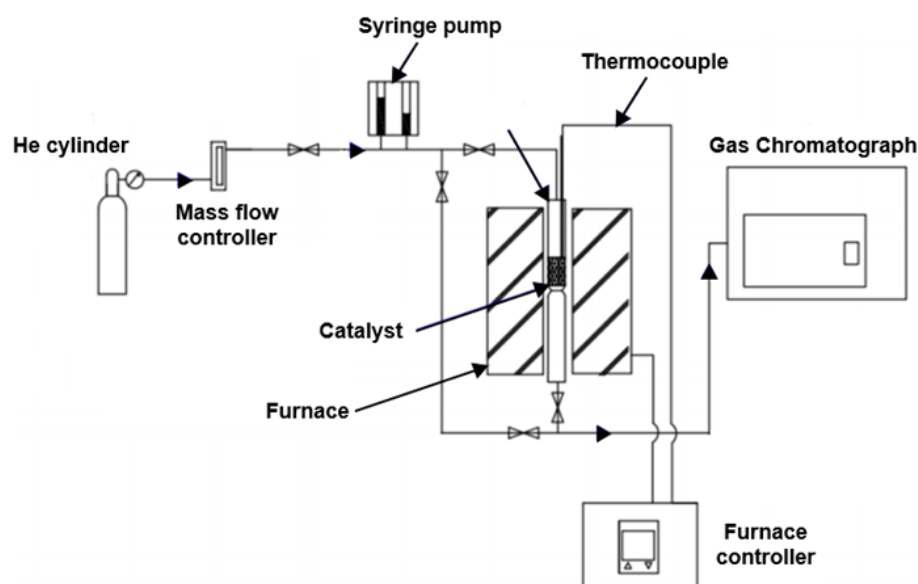

Figure 2.3. Experimental set-up for methanol dehydration experiments.

2.4.4.- Syngas to Methanol/Dimethyl ether set-up.

Methanol synthesis and direct DME synthesis experiments were carried out in an automated laboratory reactor (PID Eng. & Tech. Microactivity Reference), which is schemed in Figure 2.4. This system is equipped with:

-Stainless steel tubular reactor (Autoclave Engineers) with a 2 µm porous plate.

-Type k thermocouple in catalytic bed.

-Electrical furnace.

-Hot box for reactive system integration.

-Heater on gas output line.

-6-port valve (VICI) for reactor bypass.

-4 Mass flow controllers (Bronkhorst High-Tech).

-Safety system integrated within microprocessor.

-Pressure sensor (0-1 bar).

-Pressure control system through a servocontrolled micrometric regulating valve with stepper motor of 1^0 accuracy (P_{max} = 100 bar).
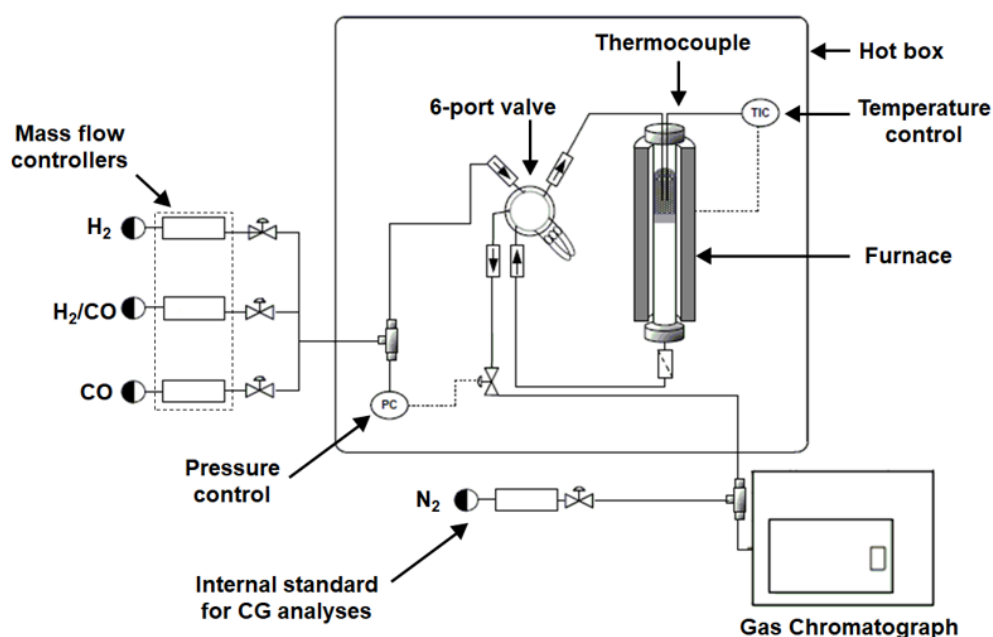

Figure 2.4. Experimental set-up for syngas to methanol/DME experiments.

Chapter 3

Methanol Dehydration to Dimethyl Ether on Zr-Loaded P-Containing Mesoporous Activated Carbon Catalysts

3.0. Abstract

Activated carbons have been prepared by the chemical activation of olive stones with phosphoric acid and loaded with Zr. The addition of Zr to the phosphorus-containing activated carbons resulted in the formation of zirconium phosphate surface groups. Gas phase methanol dehydration has been studied while using the prepared Zr-loaded P-containing activated carbons as catalysts. Carbon catalysts showed high steady-state methanol conversion values, which increased with Zr loading up to a limit that was related to P content. The selectivity towards dimethyl ether was higher than 95% for all Zr loadings. Zirconium phosphate species that were present on catalysts surface were responsible for the catalytic activity.

3.1. Introduction

Dimethyl ether (DME) is playing an important role due to its potential use as an alternative fuel in diesel engines. The use of this fuel produces lower NOx emissions and less engine noise when compared to traditional diesel fuels [1,2]. Moreover, this compound is used as a building block for many value-added chemicals, such as lower olefins, methyl acetate, and dimethyl sulphate [3,4]. Two alternatives can be used for DME production: (i) a two-step process (the so-called indirect process), which consists of one stage of methanol production from syngas while using a Cu/ZnO based catalyst [5–7], followed by a second stage of methanol dehydration over a solid acid catalyst [2,8–10]; (ii) a direct process, in which syngas is fed to a reactor that contains a bifunctional catalyst where the two aforementioned reactions take place [11–14]. The synthesis gas can be produced by partial oxidation or reforming of natural gas or by gasification of coal or biomass. In this sense, biomass represents a renewable carbon source, which would lead to a considerable reduction of greenhouse gas emissions in this process, promoting the transition to an energy system that reduces the dependence on fossil fuels in a scenario that simultaneously contemplates the scarcity of them, the growth of global demand and the impact of emissions on the environment.

The catalytic dehydration of methanol is currently the main source of DME production. In this sense, many studies have been carried out in order to obtain catalysts with a high activity and selectivity towards DME [15–21]. Among the studied catalysts, γ-Al$_2$O$_3$ and zeolites have been widely investigated. On one hand, γ-Al$_2$O$_3$ is considered to be the most efficient one, owing to its high mechanical resistance, excellent lifetime, and high selectivity towards DME [22]. However, there are some unsolved drawbacks, such as the preferential adsorption of water produced during the methanol dehydration reaction on the Lewis acid sites, reducing its catalytic activity that way. On the other hand, Zeolites (most often H-ZSM-5) are also commonly employed as catalysts for methanol dehydration [23]. These materials show high hydrothermal stability and high catalytic activity. Yet, the presence of strong acid sites yields the production of undesirable by-products and coke deposition, which lowers the productivity of DME. The acid strength of these materials must be reduced to avoid coke deposition and increase the selectivity towards DME [24].

Activated carbons that are used as catalysts and catalyst supports have received significant attention in the recent decades, owing to some great advantages, such as its high specific surface area, high thermal and chemical stability, and the possibility to modify its surface chemistry, tuning its acidity that way. These materials can be obtained from several kinds of lignocellulosic waste [25–27], producing economic as well as environmental advantages. However, the use of activated carbons as catalysts for methanol dehydration has scarcely been studied so far, despite its potential. Regarding this issue, Zawadzki et al. [28] pointed out that non-oxidized carbons are unreactive in the methanol decomposition reaction, observing certain activity only after oxidizing its surface by using gas oxygen. In this sense, some attempts have been made in order to modify the carbon surface by oxidation with chemical reagents, such as (NH$_4$)$_2$S$_2$O$_8$, H$_2$SO$_4$, and HNO$_3$ [29,30]. However, the acid groups that were created by these means have a low thermal stability, which results in a fast deactivation when the reaction temperature is increased.

Our research group has reported several works on the preparation and characterization of biomass waste derived activated carbons by chemical

activation with phosphoric acid [31–33]. The activation with phosphoric acid leads to the preparation of carbon materials, presenting oxygen-phosphorus surface groups that show a high thermal and chemical stability, remaining over the carbon surface after the washing step [34]. These phosphorus surface groups provide the activated carbons a high oxidation resistance and surface acidity, which makes them suitable for catalysis applications. According to this fact, these materials have been successfully used as catalyst in the decomposition of alcohols, mainly yielding dehydration products [35,36]. In this line, methanol dehydration has been achieved on these materials, obtaining a selectivity towards DME that is higher than 95 % when air is used as a reaction atmosphere [37]. However, when they are applied as catalysts in a non-oxidizing atmosphere, they suffer from fast deactivation due to coke deposition, only exhibiting a residual methanol conversion that is lower than 10%. Therefore, these materials cannot be applied to industrial DME production routes, that is, indirect as well as direct DME synthesis processes.

In the light of the aforementioned statements, the use of activated carbons for feasible methanol dehydration applications is still a pending issue. In this work, the modification of phosphorus-containing olive stone-derived activated carbon with zirconium has been analyzed, with the aim of preparing a carbon-based catalyst with a high resistance to coke deactivation and a tailor-made acidity for the selective methanol dehydration to DME, which would bring high added-value to this agri-food industry waste.

3.2. Materials and Methods

3.2.1. Preparation of Activated Carbon

Activated carbons were prepared by the chemical activation of olive stone, an agri-food industry waste product, with phosphoric acid. In this process, 10 g of biomass precursor, which Sociedad Cooperativa Andaluza Olivarera y Frutera San Isidro, Periana (Malaga, Spain) supplied, were impregnated with H_3PO_4 85% (w/w) aqueous solution, at room temperature and then dried for 24 h at 60 °C, in a vacuum dryer. The impregnation ratio value (H_3PO_4/olive stone mass ratio) used in this case was 2. Once impregnated and dried, the substrate was activated

in a conventional tubular furnace (Carbolite CTF 12/100/900, Thermo Fisher Scientific, Waltham, MA, USA) under continuous N_2 flow (150 cm^3/min. STP) at 800 °C for 2 h. The activated sample was cooled inside the furnace under the same N_2 flow and then washed with distilled water at 60 °C until displaying a neutral pH and a negative phosphate analysis in the eluate [38]. The final activated carbon that was prepared following this procedure presented a yield of 39% based on the mass of dried olive stone and was denoted as ACP2800.

An activated carbon was prepared by physical activation for comparative purposes. This process consisted of the carbonization of 15 g of the same carbon precursor, followed by a partial gasification step. Both of the stages were carried out in a conventional tubular furnace at a heating rate of 10 °C/min. until reaching the desired temperature. Carbonization was carried out at 800 °C for 2 h under continuous nitrogen flow (150 cm^3/min. STP). Afterwards, the carbonized precursor was activated at the same temperature in a CO_2 flow (150 cm^3/min. STP) for 7 h, reaching a 45% burn-off. The final activated carbon that was obtained by this activation process presented a yield of 13.7% based on dried olive stone and it was denoted as AC800.

3.2.2. Zr Loading over the Different Activated Carbons

Zr loading was carried out over the different activated carbons by pore-volume impregnation of the dried samples. An appropriate amount of $ZrO(NO_3)_2$ solution was added to a known quantity of activated carbon to prepare the catalysts with a Zr load ranging from 0.75 to 7.5% (w/w). The impregnated carbons were dried overnight at 120 °C and finally calcined at 250 °C for 2 h in air. Adding –ZrX to the name of the parent activated carbon denoted the catalysts that were obtained, where X refers to the Zr loading mass percentage (e.g., ACP2800Zr7.5).

3.2.3. Characterization of Carbon Catalysts

The porous texture of the prepared activated carbons and catalysts was characterized by N_2 adsorption–desorption at −196 °C and by CO_2 adsorption at 0 °C, carried out in an ASAP 2020 equipment (ASAP 2020, Micromeritics

Instruments Corp., Norcross, GA, USA). The samples were previously outgassed for at least 8 h at 150 °C. From the N_2 adsorption-desorption isotherm, the apparent surface area (A_{BET}) was determined by applying the BET equation [39]. The α_s method was used to obtain the values of the so-called external surface area (A_s), that is, the surface area associated to the non-microporous structure; and, the micropore volume (V_s), while using the high-resolution method that was proposed by Kaneko et al. [40] with a nonporous carbon black sample (Elftex-120) as standard [41]. The narrow mesopore volume was determined as the difference between the adsorbed volume of N_2 at a relative pressure of 0.99 and the micropore volume, V_s. From the CO_2 adsorption data, the narrow micropore volume (V_{DR}) and surface area (A_{DR}) were calculated while using the Dubinin–Radushkevich equation [42].

The surface chemistry of the samples was analyzed by X-ray photoelectron spectroscopy (XPS) and temperature programmed desorption (TPD). XPS analyses of the samples were obtained by a VersaProbe II ESCA 5701 model Physical Electronics apparatus (VersaProbe II ESCA 5701, Physical Electronics, Chanhassen, MN, USA), with Al Kα radiation (1486.6 eV). For the analysis of the XPS peaks, the maximum of the C1s peak was set at 284.5 eV and used as a reference for the other peaks [35]. Temperature programmed desorption (TPD) provides information regarding the nature of the oxygen groups present on the surface of activated carbons [43]. The TPD profiles were obtained in a custom fixed-bed reactor (Forns Hobersal, Barcelona, Spain) that was placed inside an electrical furnace. The samples were heated from room temperature to 1600 °C at a heating rate of 10 °C/min. in a N_2 flow (200 cm^3 STP/min). The amounts of CO and CO_2 desorbed from the samples were monitored by nondispersive infrared (NDIR) gas analyzers (ULTRAMAT 22, Siemens AG, Munich, Germany).

The total acidity and acid strength distribution of the prepared catalysts was determined by temperature programmed desorption of ammonia (NH_3-TPD). The NH_3-TPD was carried out while using 100 mg of dried material, which was saturated with NH_3 (20 % (v/v) in helium) for 15 min at 100 °C. After saturation, the weakly adsorbed NH_3 was desorbed in a helium flow at 100 °C until no NH_3 was detected in the outlet stream. The NH_3-TPD was performed by raising the

temperature up to 550 °C at a heating rate of 10 °C/min. Mass spectroscopy monitored the outlet NH_3 concentration (Pfeiffer Omnistar GSD-301, Pfeiffer Vacuum Technology AG, Asslar, Germany), registering the signal m/z 17.

3.2.4. Methanol Dehydration Catalytic Reaction

The carbon materials that were prepared were used as catalysts in the dehydration of methanol in the gas phase at atmospheric pressure in a fixed bed microreactor (i.d. 4 mm) (MERVILAB, Madrid, Spain) that was placed inside a vertical furnace (TR2-A, Forns Hobersal, Barcelona, Spain) with temperature control. In a typical experiment, 200 mg of catalyst (100–300 μm particle size) were used. Methanol was fed to the system by using a syringe pump (Cole-Parmer® 74900-00-05 model, Cole-Parmer Instrument Company, Vernon Hills, IL, USA), ensuring a constant controlled methanol flow, 0.37 g/h. The reaction was carried out in a helium atmosphere in a temperature range of 250-450 °C. All of the lines were heated up to 120 °C to avoid condensation of any compound. The feed conditions that were used were methanol partial pressures of 0.02 and 0.04 atm, water vapor partial pressures of 0 and 0.02 atm and a space time of 0.1 $(g \cdot s / \mu mol_{MeOH})$. The outlet gas concentrations were quantified by on-line gas chromatography (Perkin-Elmer Clarus 500 GC that was equipped with TCD (thermal conductivity detector) and FID (flame ionization detector) detectors (Clarus 500 GC, Perkin-Elmer, Waltham, MA, USA). The used columns were a Permanent gases active carbon 80/100 mesh for CO and CO_2 analysis (Teknokroma Analítica, Barcelona, Spain) and a 1.9 m × 1/8" × 2.1 mm Porapak N 80/100 + 0.5 m × 1/8" × 2.1 mm Porapak Q 80/100 column (Teknokroma Analítica, Barcelona, Spain) for methanol, DME, and light hydrocarbons separation.

The conversion was defined as the ratio of the amount of methanol converted to the amount of methanol that is supplied to the reactor. The selectivity (in mol%) was defined as the ratio of carbon moles in a specific product divided by the moles of converted methanol. The carbon balance was reached with an error lower than 3% in all of the experiments.

3.3. Results and Discussion

3.3.1. Characterization of the Carbon Catalysts

Figure 3.1 shows the N_2 adsorption-desorption isotherms at −196 °C for the different carbon materials that were prepared in this study. Chemically activated carbon, ACP2800, (Figure 3.1a) presents a type I b isotherm [44] corresponding to materials that have a broad range of wider micropores and narrow mesopores. The exhibition of an open knee is noticeable, which extends up to increasingly higher relative pressures and it is characteristic of a wide microporosity and mesoporosity. An H4 type hysteresis loop is observed, closing at a relative pressure value of 0.4, associated to capillary condensation in mesopores. Physically activated carbon, AC800, (Figure 3.1b) shows a type I a isotherm, which is characteristic of a typical microporous solid, adsorbing almost all N_2 volume at very low relative pressures.

The results show that the porosity of the sample ACP2800 (Figure 3.1a) seems not to be highly affected by the Zr loading. In this sense, a slight decrease in the volume of N_2 adsorbed at low relative pressures is only observed, being associated to a reduction of the wide microporosity, due to Zr deposition. The physically activated carbon, AC800 (Figure 3.1b), also experienced a porosity decrease after Zr loading, given that a reduction in the volume of N_2 was also observed, but in this case at very low relative pressures, which are associated to narrow micropore reduction or blockage.
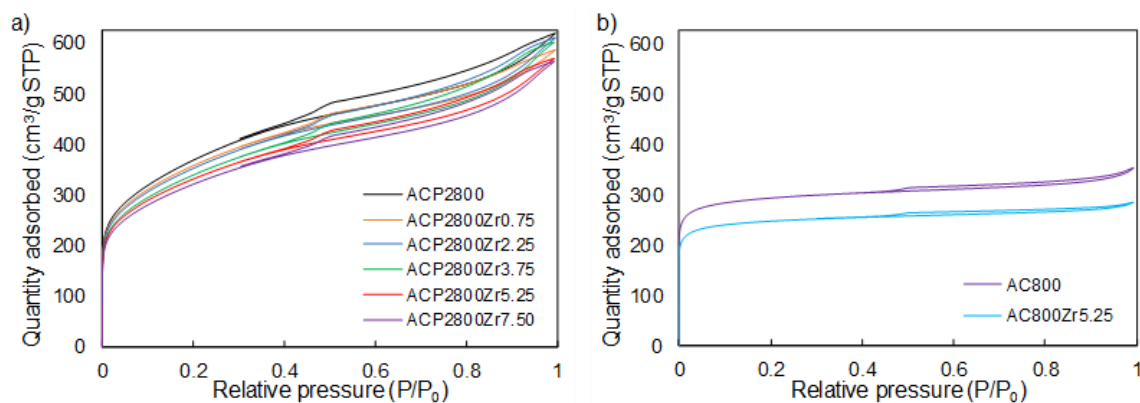
Figure 3.1. Nitrogen adsorption–desorption isotherms at −196 °C of (**a**) Chemically activated carbon (ACP2800) before and after different Zr loads. (**b**) Physically activated carbon (AC800) before and after a Zr load of 5.25 %(w/w).

Table 3.1 presents the values of the textural parameters, which were calculated from N_2 adsorption-desorption and CO_2 adsorption isotherms, of the prepared activated carbons. ACP2800 presents a value of A_{BET}^{N2} higher than that of the A_{DR}^{CO2}, which is indicative of a wide porous texture in this sample. The higher value of mesopore volume (V_{mes}) is also noticeable when comparing with the micropore value (V_s), indicating a high contribution to mesoporosity. The external surface area value (A_s) confirms this fact. Physically activated carbon (AC800) presents a specific surface area that is similar to the one that was obtained for the chemically activated carbon (ACP2800). However, the physically activated carbon (AC800) presents an A_{BET}^{N2} value that was comparable to the A_{DR}^{CO2} value, which is characteristic of a typical microporous solid. Moreover, the similarity between the values of V_s^{N2} and V_{DR}^{CO2} evidences the presence of a narrow microporous structure. The results show that, after Zr loading, all of the samples experiment a reduction in the structural parameters. On the one hand, a decrease in the V_s^{N2} values is observed when Zr loading is increased over chemically activated carbons, ACP2800ZrX. However, V_{DR}^{CO2} ones seem to be not highly affected, when increasing the Zr loading, which is indicative of Zr deposition on the surface of the wider micropores. On the other hand, when the physically activated carbon, AC800, is loaded with Zr, V_s^{N2}, and V_{DR}^{CO2} values

show a similar decrease, indicating that Zr deposition is blocking the narrow microporosity.

Table 3.1. Characteristic parameters of the porous texture and zirconium loading for the prepared activated carbons.

Sample	A_{BET}^{N2} (m^2/g)	V_p^{N2} (cm^3/g)	V_{mes}^{N2} (cm^3/g)	As^{N2} (m^2/g)	Vs^{N2} (cm^3/g)	A_{DR}^{CO2} (m^2/g)	V_{DR}^{CO2} (cm^3/g)	%Zr
			N₂ Isotherm			**CO₂ Isotherm**		
ACP2800	1280	0.95	0.44	310	0.52	471	0.19	0
ACP2800Zr0.75	1273	0.90	0.41	308	0.49	519	0.21	0.75
ACP2800Zr2.25	1195	0.94	0.45	297	0.50	511	0.21	2.25
ACP2800Zr3.75	1148	0.93	0.44	281	0.49	501	0.20	3.75
ACP2800Zr5.25	1143	0.88	0.40	247	0.48	497	0.20	5.25
ACP2800Zr7.5	1132	0.86	0.40	242	0.47	487	0.20	7.50
AC800	1127	0.55	0.10	52	0.44	865	0.35	0
AC800Zr5.25	812	0.44	0.07	43	0.37	757	0.30	5.25

X-ray photoelectron spectroscopy (XPS) analyzes were carried out in order to evaluate the surface element distribution and the surface chemical composition of the samples. Both of the activated carbons, ACP2800 and AC800, are mainly composed of carbon (89.5 and 95.4% (w/w), respectively) and oxygen (7.2 and 4.6% (w/w), respectively). However, chemically activated carbon also presents a low, but still significant, surface concentration of phosphorus (3.2% (w/w)), which has been attributed to the activation step [26,32]. Chemical activation of olive stone (and other biomass waste) with phosphoric acid seems to proceed by forming phosphate and polyphosphate bridges that crosslink the biopolymer fragments, developing the porous texture and generating these phosphorus complexes that remain chemically stable bonded to the carbon surface, even despite the washing step [34]. The P concentration for this sample was 3.6% (w/w), when it was analyzed by ICP-MS (Inductively coupled plasma mass spectrometry). The similar value that was obtained by both analytical techniques suggests that the phosphorus surface groups are very well distributed on the carbon particle surface.

Table 3.2 presents the atomic surface ratios of Zr, O, and P with respect to each other, as calculated for the different Zr loading samples. As expected, the Zr/P ratio increases and the O/Zr ratio decreases, as the zirconium amount

augments on the samples. The O/P ratio should linearly increase as the zirconium loading increases, since the salt used for the impregnation, $ZrO(NO_3)_2$, decomposes yielding ZrO_2. However, it seems that at low zirconium loadings, this ratio is not highly affected. This fact could indicate that zirconium tends to bond oxygen species present on the carbon surface at low metal loadings, such as C-O-PO_3 and C-O, hence less oxygen being necessary for the coordination of the zirconium atoms. Nevertheless, it seems that the zirconium that is incorporated to the carbon surface is accompanied by oxygen atoms at high Zr loadings, thus forming zirconium oxide species on the carbon surface.

Table 3.2. Atomic surface ratios of Zr, O, and P with respect to each other, obtained by X-ray photoelectron spectroscopy (XPS) analysis, for the Zr-loaded P-containing activated carbons.

Sample	Atomic surface ratios (XPS)		
	Zr/P	O/Zr	O/P
ACP2800	-	-	4.45
ACP2800Zr0.75	0.49	9.75	4.70
ACP2800Zr2.25	0.50	9.06	4.57
ACP2800Zr3.75	0.62	8.98	5.55
ACP2800Zr5.25	0.89	7.52	6.71
ACP2800Zr7.50	0.98	7.16	7.00

The XPS spectra were examined in order to analyze the chemical surface of the Zr-loaded samples in depth. Figure 3.2 shows the normalized high resolution XPS spectra for phosphorus, oxygen, and zirconium. The P2p spectrum of sample ACP2800 shows a main peak at a binding energy around 133 eV, which is characteristic of pentavalent tetracoordinated phosphorus [35,45]. The normalized O1s spectra for both chemically and physically prepared activated carbons show a band with a maximum at a binding energy of 532.3 eV, which is attributed to the single bonded oxygen, in the form of C-OH, C-O-C, and/or C-O-P. It can be observed that the former shows a more pronounced shoulder at a binding energy of 530.7 eV when comparing the O1s spectrum for the chemically activated carbon with the spectrum for the physically activated one, which is characteristic of C=O and/or P=O groups.

After Zr loading, all of the prepared phosphorus-containing activated carbons present similar XPS spectra. Due to this similarity, only the spectra that were obtained for sample ACP2800Zr5.25 have been shown. The normalized P2p spectrum that was obtained for this sample (Figure 3.2a) shifts to higher binding energy values when it is compared to its parent carbon, ACP2800. This displacement is a consequence of the oxidation of the phosphorus groups and now the peak appears at the binding energy characteristic of phosphates and/or polyphosphates, at 133.7 eV [34,35]. It can also be observed that the O1s and Zr3d normalized spectra for the carbons containing and not containing phosphorus exhibit significant differences between them. The normalized O1s band that was obtained for sample AC800Zr5.25 (not containing phosphorus) consists of a main peak at a binding energy of 530.2 eV, which is assigned to oxygen in metal oxides [46] and a small and broad high binding energy shoulder, which could be attributed to surface hydroxyl species, such as Zr-OH and/or C-OH [46,47]. In contrast, the normalized O1s band that was obtained from the phosphorus-containing sample, ACP2800Zr5.25, can be deconvoluted in three peaks. The main peak, which appears in this case at a binding energy of 532 eV, is associated to the oxygens of the phosphate groups. Two shoulders are also observed, one at higher binding energies that corresponds to the acidic P-OH groups and the other one at lower binding energies, which is probably due to the Zr-OH groups [48]. The normalized Zr3d band exhibits the two 3d peaks that are separated by 2.3 eV, which are characteristic of the tetravalent Zr^{4+}, in both cases. However, it is noteworthy that the binding energy at which the Zr3d appears is different when phosphorus is present in the sample. In this sense, it has been reported in the literature, when analyzing zirconium phosphates [45,48], that the coordination of Zr atoms with a high number of strongly polarized oxygens results in the displacement of the Zr3d band to higher binding energies [48]. The presence of these species could be responsible for the higher binding energy that was found in the spectra of the phosphorus-containing samples (see ACP2800Zr5.25 in Figure 3.2c).
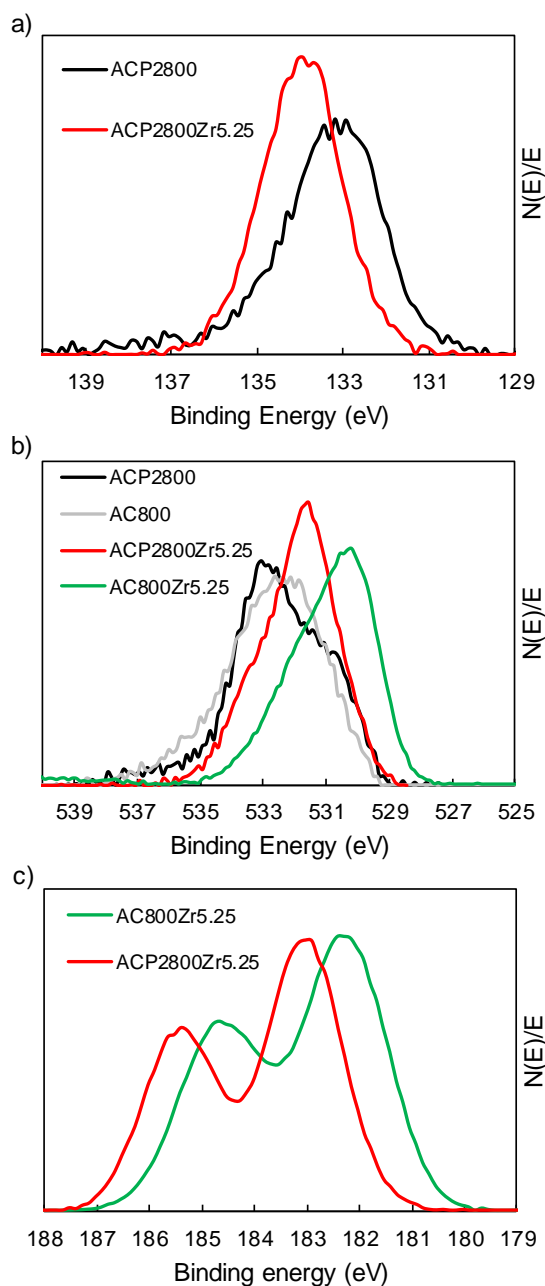
Figure 3.2. (**a**) Normalized P2p XPS spectra for ACP2800 and the 5.25% Zr loaded phosphorus containing samples; (**b**) Normalized O1s XPS spectra for ACP2800, AC800 and the 5.25% Zr loaded samples; and, (**c**) Normalized Zr3d XPS spectra for the 5.25% Zr loaded samples.

The TPD technique also analyzed the surface chemistry of the samples, which is used to characterize the oxygen groups on the surface of carbons in detail. Figure 3.3a shows the evolution of CO from the TPD analysis of the

phosphorus-containing sample, ACP2800, before and after the different Zr loadings. ACP2800 releases most of the CO at a temperature around 870 °C, which has been previously assigned to the decomposition of stable C-O-P type bonds of C-O-PO$_3$ surface groups, producing CO gas and C'-P type bonds of C-PO$_3$ surface groups, where C' represents a new carbon center [26,49]. After Zr loading on ACP2800, the CO profiles show three main peaks at 870, 1000, and 1300 °C, respectively. As it can be observed, the peak at 870 °C, which was associated to the presence of C-O-P bonds, decreased as the amount of Zr that was deposited on the carbon surface increased. On the other hand, the amount of CO that evolved at 1000 and 1300 °C increased with metal loading and it was related to the presence of zirconium species on the carbon surface. Moreover, it has to be noted that the total amount of CO evolved in the temperature range of 750–1100 °C was the same for all the samples, with a linear relationship being observed between the decrease in CO evolving at 870 °C and the increase in CO evolving at 1000 °C. The TPD CO profiles obtained for the samples not containing phosphorus, AC800 and AC800Zr5.25, were also studied in order to thoroughly analyze the nature of these surface complexes that evolved as CO at such a high temperature (see Figure 3.3b). AC800 presented a CO evolution peak at about 900 °C, which was associated to carbonyl/quinone or ether groups [34]. After Zr loading, the presence of a second peak at a temperature of 1300 °C was noticeable (see AC800Zr5.25 in Fig 3b), which has been related to the presence of C-O-Zr bonds and to the surface ZrO$_2$ carboreduction [50]. However, the CO peak that appeared at about 1000 °C was not present in this sample. Therefore, the CO that evolved at this temperature must be related to the simultaneous presence of zirconium and phosphorus, mainly in the form of zirconium phosphate groups (as already revealed by the XPS analysis), bonded to the carbon surface. Furthermore, the relationship that was observed between the decreased amount of CO that evolved at 870 and the increased amount evolved at 1000 °C with increasing Zr loading seems to indicate that the C-O-P type bonds were cleaved in favor of the formation of zirconium phosphate species. These zirconium phosphate species seem to be bonded to the carbon surface via C-O-P and C-O-Zr bonds, forming C-O-(P-O-Zr)-O-C like structures, which decompose, releasing CO at 870 °C and 1000 °C, respectively. According to these TPD results, the number for C-O-Zr bonds of the zirconium phosphate

surface groups seems to be higher than the one for C-O-P bonds in the samples with a Zr loading that was larger than 2.25.

The CO that evolved at temperatures below 800 °C for all of the samples that were loaded with Zr can be attributed to the presence of anhydride, phenol, and/or ether surface groups [43]. It is worth noting that the CO amount that evolved below this temperature was almost the same for all of the phosphorus-containing carbon samples loaded with Zr (see Figure 3.3), and therefore did not seem to have any relationship with the amount of metal loaded. These oxygenated species were probably formed during the calcination stage, at 250 °C [34]. The CO evolution at temperatures below 800 °C in the AC800Zr5.25 sample was higher than the one that was observed in the phosphorus-containing samples, due to the lower oxidation resistance of the non-phosphorus-containing activated carbons as compared to the ones containing phosphorus [31].
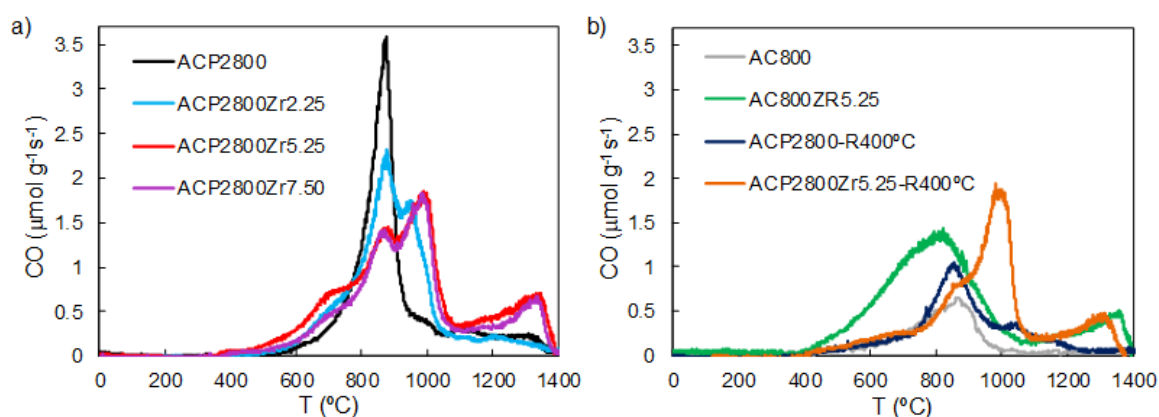

Figure 3.3. Amount of CO that evolved as a function of temperature during temperature programmed desorption (TPD) for (**a**) ACP2800, ACP2800Zr2.25, ACP2800Zr5.25 and ACP2800Zr7.50. (**b**) AC800, AC800Zr5.25 and, ACP2800 and ACP2800Zr5.25 after 4 hours on reaction at 400 °C, P_{MeOH} = 0.02 atm, W/F_{MeOH} = 0.1 g.s/µmol.

Figure 3.4 presents the NH_3-TPD profiles that were obtained for ACP2800, ACP2800Zr5.25, and AC800Zr5.25. The temperature at which ammonia desorption took place indicates the acid strength of the catalytic sites, with the sites desorbing at a lower temperature being weaker. ACP2800 desorbed most

of the ammonia at a temperature of 200 °C, which is associated to weakly (or moderately) adsorbed ammonia on the C-O-P groups, which are present on the surface of this material. The presence of a shoulder in the curve at a temperature of 250 °C and a large tail at higher temperatures is also noteworthy, being associated to the stronger adsorption of NH$_3$ on the P-OH groups present on the activated carbon surface, which act as Brönsted acid sites [36,51]. ACP2800Zr5.25 showed a similar profile to its parent carbon (ACP2800). However, it exhibited a slightly higher total amount of desorbed ammonia (175 μmol/g for ACP2800Zr5.25 vs 128 μmol/g for ACP2800). This increase in the acidity could be associated to the presence of Zr-O-P groups, which can act as acid sites. AC800 did not desorb any appreciable amount of ammonia during the NH$_3$-TPD analysis in contrast with the chemically activated carbon, which suggests that this carbon lacks the presence of acid surface groups. Once this carbon was loaded with Zr in the same conditions as those for the preparation of ACP2800Zr5.25, the resulting carbon, AC800Zr5.25, which did not contain phosphorus, exhibited a much lower amount of desorbed ammonia, 81 μmol/g, during the NH$_3$-TPD analysis than the one that was observed in the phosphorus-containing sample. The acidity of this sample (AC800Zr5.25) can be attributed to the presence of zirconium on the carbon surface, forming zirconium oxide.
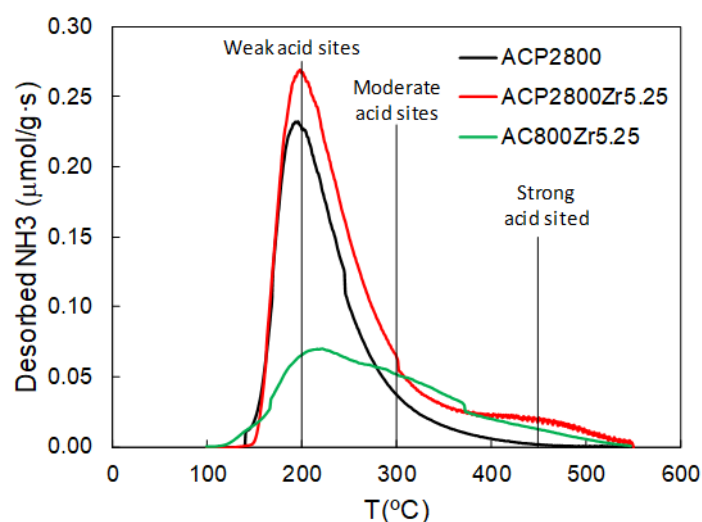

Figure 3.4. Ammonia TPD of the samples ACP2800, ACP2800Zr5.25, and AC800Zr5.25.

3.3.2. Catalytic Dehydration of Methanol

Methanol dehydration was studied for the carbon-based catalysts in a fixed bed reactor. In the absence of catalysts, no reaction occurred below 600 °C. Heat and the mass transfer limitations were theoretically checked and considered to be negligible according to the criterion that was suggested by Moulijn et al. [52].

3.3.2.1. Effect of Zr Loading

Figure 3.5 shows the steady-state methanol conversion and selectivity towards DME that was obtained for the phosphorus-containing activated carbon, ACP2800, loaded with different amounts of Zr (ACP2800ZrX), at a reaction temperature of 400 °C (P_{MeOH} = 0.02, W/F_{MeOH} = 0.1 g.s/µmol). At low metal loadings, the steady state methanol conversion increases almost linearly with the amount of zirconium being added to the P-containing activated carbon. However, it seems that there is a value of Zr loading (around 5%) from which no further increase in the methanol conversion is observed, with the methanol conversion remaining constant at 69%. The selectivity towards DME does not show a dependence with the metal loading, always presenting a value that is higher than 95%. According to these results, it seems that a Zr loading of 5.25% could be considered to be the optimum one, in terms of methanol conversion, among the prepared catalysts.
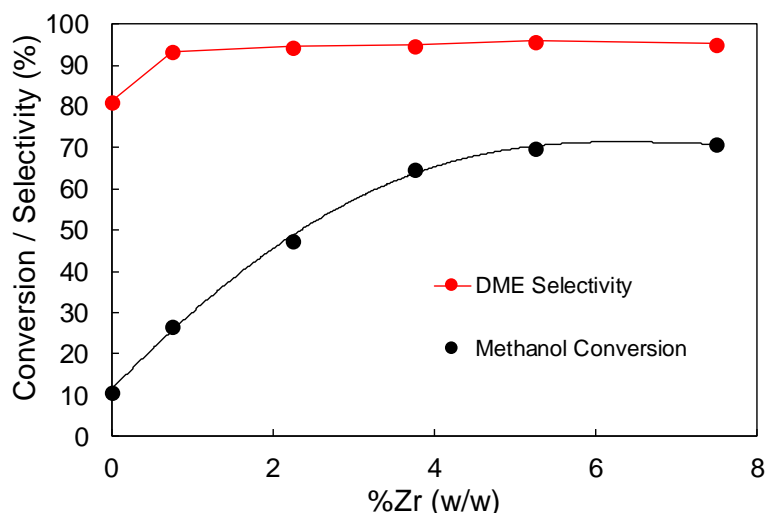
Figure 3.5. Steady-state methanol conversion and selectivity to dimethyl ether (DME) as a function of Zr loading for the sample ACP2800 (400 °C, P_{MeOH} = 0.02 atm, W/F_{MeOH} = 0.1 g.s/µmol).

3.3.2.2. Effect of Temperature

Figure 3.6 represents the methanol steady-state conversion and the selectivity towards DME as a function of the reaction temperature for the sample ACP2800Zr5.25. As expected, an increase in the reaction temperature produces an increase in the methanol steady state conversion. Regarding the selectivity towards DME, the high values exhibited by this carbon catalyst (higher than 95 %) have to be pointed out, even at temperatures as high as 400 °C. The selectivity towards DME begins to decrease at temperatures that are higher than 425 °C and CH_4 and CO appears as the main by-products, resulting from methanol/DME decomposition.
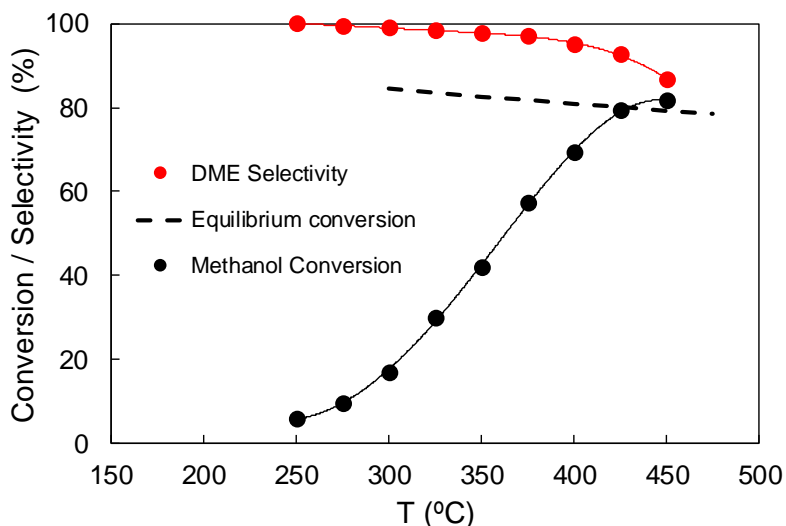
Figure 3.6. Methanol conversion and selectivity to DME as a function of the temperature for the catalyst ACP2800ZR5.25 (P_{MeOH} = 0.02 atm, W/F$_{MeOH}$ = 0.1 g.s/μmol).

3.3.2.3. Effect of Phosphorus on the Carbon Support

Figure 3.7 shows the methanol conversion, X_{MeOH}, as a function of time-on-stream (TOS) for ACP2800, ACP2800Zr5.25, and AC800Zr5.25 at the reaction temperature of 400 °C (P_{MeOH} = 0.02 atm, W/F$_{MeOH}$ = 0.1 g.s/μmol). Physically activated carbon (AC800), which did not contain P surface groups, did not show any catalytic activity. After Zr loading, AC800Zr5.25 showed some activity (an initial methanol conversion of 30%), but this decreased with time on stream, evidencing a fast deactivation process. Chemically activated carbon (ACP2800), which did contain P surface groups, exhibited a high initial methanol conversion (of about 80%). However, this value dropped in the first minutes of reaction, which indicated that the catalyst suffered from fast deactivation. Nevertheless, this P-containing carbon material that was loaded with Zr (ACP2800Zr5.25 catalyst) achieved steady-state conditions after a short period of time, showing a constant methanol conversion of 69 % and a selectivity to DME that was higher than 95%, as already shown in Figure 3.6.
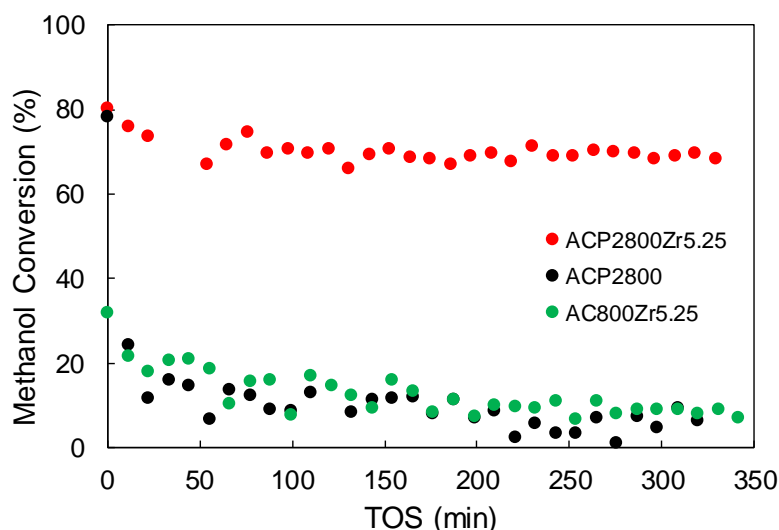
Figure 3.7. Methanol conversion as a function of time-on-stream (TOS) for ACP2800, ACP2800Zr5.25 and AC800Zr5.25 (400 °C, P_{MeOH} = 0.02 atm, W/F_{MeOH} = 0.1 g.s/µmol).

In a previous work, it was highlighted that ACP2800 presented P-OH and C-O-P type acidic surface sites, as in $C-O-PO_3$ surface groups [34]. It was also reported that the P-OH and C-O-P type sites acted as strong Brönsted and weak and/or moderate acid sites, respectively, for the methanol dehydration, although both of them were deactivated by coke deposition if oxygen was not present in the reaction gas mixture [37]. In this sense, when analyzing the CO profile that was obtained from TPD experiments for this sample after reaction (see ACP2800-R400 °C in Figure 3.3b), a decrease of the CO that evolved at 870 °C can be observed, which is associated to a lower presence of C-O-P groups on the carbons surface after the reaction. Moreover, XPS analyses showed an increase of 5% in the carbon content for this sample, evidencing the coke deposition on the P and O surface species.

In the case of AC800Zr5.25, the Zr loading only resulted in the formation of zirconium oxide species on the surface of the material (due to the absence of phosphorus in its surface), as revealed by XPS. This species provided the carbon material a low surface acidity and, thus, a low catalytic activity. Moreover, the low selectivity towards DME (34%) evidenced that methanol decomposition, rather

than methanol dehydration, was taking place in this case, as it has been reported with electrospun zirconia nanofibers [53].

ACP2800Zr5.25 mainly presented zirconium phosphate species on its surface, as revealed by XPS. C-O-P type surface sites that are present on this catalyst seemed to be deactivated by coke formation, as was revealed by the methanol conversion decay that this sample exhibited before reaching the steady state conversion, as occurred for the sample ACP2800. In this case, the CO profile that was obtained from TPD analyses for this sample after reaction (see ACP2800Zr5.25-R400 °C in Figure 3.3b) showed that the peak at 870 °C decreased when compared to the one for the fresh sample, indicating the lower presence of C-O-P surface sites. However, the peak at 1000 °C remained unaltered after reaction, indicating that the C-O-Zr bonds forming the zirconium phosphate structure are unaltered during the reaction. The steady-state methanol conversion that was achieved by this catalyst can be associated to the presence of zirconium phosphate species that are bonded to the carbon surface.

The existence of an optimum Zr loading at about 5% (w/w) (see Figure 3.5), in terms of catalytic activity, can be also explained according to the fact that zirconium phosphate groups are the actives species that are involved in the methanol dehydration reaction, in this case. The amount of phosphorus that is present on the carbon surface of ACP2800 catalyst is limited by the activation process [35,36]. In this sense, the amount of Zr is limiting the zirconium phosphate formation at low metal loadings, so the number of active sites is directly proportional to the metal loading. On the opposite, at high metal loadings, the amount of surface phosphorus is limiting the zirconium phosphate species formation and the extra amount of Zr added is forming zirconium oxide species, which does not produce significant improvement in the steady state methanol conversion, as it was observed for Zr loading higher than 5% (w/w) (see Figure 3.5).

A long-term experiment was carried out with the aim of studying the stability of the ACP2800Zr5.25 catalyst (350 °C, P_{MeOH} = 0.04 atm, W/F_{MeOH} = 0.1 g.s/µmol). Figure 3.8 depicts the evolution of methanol conversion and selectivity towards DME as a function of time-on-stream (TOS). Once the catalyst achieved

the steady-state methanol conversion, the catalytic activity remained unaltered for more than 72 h, as it can be observed. The selectivity towards DME also remained higher than 97%, without being affected by TOS.
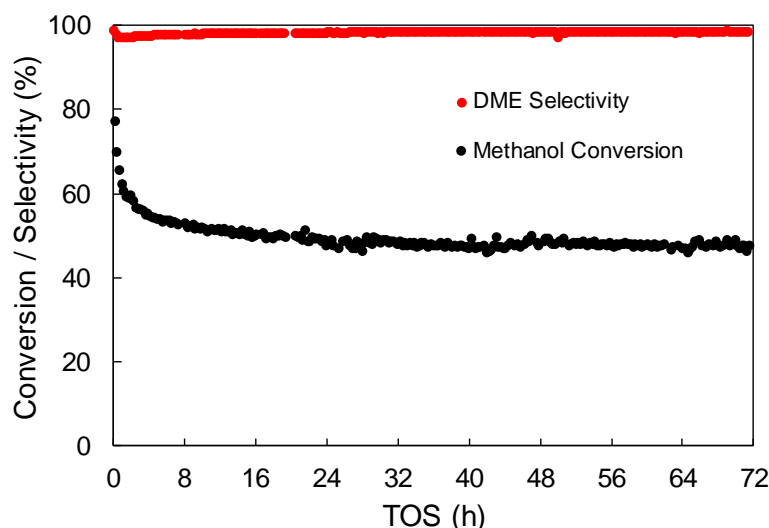

Figure 3.8. Methanol conversion and selectivity towards DME as a function of TOS for the ACP2800Zr5.25 sample (350 °C, P_{MeOH} = 0.04 atm, W/F_{MeOH} = 0.1 g.s/µmol).

3.3.2.4. Effect of Water Vapor in the Feed

The industrial methanol synthesis process, as well as DME production, involves the generation of considerable amounts of water vapor. It has been reported that the presence of water affects the catalytic activity and stability of the methanol dehydration catalysts [2,54]. In this sense, Akarmazyan et al. [15] reported a decrease in the methanol conversion, being higher than 20%, after five hours on stream when a 10 % of water vapor was present in the reactor feed, while using Al_2O_3 as catalyst. This behavior was associated to the competitive water adsorption on the active sites [55].

The influence of water vapor in the reaction gas mixture on the catalytic dehydration of methanol was studied for ACP2800Zr5.25 in order to address this issue. Figure 3.9 shows the evolution of methanol conversion with time-on-stream in the presence and absence of water vapor in the reactor feed. As it can

be observed, only a slight decrease, lower than 10%, in the initial methanol conversion is observed for this catalyst. However, it is important to mention that the methanol conversion did not change with time-on-stream at a constant water vapor partial pressure, unlike the reports for other catalysts [54]. Moreover, the methanol conversion was restored to the value that was obtained in the absence of water after removing the water vapor from the feed, evidencing that the effect of water on the catalytic performance is reversible. This behavior was also observed for other water vapor pressures studied. It is also remarkable that the presence of water vapor did not affect the selectivity towards DME, a selectivity value higher than 95% was always observed for all of the water vapor pressures studied.
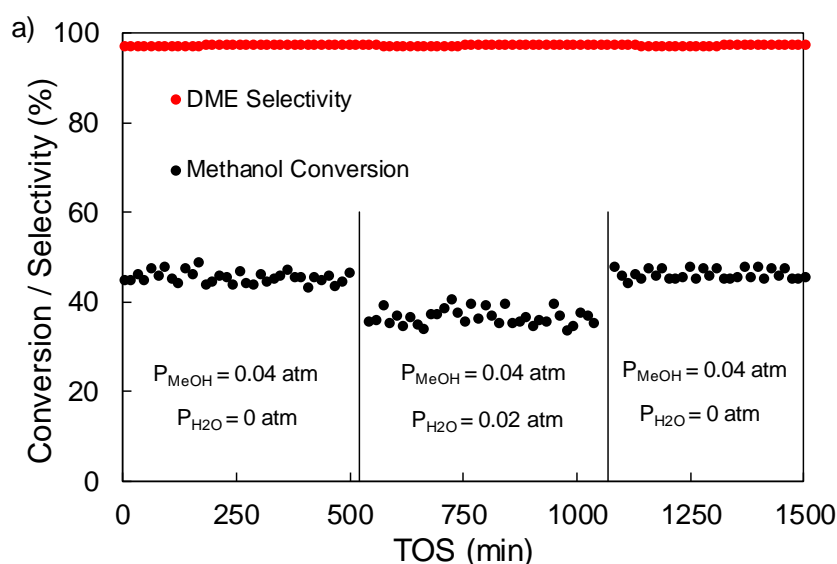

Figure 3.9. Effect of water vapor in the feed on methanol conversion at 350 °C (W/F$_{MeOH}$ = 0.1 g.s/µmol).

In the light of all the catalytic results that are presented in this study, it is remarkable that the catalyst here presented could be used in the whole range of temperatures used in the industrial methanol dehydration process (250–400 °C). Catalysts for the selective methanol dehydration to DME must show enough activity for this reaction. However, too high activity resulted in the production of hydrocarbons. Zeolites have been widely investigated [56–58]. In this sense, Rutkowska et al. [58] analyzed the catalytic performance of different zeolitic

materials, pointing out a high activity when using these materials. However, they also claimed that, at temperatures higher than 275 °C, the selectivity to DME dropped as a result of hydrocarbons formation, in the most active catalysts. Moreover, they also reported that the stability of these materials also depended on the reaction temperature, with these catalysts becoming deactivated at temperatures above 275 °C due to coke formation. Similar results have been reported for other catalysts. Nitta et al. [59] studied different sulfated zirconia catalysts for methanol dehydration, reporting a low selectivity to DME at 350 °C, due to hydrocarbons formation. Cheng et al [18] also reported the formation of hydrocarbons at 350 °C when using pillared zirconium phosphates as catalysts. Alharbi et al. [19] studied the use of different tungsten Keggin heteropolyacids as a catalyst for this reaction, exhibiting, these materials, activities higher than zeolites. Nevertheless, the formation of hydrocarbons started occurring at temperatures above 200 °C, decreasing the DME selectivity. Moreover, as it was observed for zeolites, this hydrocarbon production was accompanied by a catalyst deactivation due to coke formation.

When comparing the catalysts that are presented in this study with other catalysts that are reported in the literature, it has first to be noted that this material counts on the noticeable advantage of having been prepared from an inexpensive agri-food industrial waste. Regarding the activity, it is important to mention that, in contrast to other inorganic acid solids, such as alumina, zeolites, and Keggin heteropoly acids, in which the whole material is considered as active phase, only 5%(w/w) of this waste-derived material (for the best catalyst presented in this study) can be considered as active phase. Moreover, the operating conditions that were used in this study are significantly less favorable for achieving high conversion values. In this sense, space velocities up to 100 times higher than other studies [19] and considerably lower methanol partial pressures [60]. Despite the conditions that were used in this study, the material presented herein showed remarkable activity. In addition, when comparing the selectivity to DME and the stability on stream, this biomass-derived material exhibits noticeable features. In this regard, it has been shown that the catalyst presented here exhibits a selectivity to DME higher than 95% in the whole range of temperature studied (250–400 °C). Furthermore, this waste-derived catalyst shows a high

chemical and hydrothermal stability under the operation conditions that were studied.

3.4. Conclusions

Two kinds of activated carbons that were prepared by chemical (with phosphoric acid) and physical (by CO_2 partial gasification) activation of olive stone, an agri-food industry waste, were loaded with different Zr amounts and used as catalysts for the selective dehydration of methanol to dimethyl ether.

The presence of chemically stable phosphorus surface groups, mainly in the form of $C-O-PO_3$ groups, on the activated carbon prepared via chemical activation with phosphoric acid, seems to have great relevance in the catalytic performance of these carbon materials for methanol dehydration. XPS analysis revealed that zirconium bonded these phosphorus complexes during the metal loading, resulting in the formation of zirconium phosphate species on the activated carbon surface.

Phosphorus-containing activated carbon, ACP2800, presented a high initial methanol conversion. However, the conversion dropped in the first minutes of the reaction, evidencing a deactivation process. Once loaded with zirconium, the resulting material presented a relatively high catalytic activity and steady-state methanol conversion was observed, without deactivation. The catalytic performance was improved with the amount of zirconium that was added to the activated carbon until a fixed loading amount (of around 5% (w/w)), from which no further increasing in the steady-state methanol conversion was observed. The catalytic activity of these materials was attributed to the presence of well dispersed surface zirconium phosphate species, whose formation was limited by the amount of phosphorus that was present on the carbon surface of the chemically activated carbon.

Zr-loaded phosphorus-containing activated carbons exhibited methanol conversion values that were close to thermodynamic equilibrium, keeping selectivity towards DME higher than 95% in the whole range of temperatures that were used in the industrial DME synthesis (250–400 °C). The stability results

showed that, once the materials achieved the steady-state methanol conversion, it remained unaltered for more than 72 h.

The presence of water vapor in the reaction gas on the catalytic dehydration of methanol was studied. The results showed that the methanol conversion decreased when increasing the water vapor partial pressure. However, the methanol conversion was not affected with time-on-stream at a constant water vapor partial pressure. Moreover, the methanol conversion was restored to the value that was obtained in the absence of water once removing the water vapor from the feed, evidencing that the effect of water on the catalytic performance was reversible. The selectivity towards DME was not affected by the presence of water vapor in the feed, with a value higher than 95% being observed for all of the water vapor pressures studied.

3.5. References

[1]   Z. Azizi, M. Rezaeimanesh, T. Tohidian, M.R. Rahimpour, Dimethyl ether: A review of technologies and production challenges, Chem. Eng. Process. Process Intensif. 82 (2014) 150–172. doi:10.1016/j.cep.2014.06.007.

[2]   M. Xu, J.H. Lunsford, D.W. Goodman, A. Bhattacharyya, Synthesis of dimethyl ether (DME) from methanol over solid-acid catalysts, Appl. Catal. A Gen. 149 (1997) 289–301. doi:10.1016/S0926-860X(96)00275-X.

[3]   G. Cai, Z. Liu, R. Shi, H. Changqing, L. Yang, C. Sun, Y. Chang, Light alkenes from syngas via dimethyl ether, Appl. Catal. A, Gen. 125 (1995) 29–38. doi:10.1016/0926-860X(94)00291-6.

[4]   T. Shikada, K. Fujimoto, M. Miyauchi, H. Tominaga, Vapor phase carbonylation of dimethyl ether and methyl acetate with nickel-active carbon catalysts, Appl. Catal. 7 (1983) 361–368. doi:10.1016/0166-9834(83)80035-9.

[5]   C. Baltes, S. Vukojević, F. Schüth, Correlations between synthesis, precursor, and catalyst structure and activity of a large set of CuO/ZnO/Al2O3 catalysts for methanol synthesis, J. Catal. 258 (2008) 334–344. doi:10.1016/J.JCAT.2008.07.004.

[6]   J.D. Grunwaldt, A.M. Molenbroek, N.Y. Topsoe, H. Topsoe, B.S. Clausen, In situ investigations of structural changes in Cu/ZnO catalysts, J. Catal. 194 (2000) 452–460. doi:DOI 10.1006/jcat.2000.2930.

[7]   G.C. Chinchen, P.J. Denny, J.R. Jennings, M.S. Spencer, K.C. Waugh, Synthesis of Methanol. Part 1. Catalysts and Kinetics, Appl. Catal. 36 (1988) 1–65. doi:10.1016/S0166-9834(00)80103-7.

[8]   F. Yaripour, F. Baghaei, I. Schmidt, J. Perregaard, Catalytic dehydration of methanol to dimethyl ether (DME) over solid-acid catalysts, Catal. Commun. 6 (2005) 147–152. doi:10.1016/J.CATCOM.2004.11.012.

[9]   G. Bercic, J. Levec, Catalytic dehydration of methanol to dimethyl ether. Kinetic investigation and reactor simulation, Ind. Eng. Chem. Res. 32 (1993) 2478–2484. doi:10.1021/ie00023a006.

[10]   C.W. Seo, K.D. Jung, K.Y. Lee, K.S. Yoo, Dehydration of methanol over Nordstrandite based catalysts for dimethyl ether synthesis, J. Ind. Eng. Chem. 15 (2009) 649–652. doi:10.1016/J.JIEC.2009.09.037.

[11]   A.C. Sofianos, M.S. Scurrell, Conversion of synthesis gas to dimethyl ether over bifunctional catalytic systems, Ind. Eng. Chem. Res. 30 (1991) 2372–2378. doi:10.1021/ie00059a002.

[12]   A.T. Aguayo, J. Ereña, D. Mier, J.M. Arandes, M. Olazar, J. Bilbao, Kinetic Modeling of Dimethyl Ether Synthesis in a Single Step on a CuO−ZnO−Al_2O_3/γ-Al_2O_3 Catalyst, Ind. Eng. Chem. Res. 46 (2007) 5522–5530. doi:10.1021/ie070269s.

[13]   J. Ereña, R. Garoña, J.M. Arandes, A.T. Aguayo, J. Bilbao, Effect of operating conditions on the synthesis of dimethyl ether over a CuO-ZnO-Al_2O_3/NaHZSM-5 bifunctional catalyst, Catal. Today. 107–108 (2005) 467–473. doi:10.1016/j.cattod.2005.07.116.

[14]   M. Sánchez-Contador, A. Ateka, A.T. Aguayo, J. Bilbao, Behavior of SAPO-11 as acid function in the direct synthesis of dimethyl ether from syngas and CO_2, J. Ind. Eng. Chem. 63 (2018) 245–254. doi:10.1016/J.JIEC.2018.02.022.

[15]   S.S. Akarmazyan, P. Panagiotopoulou, A. Kambolis, C. Papadopoulou, D.I. Kondarides, Methanol dehydration to dimethylether over Al_2O_3 catalysts, Appl. Catal. B Environ. 145 (2014) 136–148. doi:10.1016/J.APCATB.2012.11.043.

[16]   G. Laugel, X. Nitsch, F. Ocampo, B. Louis, Methanol dehydration into dimethylether over ZSM-5 type zeolites: Raise in the operational temperature range, Appl. Catal. A Gen. 402 (2011) 139–145. doi:10.1016/j.apcata.2011.05.039.

[17] G. Pop, G. Bozga, R. Ganea, N. Natu, Methanol conversion to dimethyl ether over H-SAPO-34 catalyst, Ind. Eng. Chem. Res. 48 (2009) 7065–7071. doi:10.1021/ie900532y.

[18] S. Cheng, G.Z. Peng, A. Clearfield, Decomposition of Alcohols over Zirconium and Titanium Phosphates, Ind. Eng. Chem. Prod. Res. Dev. 23 (1984) 219–225. doi:10.1021/i300014a008.

[19] W. Alharbi, E.F. Kozhevnikova, I. V. Kozhevnikov, Dehydration of Methanol to Dimethyl Ether over Heteropoly Acid Catalysts: The Relationship between Reaction Rate and Catalyst Acid Strength, ACS Catal. 5 (2015) 7186–7193. doi:10.1021/acscatal.5b01911.

[20] S.Y. Hosseini, M.R. Khosravi Nikou, Investigation of different precipitating agents effects on performance of γ-Al_2O_3 nanocatalysts for methanol dehydration to dimethyl ether, J. Ind. Eng. Chem. 20 (2014) 4421–4428. doi:10.1016/J.JIEC.2014.02.010.

[21] B. Sabour, M.H. Peyrovi, T. Hamoule, M. Rashidzadeh, Catalytic dehydration of methanol to dimethyl ether (DME) over Al-HMS catalysts, J. Ind. Eng. Chem. 20 (2014) 222–227. doi:10.1016/j.jiec.2013.03.044.

[22] J. Sun, G. Yang, Y. Yoneyama, N. Tsubaki, Catalysis Chemistry of Dimethyl Ether Synthesis, ACS Catal. 4 (2014) 3346–3356. doi:10.1021/cs500967j.

[23] S. Jiang, J.-S. Hwang, T. Jin, T. Cai, W. Cho, Y.-S. Baek, S.-E. Park, Dehydration of Methanol to Dimethyl Ether over ZSM-5 Zeolite, Bull. Korean Chem. Soc. 25 (2004) 185–189. doi:10.5012/bkcs.2004.25.2.185.

[24] V. Vishwanathan, K.W. Jun, J.W. Kim, H.S. Roh, Vapour phase dehydration of crude methanol to dimethyl ether over Na-modified H-ZSM-5 catalysts, Appl. Catal. A Gen. 276 (2004) 251–255. doi:10.1016/j.apcata.2004.08.011.

[25] J.M. Rosas, J. Bedia, J. Rodríguez-Mirasol, T. Cordero, On the preparation and characterization of chars and activated carbons from

orange skin, Fuel Process. Technol. 91 (2010) 1345–1354. doi:10.1016/J.FUPROC.2010.05.006.

[26]   J.M. Rosas, J. Bedia, J. Rodríguez-Mirasol, T. Cordero, HEMP-derived activated carbon fibers by chemical activation with phosphoric acid, Fuel. 88 (2009) 19–26. doi:10.1016/J.FUEL.2008.08.004.

[27]   J. Rodríguez-Mirasol, T. Cordero, J.J. Rodríguez, Preparation and characterization of activated carbons from eucalyptus kraft lignin, Carbon N. Y. 31 (1993) 87–95. doi:10.1016/0008-6223(93)90160-C.

[28]   J. Zawadzki, B. Azambre, O. Heintz, A. Krztoń, J. Weber, IR study of the adsorption and decomposition of methanol on carbon surfaces and carbon-supported catalysts, Carbon N. Y. 38 (2000) 509–515. doi:10.1016/S0008-6223(99)00130-X.

[29]   J. Jasińska, B. Krzyżyńska, M. Kozłowski, Influence of activated carbon modifications on their catalytic activity in methanol and ethanol conversion reactions, Cent. Eur. J. Chem. 9 (2011) 925–931. doi:10.2478/s11532-011-0078-7.

[30]   C. Moreno-Castilla, F. Carrasco-Marín, C. Parejo-Pérez, M. V. López Ramón, Dehydration of methanol to dimethyl ether catalyzed by oxidized activated carbons with varying surface acidic character, Carbon N. Y. 39 (2001) 869–875. doi:10.1016/S0008-6223(00)00192-5.

[31]   J.M. Rosas, R. Ruiz-Rosas, J. Rodríguez-Mirasol, T. Cordero, Kinetic study of the oxidation resistance of phosphorus-containing activated carbons, Carbon N. Y. 0 (2012) 1523–1537. doi:10.1016/j.carbon.2011.11.030.

[32]   J.M. Rosas, J. Bedia, J. Rodríguez-Mirasol, T. Cordero, Preparation of Hemp-Derived Activated Carbon Monoliths. Adsorption of Water Vapor, Ind. Eng. Chem. Res. 47 (2008) 1288–1296. doi:10.1021/IE070924W.

[33]   J.M. Rosas, J. Rodríguez-Mirasol, T. Cordero, NO Reduction on Carbon-Supported Chromium Catalysts, Energy & Fuels. 24 (2010) 3321–3328. doi:10.1021/ef901455v.

[34]   M.J. Valero-Romero, F.J. García-Mateos, J. Rodríguez-Mirasol, T.
        Cordero, Role of surface phosphorus complexes on the oxidation of
        porous carbons, Fuel Process. Technol. 157 (2017) 116–126.
        doi:10.1016/j.fuproc.2016.11.014.

[35]   J. Bedia, R. Barrionuevo, J. Rodríguez-Mirasol, T. Cordero, Ethanol
        dehydration to ethylene on acid carbon catalysts, Appl. Catal. B Environ.
        103 (2011) 302–310. doi:10.1016/j.apcatb.2011.01.032.

[36]   J. Bedia, J.M. Rosas, J. Márquez, J. Rodríguez-Mirasol, T. Cordero,
        Preparation and characterization of carbon based acid catalysts for the
        dehydration of 2-propanol, Carbon N. Y. 47 (2009) 286–294.
        doi:10.1016/J.CARBON.2008.10.008.

[37]   M.J. Valero Romero, E.M. Calvo Muñoz, R. Ruíz Rosas, J. Rodríguez-
        Mirasol, T. Cordero, Phosphorus-containing mesoporous carbon acid
        catalyst for methanol dehydration to dimethyl ether, Ind. Eng. Chem. Res.
        58 (2019) 4042–4053. doi:10.1021/acs.iecr.8b05897.

[38]   E. Gonzalez-Serrano, T. Cordero, J. Rodriguez-Mirasol, L. Cotoruelo, J.J.
        Rodriguez, Removal of water pollutants with activated carbons prepared
        from H3PO4 activation of lignin from kraft black liquors, Water Res. 38
        (2004) 3043–3050. doi:10.1016/J.WATRES.2004.04.048.

[39]   S. Brunauer, P.H. Emmett, E. Teller, Adsorption of Gases in
        Multimolecular Layers, J. Am. Chem. Soc. 60 (1938) 309–319.
        doi:10.1021/ja01269a023.

[40]   K. Kaneko, C. Ishii, Superhigh surface area determination of microporous
        solids, Colloids and Surfaces. 67 (1992) 203–212. doi:10.1016/0166-
        6622(92)80299-H.

[41]   S.J. Gregg, K.S.W. Sing, Adsorption, Surface Area and Porosity, second
        ed., Academic Press, London, New York, 1982.
        doi:10.1002/bbpc.19820861019.

[42]   M.M. Dubinin, The potential theory of adsorption of gases and vapors for adsorbents with energetically nonuniform surfaces, Chem. Rev. 60 (1960) 235–241. doi:10.1021/cr60204a006.

[43]   J.L. Figueiredo, M.F.R. Pereira, M.M.A. Freitas, J.J.M. Órfão, Modification of the surface chemistry of activated carbons, Carbon N. Y. 37 (1999) 1379–1389. doi:10.1016/S0008-6223(98)00333-9.

[44]   M. Thommes, K. Kaneko, A. V. Neimark, J.P. Olivier, F. Rodriguez-Reinoso, J. Rouquerol, K.S.W. Sing, Physisorption of gases, with special reference to the evaluation of surface area and pore size distribution (IUPAC Technical Report), Pure Appl. Chem. 87 (2015). doi:10.1515/pac-2014-1117.

[45]   J.L. Colón, D.S. Thakur, C.-Y. Yang, A. Clearfield, C.R. Martini, X-ray photoelectron spectroscopy and catalytic activity of α-zirconium phosphate and zirconium phosphate sulfophenylphosphonate, J. Catal. 124 (1990) 148–159. doi:10.1016/0021-9517(90)90111-V.

[46]   C. Morant, J.M. Sanz, L. Galán, L. Soriano, F. Rueda, An XPS study of the interaction of oxygen with zirconium, Surf. Sci. 218 (1989) 331–345. doi:10.1016/0039-6028(89)90156-8.

[47]   L. Kumari, W.Z. Li, J.M. Xu, R.M. Leblanc, D.Z. Wang, Y. Li, H. Guo, J. Zhang, Controlled hydrothermal synthesis of zirconium oxide nanostructures and their optical properties, Cryst. Growth Des. 9 (2009) 3874–3880. doi:10.1021/cg800711m.

[48]   G. Alberti, U. Costantino, G. Marletta, O. Puglisi, S. Pignataro, ESCA investigations of amorphous and crystalline zirconium acid phosphates, J. Inorg. Nucl. Chem. 43 (1981) 3329–3334. doi:10.1016/0022-1902(81)80111-X.

[49]   X. Wu, L.R. Radovic, Inhibition of catalytic oxidation of carbon / carbon composites by phosphorus, Carbon N. Y. 44 (2006) 141–151. doi:10.1016/j.carbon.2005.06.038.

[50] C. Ang, T. Williams, A. Seeber, H. Wang, Y.B. Cheng, Synthesis and evolution of zirconium carbide via Sol-Gel route: Features of nanoparticle oxide-carbon reactions, J. Am. Ceram. Soc. 96 (2013) 1099–1106. doi:10.1111/jace.12260.

[51] J. Bedia, R. Ruiz-Rosas, J. Rodríguez-Mirasol, T. Cordero, Kinetic study of the decomposition of 2-butanol on carbon-based acid catalyst, AIChE J. 56 (2010) 1557–1568. doi:10.1002/aic.12056.

[52] J.A. Moulijn, A. Tarfaoui, F. Kapteijn, General aspects of catalyst testing, Catal. Today. 11 (1991) 1–12. doi:10.1016/0920-5861(91)87002-5.

[53] R. Ruiz-Rosas, J. Bedia, J.M. Rosas, M. Lallave, I.G. Loscertales, J. Rodríguez-Mirasol, T. Cordero, Methanol decomposition on electrospun zirconia nanofibers, Catal. Today. 187 (2012) 77–87. doi:10.1016/j.cattod.2011.10.031.

[54] M. Mollavali, F. Yaripour, H. Atashi, S. Sahebdelfar, Intrinsic kinetics study of dimethyl ether synthesis from methanol on γ-Al2O3 catalysts, Ind. Eng. Chem. Res. 47 (2008) 3265–3273. doi:10.1021/ie800051h.

[55] V. Vishwanathan, H.S. Roh, J.W. Kim, K.W. Jun, Surface properties and catalytic activity of TiO_2-ZrO_2 mixed oxides in dehydration of methanol to dimethyl ether, Catal. Letters. 96 (2004) 23–28. doi:10.1023/B:CATL.0000029524.94392.9f.

[56] A.A. Rownaghi, F. Rezaei, M. Stante, J. Hedlund, Selective dehydration of methanol to dimethyl ether on ZSM-5 nanocrystals, Appl. Catal. B Environ. 119–120 (2012) 56–61. doi:10.1016/j.apcatb.2012.02.017.

[57] E. Catizzone, A. Aloise, M. Migliori, G. Giordano, Dimethyl ether synthesis via methanol dehydration: Effect of zeolite structure, Appl. Catal. A Gen. 502 (2015) 215–220. doi:10.1016/j.apcata.2015.06.017.

[58] M. Rutkowska, D. Macina, N. Mirocha-Kubień, Z. Piwowarska, L. Chmielarz, Hierarchically structured ZSM-5 obtained by desilication as new catalyst for DME synthesis from methanol, Appl. Catal. B Environ. 174–175 (2015) 336–343. doi:10.1016/J.APCATB.2015.03.006.

[59]   M. Nitta, H. Sakoh, K. Aomura, The conversion of methanol into hydrocarbons over modified zirconia, Appl. Catal. 10 (1984) 215–217. doi:10.1016/0166-9834(84)80105-0.

[60]   A.I. Osman, J.K. Abu-Dahrieh, D.W. Rooney, S.A. Halawy, M.A. Mohamed, A. Abdelkader, Effect of precursor on the performance of alumina for the dehydration of methanol to dimethyl ether, Appl. Catal. B Environ. 127 (2012) 307–315. doi:10.1016/J.APCATB.2012.08.033.

Chapter 4

On the kinetics of methanol dehydration to dimethyl ether on Zr-loaded P-containing mesoporous activated carbon catalyst

4.0.-Abstract

Selective methanol dehydration to DME has been investigated using activated carbon-based catalysts. An activated carbon was prepared by chemical activation of olive stones, a residue of the agri-food industry, with phosphoric acid followed by Zr loading (5% (w/w)). The activation process produced a considerable amount of chemically stable surface phosphorus complexes. The addition of Zr resulted in the formation of zirconium phosphate surface species, as revealed by XPS. TPD and catalytic reaction results determined that the presence of zirconium phosphate species bonded to the carbon surface were responsible for the high steady-state methanol conversion and DME selectivity achieved by this biomass-derived catalyst. A kinetic study for the selective methanol dehydration to DME was carried out on the Zr-loaded P-containing activated carbon catalyst and the corresponding kinetic and thermodynamic parameters were obtained. The reaction seems to proceed through a modified Langmuir-Hinshelwood mechanism (LH2), in which two methanol molecules are subsequently adsorbed on one active site. The competitive adsorption of water on the active sites was also addressed in the proposed mechanism. The activation energy for the DME production was calculated and a value of 70 kJ mol^{-1} was obtained.

4.1.-Introduction

Fossil fuels depletion, together with an increasingly stringent in the environmental regulations, are the driving force in seeking for alternative clean energy resources [1]. Dimethyl ether (DME) is one of the most promising alternative due to its potential use as diesel substitute and as H_2 source via catalytic steam reforming [2–5]. Moreover, this compound presents handling characteristics similar to liquefied petroleum gas (LPG), thus it could be supplied and storage by means of the existing LPG infrastructure, reducing the investment costs [3,6].

Currently, DME production is carried out via methanol dehydration using a solid acid as catalysts [7–10]. The most common catalyst used for this aim is γ-Al_2O_3, which presents a high lifetime stability and a high selectivity to DME.

However, the hydrophilic character this catalyst presents results in the preferential adsorption of water on the active sites, reducing its activity that way [11]. Among the alternative catalysts studied for this reaction, zeolites (most often H-ZSM-5) have been widely investigated [12–15]. These materials present a high catalytic activity. Nevertheless, the presence of strong acid sites on the surface of these materials results in the formation of hydrocarbons and coke, at reaction temperatures higher than 270 ºC, hence deactivating the catalyst [13].

Methanol dehydration reaction have been reported to occur on both Brønsted and Lewis acid sites [16,17]. For solid acids presenting Lewis acid sites, such as γ-Al$_2$O$_3$, the most accepted mechanism is the proposed by Jain and Pillai [16], which involves the adsorption of two methanol molecules on an acid and an adjacent basic site, which then react according to a Langmuir-Hinshelwood mechanism. For zeolites, which present Brønsted acid sites, two different reaction mechanisms have been proposed [18,19]. On the one hand, Bandiera and Naccache [18] suggested the adsorption of two methanol molecules on Bronsted acid-Lewis base pairs, which then react yielding DME and H$_2$O. For this mechanism, so called the direct pathway, the obtained kinetic equation is consistent with a Langmuir-Hinshelwood mechanism. On the other hand, for the indirect pathway [19] only one methanol molecule adsorption is supposed to take place, yielding an adsorbed methoxy and H$_2$O, and subsequently, this intermediate methoxy species reacts with another methanol molecule coming from the gas phase yielding DME. This reaction pathway, only involving one methanol molecule adsorption, is consistent with and Eley-Rideal mechanism.

The use of activated carbons as adsorbent and catalyst support has received a great attention in the last decade due to the properties these materials present, such as a high thermal and chemical stability, a high surface area and the possibility of obtaining them from different types of lignocellulosic waste [20–22]. Moreover, the presence of different surface oxygen groups provides them with and acidic and/or basic character, making them also suitable for catalytic applications [23]. The use of activated carbons as catalyst for methanol dehydration has been little studied. On this issue, Zawadzki et al. reported that the non-oxidized carbon surface is not active for this reaction, only observing

certain activity after an oxidation treatment in oxygen [24]. Moreno-Castilla et al. studied the surface modification of activated carbons oxidizing them with different chemical reagents in order to introduce oxygen surface complexes of acidic character [25]. However, the acidic groups generated on the surface of these materials presented a low to moderate activity and thermal stability, which resulted in a fast deactivation when increasing the reaction temperature.

Our research group has reported several works regarding the preparation and characterization of biomass waste derived activated carbons via chemical activation with phosphoric acid [26,27]. The use of phosphoric acid as activating reagent, under certain conditions of temperature and impregnation ratio, leads to the preparation of carbon materials showing a particular surface chemistry, as a consequence of the presence of phosphorus surface complexes, mainly in form of $C-PO_3$ and $C-O-PO_3$ groups [28]. These surface phosphorus groups provide the activated carbon a surface acidity and a high oxidation resistance, making them suitable for applications in catalysis, such as alcohol dehydration reactions [26,29]. However, the direct use of these activated carbons for methanol dehydration results in the fast deactivation of the carbon catalyst due to coke deposition [30]. We have recently reported that the modification of these phosphorus-containing activated carbons with zirconium leads to the obtention of carbon materials presenting zirconium phosphate species, which demonstrated high methanol conversion values and a high stability in the whole range of temperature studied (200-400 ºC) [31].

In this work, we examine the dehydration of methanol for the selective production of DME by using a Zr-loaded P-containing biomass-derived catalyst. A kinetic study has been carried out and a modified Langmuir-Hinshelwood mechanism has been proposed for the reaction taking place on the carbon-based catalyst. The corresponding kinetic and thermodynamic parameters were also obtained.

4.2.-Experimental method

4.2.1.-Carbon-based catalyst preparation.

Two kinds of activated carbons were prepared. On the one hand, an activated carbon was prepared via chemical activation with phosphoric acid, using olive stones, an agri-food industry residue, as biomass precursor. Olive stones were impregnated with 85 %(w/w) aqueous solution H_3PO_4 at room temperature and dried 24 h in a vacuum dryer. An impregnation ratio (H_3PO_4/olive stone mass ratio) value of 2 was used for this process. The impregnated substrate was then activated in a tubular furnace under continuous N_2 flow (150 cm^3/min STP). The sample was heated at 10 ºC/min up to 800 ºC, keeping this temperature for 2 h. The activated sample was cooled to room temperature inside the furnace under the same N_2 flow, and then it was washed with distilled water at 60 ºC until constant pH and a negative phosphate analysis in the eluate [28]. Finally, the prepared activated carbon was grinded and sieved (100-300 µm). The final mass yield for this activated carbon showed a value of 39% based on the mass of dried olive stone and was denoted as ACP. On the other hand, an activated carbon was prepared by physical activation, which consisted of a carbonization of the biomass precursor, followed by a partial gasification step. Both stages were carried out in a conventional laboratory tubular furnace. In the carbonization step, the sample was heated at 10 ºC/min up to 800 ºC, keeping this temperature for 2 h, under continuous N_2 flow (150 cm^3/min STP). Thereafter, the carbonized sample was activated using a CO_2 flow (150 cm^3/min STP) at the same temperature for 7 h, obtaining a 45% burn-off. This sample was denoted as AC and presented a final yield of 13.5 %, based on the mass of dried olive stone.

Subsequently, these activated carbons were loaded with a 5 %(w/w) of zirconium. The use of this zirconium loading was based on a previous study [31], in which it was found that the catalytic performance of these materials was improved with the amount of Zr loaded until a fixed loading amount (of around 5 % (w/w)), from which, no further improvements on the catalytic performance were observed. The zirconium loading process was carried out via incipient wetness

impregnation, using a $ZrO(NO_3)_2$ in water solution. The impregnated carbon was dried overnight at 120 ºC and then calcined at 250 ºC for 2 h in a tubular furnace under continuous air flow (150 cm^3/min STP). Samples were denoted adding -Zr to the name of the parent carbon.

4.2.2.-Characterization of carbon catalysts

The porous texture of the samples was characterized by N_2 adsorption–desorption at -196 ºC and by CO_2 adsorption at 0 ºC, performed in an ASAP 2020 equipment (Micromeritics). Prior to adsorption, samples were outgassed for 8 h at 150 ºC. From the N_2 adsorption-desorption isotherm, the apparent surface area (A_{BET}) was determined applying the BET equation [32], the micropore volume (V_t) and the external surface area were calculated using the t-method [33] and the mesopore volume (V_{mes}) was determined as the difference between the adsorbed volume at a relative pressure of 0.99 and the micropore volume of V_t. The narrow micropore volume (V_{DR}) and surface area (A_{DR}) were calculated by the Dubinin–Radushkevich method [34] applied to the CO_2 adsorption isotherm.

The surface chemistry of the samples was analyzed by X-ray photoelectron spectroscopy (XPS), temperature programmed desorption (TPD), and transmission electron microscopy (TEM). XPS analyses of the samples were obtained using a VersaProbe II ESCA 5701 model Physical Electronics apparatus, with Al Kα radiation (1486.6 eV). For the analysis of the XPS peaks, the C1s position was set at 284.5 eV and used as reference for the other peaks [29]. TPD profiles were obtained in a custom tubular fixed-bed reactor placed inside an electrical furnace. The samples were heated from room temperature to 1500 ºC at a heating rate of 10 ºC/min, under constant N_2 flow (200cm^3 STP/min). The amounts of CO and CO_2 evolved from the samples were recorded with a nondispersive infrared (NDIR) gas analyzer (Siemens ULTRAMAT 22). The surface morphology of the samples was studied by transmission electron microscopy (TEM) in a FEI Talos F200X microscope at an accelerating voltage of 200 kV and in a high angle annular dark field (HAADF). The total acidity was determined by temperature programmed desorption of ammonia (NH_3-TPD), after NH_3 adsorption-desorption at 100 ºC.

ICP-MS analyses were carried out in a Perkin-Elmer NexION apparatus. Carbon samples were calcined in air at 800 ºC for 12 hours, and then, the resulting ashes were dissolved in acid and analyzed for determining and quantifying the amount of phosphorus and zirconium.

4.2.3.-Methanol dehydration experiments.

Catalytic experiments for the selective methanol dehydration to DME were performed in a quartz fixed bed microreactor (i.d. 4 mm) placed inside a vertical furnace with temperature control, using 150 mg of catalyst (100-300 μm particle size). Methanol was fed into the reactor using a syringe pump (Cole-Parmer® 74900-00-05 model). The reactions were performed with helium as carrier gas at atmospheric pressure. To prevent the condensation of any compound, all lines were heated up to 120 ºC. The reaction was carried out in the temperature range of 250-400 ºC, the inlet methanol partial pressure varied from 0.01 to 0.1 atm, the water vapor partial pressures from 0.02 to 0.1 atm and the space time from 0.025 to 0.125 (g·s/μmol$_M$).

The outlet gas concentrations were analyzed by on-line gas chromatography (Perkin-Elmer Clarus 500 GC equipped with TCD and FID detectors). The used columns were a Permanent gases active carbon 80/100 mesh for CO and CO_2 analysis and a 1.9m x 1/8" x 2.1mm Porapak N 80/100 + 0.5m x 1/8" x 2.1mm Porapak Q 80/100 column for methanol, DME and light hydrocarbons separation.

The reaction rate, r, was defined as the mol number of methanol converted in 1 s per gram of catalyst. The conversion was defined as the molar ratio of methanol converted (F_M-F_M^o) to the amount of methanol supplied to the reactor (F_M), Eq. (4.1). The selectivity (in mol%) was defined as the ratio of carbon moles in a specific product (F_i·nc$_i$) to the moles of methanol converted, Eq. (4.2). The carbon balance was reached with an error lower than 3% in all the experiments.

$$x_M = \frac{F_M - F_M^o}{F_M} \cdot 100 \qquad \text{(Eq. 4.1)}$$

$$S_i = \frac{F_i^o \cdot nc_i}{F_M - F_M^o} \cdot 100 \qquad\qquad \text{(Eq. 4.2)}$$

4.3.-Results and discussion

4.3.1 Characterization of the carbon catalysts

The physicochemical properties of the activated carbon materials are presented in Table 4.1. The presented data are referred to textural parameter obtained from N_2 adsorption-desorption and CO_2 adsorption isotherms and the surface atomic concentration obtained by XPS for the carbon materials prepared herein. The chemically activated carbon prepared in this work, ACP, presented a well-developed porous texture and a high apparent surface area (1260 m^2/g). It is noticeable the higher value of A_{BET} compared to the one of the A_{DR} obtained for this sample, suggesting the existence of a wide microporous texture [35]. The relatively high value of mesopore volume (V_{mes}) observed for this activated carbon indicated a high contribution to mesoporosity. The high external surface area value (A_t) also confirmed this fact. Once loaded with Zr, the chemically activated carbon catalyst (ACPZr) showed a slight decrease, in general, in the textural parameters compared to the ones of the parent activated carbon, which suggests that Zr was homogeneously distributed both on the internal and on the external surface of the carbon-based catalyst particles. It is remarkable that this activated carbon catalyst presented a very high external surface area (A_t=270 m^2/g), which is an important feature for catalytic applications.

Physically activated carbon, AC, presented a specific surface area very similar to the one obtained for the chemically activated carbon (Table 4.1). AC showed, however, a larger narrow microporosity (higher value of V_{DR}) and lower mesoporosity and external surface area (lower values of V_{mes} and A_t). As in the case of ACP, the values of the textural parameters slightly decreased, in general, after Zr loading on AC (see ACZr in Table 4.1). However, in this case, a larger decrease (of about 36%) was observed for the value of mesopore volume (V_{mes})

once Zr was loaded on this sample, suggesting that the deposition of Zr was mainly on the external surface.

X-ray photoelectron spectroscopy (XPS) analyses were performed to evaluate the surface chemical composition of the samples. The main elements present on the surface of both activated carbon supports were carbon and oxygen. It is also noticeable the presence of a considerable amount of phosphorus on the surface of the chemically activated carbon, which has been attributed to the activation step [26]. The mechanism of biomass activation with phosphoric acid to produce activated carbons has been reported to occur through the formation of phosphate and polyphosphate bridges that connect and crosslink biopolymer fragments [36]. As a result, part of these phosphorus complexes remains chemically stable bonded to the carbon surface, even after the washing step [27]. The phosphorus concentration measured by ICP-MS for ACP was 3.3 % (w/w)), which is a value very similar to the one obtained by XPS (3.2 % (w/w); see Table 4.1), indicating that phosphorus was very well distributed on the carbon particle surface of this sample. After zirconium loading, an increase in the oxygen content, as a result of the Zr incorporation and of a surface oxidation during the thermal stabilization process (calcination), was observed for both activated carbon catalysts, ACPZr and ACZr.

Table 4.1. Textural parameters, chemical surface composition by XPS and total acidity for the activated carbon materials.

	AC	ACZr	ACP	ACPZr
Surface area and porosity				
N_2 adsorption-desorption isotherm				
A_{BET} (m^2/g)	1130	810	1260	1190
V_p (cm^3/g)	0.55	0.41	0.90	0.88
V_{mes} (cm^3/g)	0.11	0.07	0.42	0.42
A_t (m^2/g)	59	44	290	270
V_t (cm^3/g)	0.44	0.37	0.49	0.46
CO_2 adsorption isotherm				
A_{DR} (m^2/g)	865	760	470	500
V_{DR} (cm^3/g)	0.35	0.30	0.19	0.20
% Surface concentración, XPS (w/w %)				
C1s	95.5	31.0	89.6	59.8
O1s	4.5	24.2	7.2	19.6
P2p	0	0	3.2	5.7
Zr3d	0	44.8	0	14.9
Acidity, determined by NH$_3$-TPD				
Desorbed NH$_3$ (μmol/g$_{cat}$)	-	80	128	175

The Zr surface concentration measured by XPS (that of the external surface) was quite different for this two samples, suggesting that Zr was very well dispersed through the whole particle surface (internal and external) in the case of ACPZr and was not so well distributed but concentrated on the external surface in the case of ACZr.

XPS spectra were analyzed in order to evaluate the chemical environment of the elements present on samples surface. The binding energies at which P and Zr appeared in the prepared carbon materials, along with the binding energy of other P and Zr compounds reported in the literature are summarized in Table 4.2. P2p spectrum of the chemically activated carbon support (ACP) showed a broad peak at 133.4 eV, suggesting the presence of C-O-P (134 eV) and C-P (133.2 eV) bonds, as those in C-O-PO$_3$ and C- PO$_3$/C$_2$-PO$_2$ surface groups [27,37]. After Zr loading, the P2p spectrum for ACPZr shifted to higher binding energies, with a peak at 134 eV, indicating the oxidation of the surface

phosphorus groups, which probably occurred during the calcination stage at 250 ⁰C (see ACPZr in Table 4.2) [28]. The Zr3d spectra for both Zr loaded activated carbon catalysts, ACPZr and ACZr, showed the two 3d peaks separated by 2.3 eV, characteristic of the Zr^{4+}. However, the binding energy at which these peaks appeared for the sample ACPZr, 183.1 eV, was higher than the corresponding for ZrO_2 (182.2 eV). This fact has been associated in the literature to the presence of zirconium phosphates, due to the coordination of Zr atoms with a high number of strongly polarized oxygens, forming P-O-Zr bonds [38,39]. The presence of these chemical species bonded to the carbon surface could be related to this high binding energy. In this sense, transmission electron microscopy energy-dispersive X-ray spectroscopy (TEM-EDXA) analyses for this sample, ACPZr, revealed uniform distribution for P and Zr on the carbon particle. (see Figure 4.1).

Table 4.2. Binding energies of P and Zr for the carbon materials. The binding energy relative to other P and Zr compounds are also reported for comparison purposes.

Compound	Binding Energies (eV)		Reference
	P2p	Zr3d$_{5/2}$	
ACZr	-	182.1	This work
ACP	133.3	-	This work
ACPZr	133.9	183.1	This work
P-containing AC	133.4	-	[28]
ZrO_2	-	181.7	[40]
Zirconium phosphate	134.1	183.7	[39]
Zirconium phosphate	133.7	183.1	[41]
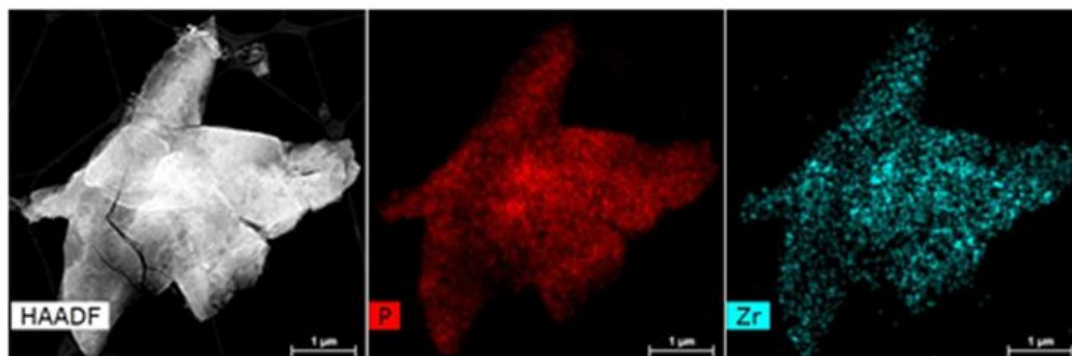
Figure 4.1. HAADF-STEM, and P and Zr EDXA elemental mappings of ACPZr.

TPD technique was used to characterize the oxygen groups present on the carbon surface [42]. Figure 4.2 presents the CO and CO_2 evolution from TPD analyses for the prepared samples. The amount of CO_2 evolved during TPD was negligible as compared to the amount of CO evolved. As can be observed in Figure 4.2a, ACP presented one peak of CO evolution at 870 ºC. This CO evolution has been previously associated to the decomposition of stable C-O-P type bonds of $C-O-PO_3$ surface groups, yielding CO gas and C'-P type bonds of $C-PO_3$ surface groups, where C' represents a different carbon atom of the carbon surface close to the one evolved as CO [27,43]. After Zr loading on this sample, the CO profile obtained showed two new peaks at 1000 and 1300 ºC, respectively, that must be related to the presence of zirconium species on the carbon surface (see ACPZr in Figure 4.2). AC presented one CO evolution peak at about 900 ºC, which has been related to carbonyl/quinone or ether groups [28]. Once Zr was loaded on this sample, the presence of a second peak at 1300 ºC was also noticeable (see ACZr in Figure 4.2). Comparing the two Zr-loaded samples, ACPZr and ACZr, it could be observed that the CO evolution peak appearing at 1300 ºC was present for both samples and could be related to the presence of C-O-Zr bonds and/or to the ZrO_2 carboreduction, which occurs also at such high temperature [44,45]. However, the CO evolution peak appearing at 1000 ºC was only observed when analyzing the ACPZr sample, therefore it could be related to the presence of P and Zr on the carbon surface in form of zirconium phosphates (as revealed by XPS). Moreover, it is interesting to mention that the total amount of CO associated to the decomposition of stable C-O-P type bonds for the ACP sample (CO evolved at 870 ºC) was the same that the total amount of CO evolved in both peaks appearing at 870 and 1000 ºC for the sample ACPZr, indicating that C-O-P bonds were cleaved to form Zr-O-P bonds, as in C-O-(P-O-Zr)-O-C like structures, during the Zr loading process (see Scheme 4.1).

CO and CO_2 evolved at temperatures below 800 ºC occurring in both samples loaded with zirconium can be related to the presence of oxygenated surface groups formed during the calcination stage, at 250 ºC [28]. It is noticeable the lower amount of CO and CO_2 evolved at a temperature below 800 ºC in the sample ACPZr. This fact is associated to the presence of phosphorus surface

complexes, which provides the activated carbon with a high oxidation resistance [46].
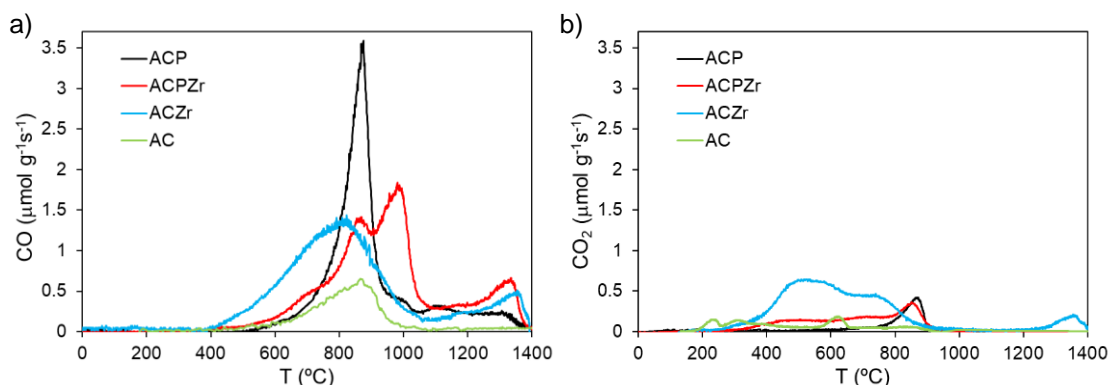
Figure. 4.2. a) CO and **b)** CO_2 evolved as a function of temperature during TPD for the samples.
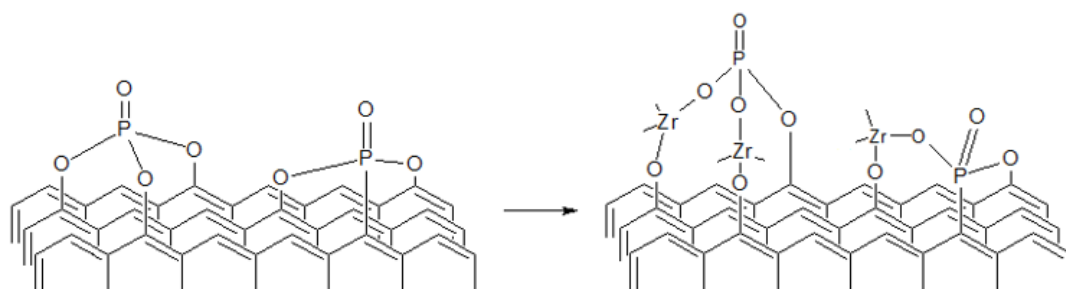
Scheme 4.1. Formation of zirconium phosphate species from C-O-P surface groups.

4.3.2 Catalytic dehydration of Methanol

4.3.2.1 Calculation of the mass and heat transfer limitations

Methanol dehydration was studied on the carbon-based catalysts in a fixed-bed microreactor. The reaction study was carried out in the temperature range from 250 to 400 °C. In the absence of catalysts, no reaction occurred below 600 °C. The calculated value of L_b/d_p (being L_b the bed length and d_p the particle diameter) was 100, which indicated negligible axial dispersion problems [47,48].

The absence of external and internal mass-transfer limitations for the studied reaction on the carbon-based catalysts in the fixed-bed reactor was checked theoretically. The effect of external mass transfer limitations was evaluated using the Carberry number (Ca) [49]. The calculated value for this number employing the conditions used in this study was $1.67 \cdot 10^{-4}$, which is well below 0.05. Therefore, external mass-transfer limitations can be neglected. The internal mass-transfer limitation was evaluated by using the isothermal intraphase internal effectiveness factor, η, which is a function of the Thiele modulus, ϕ. The values obtained for the Thiele modulus and the intraphase effectiveness factor were 0.32 and 0.993, respectively. Therefore, the internal mass transfer limitations were also considered negligible in this study.

The absence of intraparticle and extraparticle heat transfer limitations was also theoretically checked following the criteria suggested in Moulijn et al. [49]. These criteria indicate that for the consideration of negligible extraparticle and intraparticle heat transfer limitations, the system must satisfy $\gamma \cdot \beta_e \cdot C_a < 0.05$ and $\gamma \cdot \beta_i \cdot (\eta \cdot \phi^2) < 0.1$ *respectively.*

$$\gamma \cdot \beta_e \cdot Ca = \left(\frac{E_a}{R \cdot T_b}\right) \cdot \left|\frac{(-\Delta H_r) \cdot k_f \cdot c_b}{h \cdot T_b}\right| \cdot \left(\frac{r_{v,obs}}{a' \cdot k_f \cdot c_b}\right) = 5.28 \cdot 10^{-5} \ < 0.05 \qquad (Eq.\,4.3)$$

$$\gamma \cdot \beta_i \cdot (\eta \cdot \phi^2) = \left(\frac{E_a}{R \cdot T_b}\right) \cdot \left|\frac{(-\Delta H_r) \cdot D_{eff} \cdot c_s}{\lambda_{eff,p} \cdot T_b}\right| \cdot \left(\frac{r_{v,obs} \cdot L^2}{D_{eff} \cdot c_s}\right) = 1.7 \cdot 10^{-5} < 0.1 \qquad (Eq.\,4.4)$$

Here, $\gamma = E_a/R \cdot T$, is the Arrhenius number, $\beta_{e,i}$ is the external or internal temperature gradient and $\cdot (\eta \cdot \phi^2)$ is the Wheeler-Weisz modulus. The calculated values for the parameters required by this criterion using the most severe conditions analyzed in this study were well below the limit stablished. It has also to be pointed out that the internal diameter of the reactor is quite small (4 mm), which favors the heat exchange through the wall. Moreover, experiments were conducted with the catalytic bed diluted with inert particles of silicon carbide (75 µm of diameter and a mass ratio of SiC to carbon-based catalyst of 2) and similar results were obtained. Therefore, the intraparticle and extraparticle heat transfer limitations can be considered negligible in this study.

4.3.2.2 Methanol dehydration on carbon-based catalysts

Carbon-based materials prepared in this work were used as catalysts for the methanol dehydration reaction. Table 4.3 reports the steady-state methanol conversion and selectivity to DME values obtained for these samples. The total acidity for these samples (measured by NH_3 adsorption-desorption and TPD) has been also represented in Table 4.1. Physically activated carbon, AC, did not show any catalytic activity. Chemically activated carbon, ACP, showed a high initial methanol conversion with a high selectivity to DME, which dropped in the first 10 minutes of reaction at the operation conditions used, evidencing a fast deactivation process due to coke deposition. The presence of zirconium over the physically activated carbon did not produce any appreciable improvement in the steady-state methanol conversion value when using this material as catalyst (see ACZr in Table 4.3). Moreover, the low selectivity to DME observed for this catalyst suggested that methanol decomposition was taking place instead of dehydration, as reported for zirconia nanofibers [50]. On the contrary, the presence of Zr on the phosphorus-containing activated carbon resulted in a high and stable (steady-state) methanol conversion, with a high selectivity to DME (see ACPZr in Table 4.3), being this high stable catalytic activity related to the presence of zirconium phosphate species. The activity of these catalysts can be very well correlated with the total acidity of the samples (See Table 4.1). Actually, the acidity of ACP decreased from 128 µmol NH_3/g to a value of 35 µmol NH_3/g after this samples was used in reaction for 2 hours at the operation conditions indicated in Table 4.3, as a consequence of deposition of coke on P active sites (C-O-P and P-OH type). On the contrary, acidity of ACPZr was just slightly reduced (25 %) to a value of 130 µmol NH_3/g after methanol dehydration reaction for 4 h. The presence of Zr on the P-containing activated carbon seems to be responsible for the high stability of the acid sites on this catalyst and, therefore, for the high activity of this catalyst.

Table 4.3. Steady-state methanol conversion and selectivity to DME for the use of the activated carbon materials as catalysts (P_M = 0.02 atm, W_{cat}/F_M = 0.1 g·s/µmol$_M$, T = 400 ºC.

Catalyst	x_M (%)	S_{DME} (%)
AC	-	-
ACZr	13	34
ACP	11	81
ACPZr	70	96

Figure 4.3 presents the steady-state methanol conversion as a function of the temperature at different space times (W_{cat}/F_M) with a constant methanol partial pressure of 0.04 atm, using ACPZr as catalyst. The steady-state methanol conversion was achieved after 2.5 h on stream. As expected, the higher the temperature, the higher the methanol conversion value obtained. For a fixed temperature, methanol conversion increased with increasing the space time. The selectivity to DME was higher than 97 % in the whole range of temperature and space time studied.

Figure 4.4 shows the steady-state methanol conversion as a function of inlet methanol partial pressure for ACPZr at different reaction temperatures and a constant space time (W_{cat}/F_M = 0.025 g·s/µmol$_M$). For a fixed temperature, methanol conversion was almost no influenced by the inlet methanol partial pressure. These results are in agreement with those reported by Carr et al. for heteropoly acid catalysts [51]. They observed a non-dependence of conversion with inlet methanol partial pressure for values higher than 1 kPa, for this type of catalysts.
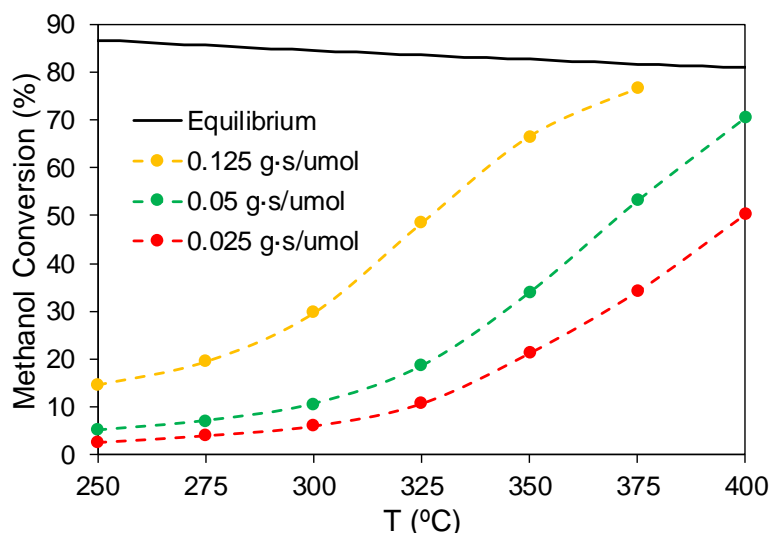
Figure 4.3. Steady-state and equilibrium methanol conversion as a function of the reaction temperature for ACPZr at different W_{cat}/F_M with a constant partial pressure of methanol $P_M = 0.06$ atm.
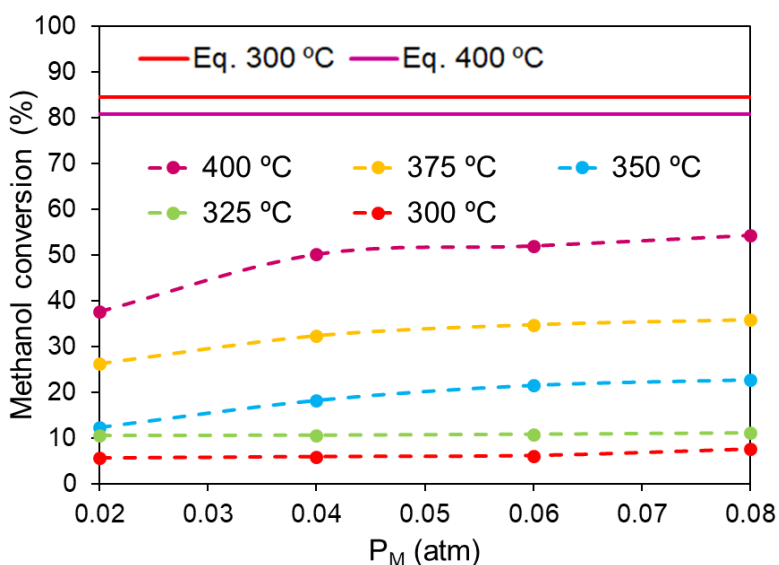
Figure. 4.4. Steady-state and equilibrium methanol conversion as a function of P_M for ACPZr at different reaction temperatures and a constant W_{cat}/F_M (0.025 g·s/μmol$_M$).

As aforementioned, the catalytic activity of the various carbon materials prepared in this study showed remarkable differences. These differences could be related to the surface chemistry of these catalysts. ACP showed only phosphorus species, presenting C-O-P and P-OH bonds as in C-O-PO$_3$ surface

groups [28], which have been reported to act as moderate and strong acid sites, respectively, for methanol dehydration. However, a fast deactivation due to coke formation was also observed if oxygen was not present in the reaction atmosphere [30]. ACZr presented ZrO_2 and oxygenated carbon groups on its surface. The low activity of this material was associated to the low thermal stability of the oxygenated surface groups and to the low catalytic activity that ZrO_2 exhibits [50]. ACPZr contained phosphorus and zirconium chemical surface groups, mainly in form of zirconium phosphate, and was the only catalyst prepared in this work exhibiting appreciable methanol conversion at steady-state conditions. Therefore, the presence of this chemical species bonded to the carbon surface seemed to be responsible for the steady-state methanol conversion presented by this catalyst. The selectivity to DME was higher than 97 % for all the conditions studied in this work, being CH_4 the main byproduct.

Methanol dehydration to DME using zirconium phosphates as catalysts has been studied. In their study, Cheng et al. proposed a reaction mechanism involving P-OH and P-O-P surface species as active sites for this reaction [52]. This mechanism considers one methanol adsorption over the active site, yielding a methoxy group, which then reacts with a methanol molecule through a four-member ring electron transfer process to form DME. According to this study, only phosphorus species are responsible for the methanol dehydration activity of these materials. Attending to this mechanism, the phosphorus-containing activated carbon presented in this study, ACP, which exhibited phosphorus surface complexes, should have efficiently catalyzed the reaction. However, after a fast deactivation process, this material only showed a residual activity, indicating that neither P-OH nor C-O-P sites are capable of achieving a significant steady-state methanol conversion. On the opposite, as mentioned above, the activated carbon containing zirconium phosphate surface species, ACPZr, did present high steady-state methanol conversion values. Thus, it seems that the active site catalyzing this reaction have to consider the presence of both P and Zr.

Scheme 4.2 represents the proposed chemical structures containing P and Zr, present on the carbon surface for the sample ACPZr. This scheme, considers the presence of Zr-O-P bond, as determined by XPS, and the existence of C-O-

P, C-O-Zr-O-P and C-O-Zr bonds, which were determined from TPD analyses (see section 4.3.1).
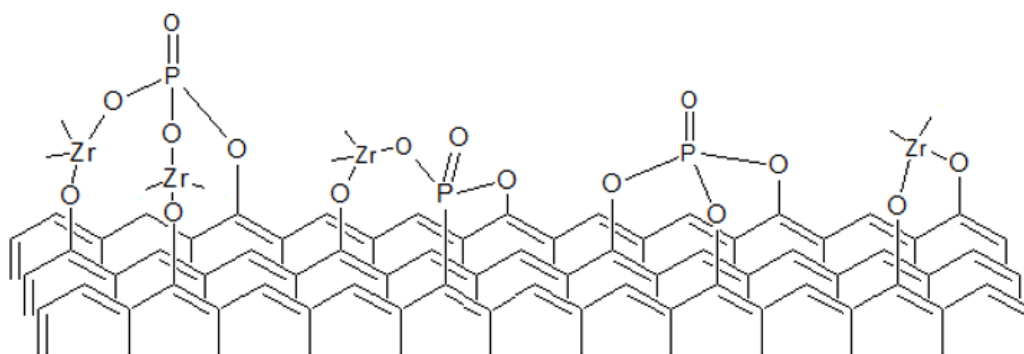
Scheme 4.2. Possible P and Zr groups on the surface of ACPZr.
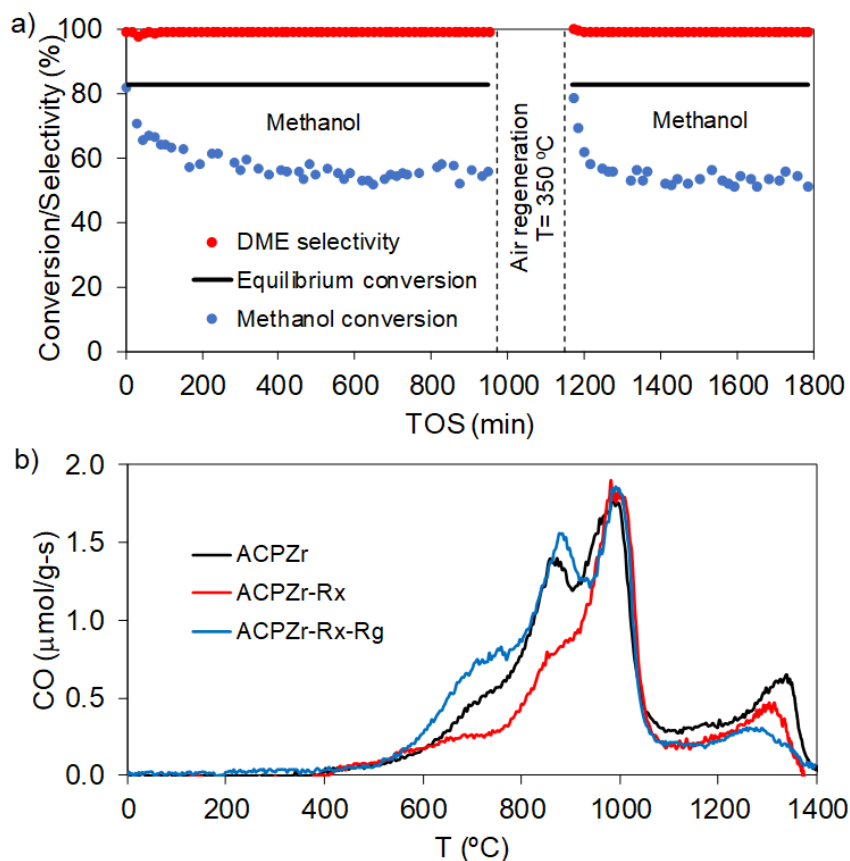
Figure 4.5a shows the methanol conversion and the selectivity to DME as a function of time-on-stream (TOS) for ACPZr at a reaction temperature of 350 ºC (P_M = 0.04 atm, W_{cat}/F_M = 0.1 g·s/µmol$_M$). In this experiment, the reaction mixture was first passed through the catalyst. As can be observed, a steady-state methanol conversion was achieved after 2.5 h, being observed a methanol conversion decay within this initial time. Once the steady-state conditions were achieved, the reaction gas was shifted to air and kept for 3 h. Subsequently, the initial reaction mixture was fed again, and it can be observed that the initial and the steady-state methanol conversion were very similar to the ones of the fresh catalyst (first step in Figure 4.5a), also showing an initial deactivation.

In order to analyze the active sites involved in both the initial conversion decay and the steady-state methanol conversion in more detail, TPD analyses were performed once achieved the steady-state methanol conversion (ACPZr-Rx), and after the air treatment at 350 ºC (ACPZr-Rx-Rg). After each treatment, and prior to TPD analyses, the samples were flushed in He at the reaction temperature for one hour and cooled to 120 ºC under constant He flow at 10 ºC/min. Figure 4.5b presents CO evolution from TPD analyses for the aforementioned samples. It could be observed that the CO evolution peak appearing at 1000 was unaffected after achieving the reaction steady-state conditions (see ACPZr and ACP-Rx in Figure 4.5b), indicating that the C-O-Zr

bonds of the C-O-Zr-O-P surface groups type were not modified under reaction conditions. However, the CO evolution peak appearing at 870 ℃ that is associated to the decomposition of C-O-P bonds significantly decreased for ACPZr-Rx, suggesting that although these groups are active for methanol dehydration, they are initially deactivated under the reaction conditions used, as it was observed for ACP, which only contained this type of active sites and were almost completely deactivated (see Table 4.3) [30]. Actually, the initial loss of activity, in terms of conversion, was about 25%, which coincides with the loss of acidity of this catalyst measured after the reaction, as indicated above (from 175 to 130 µmol NH_3/g). After the air treatment, the peak appearing at 870 ℃ was totally restored (see ACPZr-Rx-Rg in Figure 4.5b), indicating that the C-O-P sites were regenerated after this oxidative treatment, as reported by Valero-Romero et al. [30]. Furthermore, NH_3-TPD analysis further revealed a restorage of the total acidity for this catalyst after the air regeneration treatment. Actually, the initial methanol conversion decay before achieving the steady-state conversion can be observed again in the third experimental step of Figure 4.5a, which corresponds to the conversion-TOS profile for the regenerated catalyst (ACPZr-Rx). Therefore, the Zr-O-P sites, present in C-O-Zr-O-P surface groups, seems to be responsible of reaching a steady-state methanol conversion, without a significant deactivation, given that C-O-Zr groups showed a negligible activity for this reaction, as observed for ACZr (Table 4.3).

Figure 4.5. a) Methanol conversion as a function of time-on-stream (TOS) for ACPZr at a reaction temperature of 350 ºC (P_M = 0.04 atm, W_{cat}/F_M = 0.1 g·s/µmol$_M$) and equilibrium methanol conversion. **b)** CO evolved as a function of temperature during TPD for the fresh ACPZr catalyst, for that catalyst used in reaction, ACPZr-Rx (once achieved the steady-state methanol conversion) and for the regenerated catalyst, ACPZr-Rx-Rg (the used catalyst after the air treatment at 350 ºC).

4.3.2.3 Kinetic study

A kinetic study was carried out for the selective methanol dehydration to DME on the Zr-loaded P-containing activated carbon, ACPZr. Inlet methanol partial pressure and space time were varied from 0.01 to 0.1 atm and 0.025 to 0.125 g·s/µmol$_M$, respectively. The reaction was performed in the temperature range of 250-400 ºC. Since selectivity to DME was higher than 97% for all the

conditions studied, the mechanisms proposed in this work only consider the formation of DME as reaction product.

In this study, the following assumptions were accomplished: active sites were uniformly distributed on the surface of the catalyst, reactor operated at steady-state conditions and heat and mass transfer limitations were negligible (see section 4.3.1). These assumptions allowed considering plug flow integral reactor for the interpretation of the experimental data. For this aim, the reactor mass balance equation (Eq. (4.5)) was numerically integrated to calculate the exit methanol conversion.

$$-\frac{dx_M}{d\left(\frac{W}{F_M}\right)} = r_M \qquad\qquad (Eq.\,4.5)$$

For methanol dehydration reaction two different reaction routes have been proposed in the literature, so called the indirect and the direct routes [17]. In the indirect pathway [19,53,54] one methanol molecule adsorption is supposed to take place, yielding H_2O and an adsorbed methoxy group, which then reacts with another gas phase methanol molecule giving DME. This reaction pathway, only involving one methanol molecule adsorption, is consistent with and Eley-Rideal mechanism. On the other hand, for the direct route [18], two methanol molecules are adsorbed on an acid and an adjacent basic site, which then react according to a Langmuir-Hinshelwood mechanism. In addition to this Langmuig-Hinshelwood mechanism, where two methanol molecules are adsorbed on two different active sites, Carr et al. [51] proposed a reaction mechanism in which the two methanol molecules are adsorbed on the same active site, then reacting according to a direct route.

In the present study, three different kinetic models were proposed in order to describe the kinetic of the methanol dehydration on ACPZr catalyst. The first reaction mechanism studied was an Eley-Rideal mechanism (ER); the second one was a Langmuir-Hinshelwood mechanism (LH1), which considered that the two methanol molecules adsorption took place on two active sites, with the same adsorption enthalpy; and the third one was a Langmuir-Hinshelwood like mechanism (LH2), in which both methanol molecules were subsequently

adsorbed on the same active site, but with different adsorption enthalpies. For the derivation of the rate expression, the surface reaction between an adsorbed molecule and a molecule in the gas phase, in the case of the Eley-Rideal mechanism (ER), or between two adsorbed methanol molecules, in the case of the Langmuir-Hinshelwood type mechanisms (LH1 and LH2), was considered as the rate determining step. Table 4.4 summarizes the rate expressions for the reaction mechanisms studied in this work.

Table 4.4. Rate expressions for the proposed mechanisms for methanol dehydration on ACPZr catalyst.

Mechanism	Description	Rate expresion
ER	Eley-Rideal mechanism with DME production as rate determining step	$-r_{ER} = \dfrac{k_{sr}\left(K_M P_M^2 - \frac{P_W P_{DME}}{K_{sr} K_W}\right)}{1 + K_M P_M + \frac{P_W}{K_W}}$
LH1	Langmuir-Hinshelwood assuming both methanol adsortions equals	$-r_{LH1} = \dfrac{k_{sr}\left(K_M P_M^2 - \frac{P_{DME} P_W}{K_{sr} K_W}\right)}{\left(1 + K_1 P_M + \frac{P_W}{K_W}\right)^2}$
LH2	Langmuir-Hinshelwood, where methanol molecules are adsorbed on one active site, with different adsorption enthalpies.	$-r_{LH2} = \dfrac{k_{sr}\left(K_{M,1} K_{M,2} P_M^2 - \frac{P_{DME} P_W}{K_{sr} K_W}\right)}{1 + K_{M,1} P_M + K_{M,1} K_{M,2} P_M^2 + \frac{P_W}{K_W}}$

In this set of equations, k_i represents the kinetic rate constant and K_i accounts for adsorption equilibrium constant, for each reaction step. P_M, P_{DME} and P_W represent the methanol, DME and water vapor partial pressures. The dependence on temperature for the kinetic and thermodynamic parameters was considered to follow an Arrhenius law, Eq. (4.6), for the kinetic constants or Van't Hoff law, Eq. (4.7), for the adsorption constants.

$$k_i = k_{0,i} \cdot \exp\left(\frac{-E_{a,i}}{RT}\right) \qquad \text{(Eq. 4.6)}$$

$$K_i = K_{0,i} \cdot \exp\left(\frac{-\Delta H_i}{RT}\right) \qquad \text{(Eq. 4.7)}$$

In these equations (Eqs. (4.6) and (4.7)), $k_{o,i}$ and $K_{o,i}$ are the preexponential factor, R is the universal gas constant, T is the temperature, $E_{a,i}$ is the activation energy and ΔH_i is the enthalpy of adsorption.

The calculation of the kinetic parameters involved in these equations was performed using the Runge-Kutta method, implemented in Matlab 2017a software, by minimizing the objective function:

$$O.F. = \sum_j \left(x_j^{exp} - x_j^{calc} \right)^2 \qquad \text{(Eq. 4.8)}$$

Where x_j^{exp} represents the value for the experimental methanol conversion in the experiment $_j$ and x_j^{calc} the calculated value solving the differential rate equation. The optimization routine was based on the Nelder-Mead algorithm. 77 experiments at different methanol partial pressures, temperatures and space times were considered.

Figure 4.6 presents the conversion calculated by the different kinetic models vs. the experimental methanol conversions. The kinetic model based on the Eley-Rideal mechanism did not reproduce the experimental results. In the conditions studied, the model that best reproduce the experimental data was LH2. LH1 model also presented a relatively good agreement between the experimental and the calculated data. However, it provided a thermodynamically inconsistent value of heat of adsorption for methanol (0.17 kJ/mol) and, thus, it was rejected.

As can be seen, the LH2 model reproduced the experimental data with a high accuracy (see Figure 4.6c). The quality of the fitting is also observed in both Figure 4.7a and b. Figure 4.7a shows the methanol conversion as a function of the temperature for different space times at a constant methanol partial pressure of 0.04 atm. The results predicted by the model are also shown in solid lines, for the sake of comparison, and it is remarkable the good agreement between the experimental data and the calculated values provided by the model. Figure 4.7b represents the steady state methanol conversion as a function of methanol partial pressure at different space times for a constant temperature of 375 ºC. Steady-state methanol conversion increased with inlet methanol partial pressure up to a value of 0.04 atm and above this value methanol conversion showed almost no influence on the methanol partial pressure, probably due to the high affinity of methanol for the active sites of the catalyst.
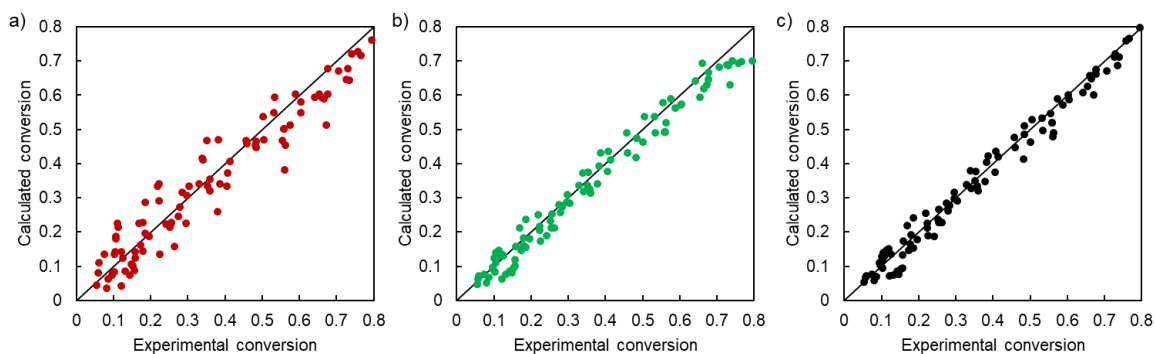
Figure 4.6. Calculated methanol conversion versus experimental conversion for a) ER b) LH1 and c) LH2 models.
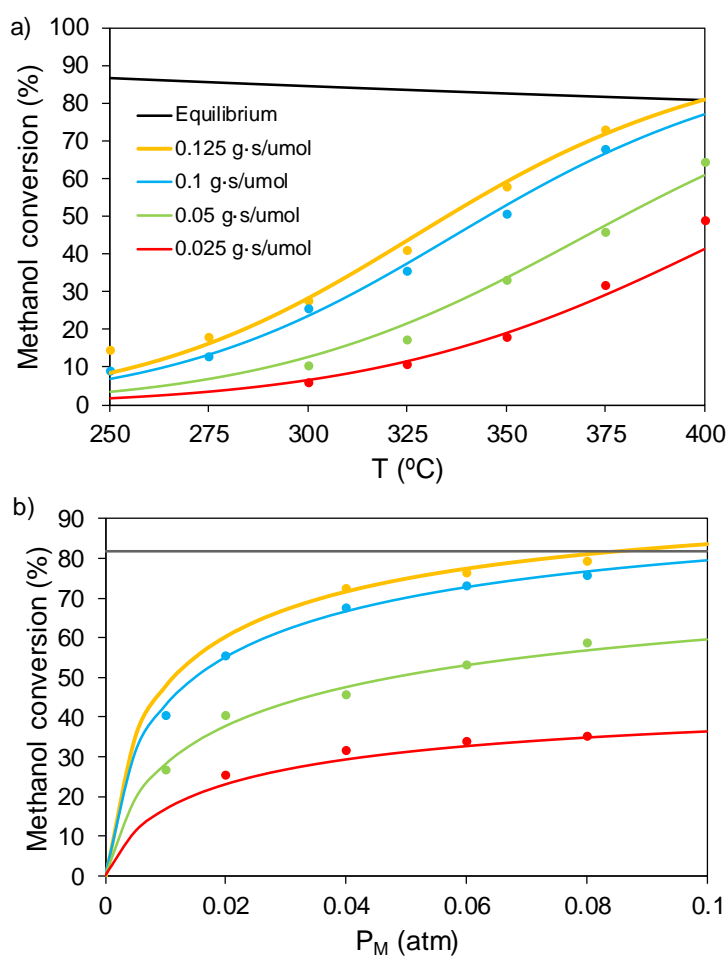
Figure 4.7. Experimental (dot), simulated (solid line) steady-state and equilibrium methanol conversion as a function of **a)** the reaction temperature at different W_{cat}/F_M with a constant partial pressure of methanol $P_M = 0.04$ atm. **b)** the methanol partial pressure at different W_{cat}/F_M at a constant temperature of 375 °C.

Scheme 4.3 represents the proposed LH2 mechanism for methanol dehydration, considering Zr-O-P groups as the active sites for this catalyst. This mechanism accounts for a first methanol adsorption on the Zr-O-P active site, which cleavages yielding a methoxy group bonded to the phosphorus and a vicinal -OH bonded to the zirconium (Step 1). Subsequently, a second methanol molecule adsorbs on the generated vicinal Zr-OH (Step 2). The methoxy group formed in Step 1 as a reaction intermediate has been reported to be a coke precursor, which could deactivate the catalyst [55]. However, in this case, this methoxy group reacts with an adsorbed methanol molecule yielding DME and H_2O, which remains adsorbed on the active site (Step 3). Finally, H_2O is desorbed, being the Zr-O-P group regenerated (Step 4). Some studies reported that DME adsorption on the active sites can be considered negligibly small compared to the methanol and water adsorptions [56,57]. Thus, DME readsorption has not been considered in this study. On the opposite, it has been also reported that water vapor molecules compete for the acid sites of the catalyst, preventing methanol from being adsorbed [58]. This competitive adsorption is accounted in this mechanism through the reversible Step 4.
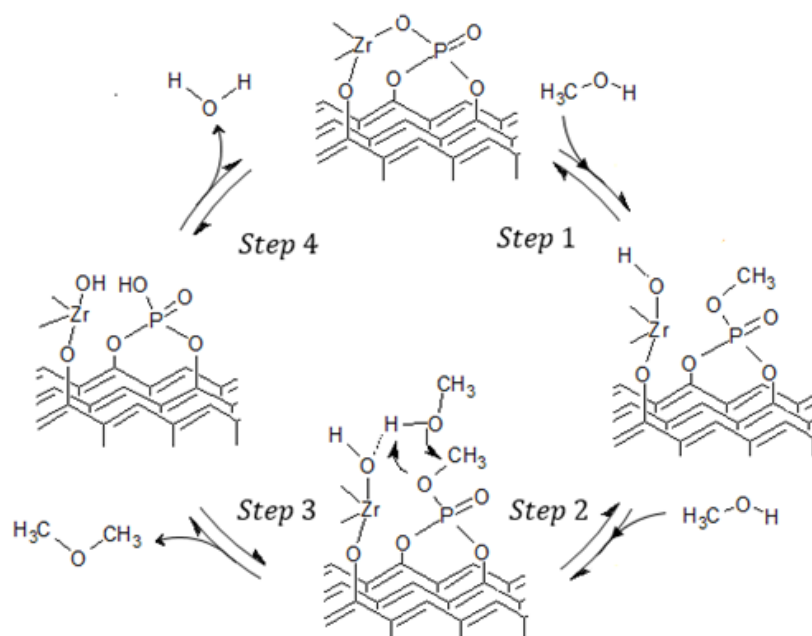
Scheme 4.3. Scheme of the proposed surface methanol dehydration mechanism on the zirconium phosphate species present on the activated carbon catalyst surface.

The rate equations for each elementary reaction step depicted in Scheme 4.3, Steps (1) – (4), are shown in Eq. (4.9) – (4.12).

$$r_1 = k_{M,1} \cdot P_M \cdot \theta_L - \frac{k_{M,1}}{K_{M,1}} \cdot \theta_{L'} \qquad \text{(Eq. 4.9)}$$

$$r_2 = k_{M,2} \cdot \theta_{L'} \cdot P_M - \frac{k_{M,2}}{K_{M,2}} \cdot \theta_{L'-M} \qquad \text{(Eq. 4.10)}$$

$$r_3 = k_{sr} \cdot \theta_{L'-M} - \frac{k_{sr}}{K_{sr}} \cdot P_{DME} \cdot \theta_{L-W} \qquad \text{(Eq. 4.11)}$$

$$r_4 = k_W \cdot \theta_{L-W} - \frac{k_W}{K_W} \cdot \theta_L \cdot P_W \qquad \text{(Eq. 4.12)}$$

Where θ_L represents the fraction of vacant Zr-O-P sites, $\theta_{L'}$ is the fractional coverage of methoxy groups with a vicinal Zr-OH site (Step 1), $\theta_{L'-M}$ is the fractional coverage of methanol adsorbed on the generated Zr-OH (Step 2), and θ_{L-W} is the fractional coverage of water adsorbed on the active sites.

For the proposed kinetic model, it was assumed that all the adsorption steps (Steps 1, 2 and 4) reached a quasi-equilibrium state. From these assumptions, it can be obtained:

$$\theta_{L'} = K_{M,1} \cdot \theta_L \cdot P_M \qquad \text{(Eq. 4.13)}$$

$$\theta_{L'-M} = K_{M,2} \cdot \theta_{L'} \cdot P_M \qquad \text{(Eq. 4.14)}$$

$$\theta_{L-W} = \frac{\theta_L \cdot P_W}{K_W} \qquad \text{(Eq. 4.15)}$$

The site balance is shown in the following equation,

$$1 = \theta_L + \theta_{L'} + \theta_{L'-M} + \theta_{L-W} \qquad \text{(Eq. 4.16)}$$

and rearranging the Eqs. (4.13) – (4.16) yields,

$$\theta_L = \frac{1}{1 + K_{M,1}P_M + K_{M,1}K_{M,2}P_M^2 + \frac{P_W}{K_W}} \qquad \text{(Eq. 4.17)}$$

Considering the surface reaction between the adsorbed methoxy and the adsorbed methanol molecule (Step 3), as the rate determining step, the rate expression presented in Table 4.4 was obtained:

$$r_{DME} = r_3 = \frac{k_{sr}\left(K_{M,1}K_{M,2}P_M^2 - \frac{P_{DME}P_W}{K_{sr}K_W}\right)}{1 + K_{M,1}P_M + K_{M,1}K_{M,2}P_M^2 + \frac{P_W}{K_W}} \qquad (Eq.\,4.18)$$

$$-r_M = 2 \cdot r_{DME} \qquad (Eq.\,4.19)$$

Table 4.5 summarizes the values of the activation energy or enthalpy of adsorption and the preexponential factors ($k_{0,i}$, $K_{0,i}$) for the reactions implied in the proposed mechanism, obtained from the numerical fitting of the experimental data to the LH2 model. The high value obtained for the surface reaction equilibrium constant (higher than $2 \cdot 10^6$, at 300 ºC), indicated that the reverse reaction could be considered negligible for the operation conditions used in this study. The negative values of the obtained enthalpies of adsorption are in agreement with an exothermic process. It is noticeable the low calculated value obtained for the enthalpy of adsorption of the second methanol molecule, -10 kJ/mol, when it is compared to the adsorption enthalpy value calculated for the first one (-28 kJ/mol), which indicated a weak adsorption for this second methanol molecule. The calculated enthalpy of adsorption of methanol presented a lower value than the reported in the literature for SAPO and zeolites [59,60], probably due to the presence of strong acid sites on these materials. In the case of the adsorption enthalpy of water, the value here obtained was similar to that reported for alumina [61] and SAPO-34 [59], and lower than the reported for zeolites [60,62]. The activation energy for the surface reaction was also calculated, obtaining a value of 70 kJ·mol^{-1}, which is similar to that reported for zirconia fibers [50], γ-Al$_2$O$_3$ [56], and zeolites [62] and slightly lower than other solid acid catalysts such as SAPO-34 [59].

Table 4.5. Kinetic parameters for methanol conversion.

	k_0 or K_0		E_a or ΔH (kJ/mol)
k_{sr}	3.7	$(mol \cdot g_{cat}^{-1} \cdot s^{-1})$	70
$K_{M,1}$	11.1	(atm^{-1})	-28
$K_{M,2}$	11.5	(atm^{-1})	-10
K_W	0.2	(atm)	41
K_{sr}	35533	-	-21

4.3.2.4 Effect of inlet water vapor on the kinetic behavior

The presence of water vapor in the reactor inlet has been reported to affect the performance of catalysts for this reaction, given that water vapor competes with methanol for the active sites of the catalyst [58]. Moreover, DME production involves the generation of appreciable amounts of water that can be also readsorbed on the catalyst active sites. This competitive adsorption is accounted in the mechanism here proposed through the reversible Step 4 (see Scheme 4.3). Figure 4.8. shows the experimental and the simulated steady-state methanol conversion as a function of the water vapor partial pressure for a constant methanol partial pressure at 400 ºC. The solid line represents the simulated methanol conversion according to LH2 model. As can be observed, the higher the water vapor partial pressure in the reactor inlet, the lower the methanol conversion reached in the reactor exit. It is noteworthy the good agreement between the experimental and the estimated methanol conversion values. Therefore, the LH2 model presented in this study exhibited robust enough for predicting the inhibition effect caused by the presence of water vapor presence.
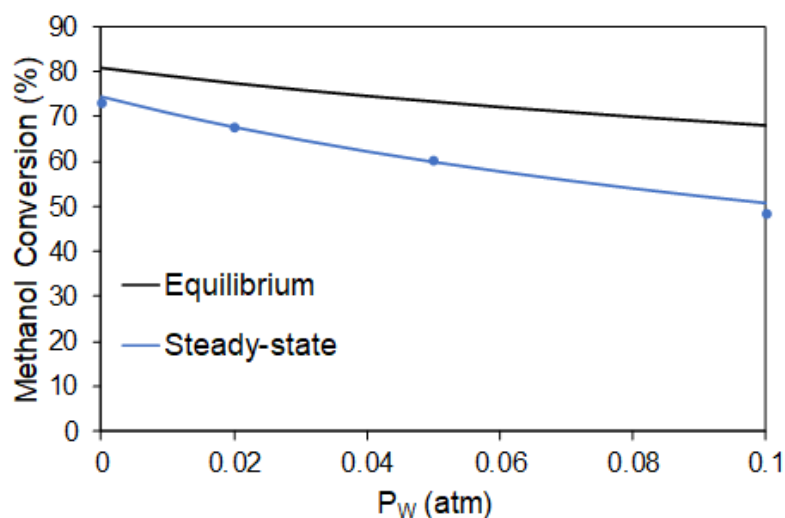
Figure 4.8. Experimental (dot), estimated (solid line) steady-state and equilibrium methanol conversion as a function of water vapor partial pressure (W_{cat}/F_M=0.025 g·s/µmol$_M$, P_M = 0.1 atm and at 400 ºC).

Figure 4.9 presents the estimated evolution of methanol conversion, the fraction of free active sites and the fractional coverage obtained by LH2 model as a function of the space time for a constant temperature of 350 ºC. As can be observed, the fraction of free active sites (θ_L) is very low, while those corresponding to methanol coverage ($\theta_{L'}$ and $\theta_{L'-M}$) showed high values. These results suggested a high affinity of methanol for the active sites of the catalyst. As the reaction proceed, it can be also seen that the fractional coverage corresponding to adsorbed water (θ_{L-W}) increased, while decreasing the fractional coverage of methanol ($\theta_{L'-M}$), highlighting the competitive adsorption of water on the active sited of the catalyst.
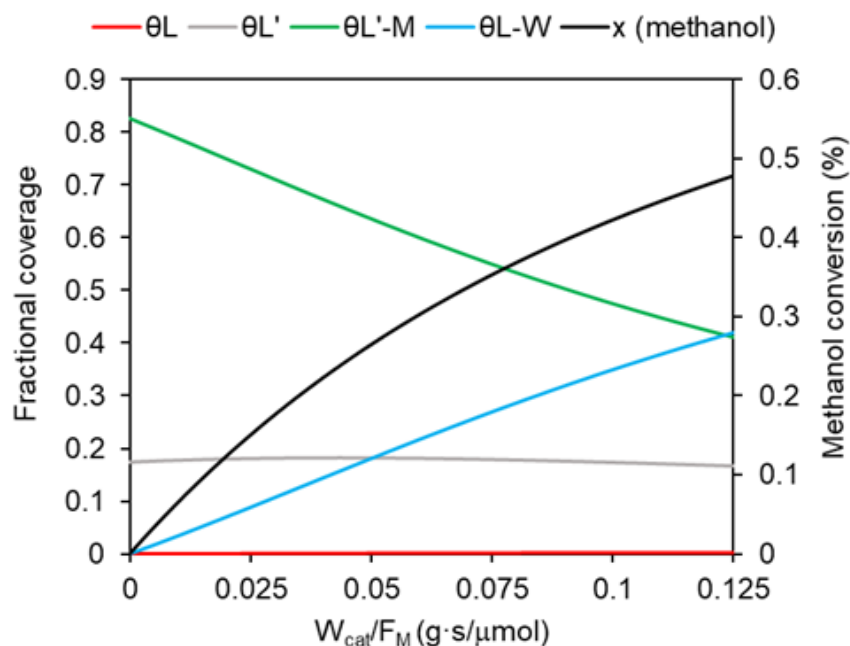
Figure 4.9. Evolution of methanol conversion, the fraction of free active sites and the fractional coverage, obtained by LH2 model (W_{cat}/F_M=0.025 g·s/µmol$_M$, P_M = 0.06 atm and at 350 ºC).

4.4.-Conclusions

Selective methanol dehydration to DME has been investigated using activated carbon catalysts. Two different kinds of activated carbons were prepared. On the one hand, an activated carbon was prepared via physical activation, by CO_2 partial gasification, and on the other hand, a chemical activation with phosphoric acid process was carried out for the preparation of the activated carbon. Both activated carbons were loaded with a 5 % (w/w) Zr.

The catalytic results showed that only the chemically activated carbon (the one containing P surface groups) loaded with Zr (ACPZr) was capable of achieving high steady-state methanol conversion and selectivity to DME values. The surface chemistry of this sample was analyzed in depth to determine the chemical species involved in its catalytic performance. The presence of zirconium phosphate species bonded to the carbon surface were determined to be the

responsible for the high steady-state methanol conversion and selectivity to DME achieved using this material as catalysts.

A kinetic study was carried out for the selective methanol dehydration to DME on ACPZr. Three different reaction mechanisms were studied. A modified Langmuir-Hinshelwood mechanism (LH2), in which two methanol molecules are subsequently adsorbed on one active site, with different adsorption enthalpies and considering the competitive adsorption of water on the active sites, was the model that best reproduce the experimental data. The activation energy for the DME production was calculated and a value of 70 kJ mol^{-1} was obtained. The kinetic model was capable of predicting the effect of water vapor in the reactor inlet, being observed a good agreement between the experimental and the calculated methanol conversion values.

4.5.-Notation

A_{BET} = apparent surface area obtained by the BET method (m^2/g).

A_{DR} = apparent area of narrow micropores from CO_2 isotherm (m^2/g).

A_t = external area obtained by the t method, (m^2/g).

BET = Brunauer, Emmett, and Teller.

Ca = Carberry number.

Da = Damköhler number.

DME = dimethyl ether.

d_p = catalyst particle diameter (mm).

DR = Dubinin-Radushkevich.

$E_{a,i}$ = activation energy for reaction i (kJ/mol).

F_i^o = molar flow of the compound i in the reactor output stream (µmol/s).

F_M = initial methanol molar flow (µmol$_M$/s).

F_M^o = methanol molar flow in the reactor output stream (µmol$_M$/s).

$k_{o,i}$ = preexponential factor of Ahrrenius equation, reaction i.

k_i = kinetic rate constant.

$k_{M,1}$ = kinetic constant for first methanol adsorption (mol_M/s-g-atm).

$k_{M,2}$ = kinetic constant for second methanol adsorption (mol_M/s-g-atm).

k_{sr} = kinetic constant for surface reaction (mol_M/s-g).

k_w = kinetic constant for water desorption (mol_W/s-g).

$K_{o,i}$ = preexponential factor of Van't Hoff equation, reaction i.

K_i = equilibrium constant.

$K_{M,1}$ = equilibrium constant for first methanol adsorption (atm^{-1}).

$K_{M,2}$ = equilibrium constant for second methanol adsorption (atm^{-1}).

K_{sr} = equilibrium constant for surface reaction (dimensionless).

K_w = equilibrium constant for water desorption (atm).

L_b = bed length (mm).

nc_i = number of carbon atoms in the product i.

O.F. = optimization function.

P_{DME} = dimethyl ether partial pressure (atm).

P_M = methanol partial pressure (atm).

P_w = water partial pressure (atm).

R = universal gas constant (J/mol-K)

r_i = rate equation for component/step i (mol_M/s-g).

$-r_M$ = methanol consumption rate (mol_M/s-g).

r_{DME} = DME formation rate (mol_M/s-g).

S_i = selectivity to i product (%).

TOS = time on stream (min).

V_{DR} = micropore volume obtained by the DR method applied to CO_2 isotherm (cm^3/g).

V_{mes} = mesopore volume (cm^3/g).

V_P = pore volume (cm^3/g).

V_t = micropore volume obtained by the t method (cm^3/g).

W_{cat} = catalyst weight (g).

W_{cat}/F_M = space time ($g·s/µmol_M$).

x_j^{exp} = experimental methanol conversion in the experiment j.

x_j^{calc} = calculated methanol conversion for the experiment j.

x_M = methanol conversion (%).

Greek Letters

β_e = external temperature gradient

β_i = internal temperature gradient.

$\gamma = E_a/R·T$ = Arrhenius number

ΔH_i = enthalpy of adsorption of component i

η = isothermal intraphase internal effectiveness factor.

$\eta\phi^2$ = Wheeler-Weisz modulus.

θ_L = fraction of vacant Zr-O-P sites.

$\theta_{L'}$ = fractional coverage of methoxy groups, with a vicinal Zr-OH site.

$\theta_{L'-M}$ = fractional coverage of methanol adsorbed on the generated Zr-OH.

θ_{L-W} = fractional coverage of water adsorbed on the active sites.

ϕ = Thiele modulus.

4.6.-References

[1] K. Saravanan, H. Ham, N. Tsubaki, J.W. Bae, Recent progress for direct synthesis of dimethyl ether from syngas on the heterogeneous bifunctional hybrid catalysts, Appl. Catal. B Environ. 217 (2017) 494–522. doi:10.1016/j.apcatb.2017.05.085.

[2] J. Vicente, J. Ereña, L. Oar-Arteta, M. Olazar, J. Bilbao, A.G. Gayubo, Effect of operating conditions on dimethyl ether steam reforming in a fluidized bed reactor with a $CuO-ZnO-Al_2O_3$ and desilicated ZSM-5 zeolite bifunctional catalyst, Ind. Eng. Chem. Res. 53 (2014) 3462–3471. doi:10.1021/ie402509c.

[3] T.A. Semelsberger, R.L. Borup, H.L. Greene, Dimethyl ether (DME) as an alternative fuel, J. Power Sources. 156 (2006) 497–511. doi:10.1016/j.jpowsour.2005.05.082.

[4] K. Takeishi, H. Suzuki, Steam reforming of dimethyl ether, Appl. Catal. A Gen. 260 (2004) 111–117. doi:10.1016/J.APCATA.2003.10.006.

[5] J. Li, Q.-J. Zhang, X. Long, P. Qi, Z.-T. Liu, Z.-W. Liu, Hydrogen production for fuel cells via steam reforming of dimethyl ether over commercial $Cu/ZnO/Al_2O_3$ and zeolite, Chem. Eng. J. 187 (2012) 299–305. doi:10.1016/J.CEJ.2012.01.126.

[6] M. Marchionna, R. Patrini, D. Sanfilippo, G. Migliavacca, Fundamental investigations on di-methyl ether (DME) as LPG substitute or make-up for domestic uses, Fuel Process. Technol. 89 (2008) 1255–1261. doi:10.1016/j.fuproc.2008.07.013.

[7] J. Sun, G. Yang, Y. Yoneyama, N. Tsubaki, Catalysis chemistry of dimethyl ether synthesis, ACS Catal. 4 (2014) 3346–3356. doi:10.1021/cs500967j.

[8] M. Xu, J.H. Lunsford, D.W. Goodman, A. Bhattacharyya, Synthesis of dimethyl ether (DME) from methanol over solid-acid catalysts, Appl. Catal. A Gen. 149 (1997) 289–301. doi:10.1016/S0926-860X(96)00275-X.

[9] K.C. Tokay, T. Dogu, G. Dogu, Dimethyl ether synthesis over alumina based catalysts, Chem. Eng. J. 184 (2012) 278–285. doi:10.1016/J.CEJ.2011.12.034.

[10] A. Ciftci, D. Varisli, K. Cem Tokay, N. Aslı Sezgi, T. Dogu, Dimethyl ether, diethyl ether & ethylene from alcohols over tungstophosphoric acid based mesoporous catalysts, Chem. Eng. J. 207–208 (2012) 85–93. doi:10.1016/J.CEJ.2012.04.016.

[11] Z. Azizi, M. Rezaeimanesh, T. Tohidian, M.R. Rahimpour, Dimethyl ether: A review of technologies and production challenges, Chem. Eng. Process. Process Intensif. 82 (2014) 150–172. doi:10.1016/j.cep.2014.06.007.

[12] G. Laugel, X. Nitsch, F. Ocampo, B. Louis, Methanol dehydration into dimethylether over ZSM-5 type zeolites: Raise in the operational temperature range, Appl. Catal. A Gen. 402 (2011) 139–145. doi:10.1016/j.apcata.2011.05.039.

[13] M. Rutkowska, D. Macina, N. Mirocha-Kubień, Z. Piwowarska, L. Chmielarz, Hierarchically structured ZSM-5 obtained by desilication as new catalyst for DME synthesis from methanol, Appl. Catal. B Environ. 174–175 (2015) 336–343. doi:10.1016/j.apcatb.2015.03.006.

[14] A.A. Rownaghi, F. Rezaei, M. Stante, J. Hedlund, Selective dehydration of methanol to dimethyl ether on ZSM-5 nanocrystals, Appl. Catal. B Environ. 119–120 (2012) 56–61. doi:10.1016/j.apcatb.2012.02.017.

[15] C. Ortega, M. Rezaei, V. Hessel, G. Kolb, Methanol to dimethyl ether conversion over a ZSM-5 catalyst: Intrinsic kinetic study on an external recycle reactor, Chem. Eng. J. 347 (2018) 741–753. doi:10.1016/J.CEJ.2018.04.160.

[16] J.R. Jain, C.N. Pillai, Catalytic Dehydration of Alcohols over Alumina Mechanism of Ether Formation, J. Catal. 9 (1967) 322–330. doi:10.1016/0021-9517(67)90260-6.

[17]   I. Štich, J.D. Gale, K. Terakura, M.C. Payne, Role of the zeolitic environment in catalytic activation of methanol, J. Am. Chem. Soc. 121 (1999) 3292–3302. doi:10.1021/ja983470q.

[18]   J. Bandiera, C. Naccache, Kinetics of methanol dehydration on dealuminated H-mordenite: Model with acid and basic active centres, Appl. Catal. 69 (1991) 139–148. doi:10.1016/S0166-9834(00)83297-2.

[19]   L. Kubelková, J. Nováková, K. Nedomová, Reactivity of surface species on zeolites in methanol conversion, J. Catal. 124 (1990) 441–450. doi:10.1016/0021-9517(90)90191-L.

[20]   L.M. Cotoruelo, M.D. Marqués, F.J. Díaz, J. Rodríguez-Mirasol, J.J. Rodríguez, T. Cordero, Equilibrium and Kinetic Study of Congo Red Adsorption onto Lignin-Based Activated Carbons, Transp. Porous Media. 83 (2010) 573–590. doi:10.1007/s11242-009-9460-8.

[21]   J.M. Rosas, J. Bedia, T. Cordero, On the preparation and characterization of chars and activated carbons from orange skin, Fuel Process. Technol. 91 (2010) 1345–1354. doi:10.1016/j.fuproc.2010.05.006.

[22]   J.M. Rosas, R. Ruiz-Rosas, J. Rodríguez-Mirasol, T. Cordero, Kinetic study of SO_2 removal over lignin-based activated carbon, Chem. Eng. J. 307 (2017) 707–721. doi:10.1016/J.CEJ.2016.08.111.

[23]   J. Bedia, J.M. Rosas, D. Vera, J. Rodríguez-Mirasol, T. Cordero, Isopropanol decomposition on carbon based acid and basic catalysts, Catal. Today. 158 (2010) 89–96. doi:10.1016/j.cattod.2010.04.043.

[24]   J. Zawadzki, M. Wiśniewski, J. Weber, O. Heintz, B. Azambre, IR study of adsorption and decomposition of propan-2-ol on carbon and carbon-supported catalysts, Carbon N. Y. 39 (2001) 187–192. doi:10.1016/S0008-6223(00)00107-X.

[25]   C. Moreno-Castilla, F. Carrasco-Marín, C. Parejo-Pérez, M. V. López Ramón, Dehydration of methanol to dimethyl ether catalyzed by oxidized activated carbons with varying surface acidic character, Carbon N. Y. 39 (2001) 869–875. doi:10.1016/S0008-6223(00)00192-5.

[26] J. Bedia, R. Ruiz-Rosas, J. Rodríguez-Mirasol, T. Cordero, Kinetic Study of the decomposition of 2-Butanol on Carbon-Based Acid Catalyst, Am. Inst. Chem. Engeeniers. 56 (2010) 1557–1568. doi:10.1002/aic.

[27] J.M. Rosas, J. Bedia, J. Rodríguez-Mirasol, T. Cordero, HEMP-derived activated carbon fibers by chemical activation with phosphoric acid, Fuel. 88 (2009) 19–26. doi:10.1016/j.fuel.2008.08.004.

[28] M.J. Valero-Romero, F.J. García-Mateos, J. Rodríguez-Mirasol, T. Cordero, Role of surface phosphorus complexes on the oxidation of porous carbons, Fuel Process. Technol. 157 (2017) 116–126. doi:10.1016/j.fuproc.2016.11.014.

[29] J. Bedia, R. Barrionuevo, J. Rodríguez-Mirasol, T. Cordero, Ethanol dehydration to ethylene on acid carbon catalysts, Appl. Catal. B Environ. 103 (2011) 302–310. doi:10.1016/j.apcatb.2011.01.032.

[30] M.J. Valero Romero, E.M. Calvo Muñoz, R. Ruíz Rosas, J. Rodríguez-Mirasol, T. Cordero, Phosphorus-containing mesoporous carbon acid catalyst for methanol dehydration to dimethyl ether, Ind. Eng. Chem. Res. 58 (2019) 4042–4053. doi:10.1021/acs.iecr.8b05897.

[31] J. Palomo, M.A. Rodríguez-Cano, J.M. Rosas, J. Rodríguez-Mirasol, T. Cordero, Kinetic study of methanol dehydration over ZrO_2 supported-activated carbons, in: The world Conference on Carbon 2018, 2018.

[32] S. Brunauer, P.H. Emmett, E. Teller, Adsorption of Gases in Multimolecular Layers, J. Am. Chem. Soc. 60 (1938) 309–319. doi:10.1021/ja01269a023.

[33] S. Lowell, J.E. Shields, J.E. Morral, Powder Surface Area and Porosity, 2nd Edition, 1985. doi:10.1115/1.3225796.

[34] M.M. Dubinin, The potential theory of adsorption of gases and vapors for adsorbents with energetically nonuniform surfaces, Chem. Rev. 60 (1960) 235–241. doi:10.1021/cr60204a006.

[35]   M. Thommes, K. Kaneko, A. V. Neimark, J.P. Olivier, F. Rodriguez-Reinoso, J. Rouquerol, K.S.W. Sing, Physisorption of gases, with special reference to the evaluation of surface area and pore size distribution (IUPAC Technical Report), Pure Appl. Chem. 87 (2015). doi:10.1515/pac-2014-1117.

[36]   M. Jagtoyen, F. Derbyshire, Activated carbons from yellow poplar and white oak by H_3PO_4 activation, Carbon N. Y. 36 (1998) 1085–1097. doi:10.1016/S0008-6223(98)00082-7.

[37]   J. Bedia, J.M. Rosas, J. Márquez, J. Rodríguez-Mirasol, T. Cordero, Preparation and characterization of carbon based acid catalysts for the dehydration of 2-propanol, Carbon N. Y. 47 (2009) 286–294. doi:10.1016/j.carbon.2008.10.008.

[38]   G. Alberti, U. Costantino, G. Marletta, O. Puglisi, S. Pignataro, ESCA investigations of amorphous and crystalline zirconium acid phosphates, J. Inorg. Nucl. Chem. 43 (1981) 3329–3334. doi:10.1016/0022-1902(81)80111-X.

[39]   J.L. Colón, D.S. Thakur, C.Y. Yang, A. Clearfield, C.R. Martini, X-ray photoelectron spectroscopy and catalytic activity of α-zirconium phosphate and zirconium phosphate sulfophenylphosphonate, J. Catal. 124 (1990) 148–159. doi:10.1016/0021-9517(90)90111-V.

[40]   D.D. Sarma, C.N.R. Rao, XPES studies of oxides of 2nd row and 3rd row transition-metals including rare-earths, J. Electron Spectros. Relat. Phenomena. 20 (1980) 25–45. doi:10.1016/0368-2048(80)85003-1.

[41]   R. Weingarten, Y.T. Kim, G.A. Tompsett, A. Fernández, K.S. Han, E.W. Hagaman, W.C. Conner, J.A. Dumesic, G.W. Huber, Conversion of glucose into levulinic acid with solid metal(IV) phosphate catalysts, J. Catal. 304 (2013) 123–134. doi:10.1016/J.JCAT.2013.03.023.

[42]   J.L. Figueiredo, M.F.R. Pereira, M.M.A. Freitas, J.J.M. Órfão, Modification of the surface chemistry of activated carbons, Carbon N. Y. 37 (1999) 1379–1389. doi:10.1016/S0008-6223(98)00333-9.

[43]   X. Wu, L.R. Radovic, Inhibition of catalytic oxidation of carbon / carbon composites by phosphorus, Carbon N. Y. 44 (2006) 141–151. doi:10.1016/j.carbon.2005.06.038.

[44]   P.L. Alexandre Maitre, Solid state reaction of zirconia with carbon, Solid State Ionics. 104 (1997) 109–122. doi:10.1016/S0167-2738(97)00398-6.

[45]   C. Ang, T. Williams, A. Seeber, H. Wang, Y.B. Cheng, Synthesis and evolution of zirconium carbide via Sol-Gel route: Features of nanoparticle oxide-carbon reactions, J. Am. Ceram. Soc. 96 (2013) 1099–1106. doi:10.1111/jace.12260.

[46]   J.M. Rosas, R. Ruiz-Rosas, J. Rodríguez-Mirasol, T. Cordero, Kinetic study of the oxidation resistance of phosphorus-containing activated carbons, Carbon N. Y. 0 (2012) 1523–1537. doi:10.1016/j.carbon.2011.11.030.

[47]   J. Perez-Ramirez, R.J. Berger, G. Mul, F. Kapteijn, J.A. Moulijn, The sixflow reactor technology - A review on fast catalyst screening and kinetic studies., Catal. Today. 60 (1999) 93–109. doi:10.1016/S0920-5861(00)00321-7.

[48]   D.E. Mears, The role of axial dispersion in trickle-flow laboratory reactors, Chem. Eng. Sci. 26 (1971) 1361–1366. doi:10.1016/0009-2509(71)80056-8.

[49]   J.A. Moulijn, A. Tarfaoui, F. Kapteijn, General aspects of catalyst testing, Catal. Today. 11 (1991) 1–12. doi:10.1016/0920-5861(91)87002-5.

[50]   R. Ruiz-Rosas, J. Bedia, J.M. Rosas, M. Lallave, I.G. Loscertales, J. Rodríguez-Mirasol, T. Cordero, Methanol decomposition on electrospun zirconia nanofibers, Catal. Today. 187 (2012) 77–87. doi:10.1016/j.cattod.2011.10.031.

[51]   R.T. Carr, M. Neurock, E. Iglesia, Catalytic consequences of acid strength in the conversion of methanol to dimethyl ether, J. Catal. 278 (2011) 78–93. doi:10.1016/j.jcat.2010.11.017.

[52] S. Cheng, G.Z. Peng, A. Clearfield, Decomposition of Alcohols over Zirconium and Titanium Phosphates, Ind. Eng. Chem. Prod. Res. Dev. 23 (1984) 219–225. doi:10.1021/i300014a008.

[53] T.R. Forester, R.F. Howe, In Situ FTIR Studies of Methanol and Dimethyl Ether in ZSM-5, J. Am. Chem. Soc. 109 (1987) 5076–5082. doi:10.1021/ja00251a004.

[54] Y. Ono, T. Mori, Mechanism of methanol conversion into hydrocarbons over ZSM-5 zeolite, J. Chem. Soc. Faraday Trans. 1 Phys. Chem. Condens. Phases. 77 (1981) 2209–2221. doi:10.1039/F19817702209.

[55] J. Ereña, I. Sierra, M. Olazar, A.G. Gayubo, A.T. Aguayo, Deactivation of a CuO-ZnO-Al_2O_3/γ-Al_2O_3 catalyst in the synthesis of dimethyl ether, Ind. Eng. Chem. Res. 47 (2008) 2238–2247. doi:10.1021/ie071478f.

[56] M. Mollavali, F. Yaripour, H. Atashi, S. Sahebdelfar, Intrinsic kinetics study of dimethyl ether synthesis from methanol on γ-Al_2O_3 catalysts, Ind. Eng. Chem. Res. 47 (2008) 3265–3273. doi:10.1021/ie800051h.

[57] B.C. Gates, L.N. Johanson, Langmuir-hinshelwood kinetics of the dehydration of methanol catalyzed by cation exchange resin, AIChE J. 17 (1971) 981–983. doi:10.1002/aic.690170435.

[58] V. Vishwanathan, H.S. Roh, J.W. Kim, K.W. Jun, Surface properties and catalytic activity of TiO_2-ZrO_2 mixed oxides in dehydration of methanol to dimethyl ether, Catal. Letters. 96 (2004) 23–28. doi:10.1023/B:CATL.0000029524.94392.9f.

[59] G. Pop, G. Bozga, R. Ganea, N. Natu, Methanol Conversion to Dimethyl Ether over H-SAPO-34 Catalyst, Ind. Eng. Chem. Res. 48 (2009) 7065–7071.

[60] K.S. Ha, Y.J. Lee, J.W. Bae, Y.W. Kim, M.H. Woo, H.S. Kim, M.J. Park, K.W. Jun, New reaction pathways and kinetic parameter estimation for methanol dehydration over modified ZSM-5 catalysts, Appl. Catal. A Gen. 395 (2011) 95–106. doi:10.1016/j.apcata.2011.01.025.

[61]   G. Berčič, J. Levee, Intrinsic and Global Reaction Rate of Methanol Dehydration over γ-Al$_2$O$_3$ Pellets, Ind. Eng. Chem. Res. 31 (1992) 1035–1040. doi:10.1021/ie00004a010.

[62]   Y. Tavan, S.H. Hosseini, From laboratory experiments to simulation studies of methanol dehydration to produce dimethyl ether reaction-Part II: Simulation and cost estimation, Chem. Eng. Process. 73 (2013) 144–150. doi:10.1016/j.cep.2013.08.006.

Chapter 5

Biomass-derived activated carbon catalysts for the direct dimethyl ether synthesis from syngas

5.0.-Abstract

The direct DME synthesis from syngas was investigated by using activated carbons as catalysts. Two kinds of activated carbons, prepared by physical (by CO_2 partial gasification) and chemical (with phosphoric acid) activation of olive stones, were used as supports for the preparation of the catalysts. The chemically activated carbon presented a considerable amount of chemically stable surface phosphorus complexes, which played an important role on the catalytic performance of the prepared catalysts. A Zr-loaded P-containing activated carbon was used as methanol dehydration catalyst. For the preparation of the methanol synthesis catalyst, Cu-Zn was loaded on the activated carbon supports. The presence of phosphorus on the carbon support resulted in a strong metal-support interaction, lowering the catalytic activity of the catalyst. The catalyst that did not contain phosphorus showed noticeable activity for methanol synthesis and, thus, it was used as the methanol synthesis catalyst for preparing bifunctional catalytic beds. The physical mixing of the methanol synthesis and methanol dehydration catalysts resulted in the preparation of carbon-based catalytic beds, which performed very efficiently in the direct DME synthesis from syngas. Different mass ratios of the individual catalysts were studied. An acid/metallic catalyst mass ratio of 2 provided the catalytic bed with enough acid sites for making the overall syngas to DME process kinetically controlled by the methanol synthesis reaction.

5.1.-Introduction

Dimethyl ether (DME) is a chemically stable, colorless, non-toxic, non-carcinogenic, and environmentally friendly compound presenting a characteristic odor. Thanks to its physical and chemical properties, similar to liquified petroleum gases (LPG) [1] and conventional diesel [2,3], plus the clean combustion achieved when used as fuel [4], this compound is considered as one of the most promising alternatives to petroleum derived fuel, and thus, its production is the object of much research [5–7].

DME can be produced by two alternative processes; a two-step catalytic process (so-called indirect process), which involves a first stage for methanol

synthesis from syngas (Eq. (5.1) and (5.2)) on Cu-based catalysts [8–10] and a second stage for the selective dehydration of methanol to DME (Eq. (5.3)) on a solid acid catalyst [11–14]; and a one-step process (so-called direct process), in which synthesis gas is fed to a single reactor containing a bifunctional catalyst, where both methanol synthesis, in parallel with the water gas shift reaction (WGSR) (Eq. (5.4)), and the selective methanol dehydration take place [6,15–19].

$$2CO + 4H_2 \leftrightarrow 2CH_3OH \quad (\Delta H_r^0 = -90.8 \text{ kJ·mol}^{-1}) \qquad \text{Eq. (5.1)}$$

$$CO_2 + 3H_2 \leftrightarrow CH_3OH + H_2O \quad (\Delta H_r^0 = -49.5 \text{ kJ·mol}^{-1}) \qquad \text{Eq. (5.2)}$$

$$2CH_3OH \leftrightarrow CH_3OCH_3 + H_2O \quad (\Delta H_r^0 = -21.3 \text{ kJ·mol}^{-1}) \qquad \text{Eq. (5.3)}$$

$$H_2O + CO \leftrightarrow H_2 + CO_2 \quad (\Delta H_r^0 = -41.1 \text{ kJ·mol}^{-1}) \qquad \text{Eq. (5.4)}$$
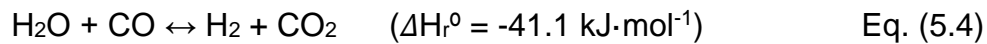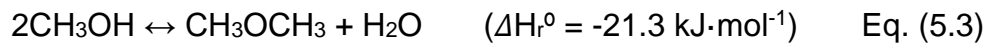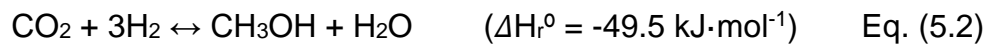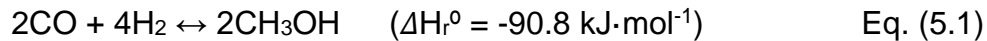
Although DME production is currently carried out by the indirect process, the prospects for the development of a DME-based economy depends on the feasibility of the direct DME synthesis route [20]. The main motivation for using the direct route instead of the indirect one relies on the thermodynamic limitations affecting the latter. Chemical reactions involved in methanol synthesis are reversible and they are limited by thermodynamic equilibrium, which is a function of the temperature, pressure and the synthesis gas composition. This thermodynamic limitation results in a low synthesis gas conversion per-pass, increasing the operating costs related to methanol separation and synthesis gas recirculation [21]. The use of the direct DME synthesis route, allows for in-situ consuming the generated methanol, via dehydration to DME, reducing the equilibrium constrains affecting the methanol synthesis in this way. This thermodynamic advantage permits work at lower pressure and/or higher temperature achieving a higher synthesis gas conversion per pass [17,22]. On the other hand, water generated in the methanol dehydration reaction (Eq. (5.3)), can be removed from the reaction media by means of the WGSR (Eq. (5.4)), yielding H_2 and favoring the methanol dehydration reaction. This feature is of high interest when using a CO-enriched synthesis gas, such as that obtained via biomass gasification [23,24]. In this sense, the use of biomass derived synthesis gas for this process would lead to a considerable reduction of greenhouse gas

emissions in this process, promoting the transition to an energy system that reduces dependence on fossil fuels in a scenario that contemplates, on the one hand, the scarcity of fossil fuels, and on the other hand the growth of global demand and the impact of emissions on the environment.

The catalysts used for the direct DME synthesis route are composed of two active phases, one accounting for the methanol synthesis and another one for the methanol dehydration. As a component for methanol synthesis, the most commonly used catalytic phase is the $Cu/ZnO/Al_2O_3$ ternary system [8]. The acid component involved in these catalysts must present a moderate acid strength, being enough so as to promote methanol dehydration, but not too high, so as to avoid further DME dehydration to olefins and higher hydrocarbons (which are related to coke formation). The most commonly studied acid functions for bifunctional catalysts are γ-Al_2O_3, HZSM-5 [18,25,26], HMCM-22 [27], ferrierite [28] and SAPOs [20].

In the last decades, activated carbons have been widely investigated as catalysts and catalyst supports. These materials present remarkable features, such as their high thermal and chemical stability, and their high specific surface area. Moreover, they can be obtained from several kinds of lignocellulosic waste [29,30], giving rise to economic as well as environmental advantages. Despite the potential they have exhibited, to the best of our knowledge, the use of activated carbon-based catalysts for the direct DME synthesis has not been reported in the literature, existing only some studies dealing with the preparation of the application of activated carbons for the methanol dehydration reaction [31–33]. The materials prepared in these studies presented low thermally stable acid groups, which resulted in a fast deactivation when the reaction temperature was increased, and thus, they cannot be applied for the preparation of bifunctional catalyst for the direct DME synthesis. On the other hand, it has been also reported that the preparation of activated carbons by chemical activation with phosphoric acid, yields activated carbons, which contain high thermal and chemically stable oxygen-phosphorus acid surface groups [34–36]. The use of these activated carbons for the methanol dehydration reaction, showed that, although these materials performed very efficiently under air atmosphere, achieving a selectivity to DME higher than 95 %, they were fast deactivated under a non-oxidizing

atmosphere [37], and thus, they cannot be applied as the acid component of bifunctional catalysts neither.

On this issue, we have recently reported that the modification of phosphorus-containing activated carbons with zirconium leads to the obtention of carbon materials presenting zirconium phosphate species, which performed very efficiently in the methanol dehydration reaction under non-oxidizing atmosphere [38]. In this sense high steady-state methanol conversion values, keeping a selectivity to DME higher than 97 %, were obtained in the whole range of temperatures studied (250-400 ºC) [39]. Therefore, these activated carbon catalysts could be feasibly used as the methanol dehydration component in the direct DME synthesis from syngas.

In this work we report the use of activated carbon catalysts for the direct syngas to DME. As for methanol synthesis component, different activated carbons were loaded with Cu/Zn, in order to study the effect of the surface chemistry on the catalytic activity, and as a component for methanol dehydration, a Zr-loaded P-containing-activated carbon was used.

5.2.-Experimental method

5.2.1.-Preparation of the activated carbons.

Two kinds of activated carbons were prepared. On the one hand, an activated carbon was prepared by physical activation. For this process, 15 g of olive stone, an agri-food industry residue, was carbonized and then it was partially gasified with CO_2. Both stages were carried out in a conventional tubular laboratory furnace. In the carbonization step, the sample was heated at 10 ºC/min up to 800 ºC, keeping this temperature for 2 h, under continuous N_2 flow (150 cm^3/min STP). Afterwards, the carbonized sample was partially gasified using a continuous CO_2 flow (150 cm^3/min STP) at the same temperature for 7 h, obtaining a 42 % burn-off. The final carbon presented a final mass yield of 14 % based on the mass of dried olive stone. Finally, this sample was grinded and sieved (100-300 μm) and was denoted as *ACG*. On the other hand, an activated carbon was prepared via chemical activation of olive stones, with phosphoric

acid. For the activation process, 10 g of olive stone was impregnated with H_3PO_4 85 %(w/w) aqueous solution, at room temperature and dried for 24 h at 60 ºC. An impregnation ratio (H_3PO_4/olive stone mass ratio) value of 2 was used in this work. Once dried, the impregnated substrate was activated in a conventional tubular furnace under continuous N_2 flow (150 cm^3/min STP) at 800 ºC for 2h. The activated sample was cooled to room temperature inside the tubular furnace, keeping the same N_2 flow and afterwards it was washed with distilled water at 60 ºC, until achieving a neutral pH and a negative phosphate analysis in the eluate [40]. The activated carbon presented a final mass yield of 39% based on the mass of dried olive stone and was denoted as *ACP*. Finally, activated carbon was grinded and sieved (100-300 μm).

5.2.2.- Catalysts preparation.

To prepare the carbon-based catalysts used in this work, the activated carbons were loaded with Cu, Zn and Zr salts. Figure 5.1 shows an outline of the procedures and nomenclature used for the preparation of the catalysts.

5.2.2.1.- Methanol dehydration catalyst preparation. Zr loading.

Zr loading was carried out by incipient wetness impregnation. A 5 %(w/w) of zirconium was loaded on the activated carbon obtained by chemical activation, ACP, using a $ZrO(NO_3)_2$ in water solution. Once impregnated, the sample was dried overnight at 120 ºC and then calcined at 250 ºC for 2 h in a tubular furnace under continuous air flow (150 cm^3/min STP). This sample was denoted as *ACPZr*.

5.2.2.2.- Methanol synthesis catalysts preparation. Cu-Zn loading.

Cu-Zn loading was carried out on the two different activated carbons, ACG and ACP. In addition, the use of the methanol dehydration catalyst, ACPZr, as support for the Cu-Zn metallic phase was addressed. The metal loading process was carried out by pore-volume impregnation of the dried samples. In this process, an appropriate amount of $Cu(NO_3)_2 \cdot 3H_2O$ and $Zn(NO_3)_2 \cdot 6H_2O$ was added to a known quantity of activated carbon to prepare catalysts with a Cu and

Zn loading of 10.5 and 5.5 %(w/w), respectively. The impregnated carbons were dried at 120 °C for 24h and finally calcined at 300 °C for 4h under continuous N_2 flow (150 cm^3/min STP). The catalyst obtained were denoted by adding *-CuZn* to the name of the parent carbon.

5.2.2.3.- Bifunctional catalytic beds preparation.

The preparation of bifunctional catalytic beds was carried out by physical mixing of the corresponding methanol synthesis and methanol dehydration components, by using different acid/metallic mass ratios. Physical mixtures were denoted as *Metallic component name + X Acid component name*, being *X* the Acid/metallic mass ratio.
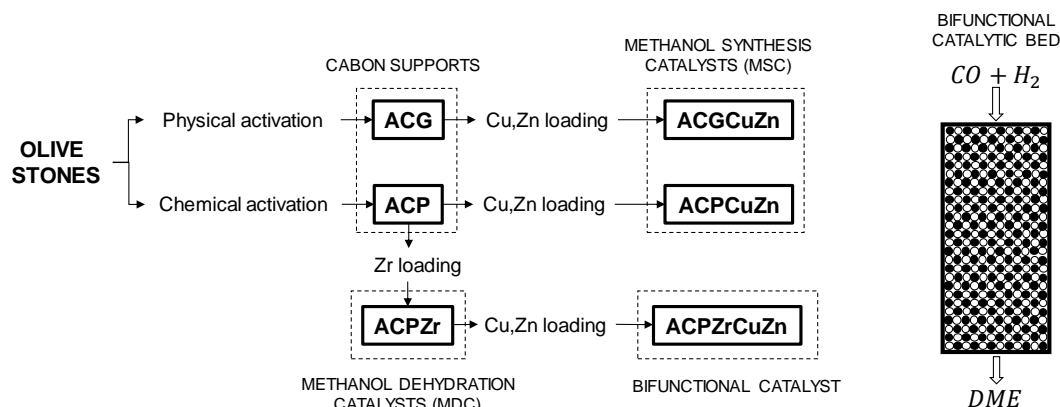
Figure 5.1. Schematic diagram of the procedures and nomenclature used for sample preparation of the catalysts and the bifunctional catalytic beds.

5.2.3.-Characterization of the carbon catalysts

The porous texture of the activated carbons and catalysts was characterized by N_2 adsorption–desorption at -196 °C and by CO_2 adsorption at 0 °C, performed in an ASAP 2020 equipment (Micromeritics). Samples were previously outgassed for 8 h at 150 °C. From the N_2 adsorption-desorption isotherm, the apparent surface area (A_{BET}) was determined applying the BET equation [41], the micropore volume (V_t^{N2}) and the external surface area were calculated using the t-method [42] and the mesopore volume (V_{mes}^{N2}) was

147

determined as the difference between the adsorbed volume at a relative pressure of 0.99 and the micropore volume of V_t^{N2}. The narrow micropore volume (V_{DR}^{CO2}) and surface area (A_{DR}^{CO2}) were calculated by the Dubinin–Radushkevich equation [43], applied to the CO_2 adsorption isotherm.

The surface chemistry of the samples was analyzed by X-ray photoelectron spectroscopy (XPS). XPS analyses of the samples were obtained using a VersaProbe II ESCA 5701 model Physical Electronics apparatus, with Al Kα radiation (1486.6 eV). For the analysis of the XPS peaks, the C1s peak position was set at 284.5 eV and used as reference for the other peaks [44,45].

The reducibility of the Cu species present on the catalysts was studied by temperature programmed reduction (H_2-TPR). For these analyses, 50 mg of dried sample was loaded in a quartz fixed-bed reactor and were heated up to 100 ºC under helium flow. Then the helium flow was switched to a 10 %(v/v) H_2 in helium stream, and kept for 30 min. Finally, the sample was heated up to 350 ºC at a heating rate of 5 ºC/min. H_2 consumption was monitored by mass spectroscopy (Pfeiffer Omnistar GCD-301), registering the signal m/z 2.

The total acidity and acid strength distribution of the methanol dehydration catalyst was determined by temperature programmed desorption of ammonia (NH_3-TPD). In these analyses 100 mg of dried sample was heated up to 100 ºC under helium flow and then it was saturated with NH_3 (20 %(v/v) in helium) for 15 minutes at this temperature. Afterwards, the weakly adsorbed NH_3 was desorbed in continuous helium flow at 100 ºC until no NH_3 was detected in the outlet stream. The NH_3-TPD experiment was carried out by rising the temperature up to 500 ºC at a heating rate of 10 ºC/min. The outlet NH_3 concentration was registered using a TCD-detector.

5.2.4.-Catalytic experiments.

The catalytic experiments for the direct DME synthesis from synthesis gas were performed in a PID Eng. & Tech. Microactivity equipment, which is provided with a stainless steel fixed-bed reactor and allows for operating at high temperature and pressures. Prior to stating the reaction, the catalyst was in-situ reduced at 270 ºC under H_2 flow (50 mL/min) for 2 h. After the reduction step, the

temperature was set to the reaction value, and afterwards, the pressure was slowly increased up to the desired value. Finally, the synthesis gas was introduced. To prevent the condensation of any compound, all lines were heated up to 120 ºC. The outlet gas concentrations were analyzed by on-line gas chromatography (Perkin-Elmer Clarus 500 GC equipped with TCD and FID detectors). The used columns were a Permanent gases active carbon 80/100 mesh for CO and CO_2 analysis and a 1.9m x 1/8" x 2.1mm Porapak N 80/100 + 0.5m x 1/8" x 2.1mm Porapak Q 80/100 column for methanol, DME and light hydrocarbons separation. N_2 was used as internal standard for CG analyses.

The conversion was defined as the ratio of the amount of CO converted to the amount of CO supplied to the reactor. The selectivity (in %mol) was defined as the mole ratio of carbon moles in a specific product referred the moles of converted CO into all the products formed. The yield to DME was calculated as the product of the CO conversion and the selectivity to DME.

5.3.-Results and discussion

5.3.1 Characterization of the carbon catalysts.

Figure 5.2 shows the N_2 adsorption-desorption isotherms at -196 ºC of the different activated carbon materials prepared in this study. Physically activated carbon, ACG, presented a type I a isotherm [46], adsorbing almost all N_2 volume at low relative pressures, which is characteristic of a predominantly microporous texture. Chemically activated carbon, ACP, showed a type I b isotherm, associated to the presence of a broad range of wider micropores and narrow mesopores. The existence of a H4 type hysteresis loop is noticeable, closing at a relative pressure value of 0.4, indicative of capillary condensation in mesopores [46].

After the metal deposition, both activated carbons presented a reduction in their porous texture. The methanol dehydration catalyst, ACPZr, showed a slight decrease in the volume of N_2 adsorbed in the range of the low relative pressures, as compared to the parent carbon, ACP, indicating a reduction of the wider microporosity, due to Zr loading. Cu-Zn loading resulted in a more

noticeable porosity reduction, given to the higher amount of metal loaded on the carbon supports. In this sense, the three samples used as Cu-Zn support, ACG, ACP and ACP-Zr, showed a reduction in the volume of N_2 adsorbed, but in this case at a very low relative pressures, which indicated a narrow micropore reduction or blockage.
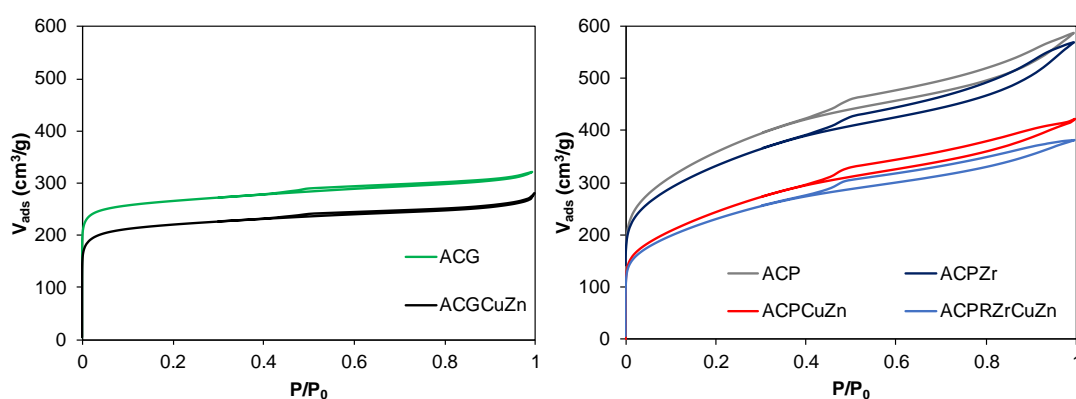
Figure 5.2. Nitrogen adsorption–desorption isotherms at −196 ∘C of the carbon materials.

Table 5.1 shows the textural parameters obtained from N_2 adsorption-desorption and CO_2 adsorption isotherms. Both activated carbons present a well-developed porous texture and high surface areas. Physically activated carbon, ACG, presented an A_{BET} value similar to A_{DR}, indicating a microporous texture. The similarity between V_t and V_{DR} further confirmed the presence of a narrow microporous texture. The chemically activated carbon, ACP, presented a comparable A_{BET} value to that obtained for the physically activated carbon, ACG. However, attending to the higher valuer of A_{BET} as compared to A_{DR}, this sample presented a wider microporous texture, as compared to the physically activated carbon. Moreover, the higher mesopore volume value (V_{mes}) when comparing with the micropore volume one (V_t), together with the high external surface area value (A_t), suggested a high contribution to mesoporosity in this sample.

Once metal loaded, both activated carbons showed a decrease in the textural parameters as compared to the parent activated carbon. The Zr loaded chemically activated carbon showed slight decrease, in general, in the textural parameters when compared to the ones of the parent activated carbon,

suggesting that Zr was homogeneously distributed both on the external and internal surface of the activated carbon particles. After Cu-Zn loading a more significant decrease in the textural parameters is observed in the samples. In these cases, A_{BET} and A_{DR} decreased in a similar way, indicating a reduction in the microporosity of these samples. The decrease in the V_t and V_{DR} values suggested the blockage of the narrow micropores due to metal deposition.

Table 5.1. Characteristic parameters of the porous texture for the prepared carbon-based materials.

	N₂ Isotherm					CO₂ Isotherm	
	A_{BET}	V_p	V_{mes}	A_t	V_t	A_{DR}	V_{DR}
	(m²/g)	(cm³/g)	(cm³/g)	(m²/g)	(cm³/g)	(m²/g)	(cm³/g)
ACG	1040	0.49	0.11	89	0.38	855	0.34
ACGCuZn	750	0.43	0.11	87	0.31	595	0.24
ACP	1260	0.9	0.42	295	0.49	470	0.19
ACPZr	1190	0.88	0.42	270	0.46	500	0.20
ACPCuZn	880	0.65	0.30	210	0.35	445	0.18
ACPZrCuZn	830	0.59	0.27	200	0.32	375	0.15

X-ray photoelectronic spectroscopy (XPS) analyses were carried out to evaluate the surface chemical composition of the carbons. Table 5.2 reports the atomic surface composition of the samples. Both activated carbon supports, ACG and ACP, were mainly composed by carbon and oxygen (91.7 and 89.7 % (w/w), respectively) and oxygen (7.3 and 7.2 % (w/w), respectively). In addition, the chemically activated carbon, ACP, presented a considerable amount of phosphorus (3.1 % (w/w)), presumably in form of phosphate groups [34]. This presence of phosphorus has been attributed to the activation step with phosphoric acid [47], which seems to proceed through the formation of phosphate and polyphosphate bridges that connect and crosslink biopolymer fragments [48]. As a result of this activation mechanism part of these phosphorus complexes remain chemically bonded to the carbon surface, even after the washing step [49].

After Zr loading on the chemically activated carbon, ACP, an increase in both Zr and O is observed. Attending to the surface composition, a higher amount of O, when compared to the maximum theoretically introduced if Zr were

deposited on the carbon surface in form of ZrO_2, was observed (see ACPZr in Table 5.2). This fact could be associated to the surface oxidation of these activated carbon catalysts during the thermal stabilization process (calcination) at 250 ºC [34]. The three samples loaded with Cu-Zn exhibited the presence of these elements, Cu and Zn, on their surface. In addition, as occurred when loading with zirconium, the oxygen content increased to a higher extent than that expected considering the incorporation of Cu and Zn as oxides (CuO and ZnO). In this case, the increase in the oxygen content could be related to the metal salts decomposition during thermal treatment, which has been reported to yield oxygen groups on the activated carbon surface [50].

Table 5.2. Mass surface concentration values obtained by XPS.

Catalyst	Mass surface concentration (%)					
	C	O	Cu	Zn	P	Zr
ACG	91.7	7.3	-	-	-	-
ACGCuZn	50.4	17.3	25.5	6.8	-	-
ACP	89.7	7.2	-	-	3.1	-
ACPZr	59.8	19.6	-	-	5.7	14.9
ACPCuZn	36.6	23.3	24.3	11.3	4.5	-
ACPZrCuZn	36.4	26.6	13.5	7.1	4.4	12.1

In order to analyze in depth the chemical surface of the activated carbon catalysts, the XPS spectra were examined. Figure 5.3 shows the normalized high resolution multiregional XPS spectra for phosphorus, zirconium and copper. The P2p spectrum of the chemically activated carbon, ACP, showed a main peak at 133.2 eV, associated to the presence of pentavalent tetracoordinated phosphorus, presumably forming $C-O-PO_3$ and $C-PO_3/C_2-PO_2$ surface groups bonded to the carbon surface [49,51]. After Zr loading, the P2p spectrum for ACPZr shifted to higher binding energy values (133.7 eV), indicating the oxidation the phosphorus surface groups, which probably occurred during the calcination stage at 250 ºC (see ACPZr in Figure 5.3a) [40]. Cu-Zn loading process did not affect the P2p spectra of the samples to a significant extent. The normalized Zr3d spectra the two Zr-containing carbons, ACPZr and ACPZrCuZn, exhibited the two 3d peaks separated by 2.3 eV, characteristic of the of the tetravalent Zr^{4+}. The binding energy at which the $Zr3d_{5/2}$ appeared (183.1 eV), in both cases, was very

similar to that reported for when analyzing zirconium phosphates [52,53], indicating the coordination of Zr atoms with a high number of strongly polarized oxygens, forming P-O-Zr bonds, and thus suggesting the presence of zirconium phosphate species bonded to the activated carbon surface [38].

The normalized $Cu2p_{3/2}$ XPS spectra of the catalysts showed appreciable differences, which could be associated to the surface chemistry of the activated carbon support. On the one hand, the catalyst prepared by using the physically activated carbon as support, ACGCuZn, showed a binding energy value of 933.8 e.V. for the $Cu2p_{3/2}$ peak, and the presence of the strong satellite peaks between 940 and 945 eV, which are characteristic of Cu^{2+} in form of CuO [54,55]. On the other hand, when analyzing the catalyst prepared by using the chemically activated carbon as support, ACPCuZn, it could be seen that the $Cu2p_{3/2}$ peak showed a doublet structure and a significant decrease of the satellite peaks between 940 and 945 eV, which suggested the co-existence of non-reduced and reduced copper species. Similar observations have been reported when analyzing copper phosphate glasses [56,57]. These studies claimed that some of the Cu^{2+} was reduced to Cu^+ upon going from CuO to Cu phosphate, being this doublet structure in the $Cu2p_{3/2}$ peak associated to the presence of both Cu^+ (932.5 eV) and Cu^{2+} (934 eV) in the copper phosphate glass [57]. Given that the chemically activated carbon used as support in this study showed the presence of phosphorus, in form of phosphate groups, chemically bonded to its surface, the results here obtained suggested that Cu was interacting with P, forming copper phosphate species. ACPZrCuZn, also containing phosphorus, showed the same doublet structure for the $Cu2p_{3/2}$ peak. The $Cu2p_{3/2}$ peak of the phosphorus-containing samples was deconvoluted into two different peaks, associated to Cu^+ and Cu^{2+}, at binding energies of 932.5 and 934 eV, respectively. The results showed that 65 % of the total Cu was in form of Cu^+ in the sample ACPCuZn, whereas a value of 45 % was obtained for ACPZrCuZn. This difference could be justified given that the presence of Zr forming zirconium phosphate species on the sample ACPZrCuZn partially avoided the formation of copper phosphate species, remaining a higher amount of the Cu as CuO.
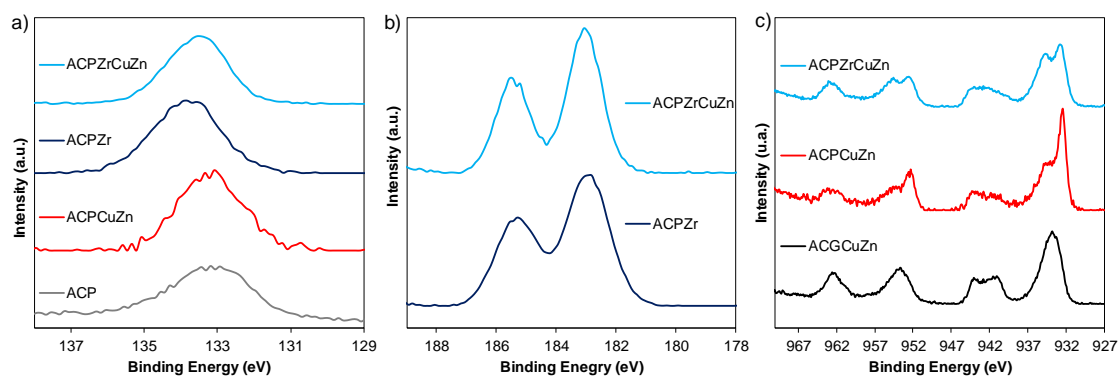
Figure 5.3. Normalized XPS spectra for the prepared activated carbon samples. **a)** P2p, **b)** Zr3d and **c)** Cu2p.

The reducibility of the Cu species present on the activated carbon catalysts was studied by temperature programmed reduction (H_2-TPR). Figure 5.4 shows the H_2 consumption as a function of the temperature during H_2-TPR analysis for the Cu-Zn-loaded activated carbos. According to the literature, ZnO is not reducible under H_2-TPR conditions [58]. Moreover, the gasification of the activated carbon support has been also reported to be very low, only being observed small amounts of methane at temperatures above 300 ºC [59]. Therefore, the H_2 consumption measured during H_2-TPR was only related to the reduction of the Cu species. ACGCuZn, presented a main H_2 consumption peak at about 175 ºC, which was associated to the reduction of highly dispersed CuO [60] and a second at about 200 ºC, related to bulk CuO reduction [61]. The temperature at which the reduction of the CuO species occur depends on their particle size (the bigger particle size, the higher reduction temperature) [24] and also on the interaction between Cu and the other compounds present in the material [62,63]. The CuO reduction temperature for this catalyst was considerably lower than that reported for CuO-ZnO-Al_2O_3-based catalysts (about 300 ºC) [15,64,65]. This fact is attributed to the weak interaction CuO-activated carbon as compared to other oxidic supports [59]. The phosphorus-containing samples, ACPCuZn and ACPZrCuZn showed a much lower H_2 consumption as compared to the sample prepared by using the physically activated carbon (not containing P) as support. Along this line, ACPCuZn, showed a negligible H_2 consumption, indicating the lack of reducibility of the Cu species present on this catalyst. ACPZrCuZn, showed a slightly higher H_2-consumption, as compared to

ACPCuZn, indicating the reducibility of only part of the Cu species on the catalyst. The above results evidenced that only CuO species were reduced, whereas Cu phosphate species present on the activated carbon surface were not reducible under H_2-TPR conditions.
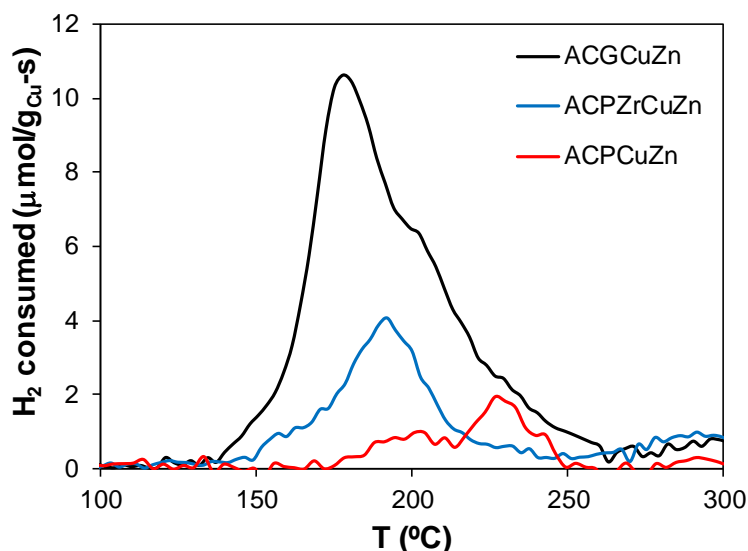
Figure 5.4. H_2-TPR profile of Cu-Zn loaded activated carbon catalysts.

Figure 5.5 presents the NH_3-TPD profile obtained for the methanol dehydration catalysts used in this study, ACPZr. The temperature at which ammonia desorption occurs depends on the strength of the acid sites present on the materials, being the weaker centers the ones in which ammonia desorption is occurring at the lower temperature. The acid strength required for efficiently dehydrating methanol to DME must be enough so as to promote methanol dehydration, but not too high, so as to avoid further DME dehydration to olefins and higher hydrocarbons (which are related to coke formation) [66]. The acid catalyst here presented desorbed most of the ammonia at a temperature lower than 300 ºC, which highlighted the existence of acid sites presenting a weak/moderate strength. In this line, this weak/moderate acid character conferred the catalyst a suitable acidity for the selective methanol dehydration to DME [38,39].
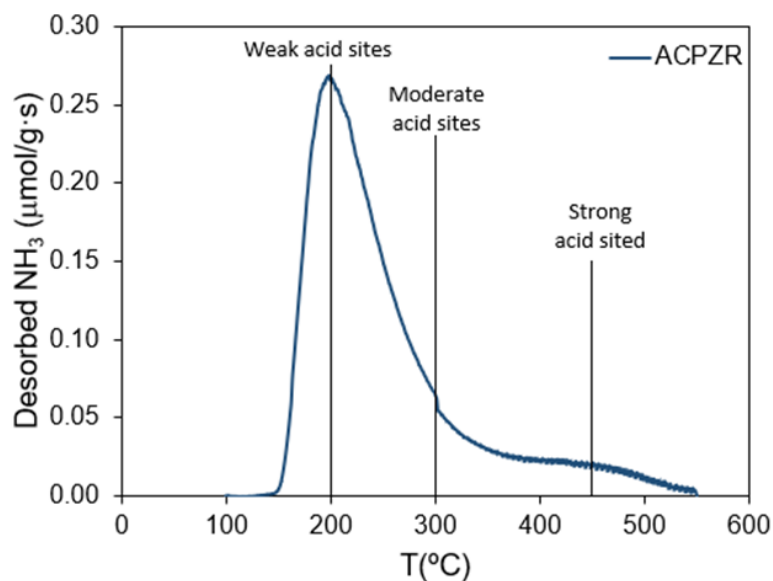
Figure 5.5. Ammonia TPD of the methanol dehydration catalyts, ACPZr.

5.3.2 Catalytic experiments.

The Cu-Zn-containing carbon catalysts, ACGCuZn, ACPCuZn, and ACPZrCuZn, were first analyzed in order to stablish the most suitable methanol synthesis catalyst for the preparation of the bifunctional catalytic beds. Figure 5.6 shows the CO conversion and selectivity to the main reaction products as a function of the temperature for the carbon catalysts (T = 250 – 300 ºC, GHSV = 36.4 $L \cdot g_{Cu}^{-1} \cdot s^{-1}$, P = 45 bar, H_2/CO = 3). ACGCuZn showed noticeable CO conversion values in the temperature range studied. Attending to the selectivity to the main reaction products, it can be observed that a high selectivity to methanol (S_{MeOH} = 82 %) was obtained at 250 ºC, which decreased when rising the temperature due to the formation of DME and CO_2, via methanol dehydration and water gas shift reaction, respectively. The dehydration capability of this catalyst under syngas to DME conditions was surprising, given that the parent activated carbon support, ACG, has been reported to be not active for methanol dehydration [38,39], and Cu-based catalysts have been also reported to form methanol through CO hydrogenation with a very high selectivity [67,68]. Therefore, the methanol dehydration capability of this material must be related to the presence of oxygen surface groups bonded to the carbon surface, which

could have been generated during the metal salts decomposition thermal treatment [69], or in-situ formed under the reaction conditions. ACPCuZn, showed very low CO conversion values, which can be justified based on the lack of reducibility of the Cu species presented on the surface of this catalyst (See Figure 5.4). ACPZrCuZn, showed a higher CO conversion value, as compared to the other phosphorus-containing sample, ACPCuZn, due to the higher proportion of reducible Cu species in the former. Regarding the selectivity to the main reaction products, it could be observed that this sample presented the highest dehydration activity amongst the prepared catalysts, due to the presence of zirconium phosphate surface groups on the carbon surface, which are capable of promoting the selective methanol dehydration to DME [38,39]. However, despite the higher selectivity to DME value obtained for ACPZrCuZn, as compared to the other catalysts here presented, ACGCuZn showed the highest methanol and DME yields, and thus, this catalyst was chosen to be used as methanol synthesis component for the preparation of bifunctional catalytic beds.
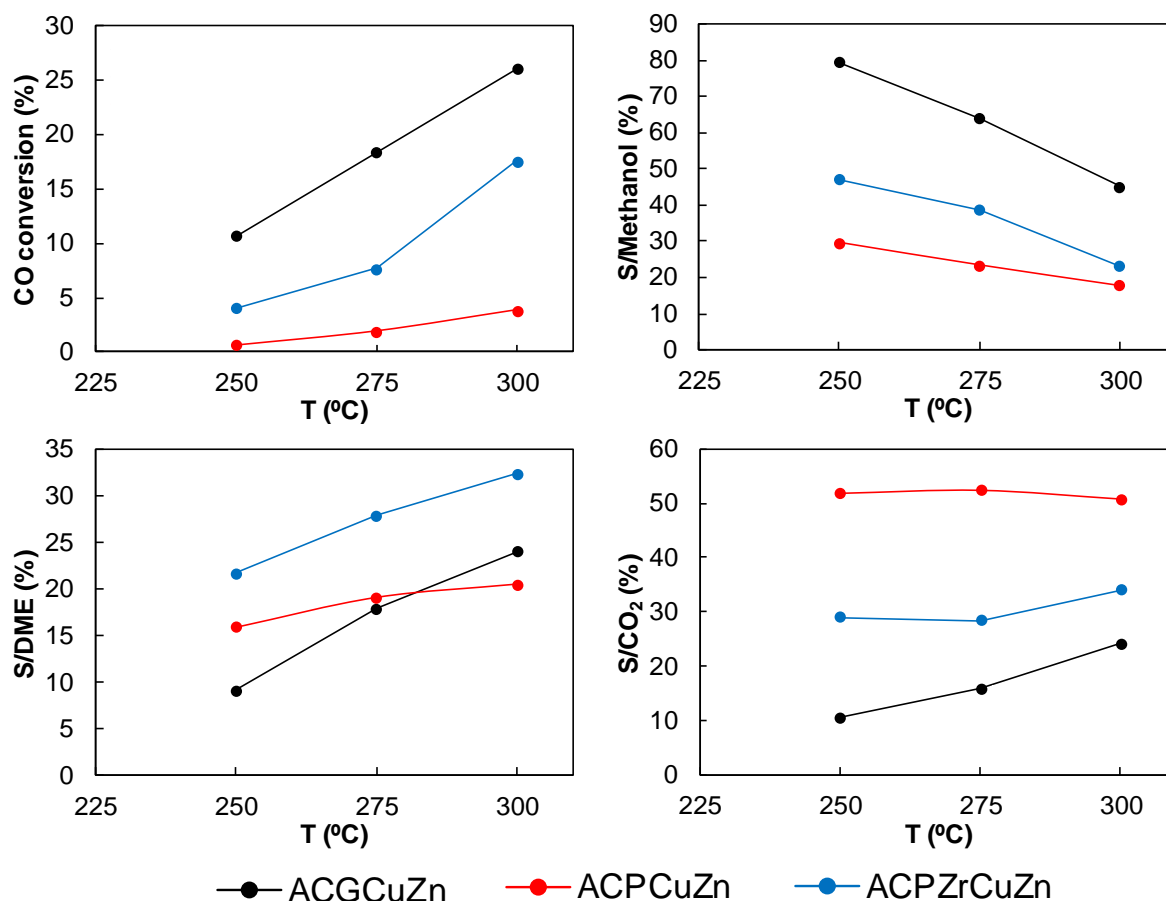
Figure 5.6. CO conversion and selectivity to main reaction products (Methanol, DME and CO_2 a function of temperature for the Cu-Zn-loaded activated carbon catalysts ($H_2/CO = 3$, GHSV=36.4 L·g$_{Cu}^{-1}$·s^{-1}, 45 bar, 3 hours on stream).

The preparation of bifunctional catalytic beds was carried out by physical mixing of the selected methanol synthesis catalyst (ACGCuZn) and the methanol dehydration catalyst (ACPZr), by using different mass ratios of the individual materials. The resulting physical mixtures were used as catalysts for the direct synthesis of DME from syngas. Figure 5.7 presents the CO conversion and selectivity to the main reaction products at different temperatures for the studied catalytic beds (T = 250 – 300 ºC, GHSV = 36.4 L·g$_{Cu}^{-1}$·s^{-1}, P = 45 bar, H_2/CO = 3). As commented above, ACGCuZn presented a high selectivity to methanol, which dropped when increasing the temperature due to the formation of DME and CO_2. When analyzing catalytic bed prepared keeping an Acid/metallic catalyst mass ratio value of 1, ACGCuZn + 1 ACPZr, it could be observed that the carbon-

based methanol dehydration catalyst, was capable of promoting the methanol dehydration reaction under the reaction conditions, thus achieving a higher selectivity to DME value than the isolated methanol synthesis catalyst, ACGCuZn. Moreover, as expected, a higher CO conversion value was obtained due to the synergic effect achieved when integrating both methanol synthesis and dehydration in the same reactor [17,22]. The increase of the acid/metallic catalyst mass ratio to a value of 2, ACGCuZn + 2 ACPZr, resulted in a further increase of the dehydration activity of the catalytic bed, achieving a higher CO conversion and selectivity to DME values as compared to the one obtained keeping an acid/metallic catalysts mass ratio of 1, ACGCuZn + 1 ACPZr. Analyzing the selectivity to the reaction products obtained for the two acid/metallic catalysts mass ratios studied, it could be observed that the products distribution was affected by the reaction temperature in the case of ACGCuZn + 1 ACPZr, showing an increase in the selectivity to DME and CO_2 by increasing the temperature from 250 to 300 ⁰C, where the same CO conversion and product distribution that the obtained for ACGCuZn + 2 ACPZr were achieved. Given that methanol dehydration reaction is kinetically faster than methanol synthesis reaction [70], these results suggested that the use of an acid/metallic catalysts mass ratio of 1 yielded a catalytic bed lacking in acid sites for promoting the methanol dehydration reaction to the maximum value obtained by the use of the catalysts here presented at low temperatures. On the contrary, the reaction product distribution remained almost unchanged when using an acid/metallic catalysts mass ratio of 2, ACGCuZn + 2 ACPZr, which suggested that, in this case, the catalytic bed counted on enough acid sites for promoting methanol dehydration to the maximum value allowable using the carbon-based catalysts here presented in the whole temperature range studied.
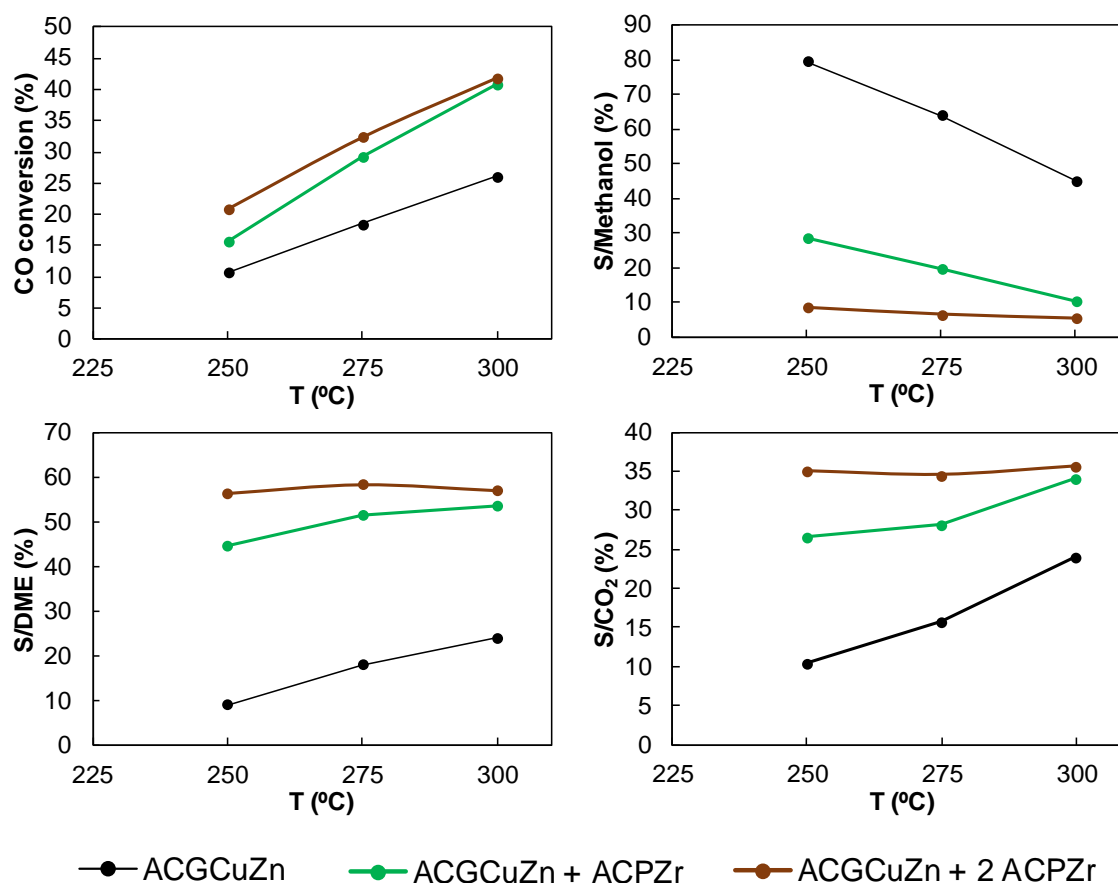
Figure 5.7. CO conversion and selectivity to main reaction products (Methanol, DME and CO_2 a function of temperature for the studied Acid/Metallic components mass ratios ($H_2/CO = 3$, GHSV=36.4 $L \cdot g_{Cu}^{-1} \cdot s^{-1}$, 45 bar, 3 hours on stream).

In the light of the above results, it can be concluded that the direct DME synthesis from syngas can be efficiently carried out by using carbon-based catalysts. In this sense, the metallic function showed a good catalytic behavior for CO hydrogenation, and on the other hand, the acid function exhibited suitable acidic properties for the selective methanol dehydration to DME under the syngas to DME reaction conditions. When comparing the catalytic beds here presented with other catalytic beds/bifunctional catalysts reported in the literature, it is worth remarking that the catalysts present in this study were prepared from inexpensive industrial waste. As regarding the CO conversion obtained, it is important to highlight that, in contrast with other inorganic catalysts [15,71], in which the whole material can be considered as an active phase for the chemical reaction involved, only 5 %(w/w) and 16 % (w/w) of the waste-derived material, for the methanol

dehydration and methanol synthesis catalysts, respectively, should be considered as an active phase for the reactions involved in the syngas to DME process. Therefore, the space velocity used in the present work is considerably higher than that reported for other catalysts. Despite this fact, the catalysts here presented showed a noticeable catalytic activity, making it possible to achieve CO conversion values comparable to that reported for other catalysts [7,20,55,67]. The selectivity to DME values were also outstanding, showing a value of 58.4 % at 275 ºC, which is a high value when compared to other catalysts reported in the literature [67,72].

5.4.-Conclusions

The direct DME synthesis from syngas was investigated by using activated carbon catalysts. Two kinds of activated carbons, prepared by physical (by CO_2 partial gasification) and chemical (with phosphoric acid) activation of olive stones, were used as supports for the preparation of the catalysts. The main difference between them was the presence of chemically stable phosphorus surface groups, mainly in form of $C-O-PO_3$ groups, on the activated carbon prepared via chemical activation with phosphoric acid.

As for the methanol dehydration catalyst, a Zr-loaded chemically activated carbon was used. The addition of Zr to the chemically activated carbon resulted in the formation of zirconium phosphate species on the carbon surface, capable of promoting the selective methanol dehydration to DME.

As for methanol synthesis component, the two activated carbons and the methanol dehydration catalyst were loaded with Cu-Zn and evaluated. The presence of phosphorus groups on the surface of the activated carbons seems to have a great relevance on the catalytic performance of the materials. The results showed strong interactions between the metallic phase and the phosphate surface groups, due to the formation Cu phosphate species, which were not active for the methanol synthesis reaction. On the contrary, the physically activated carbon, not containing phosphorus, exhibited a fairly good catalytic behavior, and thus, it was chosen to be used as the methanol synthesis catalyst for the preparation of bifunctional catalytic beds.

The preparation of bifunctional catalysts was attempted by using the methanol dehydration catalyst as support of the metallic phase. However, the detrimental interaction between Cu and the phosphate species made this preparation strategy unfeasible.

The physical mixing of the methanol synthesis and methanol dehydration catalysts resulted in the preparation of carbon-based catalytic beds, which avoided the metallic-acid detrimental interaction. These carbon-based catalytic beds performed very efficiently in the direct DME synthesis from syngas. Different mass ratios of the individual catalysts were studied. An acid/metallic catalyst mass ratio of 2 provided the catalytic bed with enough acid sites for making the overall syngas to DME process kinetically controlled by the methanol synthesis reaction.

5.5.-References

[1]   T.A. Semelsberger, R.L. Borup, H.L. Greene, Dimethyl ether (DME) as an alternative fuel, J. Power Sources. 156 (2006) 497–511. doi:10.1016/j.jpowsour.2005.05.082.

[2]   T.H. Fleisch, A. Basu, M.J. Gradassi, J.G. Masin, Dimethyl ether: A fuel for the 21st century, Stud. Surf. Sci. Catal. 107 (1997) 117–125. doi:10.1016/S0167-2991(97)80323-0.

[3]   S.C. Sorenson, Dimethyl Ether in Diesel Engines : Progress and Perspectives, J. Eng. Gas Turbines Power. 123 (2001) 652–658. doi:10.1115/1.1370373.

[4]   C. Arcoumanis, C. Bae, R. Crookes, E. Kinoshita, The potential of di-methyl ether (DME) as an alternative fuel for compression-ignition engines : A review, Fuel. 87 (2008) 1014–1030. doi:10.1016/j.fuel.2007.06.007.

[5]   Z. Azizi, M. Rezaeimanesh, T. Tohidian, M.R. Rahimpour, Dimethyl ether: A review of technologies and production challenges, Chem. Eng. Process. Process Intensif. 82 (2014) 150–172. doi:10.1016/j.cep.2014.06.007.

[6]   J. Sun, G. Yang, Y. Yoneyama, N. Tsubaki, Catalysis Chemistry of Dimethyl Ether Synthesis, ACS Catal. 4 (2014) 3346–3356. doi:10.1021/cs500967j.

[7]   K. Saravanan, H. Ham, N. Tsubaki, J.W. Bae, Recent progress for direct synthesis of dimethyl ether from syngas on the heterogeneous bifunctional hybrid catalysts, Appl. Catal. B Environ. 217 (2017) 494–522. doi:10.1016/J.APCATB.2017.05.085.

[8]   C. Baltes, S. Vukojević, F. Schüth, Correlations between synthesis, precursor, and catalyst structure and activity of a large set of $CuO/ZnO/Al_2O_3$ catalysts for methanol synthesis, J. Catal. 258 (2008) 334–344. doi:10.1016/j.jcat.2008.07.004.

[9]   J.D. Grunwaldt, A.M. Molenbroek, N.Y. Topsoe, H. Topsoe, B.S. Clausen, In situ investigations of structural changes in Cu/ZnO catalysts, J. Catal. 194 (2000) 452–460. doi:DOI 10.1006/jcat.2000.2930.

[10]   G.C. Chinchen, P.J. Denny, J.R. Jennings, M.S. Spencer, K.C. Waugh, Synthesis of Methanol. Part 1. Catalysts and Kinetics, Appl. Catal. 36 (1988) 1–65. doi:10.1016/S0166-9834(00)80103-7.

[11]   C.W. Seo, K.D. Jung, K.Y. Lee, K.S. Yoo, Dehydration of methanol over Nordstrandite based catalysts for dimethyl ether synthesis, J. Ind. Eng. Chem. 15 (2009) 649–652. doi:10.1016/J.JIEC.2009.09.037.

[12]   G. Bercic, J. Levec, Catalytic dehydration of methanol to dimethyl ether. Kinetic investigation and reactor simulation, Ind. Eng. Chem. Res. 32 (1993) 2478–2484. doi:10.1021/ie00023a006.

[13]   F. Yaripour, F. Baghaei, I. Schmidt, J. Perregaard, Catalytic dehydration of methanol to dimethyl ether (DME) over solid-acid catalysts, Catal. Commun. 6 (2005) 147–152. doi:10.1016/J.CATCOM.2004.11.012.

[14]   M. Xu, J.H. Lunsford, D.W. Goodman, A. Bhattacharyya, Synthesis of dimethyl ether (DME) from methanol over solid-acid catalysts, Appl. Catal. A Gen. 149 (1997) 289–301. doi:10.1016/S0926-860X(96)00275-X.

[15]   A. Ateka, I. Sierra, J. Ereña, J. Bilbao, A.T. Aguayo, Performance of CuO-ZnO-ZrO$_2$ and CuO-ZnO-MnO as metallic functions and SAPO-18 as acid function of the catalyst for the synthesis of DME co-feeding CO$_2$, Fuel Process. Technol. 152 (2016) 34–45. doi:10.1016/j.fuproc.2016.05.041.

[16]   F. Dadgar, R. Myrstad, P. Pfeifer, A. Holmen, H.J. Venvik, Direct dimethyl ether synthesis from synthesis gas: The influence of methanol dehydration on methanol synthesis reaction, Catal. Today. 270 (2016) 76–84. doi:10.1016/j.cattod.2015.09.024.

[17]   A.T. Aguayo, J. Ereña, D. Mier, J.M. Arandes, M. Olazar, J. Bilbao, Kinetic Modeling of Dimethyl Ether Synthesis in a Single Step on a CuO−ZnO−Al$_2$O$_3$/γ-Al$_2$O$_3$ Catalyst, Ind. Eng. Chem. Res. 46 (2007) 5522–5530. doi:10.1021/IE070269S.

[18]   A. García-Trenco, A. Martínez, Direct synthesis of DME from syngas on hybrid CuZnAl/ZSM-5 catalysts: New insights into the role of zeolite acidity, Appl. Catal. A Gen. 411–412 (2012) 170–179. doi:10.1016/j.apcata.2011.10.036.

[19]   J. Ereña, R. Garoña, J.M. Arandes, A.T. Aguayo, J. Bilbao, Effect of operating conditions on the synthesis of dimethyl ether over a CuO-ZnO-Al$_2$O$_3$/NaHZSM-5 bifunctional catalyst, Catal. Today. 107–108 (2005) 467–473. doi:10.1016/j.cattod.2005.07.116.

[20]   A. Ateka, P. Pérez-Uriarte, M. Sánchez-Contador, J. Ereña, A.T. Aguayo, J. Bilbao, Direct synthesis of dimethyl ether from syngas on CuO-ZnO-MnO/SAPO-18 bifunctional catalyst, Int. J. Hydrogen Energy. 41 (2016) 18015–18026. doi:10.1016/j.ijhydene.2016.07.195.

[21]   G.A. Olah, A. Goeppert, G.K.S. Prakash, Beyond oil and gas : the methanol economy, Wiley-VCH, 2009.

[22]   W.-J. Shen, K.-W. Jun, H.-S. Choi, K.-W. Lee, Thermodynamic investigation of methanol and dimethyl ether synthesis from CO$_2$ Hydrogenation, Korean J. Chem. Eng. 17 (2000) 210–216. doi:10.1007/BF02707145.

[23]   W. Lu, L. Teng, W. Xiao, Simulation and experiment study of dimethyl ether synthesis from syngas in a fluidized-bed reactor, Chem. Eng. Sci. 59 (2004) 5455–5464. doi:10.1016/j.ces.2004.07.031.

[24]   Y. Hua, X. Guo, D. Mao, G. Lu, G.L. Rempel, F.T.T. Ng, Single-step synthesis of dimethyl ether from biomass-derived syngas over CuO-ZnO-MOx(M = Zr, Al, Cr, Ti)/HZSM-5 hybrid catalyst: Effects of MOx, Appl. Catal. A Gen. 540 (2017) 68–74. doi:10.1016/j.apcata.2017.04.015.

[25]   Q. Ge, Y. Huang, F. Qiu, S. Li, Bifunctional catalysts for conversion of synthesis gas to dimethyl ether, Appl. Catal. A Gen. 167 (1998) 23–30.

[26]   J. Ereña, I. Sierra, M. Olazar, A.G. Gayubo, A.T. Aguayo, Deactivation of a CuO-ZnO-Al$_2$O$_3$/γ-Al$_2$O$_3$ catalyst in the synthesis of dimethyl ether, Ind. Eng. Chem. Res. 47 (2008) 2238–2247.

[27]   J. Xia, D. Mao, W. Tao, Q. Chen, Y. Zhang, Y. Tang, Dealumination of HMCM-22 by various methods and its application in one-step synthesis of dimethyl ether from syngas, Microporous Mesoporous Mater. 91 (2006) 33–39. doi:10.1016/J.MICROMESO.2005.11.014.

[28]   G. Bonura, C. Cannilla, L. Frusteri, A. Mezzapica, F. Frusteri, DME production by CO_2 hydrogenation: Key factors affecting the behaviour of CuZnZr/ferrierite catalysts, Catal. Today. 281 (2017) 337–344. doi:10.1016/J.CATTOD.2016.05.057.

[29]   L.M. Cotoruelo, M.D. Marqués, F.J. Díaz, J. Rodríguez-Mirasol, J.J. Rodríguez, T. Cordero, Equilibrium and Kinetic Study of Congo Red Adsorption onto Lignin-Based Activated Carbons, Transp. Porous Media. 83 (2010) 573–590. doi:10.1007/s11242-009-9460-8.

[30]   J.M. Rosas, J. Bedia, T. Cordero, On the preparation and characterization of chars and activated carbons from orange skin, Fuel Process. Technol. 91 (2010) 1345–1354. doi:10.1016/j.fuproc.2010.05.006.

[31]   J. Zawadzki, M. Wiśniewski, J. Weber, O. Heintz, B. Azambre, IR study of adsorption and decomposition of propan-2-ol on carbon and carbon-supported catalysts, Carbon N. Y. 39 (2001) 187–192. doi:10.1016/S0008-6223(00)00107-X.

[32]   J. Jasińska, B. Krzyżyńska, M. Kozłowski, Influence of activated carbon modifications on their catalytic activity in methanol and ethanol conversion reactions, Cent. Eur. J. Chem. 9 (2011) 925–931. doi:10.2478/s11532-011-0078-7.

[33]   C. Moreno-Castilla, F. Carrasco-Marín, C. Parejo-Pérez, M. V. López Ramón, Dehydration of methanol to dimethyl ether catalyzed by oxidized activated carbons with varying surface acidic character, Carbon N. Y. 39 (2001) 869–875. doi:10.1016/S0008-6223(00)00192-5.

[34]   M.J. Valero-Romero, F.J. García-Mateos, J. Rodríguez-Mirasol, T. Cordero, Role of surface phosphorus complexes on the oxidation of

porous carbons, Fuel Process. Technol. 157 (2017) 116–126. doi:10.1016/J.FUPROC.2016.11.014.

[35]   J. Bedia, R. Barrionuevo, J. Rodríguez-Mirasol, T. Cordero, Ethanol dehydration to ethylene on acid carbon catalysts, Appl. Catal. B Environ. 103 (2011) 302–310. doi:10.1016/J.APCATB.2011.01.032.

[36]   J. Bedia, R. Ruiz-Rosas, J. Rodríguez-Mirasol, T. Cordero, Kinetic study of the decomposition of 2-butanol on carbon-based acid catalyst, AIChE J. 56 (2010) 1557–1568. doi:10.1002/aic.12056.

[37]   M.J. Valero Romero, E.M. Calvo Muñoz, R. Ruíz Rosas, J. Rodríguez-Mirasol, T. Cordero, Phosphorus-containing mesoporous carbon acid catalyst for methanol dehydration to dimethyl ether, Ind. Eng. Chem. Res. 58 (2019) 4042–4053. doi:10.1021/acs.iecr.8b05897.

[38]   J. Palomo, J. Rodríguez-Mirasol, T. Cordero, Methanol Dehydration to Dimethyl Ether on Zr-Loaded P-Containing Mesoporous Activated Carbon Catalysts, Materials (Basel). 12 (2019) 2204. doi:10.3390/ma12132204.

[39]   J. Palomo, M.A. Rodríguez-Cano, J. Rodríguez-Mirasol, T. Cordero, On the kinetics of methanol dehydration to dimethyl ether on Zr-loaded P-containing mesoporous activated carbon catalyst, Chem. Eng. J. 378 (2019) 122198. doi:10.1016/J.CEJ.2019.122198.

[40]   M.J. Valero-Romero, F.J. García-Mateos, J. Rodríguez-Mirasol, T. Cordero, Role of surface phosphorus complexes on the oxidation of porous carbons, Fuel Process. Technol. 157 (2017) 116–126. doi:10.1016/j.fuproc.2016.11.014.

[41]   S. Brunauer, P.H. Emmett, E. Teller, Adsorption of Gases in Multimolecular Layers, J. Am. Chem. Soc. 60 (1938) 309–319. doi:10.1021/ja01269a023.

[42]   S. Lowell, J.E. Shields, J.E. Morral, Powder Surface Area and Porosity, 2nd Edition, 1985. doi:10.1115/1.3225796.

[43]   M.M. Dubinin, The potential theory of adsorption of gases and vapors for adsorbents with energetically nonuniform surfaces, Chem. Rev. 60 (1960) 235–241. doi:10.1021/cr60204a006.

[44]   S. Biniak, G. Szymansky, J. Siedlewski, A. Swiatkowski, The Characterization of Activated Carbons With Oxygen and Nitrogen Surface Groups, Carbon N. Y. 35 (1997) 1799–1810. doi:10.1016/S0008-6223(97)00096-1.

[45]   E. Desimoni, G.I. Casella, A. Morone, A.M. Salvi, XPS determination of oxygen-containing functional groups on carbon-fibre surfaces and the cleaning of these surfaces, Surf. Interface Anal. 15 (1990) 627–634. doi:10.1002/sia.740151011.

[46]   M. Thommes, K. Kaneko, A. V. Neimark, J.P. Olivier, F. Rodriguez-Reinoso, J. Rouquerol, K.S.W. Sing, Physisorption of gases, with special reference to the evaluation of surface area and pore size distribution (IUPAC Technical Report), Pure Appl. Chem. 87 (2015). doi:10.1515/pac-2014-1117.

[47]   J. Bedia, R. Ruiz-Rosas, J. Rodríguez-Mirasol, T. Cordero, Kinetic Study of the decomposition of 2-Butanol on Carbon-Based Acid Catalyst, Am. Inst. Chem. Engeeniers. 56 (2010) 1557–1568. doi:10.1002/aic.

[48]   M. Jagtoyen, F. Derbyshire, Activated carbons from yellow poplar and white oak by H3PO4 activation, Carbon N. Y. 36 (1998) 1085–1097. doi:10.1016/S0008-6223(98)00082-7.

[49]   J.M. Rosas, J. Bedia, J. Rodríguez-Mirasol, T. Cordero, HEMP-derived activated carbon fibers by chemical activation with phosphoric acid, Fuel. 88 (2009) 19–26. doi:10.1016/j.fuel.2008.08.004.

[50]   M. Molina-Sabio, V. Pérez, F. Rodríguez-Reinoso, Impregnation of activated carbon with chromium and copper salts: Effect of porosity and metal content, Carbon N. Y. 32 (1994) 1259–1265. doi:10.1016/0008-6223(94)90111-2.

[51]   J. Bedia, J.M. Rosas, J. Márquez, J. Rodríguez-Mirasol, T. Cordero, Preparation and characterization of carbon based acid catalysts for the dehydration of 2-propanol, Carbon N. Y. 47 (2009) 286–294. doi:10.1016/j.carbon.2008.10.008.

[52]   G. Alberti, U. Costantino, G. Marletta, O. Puglisi, S. Pignataro, ESCA investigations of amorphous and crystalline zirconium acid phosphates, J. Inorg. Nucl. Chem. 43 (1981) 3329–3334. doi:10.1016/0022-1902(81)80111-X.

[53]   J.L. Colón, D.S. Thakur, C.Y. Yang, A. Clearfield, C.R. Martini, X-ray photoelectron spectroscopy and catalytic activity of α-zirconium phosphate and zirconium phosphate sulfophenylphosphonate, J. Catal. 124 (1990) 148–159. doi:10.1016/0021-9517(90)90111-V.

[54]   E. Simón, J.M. Rosas, A. Santos, A. Romero, Study of the deactivation of copper-based catalysts for dehydrogenation of cyclohexanol to cyclohexanone, Catal. Today. 187 (2012) 150–158. doi:10.1016/j.cattod.2011.10.010.

[55]   J.W. Bae, S.-H. Kang, Y.-J. Lee, K.-W. Jun, Synthesis of DME from syngas on the bifunctional $Cu–ZnO–Al_2O_3$/Zr-modified ferrierite: Effect of Zr content, Appl. Catal. B Environ. 90 (2009) 426–435. doi:10.1016/J.APCATB.2009.04.002.

[56]   G.D. Khattak, M.A. Salim, A.B. Hallak, M.A. Daous, E.E. Khawaja, L.E. Wenger, D.J. Thompson, Study of valence states of copper in copper-phosphate glasses, J. Mater. Sci. 30 (1995) 4032–4036. doi:10.1007/BF00360705.

[57]   M.A. Salim, G.D. Khattak, M.S. Hussain, X-ray photoelectron spectroscopy, fourier transform infrared spectroscopy and electrical conductivity studies of copper phosphate glasses, J. Non. Cryst. Solids. 185 (1995) 101–108. doi:10.1016/0022-3093(94)00683-0.

[58]   T. Witoon, J. Chalorngtham, P. Dumrongbunditkul, M. Chareonpanich, J. Limtrakul, CO_2 hydrogenation to methanol over Cu/ZrO_2 catalysts: Effects

of zirconia phases, Chem. Eng. J. 293 (2016) 327–336. doi:10.1016/j.cej.2016.02.069.

[59] W.R.A.M. Robinson, J.C. Mol, Support effects in methanol synthesis over copper-containing catalysts, Appl. Catal. 76 (1991) 117–129. doi:10.1016/0166-9834(91)80008-K.

[60] X. Guo, D. Mao, G. Lu, S. Wang, G. Wu, Glycine–nitrate combustion synthesis of $CuO–ZnO–ZrO_2$ catalysts for methanol synthesis from CO_2 hydrogenation, J. Catal. 271 (2010) 178–185. doi:10.1016/J.JCAT.2010.01.009.

[61] G. Avgouropoulos, T. Ioannides, H. Matralis, Influence of the preparation method on the performance of $CuO–CeO_2$ catalysts for the selective oxidation of CO, Appl. Catal. B Environ. 56 (2005) 87–93. doi:10.1016/J.APCATB.2004.07.017.

[62] C. Liu, X. Guo, Q. Guo, D. Mao, J. Yu, G. Lu, Methanol synthesis from CO_2 hydrogenation over copper catalysts supported on MgO-modified TiO_2, J. Mol. Catal. A Chem. 425 (2016) 86–93. doi:10.1016/J.MOLCATA.2016.09.032.

[63] G.R. Moradi, S. Nosrati, F. Yaripor, Effect of the hybrid catalysts preparation method upon direct synthesis of dimethyl ether from synthesis gas, Catal. Commun. 8 (2007) 598–606. doi:10.1016/J.CATCOM.2006.08.023.

[64] S.-C. Baek, S.-H. Kang, J.W. Bae, Y.-J. Lee, D.-H. Lee, K.-Y. Lee, Effect of copper precursors to the activity for dimethyl ether synthesis from syngas over $Cu-ZnO/\gamma-Al_2O_3$ bifunctional catalysts, Energy & Fuels. 25 (2011) 2438–2443. doi:10.1021/ef200504p.

[65] S. Asthana, C. Samanta, A. Bhaumik, B. Banerjee, R.K. Voolapalli, B. Saha, Direct synthesis of dimethyl ether from syngas over Cu-based catalysts: Enhanced selectivity in the presence of MgO, J. Catal. 334 (2016) 89–101. doi:10.1016/J.JCAT.2015.10.020.

[66] V. Vishwanathan, K.W. Jun, J.W. Kim, H.S. Roh, Vapour phase dehydration of crude methanol to dimethyl ether over Na-modified H-ZSM-5 catalysts, Appl. Catal. A Gen. 276 (2004) 251–255. doi:10.1016/j.apcata.2004.08.011.

[67] X.K. Phan, H.D. Bakhtiary, R. Myrstad, J. Thormann, P. Pfeifer, H.J. Venvik, A. Holmen, Preparation and Performance of a Catalyst-Coated Stacked Foil Microreactor for the Methanol Synthesis, Ind. Eng. Chem. Res. 49 (2010) 10934–10941. doi:10.1021/ie1005405.

[68] X.K. Phan, H. Bakhtiary-Davijany, R. Myrstad, P. Pfeifer, H.J. Venvik, A. Holmen, Preparation and performance of Cu-based monoliths for methanol synthesis, Appl. Catal. A Gen. 405 (2011) 1–7. doi:10.1016/j.apcata.2011.07.005.

[69] M. Molina-Sabio, V. Pérez, F. Rodríguez-Reinoso, Impregnation of activated carbon with chromium and copper salts: Effect of porosity and metal content, Carbon N. Y. 32 (1994) 1259–1265. doi:10.1016/0008-6223(94)90111-2.

[70] A. García-Trenco, S. Valencia, A. Martínez, The impact of zeolite pore structure on the catalytic behavior of CuZnAl/zeolite hybrid catalysts for the direct DME synthesis, Appl. Catal. A Gen. 468 (2013) 102–111. doi:10.1016/J.APCATA.2013.08.038.

[71] P.S.S. Prasad, J.W. Bae, S. Kang, Y. Lee, K. Jun, Single-step synthesis of DME from syngas on Cu – ZnO – Al_2O_3/zeolite bifunctional catalysts : The superiority of ferrierite over the other zeolites, Fuel Process. Technol. 89 (2008) 1281–1286. doi:10.1016/j.fuproc.2008.07.014.

[72] J.W. Jung, Y.J. Lee, S.H. Um, P.J. Yoo, D.H. Lee, K.-W. Jun, J.W. Bae, Effect of copper surface area and acidic sites to intrinsic catalytic activity for dimethyl ether synthesis from biomass-derived syngas, Appl. Catal. B Environ. 126 (2012) 1–8. doi:10.1016/J.APCATB.2012.06.026.

Chapter 6

On the one step preparation of core-shell CuO/ZnO/ZrO$_2$-ZSM-5 fibrillar bifunctional catalysts by electrospinning for the efficient direct synthesis of dimethyl ether from syngas.

6.0.-Abstract

In this work, we report the use of the electrospinning technique for the one-step preparation of nanostructured ZrO_2-ZSM-5 fibrillar materials. TEM images showed fibers with a mean size of 275 nm and the presence of zeolite aggregates around the ZrO_2 nanofiber, in the form of core-shell like structures. The addition of copper and zinc salts to the electrospinning solution allowed preparing fibrillar bifunctional catalysts, presenting the same core-shell like structures. These fibrillar bifunctional materials were directly used as catalysts for the direct DME synthesis from syngas in a fixed-bed reactor, obtaining by this way spongy-like bifunctional catalytic beds, which presented an enhanced contact, in the submicrometric scale, between the two active phases involved in the syngas to DME process. These catalytic beds worked very efficiently in the direct DME synthesis from syngas, avoiding the problems related to pressure drops of fixed-bed reactors working with such a reduced particle size. A comparison between the fibrillar and a conventional particle catalyst was accomplished. The conformation of the catalyst in a fibrillar morphology, in the submicrometric scale, was of great importance for the metallic surface properties development. The bifunctional catalyst presenting a fibrillar morphology yielded a CO conversion two times higher than that obtained for the powder catalyst. The pressure drop inside the fixed-bed reactor was also calculated for both the fibrillar and the conventional particle packed bed. The results showed a value more than 10000 times smaller for the fibrillar packed bed as compared to the value calculated for a packed bed of particles presenting the same particle dimension.

6.1.-Introduction

Zeolites, an important kind of crystalline aluminosilicates, are widely used in many applications, such as, carbon dioxide capturing [1], catalysis [2,3] and gas sensing [4]. These materials present a network of channels at a molecular scale, which provides these aluminosilicates a uniform and ordered microporous structure [5]. This well-defined microporosity confers the materials a high surface area, along with an excellent stability and unique shape selectivity.

Most of the current zeolites are used in a particulate form or structure according to their applications [6–9]. These materials are usually commercialized in powder form, with particle sizes ranging from several thousands of nanometers to several microns [10]. This small particle size favors the intraparticle mass transfer of the reactants and products, but also results in high pressure drops in fixed-bed reactors, making these materials non-applicable directly. To overcome this issue, zeolites need to be pelletized or mixed with other materials in order to prepare structured materials, such as monoliths. However, this packing process usually results in the decrease of the specific surface area and, thus, in the loss of efficiency of the material [11,12]. In addition, the microporous size of the channels present in the structure of the zeolite is frequently translated into intraparticle diffusion limitations [5,13], especially in catalysis applications. Moreover, highly exothermic reactions introduce heat transfer problems, giving rise to hotspots in chemical reactors that may seriously damage the catalyst. Regarding these issues, there is a growing interest in using nanosized zeolites [14–16], due to the improvement of mass transfer of the reactant to the active sites.

One of the applications for zeolite materials that is receiving a great deal of attention is their use as acid catalysts for the synthesis of dimethyl ether (DME). DME has been traditionally produced via methanol dehydration on a solid acid catalyst [7,8,15,17]. Nevertheless, a one-step process for the direct synthesis of DME has been intensively studied in the last decades [18–23]. In this process, synthesis gas is fed to a single reactor containing a bifunctional catalyst, where both methanol synthesis, in parallel with water gas shift reaction, and methanol dehydration take place.

The catalysts used in the direct DME synthesis must present two well-defined catalytic active phases, one accounting for methanol synthesis and the other for methanol dehydration. As a component for methanol synthesis, the most commonly used catalytic phase is based on the Cu/ZnO metallic function [18,24,25] and as for the acid component of bifunctional catalysts, zeolites have been widely investigated [21,26,27]. When preparing bifunctional catalysts, an adequate balance between the metal and acid sites must be achieved, keeping a close proximity among them [26]. The preparation of bifunctional catalysts for

this process is usually carried out by physical mixing of their individual components [21,28–30]. Nevertheless, the catalysts prepared following this procedure present too great a distance between the two active sites involved in the syngas-to-DME process, thus lowering the performance of the catalyst.

An alternative to these physical mixtures is the use of supported catalysts, in which the solid acid acts as support for the metallic phase [31–33]. By this way, the tandem process from synthesis gas to DME is achieved on the surface of one particle of the catalyst [23]. However, these catalysts lack uniformity for the metallic phase given that this phase is randomly distributed on the support, forming aggregates that can sinterize in the catalyst calcination stage [23]. Furthermore, metal deposition on the support results in a strong metal-support interaction, resulting in problems for the reducibility of the metallic phase, and thus, partially deactivating the catalyst [34].

In addition, the use of bifunctional capsule catalysts, co-called core-shell catalysts, has been also proposed for direct synthesis of DME [35–38]. In these catalysts, the metallic component is conforming the core of the catalyst and it is confined by a lower thickness acid phase. The preparation of these catalysts involves complex methodologies and a granulation stage at some point of their preparation procedure is required for their application in a fixed-bed reactor. This granulation stage, needed for avoiding the pressure drops inside the reactor, limits the size of the core-shell material.

Electrospinning is a simple and straightforward technique that has been used to obtain carbon and polymer fibers in the submicron and nanoscale [39–42]. In this process, a viscous polymer solution, held by its surface tension at the end of a capillary tube, is subjected to a high voltage electric field, inducing the ejection of a charged liquid jet. Due to the electrostatic repulsions between the surface charges, an unstable whipping of the jet occurs in the space between the capillary tip and the collector electrodes, provoking the solvent evaporation and leading to the deposition of polymer fibers on the collector [43]. This technique has been used for the preparation of different catalysts [40,44–46]. The use of fibrillar structured bifunctional catalysts in the submicrometric scale could be very efficient for the direct production of DME from syngas in fixed-bed reactors, in

terms of intraparticle mass and heat transfer, avoiding, at the same time, the problems related to pressure drops when working with such a reduced particle size in this type of reactor.

In this study, we report a straightforward method for the one-step preparation of nanostructured zirconia-zeolite fibrillar materials by using the electrospinning technique. By this way, we have prepared homogeneously separated zeolite-zirconia aggregates along a zirconia fiber, in a core-shell like structure. Moreover, we have obtained materials presenting two well-defined catalytic active phases by adding copper and zinc salts to the electrospinning solutions. We also report the use of these materials as efficient catalysts for methanol dehydration to dimethyl ether and for the direct synthesis of dimethyl ether from syngas, respectively.

6.2.- Experimental method

6.2.1.- Fibers preparation

The experimental procedure followed for the preparation of the fibers presented in this work involves the preparation of a polymer solution, the electrospinning of the resulting solution and the calcination of the prepared fibers.

Zirconium acetate solution was used as zirconia precursor, and PVP was added to obtain the polymeric solution, giving the suitable viscosity to make the solution electrospinnable [40]. The Zirconium-PVP solution was prepared by mixing 5 g of zirconium acetate solution diluted in acetic acid (Sigma–Aldrich, CAS 7585-20-8, $Zr^{+x} \cdot xCH_3COOH$, Zr ~16 wt.%) and 350 mg of polyvinylpyrrolidone, PVP (CAS 9003-39-8, Mw = 1,300,000). The resulted solution was vigorously stirred for 12 h up to transparency. The addition of different amounts of ZSM-5 zeolite (Zeolyst international, CBV 5524G, Si/Al 50, with mean crystal size of 120 nm [47]) and 1 g of acetic acid to this zirconium-PVP solution resulted in the preparation of different zeolite-zirconium-PVP suspensions, which were vigorously stirred for 10 hours. The concentrations of zeolite in the polymeric solutions were adjusted to obtain zeolite contents ranging from 5 to 50 %(w/w) in the final fiber, after calcination. The electrospinning set-

up used for the electrospun process consisted of a syringe pump, a needle or spinneret, a plate collector and two high voltage power suppliers. In a typical experiment, the flow rate of the solution through the spinneret was set to 0.5 mL/h, the tip-to-collector distance was 20 cm and the electrical potential difference was 14 kV. Samples prepared following this procedure were denoted as FZrXZ, where X refers to the zeolite loading mass percentage.

For the preparation of Cu/Zn containing zirconia-zeolite, a proper amount of copper and zinc nitrates was dissolved into a 5% (w/w) PVP in 1-propanol solution, to achieve a 4.5 % (w/w) Cu+Zn (mol$_{Cu}$/mol$_{Zn}$= 2). Then, 3 g of this solution, together with 3 g of the Zirconium-PVP solution were mixed and stirred until homogeneity. Finally, different amounts of ZSM-5 zeolite were added to the solution, with the aim of generating several zeolite suspensions and, then, these suspensions were vigorously stirred for 10 hours. In this case, the resulting calcined fibers had a 20 %(w/w) Cu+Zn and zeolite contents ranging from 5 to 50 %(w/w). A typical problem when electrospinning containing rather volatile solvents solutions is the eventual solidification of the Taylor cone (or part of it) [48]. In this case, we used a co-axial spinneret to overcome this problem, pumping 2-propanol through the outermost capillary needle. For these experiments, the flow rate of the inner/outer solutions were set to 0.5/0.1 mL/h, the tip-to-collector distance was 20 cm and the electrical potential difference was 17 kV. Bifunctional materials were denoted as FCuZnZrXZ, where X refers to the zeolite loading mass percentage.

Finally, the electrospun fibers were recovered in form of non-woven cloth and then calcined in a muffle furnace at 500 °C for 4 h under air atmosphere, to eliminate the remaining solvent and the polymer, stabilize the zirconia fibers and to transform the zeolite from the ammonium to the hydrogen form.

For comparative purposes, a powder-like catalyst was prepared. For this aim the aforementioned Cu-Zn-Zr-zeolite suspensions were dried overnight at 120 °C and then calcined a at 500 °C for 4 h under air atmosphere. This material was sieved to 100 – 300 μm and was denoted as PCuZnZrXZ, where X referes to the zeolite mass percentage.

6.2.2.- Characterization of the fibers

The surface morphology of the samples was studied by scanning electron microscopy (SEM) using a Jeol JSM-6490LV microscope working at 25 kV voltage and by transmission electron microscopy (TEM) in a FEI Talos F200X microscope at an accelerating voltage of 200 kV and in a high annular dark field (HAADF).

The porous texture of the prepared fibers was characterized by N$_2$ adsorption-desorption at -196 ºC and by CO$_2$ adsorption at 0 ºC, carried out in an ASAP 2020 equipment (Micromeritics). Samples were previously outgassed for 8 h at 150 ºC under vacuum. From the N$_2$ isotherm, the apparent surface area (A$_{BET}$) was determined by applying the BET equation [49]; the application of t method using Harkins and Jura equation allowed the estimation of the micropore volume (V$_t$) and the external surface area (A$_t$) [50]; mesopore volume (V$_{mes}$) was calculated as the difference between the maximum adsorbed volume of N$_2$ (V$_p$), at a relative pressure of 0.99 and the micropore volume (V$_t$). From CO$_2$ adsorption data, the narrow micropore surface area (A$_{DR}$) and the narrow micropore volume (V$_{DR}$) were assessed using the Dubinin-Radushkevich equation [51].

X-ray diffraction patterns (XRD) of the calcined fibers were recorded in the region 2θ=5-90º on an EMPYREAN PANalytical diffractometer using CuKα monochromatic radiation (operation value 45 kV and 40 mA), using a PIXcel detector and Soller slits (incident and diffracted beam) of 0.04 rad. The average size of the crystal phases was calculated by applying the Williamson-Hall method [52].

The acid strength distribution and total acidity of the prepared fibers were determined by temperature programmed desorption of ammonia (NH$_3$-TPD). For NH$_3$-TPD analyses, 100 mg of the prepared material was firstly heated up to 500 ºC at a heating rate of 10 ºC/min, and then cooled to 100 ºC under helium flow. Then the sample was saturated with NH$_3$ (20 %(v/v) in helium) for 15 minutes at 100 ºC. After saturation, the weakly adsorbed NH$_3$ was desorbed in helium flow at the same temperature, until no NH$_3$ was detected in the outlet stream. The NH$_3$-TPD was carried out rising the temperature up to 500 ºC at a heating rate of

10 ºC/min under continuous helium flow. The outlet NH_3 concentration was registered using a TCD-detector.

The reducibility of the metallic phases present in the bifunctional catalysts was studied by temperature programmed reduction (H_2-TPR). For this analysis, 50 mg of sample was loaded in a quartz fixed-bed microreactor and dried under helium flow at 100 ºC. Then helium flow was switched to a 10 %(v/v) H_2 in helium stream, and kept for 15 min. Finally, the sample was heated up to 400 ºC, at a heating rate of 5 ºC/min, under the H_2 stream. H_2 consumption was monitored by mass spectroscopy (Pfeiffer Omnistar GCD-301), registering the signal m/z 2.

The Cu dispersion and the Cu metallic surface area of the bifunctional catalysts were determined by N_2O selective chemisorption. For this analysis, the sample was firstly reduced under H_2 flow at a temperature of 270 ºC for 2 hours. Thereafter, the sample was cooled to 60 ºC, and the H_2 stream was switched to a N_2O diluted in He stream for the oxidation of the Cu^0 species [53]. N_2O consumption was registered using an ECD-detector, enabling the determination of the copper dispersion and the active copper area.

6.2.3.- Catalytic experiments

Gas phase methanol dehydration experiments were carried at atmospheric pressure in a fixed-bed microreactor (i.d. 4 mm) placed inside a vertical furnace with temperature control. In a typical experiment, 150 mg of fibers were used. Methanol was fed to the system by using a syringe pump (Cole-Parmer® 74900-00-05 model), using helium as carrier gas, which ensured a constant controlled methanol flow. The reaction was carried out in the temperature range of 200-450 ºC. To avoid condensation of any compound, all lines were heated up to 120 ºC. The feed conditions used were a methanol partial pressure of 0.10 atm and a space time of 0.02 (g·s/μmol_{MeOH}). The conversion was defined as the ratio of the amount of methanol converted to the amount of methanol supplied to the reactor. The selectivity (in %mol) was defined as the ratio of carbon moles in a specific product divided by moles of converted methanol.

The direct dimethyl ether synthesis experiments were carried out in a PID Eng. & Tech. Microactivity equipment, which is provided with a stainless steel fixed-bed reactor and allows for operating at high temperature and pressures. Before starting the reaction, 500 mg catalyst were in-situ reduced at 270 ºC under H$_2$ flow (50 mL/min) for 2 h. After the reduction stage, the temperature was set to the reaction value (250-325 ºC) and then the pressure was increased up to 45 bar. Finally, the syngas was introduced. In this case, the conversion was defined as the ratio of the amount of CO converted to the amount of CO supplied to the reactor. The selectivity (in %mol) was defined as the ratio of carbon moles in a specific product divided by moles of converted CO.

The outlet gas concentrations were quantified by on-line gas chromatography (Perkin-Elmer Clarus 500 GC equipped with TCD and FID detectors). The columns used were a Permanent gases active carbón 80/100 mesh for CO, CO$_2$ analysis, and a 1.9m x 1/8" x 2.1mm Porapak N 80/100 + 0.5m x 1/8" x 2.1mm Porapak Q 80/100 column for methanol, DME and light hydrocarbons separation. N$_2$ was used as internal standard for GC analyses.

6.3.- Results and discussion

6.3.1.- Zirconia-Zeolite fibers characterization

The morphology of the zirconia-zeolite fibers was examined by scanning electron microscopy (SEM) and transmission electron microscopy (TEM). Figure 6.1a presents a SEM image of the prepared zirconia fibers. The size and shape of these fibers was highly uniform, with diameters ranging from 200 to 300 nm. Moreover, it could be observed the absence of fused zones or beads. Figure 6.1b shows a SEM image of the zirconia-zeolite fibers with 10 %(w/w) of zeolite. In this case, two well-defined structures could be appreciated. The material was mainly composed by smooth fibers, similar to the zirconia fibers observed in Figure 6.1a, and particle aggregations along the fibers, presenting an average size of 550 nm.
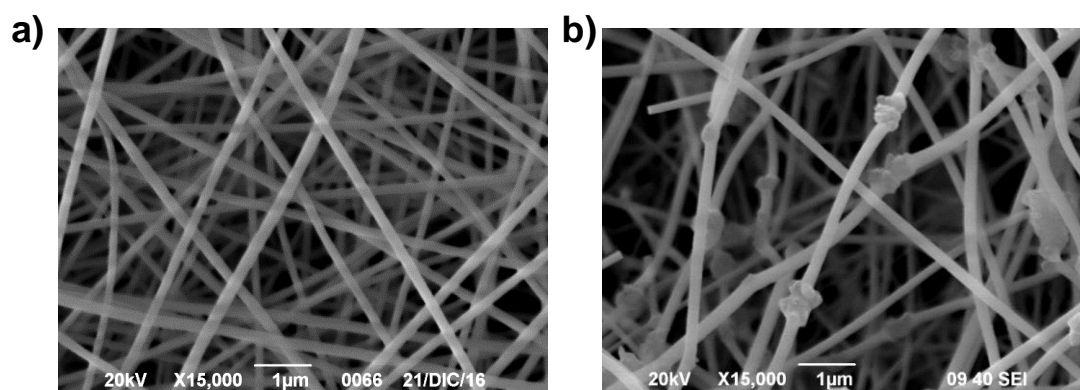
Figure 6.1. Scanning electron micrographs of the fibers calcined at 500 ºC **(a)** calcined zirconia nanofibers, **(b)** zirconia-zeolite nanofibers, 10 % (w/w) zeolite.

The chemical composition of the two different phases presented on the zirconia-zeolite fibrillar materials was analyzed by transmission electron microscopy energy-dispersive X-ray spectroscopy (TEM-EDXA). Figure 6.2a shows a high-angle annular dark field scanning transmission electron microscopy (HAADF-STEM) image along with the Zr and Si EDXA elemental mappings composite of a region of the material containing a particle aggregation. As expected, the smooth fibrillar part of the material was only composed by zirconium oxide, since no Si was detected in this region. In contrast, the particles aggregation region exhibited the presence of both Zr and Si, evidencing the presence of aggregates of zeolite particles, in a similar way to the ones reported for SiO_2 [54] and polystyrene nanoparticles [55]. These zeolite particles assembling seemed to occur, in this case, surrounding the zirconium oxide nanofiber, creating local core-shell like structures with sizes ranging from 350 to 550 nm. The average size of these zeolite particles obtained from TEM analyses showed a value of 120 nm. X-ray diffraction (XRD) analyses of the zeolite containing samples further confirmed the presence of the two crystalline phases, zeolite (ZSM-5) and tetragonal zirconium oxide (see Figure 6.2b). From XRD analyses, the mean crystal size value of these zeolite particles was estimated as 60 nm, by applying the Williamson-Hall method.

a)

b)
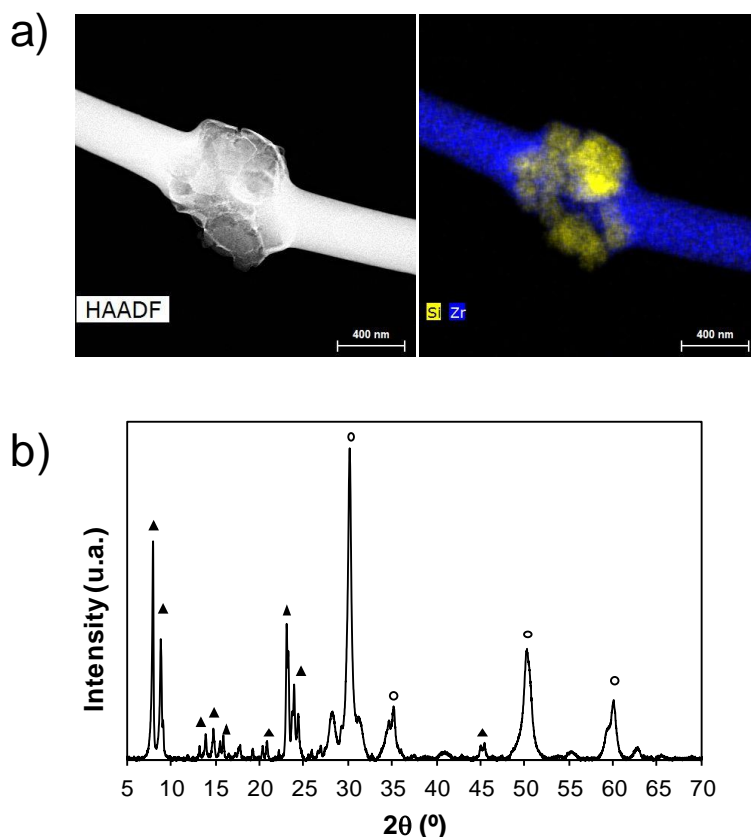
Figure 6.2. a) HAADF-STEM image, and Si (yellow) and Zr (blue) EDXA elemental mappings composite, of a zeolite particles aggregation in the zirconia-zeolite fibers. Scale bar is 400 nm. **b)** XRD patterns of the zirconia-zeolite fibers. ZSM-5 (▲), Tetragonal zirconia (o).

The increase of the zeolite concentration in the electrospinning solution resulted in a higher proportion of the local zirconia-zeolite core-shell like structures, with the corresponding reduction of the length of the fiber between two of these zirconia-zeolite core-shell like structures (see Figure 6.3). In this study, the average measured distance for the separation between the zeolite aggregates showed values of 9.5, 4.5 and 1.75 µm, for zeolite concentrations of a 5, 10 and 15 %(w/w), respectively, being observed a linear relationship between the zeolite content and the space separating the local core-shell like structures in the fibers, up to this loading. When analyzing the fibers containing a zeolite content of 20 %(w/w), the distance between the local zeolite aggregates along the fiber continued shrinking, showing an average value of 0.91 µm. Moreover, it

was observed that the local zirconia-zeolite core-shell like structures started to join for zeolite loadings higher than 20 %(w/w), where these zeolite aggregates structures were closer and closer, forming core-shell like fibers, with zeolites surrounding (covering) the zirconia fibers, as it can be observed for the case of the material containing a 50 %(w/w) of zeolite (see Figure 6.3b).

a)

| 5 %(w/w) | 10 %(w/w) | 15 %(w/w) |

b)

| 15 %(w/w) | 20 %(w/w) | 50 %(w/w) |
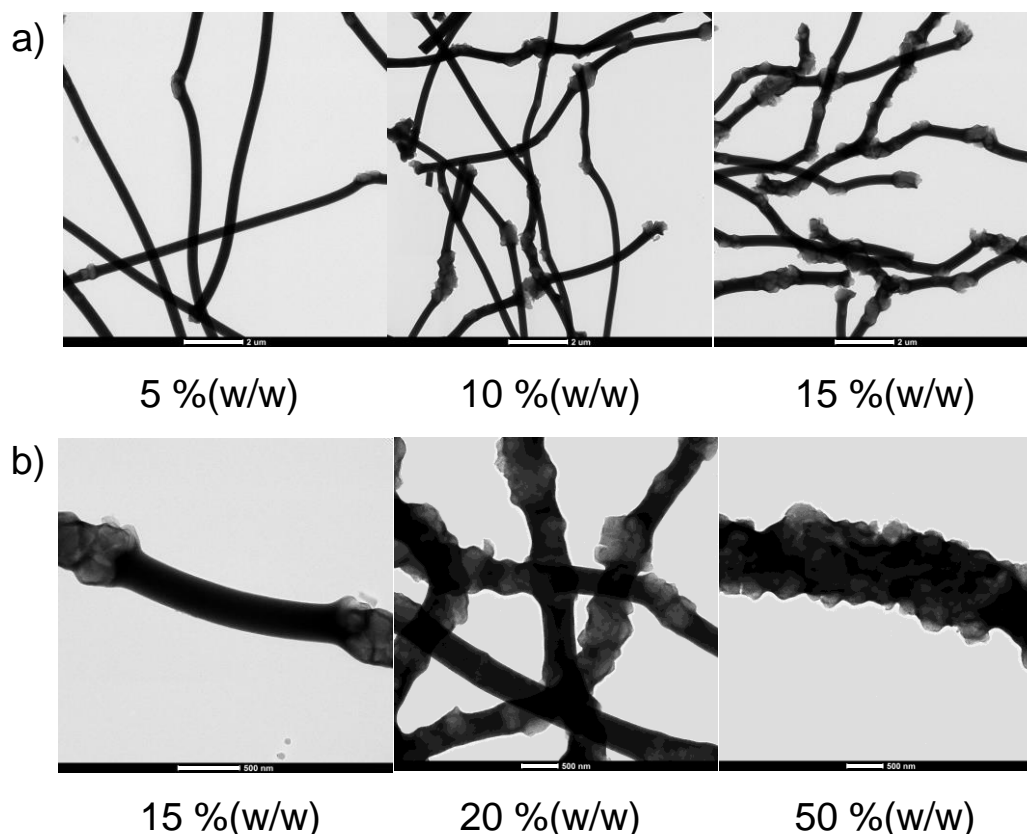
Figure 6.3. Transmission electron micrographs for the zirconia-zeolite fibers. Effect of % (w/w) zeolite in the final fiber. a) Scale bar is 2 µm. b) Scale bar is 500 nm.

N$_2$ adsorption-desorption studies were carried out in order to evaluate the possible loss of textural properties in the zeolite as a consequence of the preparation process. Figure 6.4a presents the N$_2$ adsorption-desorption isotherms at -196 ºC for the ZSM-5 zeolite along with the zirconia and the zirconia-zeolite fibrillar materials prepared in this study. Zirconia fibers, FZr, showed very low N$_2$ adsorption, suggesting a non-porous texture. ZSM-5 zeolite showed a type Ib isotherm, which is characteristic of solids with narrow

microporosity [56]. N$_2$ uptake of the zirconia-zeolite fibers showed a high dependence on the zeolite content, especially in the range of low relative pressures. In this sense, the higher the zeolite content, the higher the N$_2$ adsorption. H4 hysteresis loop was observed for the zeolite and zirconia-zeolite fibers, which is associated to zeolite nanocrystal aggregations [56]. CO$_2$ adsorption isotherms showed the same trend, indicating that the presence of the narrow microporosity is mainly related to the zeolite presence in the fibrillar materials (Figure 6.4b).
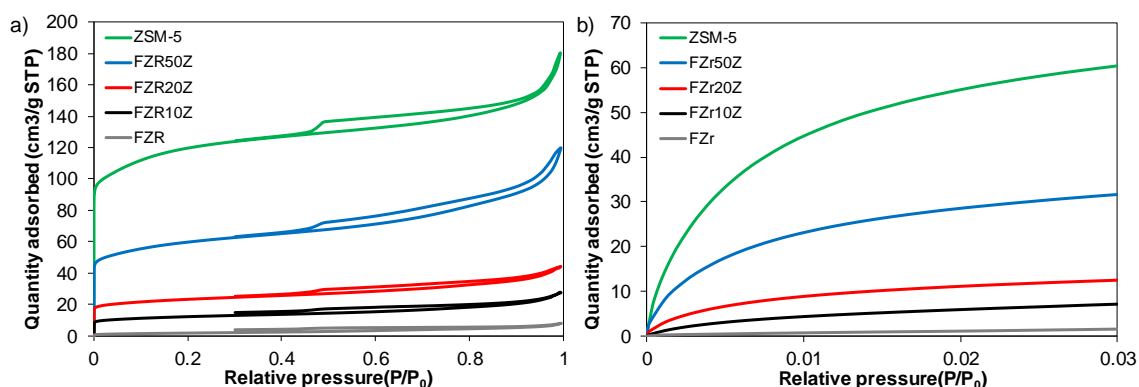
Figure 6.4. a) N$_2$ adsorption–desorption isotherms at −196 ∘C and **b)** CO$_2$ adsorption at 0 °C of ZSM-5 zeolite, the zirconia and the zirconia zeolite fibers.

Table 6.1 summarizes the characteristic parameters derived from the N$_2$ adsorption-desorption and the CO$_2$ adsorption isotherms. In this study, the calculated Bruneauer-Emmett-Teller (BET) surface area for the powder zeolite, ZSM-5, and the zirconia fibers, FZr, showed a value of 442 and 7 m^2/g, respectively. When analyzing the zirconia-zeolite fibers, it was found that this parameter increased with the zeolite content in the sample, showing values close to the proportional sum of the pure zeolite and the zirconia fibers. In this sense, the calculated values for the fibers containing a 10, 20 and 50 %(w/w) of zeolite, were 42, 82 and 217 m^2/g, respectively. A$_{DR}$ values calculated from CO$_2$ adsorption isotherms showed the same trend. However, this trend was not observed when analyzing the external surface area A$_t^{N2}$, which showed higher values than the predicted by the proportional sum of their individual components in all the prepared zirconia-zeolite fibers. Therefore, the preparation procedure here presented not only is not causing a loss of accessibility to the internal zeolite

surface, but also results into a higher external surface area, which is very important for catalysis applications.

Table 6.1. ZSM-5 loading, characteristic parameters of the porous texture, and acidity determined by NH_3-TPD.

	% ZSM-5 %(w/w)	A_{BET}^{N2} (m²/g)	V_p^{N2} (cm³/g)	A_t^{N2} (m²/g)	V_t^{N2} (cm³/g)	A_{DR}^{CO2} (m²/g)	V_{DR}^{CO2} (cm³/g)	Acidity (µmol NH_3/g)
FZr	0	7	0.01	7	0	4	0	31
FZr10Z	10	42	0.04	15	0.01	53	0.02	181
FZr20Z	20	82	0.07	24	0.03	95	0.04	280
FZr50Z	50	217	0.19	56	0.07	229	0.09	585
ZSM-5	100	442	0.28	51	0.17	509	0.20	977

Acid properties of the materials here presented were studied by temperature programmed desorption of ammonia (NH_3-TPD). Table 6.1 contains the total amount of ammonia desorbed during TPD, obtained by the integration of the area under NH_3-TPD curves. Zirconia fibers, FZr, desorbed a negligible amount of ammonia during NH_3-TPD analysis, which indicated a low acidity in this material. As occurred with textural parameters, the total acidity of the zirconia-zeolite materials linearly increased with the ZSM-5, indicating that the acidity these materials presented was mainly attributed to the presence of zeolite. Figure 6.5 presents the NH_3-TPD profiles obtained for the parent ZSM-5 zeolite along with the prepared zirconia and the zirconia-zeolite fibers. ZSM-5 zeolite showed two ammonia desorption peaks, with a maximum at 225 and at 410 ºC, respectively. The former could be associated to weak acid sites, probably of Lewis nature, while the latter could be related to ammonia interacting with strong Bronsted acid sites present on zeolite materials [57]. The ammonia desorption profiles obtained for the zirconia-zeolite fibers showed the same shape that the one of the ZSM-5 zeolite, been the main difference the intensity of the ammonia desorption peaks, associated to the zeolite content in the fibrillar material. Hence, it can be concluded that the acid sites of the parent zeolite and their acid strength distribution remained unaltered when preparing the fibrillar materials.
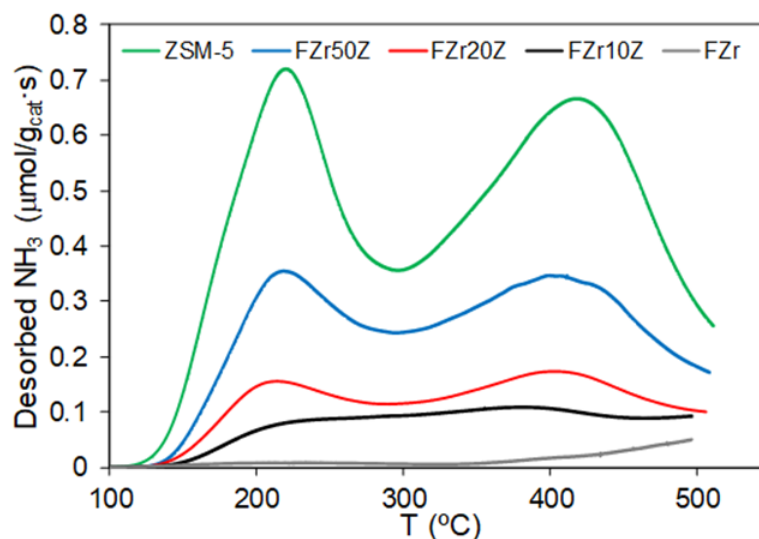
Figure 6.5. Ammonia TPD profiles of the ZSM-5 zeolite along with the zirconia and the zirconia-zeolite fibers.

6.3.2.- Catalytic dehydration of methanol

These zirconia-zeolite fibrillar materials were used as catalysts for the methanol dehydration reaction. Fig. 6 shows the steady-state methanol conversion as a function of the ZSM-5 loading for the fiber-based catalysts at a reaction temperature of 250 ºC (P_{MeOH} = 0.10 atm, W/F_{MeOH} = 0.02 g·s/μmol_{MeOH}). Zirconia fibers, FZr, not containing zeolite, showed a negligible catalytic activity for this reaction at these conditions, due to the low acidity this material presented. As expected, methanol conversion increased with ZSM-5 content in the zirconia-zeolite fibers, since the surface acidity and thus the catalytic activity was related to the presence of this phase in the material. The selectivity to DME was 100 % for all the materials studied at these operating conditions.
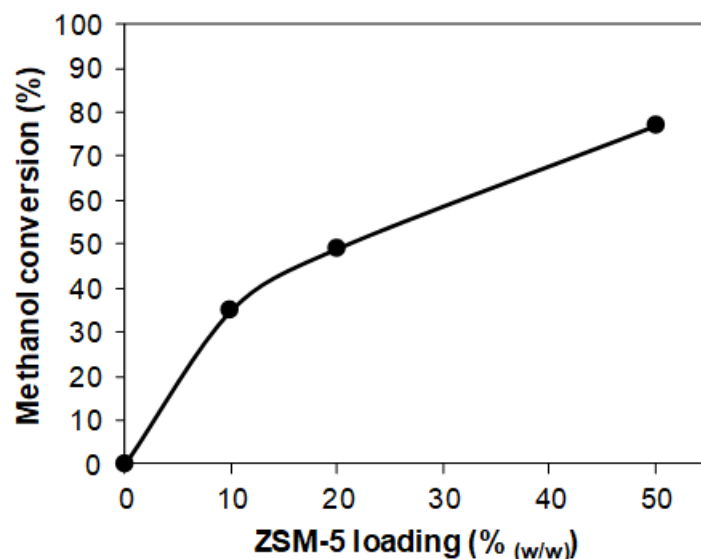
Figure 6.6. Methanol conversion as a function of Zeolite loading for zirconia-zeolite fibers at a constant temperature of 250 ºC (P_{MeOH}=0.10 atm, W/F_{MeOH}=0.02 g·s/μmol$_{MeOH}$).

Figure 6.7a and b show the evolution of the methanol conversion and selectivity to the main products as a function of the temperature, respectively, for a fibrillar catalyst containing a 20 %(w/w) zeolite. An increase in the reaction temperature resulted in a higher methanol conversion. Regarding the selectivity to the main reaction products, it was remarkable the high selectivity (100%) to DME in the temperature range of 200-300 ºC. At higher temperatures (350-400 ºC), the selectivity to light olefins was also outstanding (higher than 60 %), with no deactivation observed up to 10 hours on stream (400 ºC), which makes these materials also very attractive for the methanol to olefins (MTO) process [58].
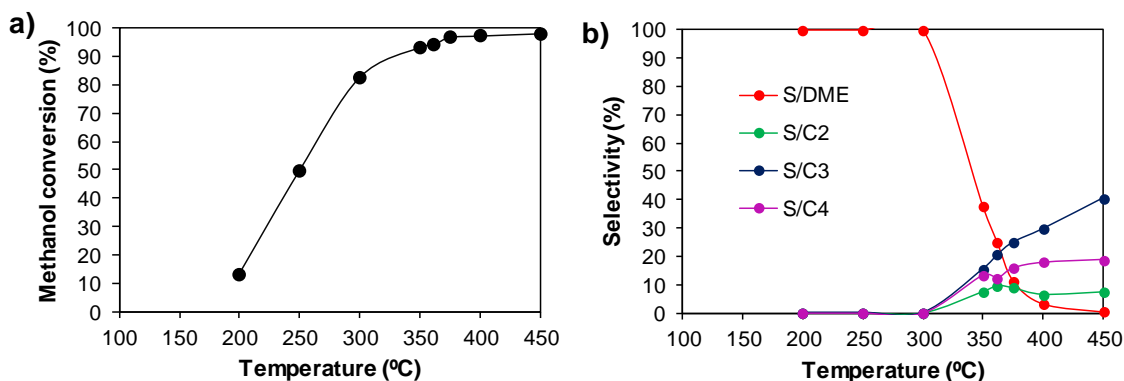
Figure 6.7. a) Methanol conversion and **b)** selectivity to DME and light olefins as a function of the temperature for the catalyst containing a 20 %(w/w) zeolite (P_{MeOH}=0.10 atm, W/F_{MeOH}=0.02 g.s/μmol$_{MeOH}$).

The selectivity towards DME and light olefins at different temperatures for the zirconia-zeolite fibrillar catalysts with zeolite loadings of 10, 20 and 50 %(w/w) are summarized in Table 6.2. DME was further converted to light olefins when rising the temperature. The temperature value at which selectivity to DME drops was related to the zeolite content. In this sense, the formation of light olefins could be controlled not only by adjusting the reaction conditions, but also by the zeolite loading in the catalyst.

Table 6.2. Methanol conversion and selectivity to DME and light hydrocarbons, at different temperatures, for the zirconia-zeolite fibrillar catalysts with zeolite loadings of 10, 20 and 50 %(w/w), (P_{MeOH} = 0.10 atm, W/F_{MeOH} = 0.02 g·s/μmol$_{MeOH}$).

Catalyst	T (ºC)	X_{MeOH} (%)	S_{DME} (%)	S_{HC} (%)
	300	65.8	100	0
FZr10Z	350	82.1	100	0
	375	87.9	48.5	51.5
	300	82.4	100	0
FZr20Z	350	93.2	37.5	62.5
	375	96.5	11.4	88.6
	300	90.2	63.7	36.3
FZr50Z	350	93.5	1.7	98.3
	375	97.7	0.4	99.6

Zeolite materials have been widely investigated for the selective dehydration of methanol to DME [7,8,15,17]. Rownaghi et al. [15] studied the effect of the zeolite crystal size in methanol conversion and DME selectivity. In their study they observed that scaling down the zeolite crystal size to the nanometric size resulted in a higher methanol conversion. This fact was attributed to the higher number of pore entrances available on the nanocrystal surface, as compared to the one of the conventional zeolite particle size [15]. However, for the application of nanocrystal zeolite materials in a fixed-bed reactor, these nanocrystals must be pelletized in order to avoid high pressure drops and this packing process has been reported to decrease the textural properties of zeolite materials, reducing thus the performance of these materials [12]. Moreover, for very high exothermic reactions, conventional catalyst size particles need to be diluted in the fixed-bed to avoid hotspots inside the reactor [59]. In contrast to the conventional catalysts, the fibrillar catalysts reported in the present work, presenting a nanometric size, were synthetized through a one-step process and were directly used in a fixed-bed reactor avoiding any pressure drop limitation. In addition, by the preparation methodology here reported, it is possible to obtain homogeneously separated nanometric zeolite particle aggregates along the zirconia fibers in a nanostructured catalytic system, which allowed controlling the catalytic active sites density inside a fixed-bed reactor, avoiding the generation of hotspots, without the need of adding a further phase in the reactor. The fibrillar catalysts here presented performed very efficient, achieving higher conversion values than the reported in other studies [15,60], working in the present study at higher space velocities.

6.3.3.- Fibrillar bifunctional catalyst characterization

To produce the bifunctional catalysts, Cu/Zn salts were added to the electrospinning solutions and the electrospinning operating parameters were adjusted. The fibrillar materials prepared following this procedure showed the same morphology as the zirconia-zeolite fibers. A HAADF-STEM image, together with the elemental mappings of Cu and Si for a region of a catalyst containing a 20%(w/w) Cu+Zn and a 10%(w/w) zeolite, FCuZnZr10Z, which shows zeolite particles aggregation, are presented in Figure 6.8a. The same local core-shell

like structure observed for the zirconia-zeolite materials was observed in this case, showing that the presence of copper and zinc is not affecting the morphology of the material. When increasing the zeolite loading, the local core-shell like structures joined forming a continuous fibrillar core-shell like structure, as occurred with the zirconia-zeolite fibers (see FCuZnZr30Z, with 30% (w/w) of zeolite, in Figure 6.8b). Regarding the distribution of Cu, a high dispersion of this metal along the zirconia fiber surface was achieved. Besides, analyzing in depth the core-shell like regions of the material, it could be observed that this element was clearly laid on the surface of the core, while the zeolite particles were allocated surrounding (covering) the copper core, acting as a shell. This configuration provides the material with an enhanced interaction between the phases, making it suitable for catalysis applications, especially, for the direct syngas to DME reaction.
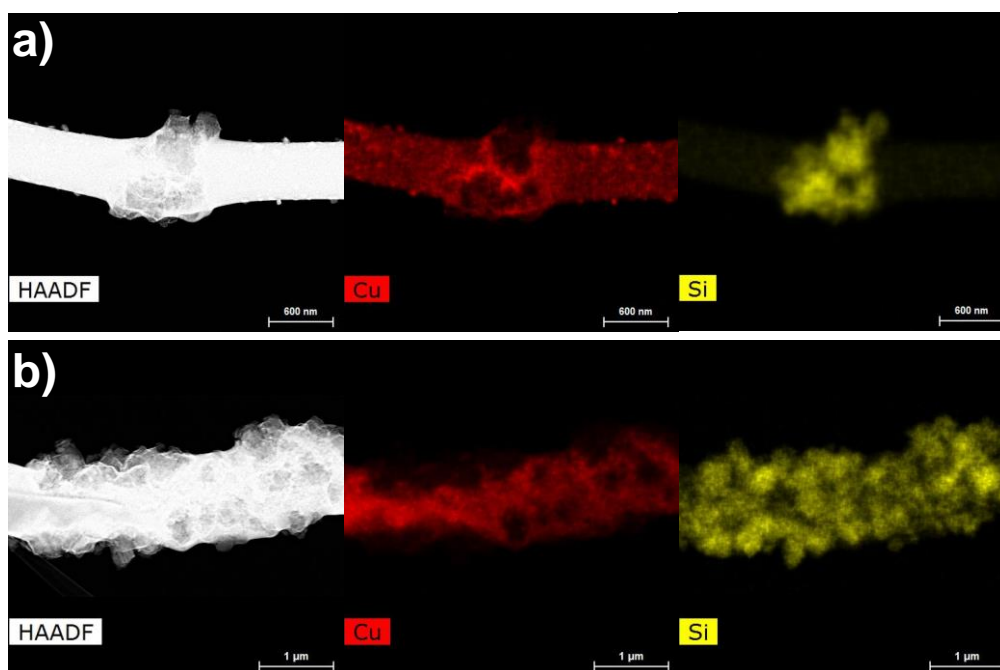
Figure 6.8. HAADF-STEM image and EDXA elemental mappings of Cu (red) and Si (yellow), of a region containing **a)** a local zeolite particles aggregation in FCuZnZr10Z, and **b)** a continuous core-shell like structure in the bifunctional catalyst FCuZnZr30Z. Scalebars are a) 600 nm. and b) 1 μm.

In the case of Cu-based bifunctional catalysts for the direct dimethyl ether synthesis, it has been reported that a mass ratio between the metallic and the acid phases of 2, in the case of using ZSM-5 zeolite as acid phase, provides the catalyst with an excess of acid sites so as to make this process controlled by the methanol synthesis step [21]. Therefore, a fibrillar bifunctional catalyst presenting a mass ratio between the metallic and the acid phases of 2 will be further characterized and used as catalyst for the direct DME synthesis from syngas. Fig. 9 shows the XRD pattern obtained for a fibrillar bifunctional catalyst containing a 20%(w/w) Cu+Zn and a 10%(w/w) zeolite (FCuZnZr10Z). This pattern showed intensive diffraction peaks at 2θ = 30.2 º, 35.2 º, 50.6 º and 60.2 º, which correspond to tetragonal zirconia crystal phase. The diffraction peaks at 2θ = 7.9 º, 8.9 º, 20.9 º and 23.9 º were also appreciated and identified as ZSM-5 zeolite. This diffraction pattern also highlighted the presence of a low intensity diffraction peak at 2θ = 38.8 º, associated to CuO crystal phase. The average crystallite size of CuO was estimated as 7.3 nm by using the Williamson-Hall method. The low CuO crystallite size observed for this material is remarkable when it is compared with other catalysts reported in the literature [61,62], despite the higher calcination temperature used in the present study. This fact has been associated to the presence of Zr, which favors the thermal resistance of Cu and also prevents the catalyst from irreversible deactivation by sintering of the metallic phase, when operating under STD conditions [24].
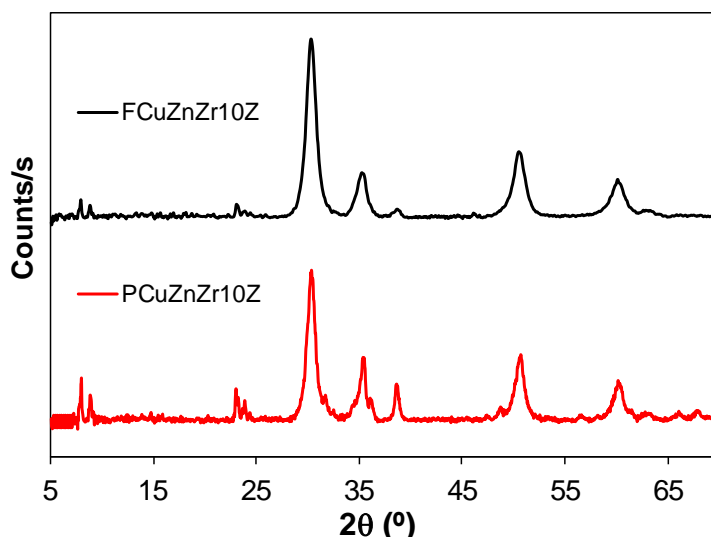
Figure 6.9. XRD pattern of the fibrillar (FCuZnZr10Z) and powder (PCuZnZr10Z) bifunctional catalysts containing a 20%(w/w) Cu+Zn and 10%(w/w) zeolite.

Table 6.3 summarizes the textural and metallic surface properties for this fibrillar bifunctional catalyst (FCuZnZr10Z). The calculated BET surface area value for this catalyst was higher than the one for the zirconia-zeolite containing the same zeolite loading, FZr10Z, indicating that the presence of Cu and Zn in the composition of the electrospun fibers resulted in a higher porous texture development of the final catalytic fibrillar material (see Tables 6.1 and 6.3). The Cu metallic surface area and Cu dispersion was determined using N_2O decomposition method. This material presented high Cu surface area and metal dispersion values, as a consequence of the high metal dispersion capability that ZrO_2 has demonstrated when it is present in this kind of catalysts [24,63].

Table 6.3. Textural and metallic surface properties for the fibrillar (FCuZnZr10Z) and powder (PCuZnZr10Z) bifunctional catalysts containing a 20%(w/w) Cu+Zn and 10%(w/w) zeolite.

	A_{BET}	V_p	S_{Cu}[a]	S'_{Cu}[a]	Cu disp.[a]
	(m²/g)	(cm³/g)	(m²/g_Cu)	m²/g_Cat)	(%)
FCuZnZr10Z	68	0.10	61	7.7	9.5
PCuZnZr10Z	53	0.08	41	5.2	6.3

[a] Calculated using N_2O decomposition method.

193

Figure 6.10 shows the H_2 consumption as a function of the temperature during H_2-TPR analysis for FCuZnZr10Z. According to the literature, ZnO and ZrO_2 are not reducible under the TPR conditions, thus, the H_2 consumption was exclusively related to the CuO reduction [64]. It has been also reported that the temperature at which CuO reduction takes place is related to the CuO particle size and to the interaction between CuO and other components of the catalyst system [65,66], being this temperature lower for smaller CuO particles. As can be observed, FCuZnZr10Z showed a main H_2 consumption peak at about 190 ºC, suggesting the presence, mainly, of homogeneously dispersed CuO. It is also noticeable that the reduction temperature for CuO in this study was considerably lower than the one reported for CuO-ZnO-Al_2O_3 metallic phases (about 300ºC) [18,67]. This fact is attributed to the favorable interaction CuO-ZrO_2, which results in a lower reduction temperature [68].
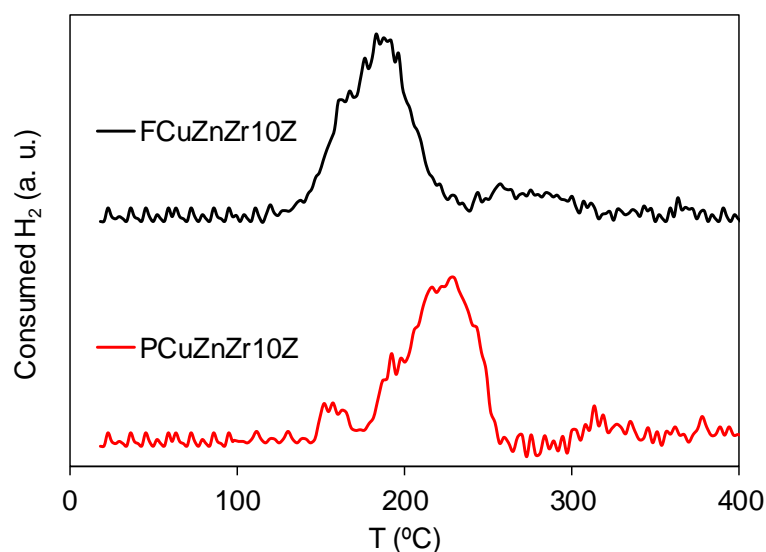
Figure 6.10. H_2-TPR profile of the fibrillar (FCuZnZr10Z) and powder (PCuZnZr10Z) bifunctional catalysts containing a 20%(w/w) Cu+Zn and 10%(w/w) zeolite.

6.3.4.- Syngas to DME catalytic reaction

The CuO/ZnO/ZrO$_2$-ZSM-5 fibrillar material obtained was studied as a bifunctional catalyst for the direct dimethyl ether synthesis from syngas. In these experiments, a high pressure fixed-bed reactor was used. Figure 6.11 shows the steady state CO conversion and the selectivity to the main reaction products as a function of temperature for FCuZnZr10Z (H$_2$/CO = 2, GHSV=4800 ml/g$_{cat}$·h, 45 bar, 4 hours on stream). The results pointed out that the CO conversion increased with temperature in the temperature range studied, reaching a value of 60% at 300 ºC. Very high selectivity values to DME were achieved in the whole range of temperature studied (>60 %). The CO conversion and selectivity to DME values were higher when increasing the H$_2$/CO ratio from 2 to 3 (X$_{CO}$ = 70 %, S$_{DME}$ = 64 %) at the same operating conditions (T= 300 ºC, GHSV=4800 ml/g$_{cat}$·h, 45 bar, 4 hours on stream). The higher CO conversion can be justified based on the overall syngas-to-DME process is kinetically controlled by the methanol synthesis stage under the conditions used in this work, which is favored by a H$_2$-rich environment [69,70]. In addition, the higher the H$_2$ content in the synthesis gas, the lower the amount of CO$_2$ generated through the water gas shift reaction, giving rise to a higher selectivity to DME. When comparing the selectivity towards DME value with the reported using other catalysts reported in the literature, it has to be noted that for the calculation of the selectivity some authors include CO$_2$ as a reaction product, while others just report this calculation on the basis of the organic products [71]. The selectivity to DME values obtained in this study considering and not-considering the CO$_2$ as a reaction product were 62% and 94%, respectively, working at H$_2$/CO = 2, GHSV=4800 ml/g$_{cat}$·h, a pressure of 45 bar and a time on stream of 4 hours. The fibrillar bifunctional catalyst presented in this work performed very efficient as compared to other advanced catalysts reported in the literature. In this line, Yang et al. [35] reported CO conversion values ranging from 5.59 to 58.07 % with selectivity to DME values (not considering CO$_2$ as a reaction product) of 96.59 and 40.51 %, respectively, using core-shell catalysts working at 250 ºC, H$_2$/CO = 2, W$_{CZA}$/F$_{syngas}$ = 10 g·h/mol and 50 bar. Wang et al. [37] also reported the use of core-shell catalysts for this reaction, obtaining CO conversion values ranging from 28 to 71.1 % and selectivity to DME values ranging from 51.6 to 61.9 % (considering CO$_2$ as

reaction product) at 260 ºC, H_2/CO = 2, GHSV = 1500 mL/(g_{cat}·h) and 50 bar. The fibrillar catalyst here presented showed CO conversion values of 21 and 37 %, working at 250 and 260 ºC, respectively, and H_2/CO = 2. However, it has to be noted that the operating conditions used in the present study were less favorable, being the reaction pressure 5 bar lower and the space velocity more than 3 times higher. Regarding the selectivity to DME, the results here obtained (reaching values higher than 62 and 94 %, considering and not-considering the CO_2 as a reaction product, respectively) were remarkably high as compare to that obtained for other advanced catalysts [36,37]. The high selectivity to DME values here obtained could be attributed to the fairly good contact between the two active phases present in the catalytic bed. A schematic representation of the reaction tandem on a section of the fibrillar bifunctional catalytic bed is shown in Figure 6.12.
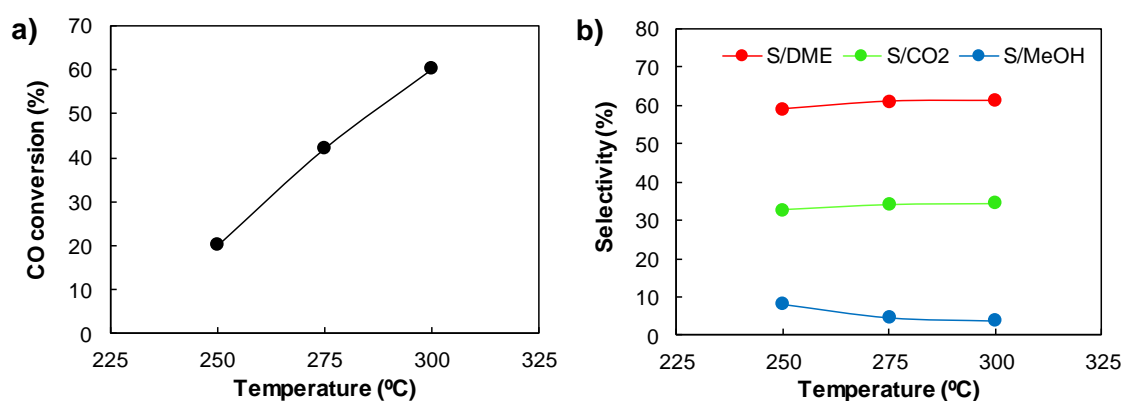
Figure 6.11. a) CO conversion and **b)** selectivity to main reaction products (DME, CO_2 and methanol (MeOH)) as a function of the temperature on FCuZnZr10Z catalyst (H_2/CO = 2, GHSV=4800 ml/g_{cat}·h, 45 bar).
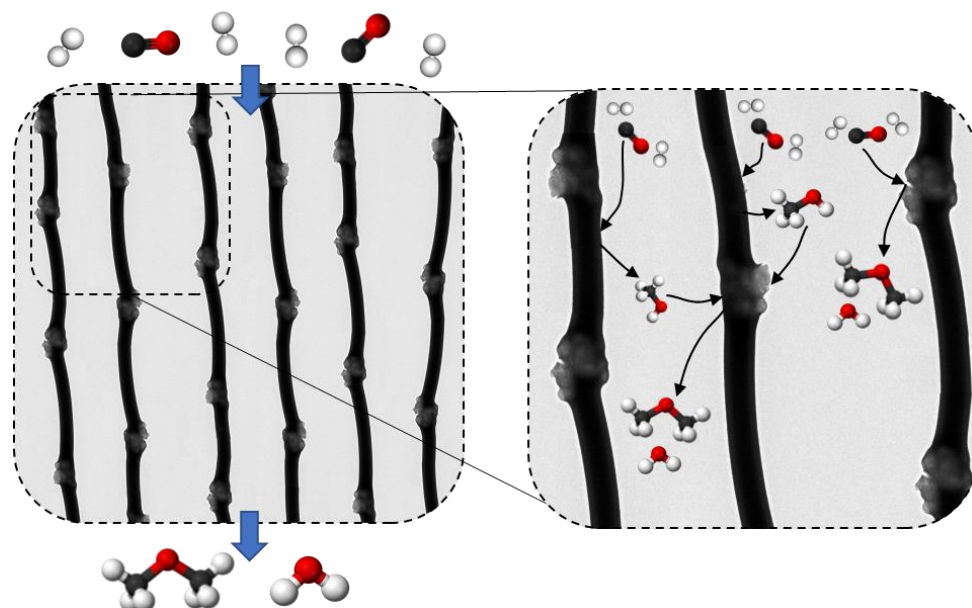
Figure 6.12. Schematic representation of the direct DME synthesis from syngas reactions on a section of the fibrillar bifunctional catalytic bed FCuZnZr10Z.

In addition, for comparative purposes, a powder catalyst (PCuZnZr10Z) was prepared keeping the same composition that the bifunctional catalyst here analyzed (20 %(w/w) Cu+Zn and 10 %(w/w) of zeolite). This material was sieved to a particle size 100 – 300 µm and used as catalyst for the direct synthesis of DME from syngas. The results showed that both the fibrillar (FCuZnZr10Z) and the powder (PCuZnZr10Z) catalysts presented the same product distribution, indicating that both catalysts possessed enough acid sites for promoting the methanol dehydration reaction. However, the powder catalyst presented a 50 % lower CO conversion value as compared to one obtained for the fibrillar bifunctional catalyst (70 % and 35 % for the fibrillar and powder catalysts, respectively, at T= 300 ºC, H$_2$/CO = 2, GHSV=4800 ml/g$_{cat}$·h, 45 bar, 4 hours on stream).

In order to explain the lower CO conversion achieved by using the powder catalyst (PCuZnZr10Z) as compared to the fibrillar one (FCuZnZr10Z), the former was also characterized. The results showed that, although both catalysts presented the same composition and were prepared by using the same metal oxide precursors, the chemical and metallic surface properties were highly

influenced by the morphology of the material. Fig. 9 also shows the XRD pattern obtained for the powder bifunctional catalyst (PCuZnZr10Z). As can be appreciated, the diffraction peak at $2\theta = 38.8$ º, associated to CuO crystal phase, was more intense and narrower in the case of the powder catalyst, indicating a higher crystallite size for CuO. The mean CuO crystal size was calculated for the powder catalyst by using the Williamson-Hall method, being obtained a value of 27 nm, which is considerably higher than the one obtained for the fibrillar (FCuZnZr10Z) catalyst, 7.3 nm. In addition, H_2-TPR analyses, showed that CuO reduction took place at higher temperature in the powder catalyst, which evidenced the presence of bigger CuO particles in this catalyst (See Fig. 10). In the same line, the Cu metallic surface area obtained showed a much lower value (about 35 % lower) as compared to the one obtained for the fibrillar catalyst (FCuZnZr10Z) (see Table 6.3), which is in good agreement with the bigger CuO particle and crystal size in the powder catalyst (PCuZnZr10Z), as revealed by H_2-TPR and XRD analyses, respectively.

These results clearly highlight that conformation of the catalyst to a fibrillar morphology in the submicrometric scale by using the electrospinning technique was of great importance for the metallic surface properties development and for the efficient performance of the catalyst.

It is also worth to remark that the fibrillar nanostructured catalyst loading in the fixed-bed reactor resulted in the obtention of a spongy-like catalytic bed, which presented an enhanced contact, in the submicrometric scale, between the two active phases involved in the syngas to DME process (see Figure 6.12). This catalytic bed performed very efficient in terms of intraparticle mass and heat transfer, avoiding, at the same time, the problems related to pressure drops of fixed-bed reactors working with such a reduced particle size.

The advantage of using a fibrillar structured catalyst instead of a conventional particles packed bed, in terms of avoiding pressure drop inside the fixed-bed reactor, was also theoretically addressed in the present work. In this line, the pressure drop inside the reactor was calculated for the fibrillar catalytic bed and it was compared to the value obtained for a powder catalyst with the same effective dimension. For the conditions used in this study, the Re_{mp}

(Reynolds number for porous media) showed a value of $1.73 \cdot 10^{-4}$, which indicated a laminar flow regime. Under these conditions, the pressure drop can be calculated by combining the Darcy's Law along with the Kozeny-Carman equation, which yields the following equation [72]:

$$\frac{\Delta P}{L} = k \cdot \mu \cdot A_v^2 \cdot \frac{(1-\varepsilon)^2}{\varepsilon^3} \cdot u_0 \qquad \text{Eq. (6.1)}$$

Where, ΔP is the pressure drop, L is the bed length, k is the Kozeny constant, A_v is the geometrical surface area, ε is the bed porosity and u_0 is the superficial velocity. The Kozeny constant characterizes the shape and the orientation of the material, for highly porous media, the Kozeny constant has been also reported to be a function of the porosity [73], and several empirical correlations have been proposed for the estimation of this factor [72].

The fibrillar catalytic bed analyzed in the present work (radius of the fibers 350 nm) showed a porosity value of 0.97 was obtained, which is in good agreement with the porosity values reported by Jackson and James [74]. This porosity value is very high as compared to the values usually found for particle packed beds, which ranges from 0.25 to 0.47. For the fibrillar catalytic bed studied in the present work, the Kozeny factor was calculated by using the empirical correlation reported by Ingmanson et al. [75]. The pressure drop for this fibrillar packed bed showed a value of 0.59 bar/m. On the other hand, the pressure drop was also calculated for a packed bed reactor containing spherical particles presenting the same dimension than the fibers (r = 250 nm), by using the Ergun equation for laminar flow [76]. The value obtained for the pressure drop was, in the case of this particle packed bed, 6500 bar/m, which is more than 10000 times higher than the value calculated for the fibrillar packed bed. These results clearly highlight the advantage of using the catalyst in a fibrillar conformation for its application in a fixed bed reactor.

Regarding the preparation of advanced catalysts, some studies dealing with the preparation of core-shell catalysts for this reaction can be found in the literature [35,37,38]. The preparation of these catalysts involves complex methodologies and a granulation stage at some point of their preparation procedure is required for their application in a fixed-bed reactor. Furthermore, this

granulation stage, needed for avoiding the pressure drops inside the reactor, limits the size of the core-shell material, which have been reported to be in the order of several hundreds of microns, with a shell thickness ranging from 3 to 5 µm [35]. However, the fibrillar nanostructured catalysts we are reporting in the present study were prepared in a one-step process and were directly used as catalysts in a fixed bed reactor, avoiding any pressure drop limitation, as theoretically checked. Moreover, it has to be highlighted that the core-shell like structure dimension of these fibrillar catalysts presents values 1000 times smaller than the ones reported in the literature for powder core-shell type catalysts [35,38], enhancing the contact between the two active phases.

6.4.- Conclusions

In conclusion, electrospinning is a useful technique for the one-step preparation of submicron (nanostructured) ZrO_2-ZSM-5 fibrillar materials in the form of core-shell like structures. For this aim, different amounts of ZSM-5 zeolite were added to a PVP-zirconium acetate solution. These polymeric suspensions were electrospun and calcined in a muffle furnace at 500 ºC. SEM and TEM images showed fibers with a high aspect ratio and mean sizes of 275 nm and the presence of zeolite aggregates around the zirconium oxide nanofiber, in the form of core-shell like structures. X-ray diffraction (XRD) analyses further confirmed the presence of both the zirconia and ZSM-5 zeolite crystal phases. The addition of copper and zinc salts to the electrospinning solution resulted in the preparation of fibrillar bifunctional catalysts, presenting the same core-shell like structures. These materials worked very efficiently as catalysts in the methanol dehydration reaction and in the direct synthesis of dimethyl ether (DME) in a fixed-bed reactor.

For comparative purposes, a powder catalyst keeping the same composition that the fibrillar bifunctional catalyst was prepared. The results clearly highlighted that conformation of the catalyst in a fibrillar morphology, in the submicrometric scale, by using the electrospinning technique was of great importance for the metallic surface properties development and for the efficient operation of the catalyst. In this sense, the bifunctional catalysts presenting a

fibrillar morphology yielded a CO conversion two times higher than that obtained for the powder catalyst.

It is also worth to remark that the fibrillar nanostructured catalyst loading in the fixed-bed reactor resulted in the obtention of a spongy-like catalytic bed, which presented an enhanced contact, in the submicrometric scale, between the two active phases involved in the syngas to DME process. This catalytic bed worked very efficient in the direct DME synthesis from syngas in terms of intraparticle mass and heat transfer, avoiding, at the same time, the problems related to pressure drops of fixed-bed reactors working with such a reduced particle size. The advantage of using a fibrillar structured catalyst instead of a conventional particles packed bed, in terms of avoiding pressure drop inside the fixed-bed reactor, was also theoretically addressed in the present work. The pressure drop calculation results showed a value more than 10000 times smaller for the fibrillar packed bed than the value calculated for the particles packed bed, which clearly highlight the advantage of the use of the catalyst in a fibrillar conformation for its application in a fixed bed reactor.

6.5.-References

[1]   D.M. D'Alessandro, B. Smit, J.R. Long, Carbon Dioxide Capture: Prospects for New Materials, Angew. Chemie Int. Ed. 49 (2010) 6058–6082. doi:10.1002/anie.201000431.

[2]   A. Corma, Inorganic Solid Acids and Their Use in Acid-Catalyzed Hydrocarbon Reactions, Chem. Rev. 95 (1995) 559–614. doi:10.1021/cr00035a006.

[3]   F. Li, S. Ding, Z. Wang, Z. Li, L. Li, C. Gao, Z. Zhong, H. Lin, C. Chen, Production of Light Olefins from Catalytic Cracking Bio-oil Model Compounds over La $_2$ O $_3$ -Modified ZSM-5 Zeolite, Energy & Fuels. 32 (2018) 5910–5922. doi:10.1021/acs.energyfuels.7b04150.

[4]   D. Srinivasan, R. Rao, A. Zribi, Synthesis of novel micro- and mesoporous zeolite nanostructures using electrospinning techniques, J. Electron. Mater. 35 (2006) 504–509. doi:10.1007/BF02690538.

[5]   A. Corma, From microporous to mesoporous molecular sieve materials and their use in catalysis, Chem. Rev. 97 (1997) 2373–2420. doi:10.1021/CR960406N.

[6]   D.E. Bryant, W.L. Kranich, Dehydration of alcohols over zeolite catalysts, J. Catal. 8 (1967) 8–13. doi:10.1016/0021-9517(67)90275-8.

[7]   E. Catizzone, A. Aloise, M. Migliori, G. Giordano, Dimethyl ether synthesis via methanol dehydration: Effect of zeolite structure, Appl. Catal. A Gen. 502 (2015) 215–220. doi:10.1016/j.apcata.2015.06.017.

[8]   S. Jiang, J.-S. Hwang, T. Jin, T. Cai, W. Cho, Y.-S. Baek, S.-E. Park, Dehydration of Methanol to Dimethyl Ether over ZSM-5 Zeolite, Bull. Korean Chem. Soc. 25 (2004) 185–189. doi:10.5012/bkcs.2004.25.2.185.

[9]   F. Pan, X. Lu, Q. Zhu, Z. Zhang, Y. Yan, T. Wang, S. Chen, A fast route for synthesizing nano-sized ZSM-5 aggregates, J. Mater. Chem. A. 2 (2014) 20667–20675. doi:10.1039/C4TA04073B.

[10]   S.F. Anis, A. Khalil, Saepurahman, G. Singaravel, R. Hashaikeh, A review on the fabrication of zeolite and mesoporous inorganic nanofibers formation for catalytic applications, Microporous Mesoporous Mater. 236 (2016) 176–192. doi:10.1016/J.MICROMESO.2016.08.043.

[11]   A. Aranzabal, D. Iturbe, M. Romero-Sáez, M.P. González-Marcos, J.R. González-Velasco, J.A. González-Marcos, Optimization of process parameters on the extrusion of honeycomb shaped monolith of H-ZSM-5 zeolite, Chem. Eng. J. 162 (2010) 415–423. doi:10.1016/J.CEJ.2010.05.043.

[12]   Y. Park, Y. Ju, D. Park, C.-H. Lee, Adsorption equilibria and kinetics of six pure gases on pelletized zeolite 13X up to 1.0 MPa: CO2, CO, N2, CH4, Ar and H2, Chem. Eng. J. 292 (2016) 348–365. doi:10.1016/J.CEJ.2016.02.046.

[13]   J. Pérez-Ramírez, C.H. Christensen, K. Egeblad, C.H. Christensen, J.C. Groen, Hierarchical zeolites: enhanced utilisation of microporous crystals in catalysis by advances in materials design, Chem. Soc. Rev. 37 (2008) 2530. doi:10.1039/b809030k.

[14]   L. Tosheva, V.P. Valtchev, Nanozeolites: Synthesis, Crystallization Mechanism, and Applications, Chem. Mater. 17 (2005) 2494–2513. doi:10.1021/cm047908z.

[15]   A.A. Rownaghi, F. Rezaei, M. Stante, J. Hedlund, Selective dehydration of methanol to dimethyl ether on ZSM-5 nanocrystals, Appl. Catal. B Environ. 119–120 (2012) 56–61. doi:10.1016/J.APCATB.2012.02.017.

[16]   G.-T. Vuong, V.-T. Hoang, D.-T. Nguyen, T.-O. Do, Synthesis of nanozeolites and nanozeolite-based FCC catalysts, and their catalytic activity in gas oil cracking reaction, Appl. Catal. A Gen. 382 (2010) 231–239. doi:10.1016/J.APCATA.2010.04.049.

[17]   M. Rutkowska, D. Macina, N. Mirocha-Kubień, Z. Piwowarska, L. Chmielarz, Hierarchically structured ZSM-5 obtained by desilication as

new catalyst for DME synthesis from methanol, Appl. Catal. B Environ. 174–175 (2015) 336–343. doi:10.1016/J.APCATB.2015.03.006.

[18] A. Ateka, I. Sierra, J. Ereña, J. Bilbao, A.T. Aguayo, Performance of CuO-ZnO-ZrO$_2$ and CuO-ZnO-MnO as metallic functions and SAPO-18 as acid function of the catalyst for the synthesis of DME co-feeding CO$_2$, Fuel Process. Technol. 152 (2016) 34–45. doi:10.1016/j.fuproc.2016.05.041.

[19] F. Dadgar, R. Myrstad, P. Pfeifer, A. Holmen, H.J. Venvik, Direct dimethyl ether synthesis from synthesis gas: The influence of methanol dehydration on methanol synthesis reaction, Catal. Today. 270 (2016) 76–84. doi:10.1016/j.cattod.2015.09.024.

[20] A.T. Aguayo, J. Ereña, D. Mier, J.M. Arandes, M. Olazar, J. Bilbao, Kinetic Modeling of Dimethyl Ether Synthesis in a Single Step on a CuO−ZnO−Al$_2$O$_3$/γ-Al$_2$O$_3$ Catalyst, Ind. Eng. Chem. Res. 46 (2007) 5522–5530. doi:10.1021/IE070269S.

[21] A. García-Trenco, A. Martínez, Direct synthesis of DME from syngas on hybrid CuZnAl/ZSM-5 catalysts: New insights into the role of zeolite acidity, Appl. Catal. A Gen. 411–412 (2012) 170–179. doi:10.1016/j.apcata.2011.10.036.

[22] J. Ereña, R. Garoña, J.M. Arandes, A.T. Aguayo, J. Bilbao, Effect of operating conditions on the synthesis of dimethyl ether over a CuO-ZnO-Al$_2$O$_3$/NaHZSM-5 bifunctional catalyst, Catal. Today. 107–108 (2005) 467–473. doi:10.1016/j.cattod.2005.07.116.

[23] J. Sun, G. Yang, Y. Yoneyama, N. Tsubaki, Catalysis Chemistry of Dimethyl Ether Synthesis, ACS Catal. 4 (2014) 3346–3356. doi:10.1021/cs500967j.

[24] M. Sánchez-Contador, A. Ateka, P. Rodriguez-Vega, J. Bilbao, A.T. Aguayo, Optimization of the Zr Content in the CuO-ZnO-ZrO$_2$/SAPO-11 Catalyst for the Selective Hydrogenation of CO+CO$_2$ Mixtures in the Direct Synthesis of Dimethyl Ether, Ind. Eng. Chem. Res. 57 (2018) 1169–1178. doi:10.1021/acs.iecr.7b04345.

[25] T. Witoon, N. Kachaban, W. Donphai, P. Kidkhunthod, K. Faungnawakij, M. Chareonpanich, J. Limtrakul, Tuning of catalytic CO$_2$ hydrogenation by changing composition of CuO–ZnO–ZrO$_2$ catalysts, Energy Convers. Manag. 118 (2016) 21–31. doi:10.1016/J.ENCONMAN.2016.03.075.

[26] Q. Ge, Y. Huang, F. Qiu, S. Li, Bifunctional catalysts for conversion of synthesis gas to dimethyl ether, Appl. Catal. A Gen. 167 (1998) 23–30.

[27] J. Ereña, I. Sierra, M. Olazar, A.G. Gayubo, A.T. Aguayo, Deactivation of a CuO-ZnO-Al$_2$O$_3$/γ-Al$_2$O$_3$ catalyst in the synthesis of dimethyl ether, Ind. Eng. Chem. Res. 47 (2008) 2238–2247.

[28] M. Stiefel, R. Ahmad, U. Arnold, M. Döring, Direct synthesis of dimethyl ether from carbon-monoxide-rich synthesis gas: Influence of dehydration catalysts and operating conditions, Fuel Process. Technol. 92 (2011) 1466–1474. doi:10.1016/J.FUPROC.2011.03.007.

[29] D. Mao, W. Yang, J. Xia, B. Zhang, Q. Song, Q. Chen, Highly effective hybrid catalyst for the direct synthesis of dimethyl ether from syngas with magnesium oxide-modified HZSM-5 as a dehydration component, J. Catal. 230 (2005) 140–149. doi:10.1016/J.JCAT.2004.12.007.

[30] G. Bonura, M. Cordaro, L. Spadaro, C. Cannilla, F. Arena, F. Frusteri, Hybrid Cu–ZnO–ZrO$_2$/H-ZSM5 system for the direct synthesis of DME by CO$_2$ hydrogenation, Appl. Catal. B Environ. 140–141 (2013) 16–24. doi:10.1016/J.APCATB.2013.03.048.

[31] P.S.S. Prasad, J.W. Bae, S. Kang, Y. Lee, K. Jun, Single-step synthesis of DME from syngas on Cu – ZnO – Al$_2$O$_3$/zeolite bifunctional catalysts : The superiority of ferrierite over the other zeolites, Fuel Process. Technol. 89 (2008) 1281–1286. doi:10.1016/j.fuproc.2008.07.014.

[32] S.-H. Kang, J.W. Bae, H.-S. Kim, G.M. Dhar, K.-W. Jun, Enhanced catalytic performance for dimethyl ether synthesis from syngas with the addition of Zr or Ga on a Cu−ZnO−Al$_2$O$_3$/γ-Al$_2$O$_3$ bifunctional catalyst, Energy & Fuels. 24 (2010) 804–810. doi:10.1021/ef901133z.

[33]   J. Sun, G. Yang, Q. Ma, I. Ooki, A. Taguchi, T. Abe, Q. Xie, Y. Yoneyama, N. Tsubaki, Fabrication of active Cu–Zn nanoalloys on H-ZSM5 zeolite for enhanced dimethyl ether synthesis via syngas, J. Mater. Chem. A. 2 (2014) 8637. doi:10.1039/c3ta14936f.

[34]   X. Liu, M.-H. Liu, Y.-C. Luo, C.-Y. Mou, S.D. Lin, H. Cheng, J.-M. Chen, J.-F. Lee, T.-S. Lin, Strong metal-support interactions between gold nanoparticles and ZnO nanorods in CO oxidation, J. Am. Chem. Soc. 134 (2012) 10251–10258. doi:10.1021/ja3033235.

[35]   G. Yang, N. Tsubaki, J. Shamoto, Y. Yoneyama, Y. Zhang, Confinement effect and synergistic function of H-ZSM-5/Cu-ZnO-Al$_2$O$_3$ capsule catalyst for one-step controlled synthesis, J. Am. Chem. Soc. 132 (2010) 8129–8136. doi:10.1021/ja101882a.

[36]   R. Phienluphon, K. Pinkaew, G. Yang, J. Li, Q. Wei, Y. Yoneyama, T. Vitidsant, N. Tsubaki, Designing core (Cu/ZnO/Al$_2$O$_3$)–shell (SAPO-11) zeolite capsule catalyst with a facile physical way for dimethyl ether direct synthesis from syngas, Chem. Eng. J. 270 (2015) 605–611. doi:10.1016/J.CEJ.2015.02.071.

[37]   Y. Wang, W. Wang, Y. Chen, J. Ma, R. Li, Synthesis of dimethyl ether from syngas over core–shell structure catalyst CuO–ZnO–Al$_2$O$_3$@SiO$_2$–Al$_2$O$_3$, Chem. Eng. J. 250 (2014) 248–256. doi:10.1016/j.cej.2014.04.018.

[38]   M. Sánchez-Contador, A. Ateka, A.T. Aguayo, J. Bilbao, Direct synthesis of dimethyl ether from CO and CO$_2$ over a core-shell structured CuO-ZnO-ZrO$_2$@SAPO-11 catalyst, Fuel Process. Technol. 179 (2018) 258–268. doi:10.1016/J.FUPROC.2018.07.009.

[39]   R. Ruiz-Rosas, J. Bedia, M. Lallave, I.G. Loscertales, A. Barrero, J. Rodríguez-Mirasol, T. Cordero, The production of submicron diameter carbon fibers by the electrospinning of lignin, Carbon N. Y. 48 (2010) 696–705. doi:10.1016/J.CARBON.2009.10.014.

[40]   R. Ruiz-Rosas, J. Bedia, J.M. Rosas, M. Lallave, I.G. Loscertales, J. Rodríguez-Mirasol, T. Cordero, Methanol decomposition on electrospun

zirconia nanofibers, Catal. Today. 187 (2012) 77–87. doi:10.1016/j.cattod.2011.10.031.

[41]   G. Larsen, R. Velarde-Ortiz, K. Minchow, A. Barrero, I.G. Loscertales, A Method for Making Inorganic and Hybrid (Organic/Inorganic) Fibers and Vesicles with Diameters in the Submicrometer and Micrometer Range via Sol−Gel Chemistry and Electrically Forced Liquid Jets, J. Am. Chem. Soc. 125 (2003) 1154–1155. doi:10.1021/JA028983I.

[42]   F.J. García-Mateos, R. Berenguer, M.J. Valero-Romero, J. Rodríguez-Mirasol, T. Cordero, Phosphorus functionalization for the rapid preparation of highly nanoporous submicron-diameter carbon fibers by electrospinning of lignin solutions, J. Mater. Chem. A. 6 (2018) 1219–1233. doi:10.1039/C7TA08788H.

[43]   I.G. Loscertales, A. Barrero, M. Márquez, R. Spretz, R. Velarde-Ortiz, G. Larsen, Electrically Forced Coaxial Nanojets for One-Step Hollow Nanofiber Design, J. Am. Chem. Soc. 126 (2004) 5376–5377. doi:10.1021/JA049443J.

[44]   K. Huang, X. Chu, W. Feng, C. Zhou, W. Si, X. Wu, L. Yuan, S. Feng, Catalytic behavior of electrospinning synthesized $La_{0.75}Sr_{0.25}MnO_3$ nanofibers in the oxidation of CO and CH_4, Chem. Eng. J. 244 (2014) 27–32. doi:10.1016/J.CEJ.2014.01.056.

[45]   R. Ruiz-Rosas, J.M. Rosas, I.G. Loscertales, J. Rodríguez-Mirasol, T. Cordero, Electrospinning of silica sub-microtubes mats with platinum nanoparticles for NO catalytic reduction, Appl. Catal. B Environ. 156–157 (2014) 15–24. doi:10.1016/J.APCATB.2014.02.047.

[46]   J. Liu, G. Jiang, Y. Liu, J. Di, Y. Wang, Z. Zhao, Q. Sun, C. Xu, J. Gao, A. Duan, J. Liu, Y. Wei, Y. Zhao, L. Jiang, Hierarchical Macro-meso-microporous ZSM-5 Zeolite Hollow Fibers With Highly Efficient Catalytic Cracking Capability, Sci. Rep. 4 (2015) 7276. doi:10.1038/srep07276.

[47]   M.J. Valero-Romero, E.M. Márquez-Franco, J. Bedia, J. Rodríguez-Mirasol, T. Cordero, Hierarchical porous carbons by liquid phase

impregnation of zeolite templates with lignin solution, Microporous Mesoporous Mater. 196 (2014) 68–78. doi:10.1016/J.MICROMESO.2014.04.055.

[48] M. Lallave, J. Bedia, R. Ruiz-Rosas, J. Rodríguez-Mirasol, T. Cordero, J.C. Otero, M. Marquez, A. Barrero, I.G. Loscertales, Filled and Hollow Carbon Nanofibers by Coaxial Electrospinning of Alcell Lignin without Binder Polymers, Adv. Mater. 19 (2007) 4292–4296. doi:10.1002/adma.200700963.

[49] S. Brunauer, P.H. Emmett, E. Teller, Adsorption of Gases in Multimolecular Layers, J. Am. Chem. Soc. 60 (1938) 309–319. doi:10.1021/ja01269a023.

[50] S. Lowell, J.E. Shields, J.E. Morral, Powder Surface Area and Porosity, 2nd Edition, 1985. doi:10.1115/1.3225796.

[51] M.M. Dubinin, The Potential Theory of Adsorption of Gases and Vapors for Adsorbents with Energetically Nonuniform Surfaces., Chem. Rev. 60 (1960) 235–241. doi:10.1021/cr60204a006.

[52] A. Khorsand Zak, W.H. Abd. Majid, M.E. Abrishami, R. Yousefi, X-ray analysis of ZnO nanoparticles by Williamson–Hall and size–strain plot methods, Solid State Sci. 13 (2011) 251–256. doi:10.1016/J.SOLIDSTATESCIENCES.2010.11.024.

[53] G.C. Chinchen, C.M. Hay, H.D. Vandervell, K.C. Waugh, The measurement of copper surface areas by reactive frontal chromatography, J. Catal. 103 (1987) 79–86. doi:10.1016/0021-9517(87)90094-7.

[54] Y. Jin, D. Yang, D. Kang, X. Jiang, Fabrication of Necklace-like Structures via Electrospinning, Langmuir. 26 (2010) 1186–1190. doi:10.1021/la902313t.

[55] S. Jiang, W. He, K. Landfester, D. Crespy, S.E. Mylon, The structure of fibers produced by colloid-electrospinning depends on the aggregation state of particles in the electrospinning feed, Polymer (Guildf). 127 (2017) 101–105. doi:10.1016/J.POLYMER.2017.08.061.

[56]   M. Thommes, K. Kaneko, A. V. Neimark, J.P. Olivier, F. Rodriguez-Reinoso, J. Rouquerol, K.S.W. Sing, Physisorption of gases, with special reference to the evaluation of surface area and pore size distribution (IUPAC Technical Report), Pure Appl. Chem. 87 (2015). doi:10.1515/pac-2014-1117.

[57]   J.C. Groen, L.A.A. Peffer, J.A. Moulijn, J. Pérez-Ramírez, Mechanism of Hierarchical Porosity Development in MFI Zeolites by Desilication: The Role of Aluminium as a Pore-Directing Agent, Chem. - A Eur. J. 11 (2005) 4983–4994. doi:10.1002/chem.200500045.

[58]   P. Losch, A.B. Pinar, M.G. Willinger, K. Soukup, S. Chavan, B. Vincent, P. Pale, B. Louis, H-ZSM-5 zeolite model crystals: Structure-diffusion-activity relationship in methanol-to-olefins catalysis, J. Catal. 345 (2017) 11–23. doi:10.1016/J.JCAT.2016.11.005.

[59]   K.S. Ha, Y.J. Lee, J.W. Bae, Y.W. Kim, M.H. Woo, H.S. Kim, M.J. Park, K.W. Jun, New reaction pathways and kinetic parameter estimation for methanol dehydration over modified ZSM-5 catalysts, Appl. Catal. A Gen. 395 (2011) 95–106. doi:10.1016/j.apcata.2011.01.025.

[60]   Y.H. Seo, E.A. Prasetyanto, N. Jiang, S.M. Oh, S.E. Park, Catalytic dehydration of methanol over synthetic zeolite W, Microporous Mesoporous Mater. 128 (2010) 108–114. doi:10.1016/j.micromeso.2009.08.011.

[61]   J.W. Bae, S.-H. Kang, Y.-J. Lee, K.-W. Jun, Synthesis of DME from syngas on the bifunctional Cu–ZnO–Al₂O₃/Zr-modified ferrierite: Effect of Zr content, Appl. Catal. B Environ. 90 (2009) 426–435. doi:10.1016/J.APCATB.2009.04.002.

[62]   R. Ahmad, D. Schrempp, S. Behrens, J. Sauer, M. Döring, U. Arnold, Zeolite-based bifunctional catalysts for the single step synthesis of dimethyl ether from CO-rich synthesis gas, Fuel Process. Technol. 121 (2014) 38–46. doi:10.1016/J.FUPROC.2014.01.006.

[63] Y. Hua, X. Guo, D. Mao, G. Lu, G.L. Rempel, F.T.T. Ng, Single-step synthesis of dimethyl ether from biomass-derived syngas over CuO-ZnO-MOx(M = Zr, Al, Cr, Ti)/HZSM-5 hybrid catalyst: Effects of MOx, Appl. Catal. A Gen. 540 (2017) 68–74. doi:10.1016/j.apcata.2017.04.015.

[64] T. Witoon, J. Chalorngtham, P. Dumrongbunditkul, M. Chareonpanich, J. Limtrakul, CO_2 hydrogenation to methanol over Cu/ZrO_2 catalysts: Effects of zirconia phases, Chem. Eng. J. 293 (2016) 327–336. doi:10.1016/j.cej.2016.02.069.

[65] C. Liu, X. Guo, Q. Guo, D. Mao, J. Yu, G. Lu, Methanol synthesis from CO_2 hydrogenation over copper catalysts supported on MgO-modified TiO_2, J. Mol. Catal. A Chem. 425 (2016) 86–93. doi:10.1016/J.MOLCATA.2016.09.032.

[66] G.R. Moradi, S. Nosrati, F. Yaripor, Effect of the hybrid catalysts preparation method upon direct synthesis of dimethyl ether from synthesis gas, Catal. Commun. 8 (2007) 598–606. doi:10.1016/J.CATCOM.2006.08.023.

[67] S. Asthana, C. Samanta, A. Bhaumik, B. Banerjee, R.K. Voolapalli, B. Saha, Direct synthesis of dimethyl ether from syngas over Cu-based catalysts: Enhanced selectivity in the presence of MgO, J. Catal. 334 (2016) 89–101. doi:10.1016/J.JCAT.2015.10.020.

[68] J. Agrell, H. Birgersson, M. Boutonnet, I. Melián-Cabrera, R.M. Navarro, J.L.G. Fierro, Production of hydrogen from methanol over Cu/ZnO catalysts promoted by ZrO_2 and Al_2O_3, J. Catal. 219 (2003) 389–403. doi:10.1016/S0021-9517(03)00221-5.

[69] J. Ereña, I. Sierra, A.T. Aguayo, A. Ateka, M. Olazar, J. Bilbao, Kinetic modelling of dimethyl ether synthesis from (H_2 + CO_2) by considering catalyst deactivation, Chem. Eng. J. 174 (2011) 660–667. doi:10.1016/J.CEJ.2011.09.067.

[70] W. Lu, L. Teng, W. Xiao, Simulation and experiment study of dimethyl ether synthesis from syngas in a fluidized-bed reactor, Chem. Eng. Sci. 59 (2004) 5455–5464. doi:10.1016/j.ces.2004.07.031.

[71] K. Saravanan, H. Ham, N. Tsubaki, J.W. Bae, Recent progress for direct synthesis of dimethyl ether from syngas on the heterogeneous bifunctional hybrid catalysts, Appl. Catal. B Environ. 217 (2017) 494–522. doi:10.1016/J.APCATB.2017.05.085.

[72] E. Mauret, M. Renaud, Transport phenomena in multi-particle systems— I. Limits of applicability of capillary model in high voidage beds-application to fixed beds of fibers and fluidized beds of spheres, Chem. Eng. Sci. 52 (1997) 1807–1817. doi:10.1016/S0009-2509(96)00499-X.

[73] S. Zhu, R.H. Pelton, K. Collver, Mechanistic modelling of fluid permeation through compressible fiber beds, Chem. Eng. Sci. 50 (1995) 3557–3572. doi:10.1016/0009-2509(95)00205-J.

[74] G.W. Jackson, D.F. James, The permeability of fibrous porous media, Can. J. Chem. Eng. 64 (1986) 364–374. doi:10.1002/cjce.5450640302.

[75] W.L. Ingmanson, B.D. Andrews, J.R. C., Internal pressure distributions in compressible mats under fluid stress., Tappi. 42 (1959) 840–849.

[76] S. Ergun, Fluid flow through packed columns, Chem. Eng. Prog. 48 (1952) 89–94.

Chapter 7

ZSM-5-decorated CuO/ZnO/ZrO$_2$ fibers as efficient bifunctional catalysts for the direct synthesis of DME from syngas.

7.0.-Abstract

CuO/ZnO/ZrO$_2$-ZSM-5 fibrillar bifunctional catalysts were prepared in flexible non-woven mats by using electrospinning technique. SEM and TEM images showed fibers presenting a high aspect ratio with a mean diameter of 1.5 µm and the presence of well-dispersed zeolite aggregates, with a mean size of 300 nm, attached to (or decorating) the surface of the CuO/ZnO/ZrO$_2$ fibers. The fibrillar bifunctional materials were used as catalysts for the direct dimethyl ether (DME) synthesis from syngas and the catalytic activity was well correlated with the textural, structural and surface chemistry of the bifunctional fibrillary catalysts studied. A comparison between the fibrillar catalysts here presented and a conventional powder catalyst was carried out. The conformation of the catalysts in a fibrillar morphology by a one-step electrospinning procedure was of great importance for the textural, structural and chemical properties development of these materials and, thus, for their catalytic efficiency. These fibrillar bifunctional catalysts presented a spongy-like structure, which allowed the use of these materials directly as catalytic bed in a packed-bed reactor without further modifications, operating very efficiently in this type of reactor (very low pressure drop and enhanced mass and heat transport). Beside, these fibrillar bifunctional catalysts showed an enhanced contact between the two active phases involved in the direct syngas-to-DME process, metallic and acid, which gave rise to high CO conversions and a selectivity to DME higher than 63% (95 % when considering only the products in the organic phase, without taking into account the CO$_2$). The acidity measurements determined by NH$_3$-TPD seem not to be suitable for evaluating the dehydration activity of bifunctional catalysts and more reliable results were obtained by comparing the acidity of the isolated active phases (the ones for methanol formation and dehydration).

7.1.-Introduction

The growing concerns about climate change, environmental pollution and energy consumption have been the driving force in seeking for alternative fuels [1,2]. In this scenario, DME is receiving a great deal of attention as an eco-friendly alternative fuel, since it can be produced from syngas coming from biomass

gasification [3–5]. DME shows a high cetane number (CN=55-60) when compared to refinery diesel (CN=40-55), making this compound a suitable alternative to diesel fuel for compression-ignition engines [6,7]. Apart from its high cetane number, it presents a high oxygen content (34.8 %) and the absence of C-C bonds, resulting in a smokeless combustion and low particle emissions [8]. In addition, CO and NO$_x$ emissions have been demonstrated to be also very low [9,10]. Moreover, the use of DME in compression-ignition engines reduces the noise of the motor to the level of a gasoline spark-ignited engine, keeping the fuel consumption close to diesel on an energy basis [8]. Regarding its properties, DME presents a similar boiling point and density as compared with LPG (mostly C$_3$ and C$_4$). These handling characteristics make its supply and storage feasible by using the already existing infrastructure and equipment as those used for LPG with minor modifications, reducing in this way the investment costs [11].

DME has been traditionally produced by a two-step catalytic process (so called indirect process) using synthesis gas (H$_2$ + CO/CO$_2$) as raw material. The first stage, Eq. (7.1) and (7.2), consists of the methanol synthesis by CO and/or CO$_2$ hydrogenation using a Cu/ZnO-based catalyst [12–14]. In the second one, selective methanol dehydration on a solid acid catalyst produces DME [15–18], Eq. (7.3). The main drawback of this process is the strong thermodynamic limitation affecting the methanol synthesis stage, which results in a low conversion per-pass and high gas recirculation costs [2].

$$CO + 2H_2 \leftrightarrow CH_3OH \qquad (\Delta H_r^0 = \text{-90.8 kJ·mol}^{-1}) \qquad \text{Eq. (7.1)}$$

$$CO_2 + 3H_2 \leftrightarrow CH_3OH + H_2O \qquad (\Delta H_r^0 = \text{-49.5 kJ·mol}^{-1}) \qquad \text{Eq. (7.2)}$$

$$2CH_3OH \leftrightarrow CH_3OCH_3 + H_2O \qquad (\Delta H_r^0 = \text{-21.3 kJ·mol}^{-1}) \qquad \text{Eq. (7.3)}$$

$$H_2O + CO \leftrightarrow H_2 + CO_2 \qquad (\Delta H_r^0 = \text{-41.1 kJ·mol}^{-1}) \qquad \text{Eq. (7.4)}$$
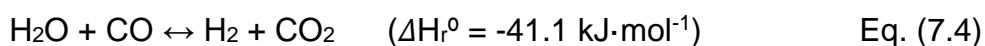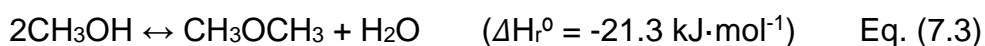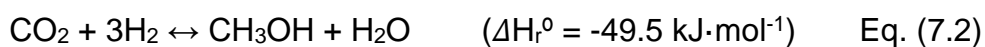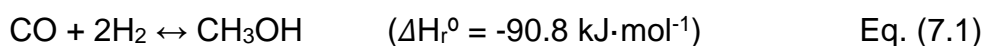
Recently, a one-step process for the direct synthesis of DME has been intensively studied [19–24]. In this process, synthesis gas is fed to a reactor containing a bifunctional catalyst, where both methanol synthesis (on the Cu-based sites of the bifunctional catalyst), Eq. (7.1) and (7.2), in parallel with the water gas shift reaction (WGSR) (Eq. 7.4), and methanol dehydration (on the acid sites of the catalyst), Eq. (7.3), take place.

The use of this direct route presents two main advantages when compared to the indirect route. On the one hand, since both methanol synthesis and dehydration occur in only one reactor, there is a reduction in the investment costs related to equipment and infrastructures. On the other hand, as the generated methanol is in-situ consumed, equilibrium constraints related to methanol synthesis are reduced. This thermodynamic advantage makes it possible to work at lower pressure and/or higher temperature achieving a higher synthesis gas conversion per pass [22,25]. In the same way, water generated in methanol dehydration (Eq. (7.3)) can be removed through the WGSR (Eq. (7.4)), also favoring the methanol dehydration reaction and yielding more H_2, which is of the utmost interest when using a synthesis gas presenting a low H_2/CO ratio, such as biomass derived syngas [4].

When preparing bifunctional catalysts, an adequate balance between the two phases (metal and acid sites, in this case) must be achieved, keeping a close proximity among them [26]. The preparation of bifunctional catalysts for this process is usually accomplished by physical mixing of their individual components [23,27–29]. Although this preparation procedure is simple and easy to scale-up, the catalysts prepared by this procedure present too great a distance between the two active sites involved in the syngas-to-DME process, thus lowering the performance of the catalyst.

As an alternative to these physical mixtures, the use of supported catalysts, in which the solid acid phase acts as support for the metallic phase, has been studied. In this way, the tandem process from synthesis gas to DME is achieved on the surface of one particle of the catalyst [30]. Conventional supported catalysts have been prepared by coprecipitation [31,32], impregnation [33] and sol-gel [34] methods. In addition to these methods, other preparation procedures have been reported for the preparation of supported bifunctional catalysts. Along this line, Gentzen et al. prepared this type of catalysts by supporting pre-synthesized Cu and ZnO nanoparticles on the acid support [35]. Zeng et al. used a physical sputtering technique for the preparation of the supported catalysts [36]. The advantages of using supported catalysts reside in the higher metallic surface area, the higher metal dispersion and a higher number of acid sites, allowing a better catalytic activity and selectivity to DME [36–38].

However, they present some drawbacks, such as their complex preparation methodologies.

All of the aforementioned catalysts are mostly prepared in powder form and, thus, for their application in industrial catalytic reactors, they need to be pelletized to a particle size in the range of 4 - 6 mm [39,40] in order to avoid high pressure drops. However, the use of such particle size gives rise to intraparticle diffuse limitations, as observed by Graaf et al. [41,42] for the methanol synthesis reaction, being the efficiency of the catalysts reduced in this way.

The use of structured catalysts could overcome the problems related to high pressure drops and enhance transport phenomena. In this line, electrospinning is a simple and straightforward technique that has been successfully applied for the preparation of carbonaceous and polymeric fibers in the submicro and nanoscale [43,44]. In this process, a viscous polymer solution held by its surface tension at the end of a capillary tube is subjected to a high voltage electric field, inducing the ejection of a charged liquid jet. As a result of the electrostatic repulsions between the surface charges, a whipping phenomenon occurs in the space between the tip of the spinneret and the collector, causing the solvent evaporation, stretching the polymeric filament and leading to the deposition of the polymer fibers on the collector [45]. The preparation of different catalysts by using the electrospinning technique has also been reported [46–48]. The use of fibrillar structured catalysts in the submicrometric scale for the direct DME synthesis from syngas could be very efficient in terms of intraparticle mass and heat transport, avoiding, at the same time, the problems of pressure drops of fixed-bed reactors working with such a reduced particle size.

In this work, we show the results on the preparation, characterization and application of one-dimensional structured bifunctional catalyst, presenting two well-defined and connected catalytic phases, metallic and acid. The use of the electrospinning technique has been highlighted as a straightforward solution to prepare bifunctional fibrillar catalysts in one step. A detailed parametric study of the direct synthesis of DME from syngas on these bifunctional fibrillar catalysts has been carried out in a continuous fixed-bed reactor. These bifunctional fibrillar

catalysts have shown a high efficiency for the direct DME synthesis from syngas and the catalytic activity has been well correlated with the textural, structural and surface chemistry of the bifunctional fibrillary catalysts studied.

7.2.-Experimental method

7.2.1.-Fibrillar catalysts preparation

The experimental procedure carried out for the preparation of the fibrillar materials presented in here involved three stages; the preparation of a polymer-based solutions, the electrospinning of the resulting solution and the calcination of the fibrillar materials.

7.2.1.1.-Polymeric solutions preparation

Two different polymeric solutions, based on different oxide precursors, were used for the preparation of the fibrillar materials. The selection of each group of oxide precursors was based on the possibility of their being dissolved together to form a homogeneous solution.

On the one hand, polymeric solutions based on zirconium (IV) propoxide (70 wt % in 1-propanol), polyvinylpyrrolidone (PVP), 1-propanol, zinc acetate and copper acetate were prepared. For the preparation of these polymeric solutions 2.74 g of zirconium (IV) propoxide solution, 3 g of 1-propanol and 0.325 g of PVP were mixed. Moreover, an appropriate amount of Cu and Zn acetates were added to the polymeric solution in order to obtain CuO+ZnO concentrations of 25 and 35 %(w/w), keeping a molar Cu/Zn ratio of 2, in the final calcined fiber. The resulting polymeric solutions were vigorously stirred for 12 h at room temperature. Samples prepared following this procedure were denoted as *FCZZX(A)*, where *X* represents the %(w/w) of CuO+ZnO in the final fiber and *(A)* refers to the use of Cu and Zn acetate as metal precursors.

On the other hand, a polymeric solution based on zirconium acetate (16 %(w/w) in acetic acid), polyvinylpyrrolidone (PVP) and 1-propanol was prepared. In this case, copper nitrate trihydrate and zinc nitrate hexahydrate were used as CuO and ZnO precursors. These polymeric solutions contained 3 g of zirconium

acetate solution, 0.325 g of PVP, 3 g of 1-propanol, with the appropriate amount of copper and zinc nitrate to obtain a final CuO+ZnO concentration of 25 and 35 %(w/w), keeping a molar Cu/Zn ratio of 2 in the final calcined fiber. The resulted polymeric solutions were vigorously stirred for 12 h at room temperature. Samples prepared from this polymeric solution were denoted as *FCZZX(N)*, where *X* represents the %(w/w) of CuO+ZnO in the final fiber and *(N)* refers to the use of Cu and Zn nitrate as metal precursors.

For the preparation of the bifunctional catalysts, different amounts of ZSM-5 zeolite (Zeolyst international, CBV 5524G, Si/Al 50, with mean crystal size of 120 nm) were also added to the polymeric solutions, to obtain a final fiber with a zeolite mass concentration ranging from 5 to 15 %(w/w). The addition of zeolite to the polymeric solutions resulted in the preparation of different polymeric suspensions, which were vigorously stirred for 8 h, prior to the electrospinning process. The bifunctional catalysts were denoted by adding *-YZ* to the name of the parent fiber, where Y accounts on the zeolite mass concentration in the final fiber.

7.2.1.2.-Electrospinning of the polymer-based solutions

The set-up used for the electrospinning process consisted of a syringe pump, a needle, a plate collector and two high voltage power suppliers; one positively polarized and connected to the needle and the other, negatively polarized, attached to the collector. By using this configuration, better electrostatic conditions to prevent fibers from flying to any grounded piece near the set-up are achieved [46].

In a usual run, the flow rate through the spinneret was set to 1.2 mL/h and the tip-to-collector distance was set to 20 cm. The electrical potential differences for the zirconium propoxide-based solutions (FCZZX(A)) and the zirconium acetate-based solutions (FCZZX(N)) were 12 and 18 kV, respectively

The eventual partial or total solidification of the Taylor cone is usually a typical problem when the electrospinning of rather volatile solvent solutions is carried out, causing the interruption of the process [47]. To address this issue, a

co-axial spinneret was used in this work, pumping 1-propanol through the outermost capillary needle at a flow rate of 0.2 mL/h.

7.2.1.3.-Calcination of the electrospun fibers.

The electrospun fiber mats were recovered in a non-woven cloth and calcined in a muffle furnace at 500 ºC for 4 h under air atmosphere, with the aim of eliminating the remaining solvent and the polymer, stabilizing the zirconia-based fibers and to transform the zeolite from the ammonium to the protonic form.

7.2.2.-Characterization of catalysts

The morphology of the prepared fibers was studied by scanning electron microscopy (SEM) using a Jeol JSM-840 microscope working at 25 kV voltage and by transmission electron microscopy (TEM) in a FEI Talos F200X microscope at an accelerating voltage of 200 kV and in a high annular dark field (HAADF).

The porous texture of the prepared fibrillar catalysts was characterized by N_2 adsorption–desorption at -196 ºC, performed in an ASAP 2020 equipment (Micromeritics). Samples were previously outgassed for at least 8 h at 150 ºC. From the N_2 adsorption-desorption isotherm, the apparent surface area (A_{BET}) was determined by applying the BET equation [48] and the estimation of the micropore volume (V_t) and the external surface (A_t) area was accomplished by the application of the t-method, using the Harkins and Jura equation [49]. The mesopore volume was determined as the difference between the adsorbed volume of N_2 at a relative pressure of 0.99 and the micropore volume, V_t.

X-ray diffraction patterns (XRD) of the prepared materials were recorded in the region 2θ = 5-90 º on a EMPYREAN diffractometer of PANalytical using CuKα monochromatic radiation (operation value 45 kV and 40 mA), a detector PIXcel and Soller slits (incident and diffracted beam) of 0.04 rad. The average crystallite sizes were estimated by the application of the Williamson-Hall method [50].

The reducibility of the metallic surface species presented on the surface of the fibers was studied by temperature programmed reduction (H_2-TPR). In these

experiments, 50 mg of sample were loaded in a quartz fixed-bed microreactor, placed inside a vertical furnace with temperature control and heated up to 100 ºC under helium. Thereafter, the helium flow was switched to a 10 %(v/v) H$_2$ in helium stream and the sample was heated up to 400 ºC, at a heating rate of 5 ºC·min^{-1}. H$_2$ consumption was monitored by mass spectroscopy (Pfeifer Omnistar GCD-301), recording the signal m/z = 2.

The Cu surface area of the prepared fibers was estimated by N$_2$O selective chemisorption. In these experiments, 100 mg of dried sample were firstly reduced under H$_2$ flow for 2 hours at a temperature of 270 ºC. Then, the sample was cooled to 60 ºC and afterwards the H$_2$ stream was switched to a N$_2$O, diluted in helium stream (2000 ppm), for the selective oxidation of the Cu^0 species [51]. N$_2$O consumption was recorded using an ECD-detector, enabling the determination of the copper dispersion and the metallic copper surface.

The total acidity of the prepared fibers was determined by temperature programmed desorption of ammonia (NH$_3$-TPD). The NH$_3$-TPD was carried out using 100 mg of dried material, which was firstly heated up to 500 ºC at a heating rate of 10 ºC/min and then cooled to 100 ºC under constant helium flow. Thereafter, the sample was saturated with NH$_3$ (20 %(v/v) in helium) for 15 minutes at 100 ºC. After saturation, the weakly adsorbed NH$_3$ was desorbed under helium flow at 100 ºC until no NH$_3$ was detected in the outlet stream. Finally, the NH$_3$-TPD was performed by raising the temperature up to 500 ºC at a heating rate of 10 ºC/min, under constant helium flow. Outlet NH$_3$ concentration was recorded using a TCD-detector.

7.2.3.-Experimental setup and procedures.

The methanol dehydration experiments were carried out at atmospheric pressure in a flow fixed-bed reactor placed in a vertical furnace with temperature control. In these experiments, methanol was fed to the system by using a syringe pump (Cole-Parmer® 74900-00-05 model), using helium as carrier gas. All lines were heated up to 120 ºC in order to avoid the condensation of any compound. The conditions used in this study were a methanol partial pressure of 0.10 atm

and a space time of 0.02 g·s·µmol$_{MeOH}^{-1}$. The DME productivity was defined as the micromole of DME generated per gram of catalyst per second.

The methanol synthesis and the direct dimethyl ether synthesis from syngas experiments were performed in a PID Eng. & Tech. Microactivity equipment, which is provided with a stainless steel fixed-bed reactor and allows for high pressure and temperature operation. Prior to starting the reaction, 500 mg of catalyst was in-situ reduced at 270 ºC under pure H$_2$ flow (50 mL·min^{-1}) for 2 h. Once carried out the reduction stage, the reaction temperature was set to the reaction value and then the pressure was slowly increased up to the desired value. Finally, the syngas was introduced. The conversion was defined as the ratio of the amount of CO converted to the amount of CO supplied to the reactor and was expressed in molar %. The selectivity (%mol) to each product was defined as the mole ratio of each product referred to the moles of CO converted.

The outlet gas concentrations were quantified by on-line gas chromatography (Perkin-Elmer Clarus 500 GC equipped with TCD and FID detectors). The columns used were a Permanent gases active carbón 80/100 mesh for CO, CO$_2$ analysis, and a 1.9m x 1/8" x 2.1mm Porapak N 80/100 + 0.5m x 1/8" x 2.1mm Porapak Q 80/100 column for methanol, DME and light hydrocarbons separation. N$_2$ was used as internal standard for GC analyses.

7.3.-Results and discussion

7.3.1 Effect of CuO-ZnO content and precursors of fibrillar catalysts on the synthesis of methanol.

The morphology of the materials was examined by scanning electron microscopy (SEM). Figure 7.1 presents the SEM micrographs of the samples prepared using the two polymeric solutions (Cu and Zn acetate (A) vs nitrate (N)) and containing different %(w/w) of CuO+ZnO. As it can be observed, the mats obtained consisted of a non-woven fabric of fibers, showing a high aspect (length to diameter) ratio and the absence of fused zones, with diameters ranging from 0.7 to 1.7 µm (Figure 7.1a-d). For both polymeric solutions, the mean diameter of the fibers slightly increased with the metal loading due to the higher concentration

of the oxide precursor in the electrospinning solution. In this sense, the average diameter obtained from SEM images for the samples FCZZ25(A), FCZZ35(A), FCZZ25(N) and FCZZ35(N) showed values of 1.2, 1.5, 1.1 and 1.5 □m, respectively. The surface morphology of the fibers was also influenced by the metal content. The fibers containing a 25 %(w/w) of CuO+ZnO, FZCZZ25(A) and FZCZZ25(N), presented a very smooth surface (See Figure 7.1a and c). On the contrary, the presence of aggregated particles on the surface of the fibers containing a 35 %(w/w) of CuO+ZnO, FZCZZ35(A) and FZCZZ35(N), is clear, showing a rough surface (See Figures 7.1b and d and Figures 7.2b and d).
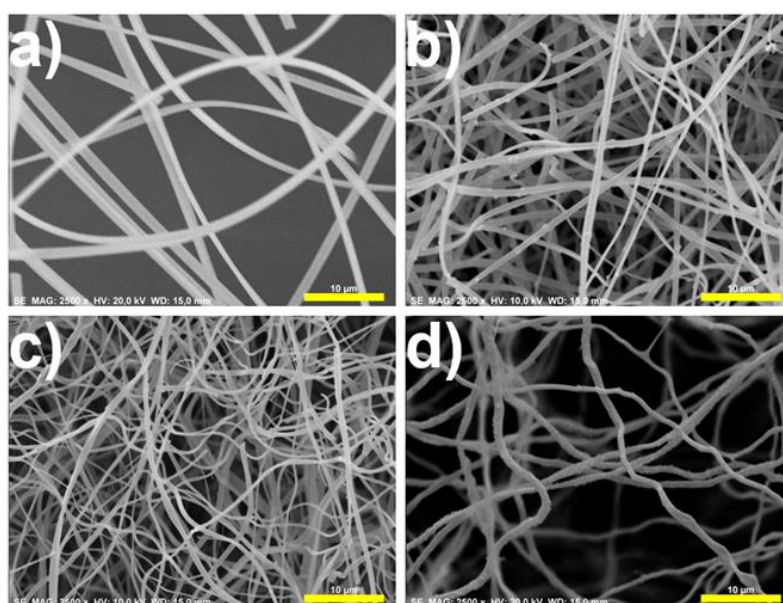
Figure 7.1. Scanning electron micrographs of the fibers **a)** FCZZ25(A), **b)** FCZZ35(A), **c)** FCZZ25(N), and **d)** FCZZ35(N). Bar lengths are 10 μm.

The chemical composition and the elemental distribution of the fibers was analyzed by transmission electron microscopy energy-dispersive X-ray spectroscopy (TEM-EDXA). Figure 7.2 shows selected high-angle annular dark field scanning electron microscopy (HAADF-STEM) images, along with the O, Zr, Cu and Zn EDXA elemental mappings of these regions of the samples. O and Zr elemental mappings showed a good dispersion for this element in all the samples. It is noteworthy that the elemental distribution for Cu and Zn was highly influenced by the metal content. The fibers containing a 25 %(w/w) of CuO+ZnO, FZCZZ25(A) and FZCZZ25(N), presented a uniform distribution of these

elements, indicating an intimate interaction between them and all the elements present in the material. On the other hand, the samples containing a 35 %(w/w) of CuO+ZnO, FZCZZ35(A) and FZCZZ35(N), did not exhibit so homogeneous Cu and Zn elemental surface distributions, evidencing the presence of CuO and ZnO aggregates, with sizes varying from 50 to 200 nm. The high concentration of Cu in the particles observed on the surface of the fibers with the highest concentration of Cu+Zn (35% (w/w)) indicated that part of the copper present in these fibers sintered during the calcination stage at 500 ºC.

It has been reported in the literature that ZrO_2, in addition to favoring the dispersion of CuO, also improves its thermal resistance, avoiding its sintering [5]. In their study Sanchez-Contador et al. [54] demonstrated that the temperature at which this sintering process occurred depended on the Zr content in the material, being observed CuO sintering temperatures of 550 and 600 ºC for the sample presenting Cu:Zn:Zr molar ratios of 2:1:1 and 2:1:2, respectively. In the present study, the molar ratio for the samples containing a 25 and a 35 %(w/w) of CuO + ZnO were 2:1:5.8 and 2:1:3.6, respectively, and the calcination stage was carried out at 500 ºC. Therefore, CuO sintering should not have occurred in these samples. However, the combustion of the polymer (PVP) and the organic part of the metal precursors during the calcination stage could have given rise to hot spots in the fibrillar material, thus reaching a higher local temperature in some points of the fiber, yielding the sintering of CuO in the case of the fibers with the highest concentration of metal content (35 % (w/w)).
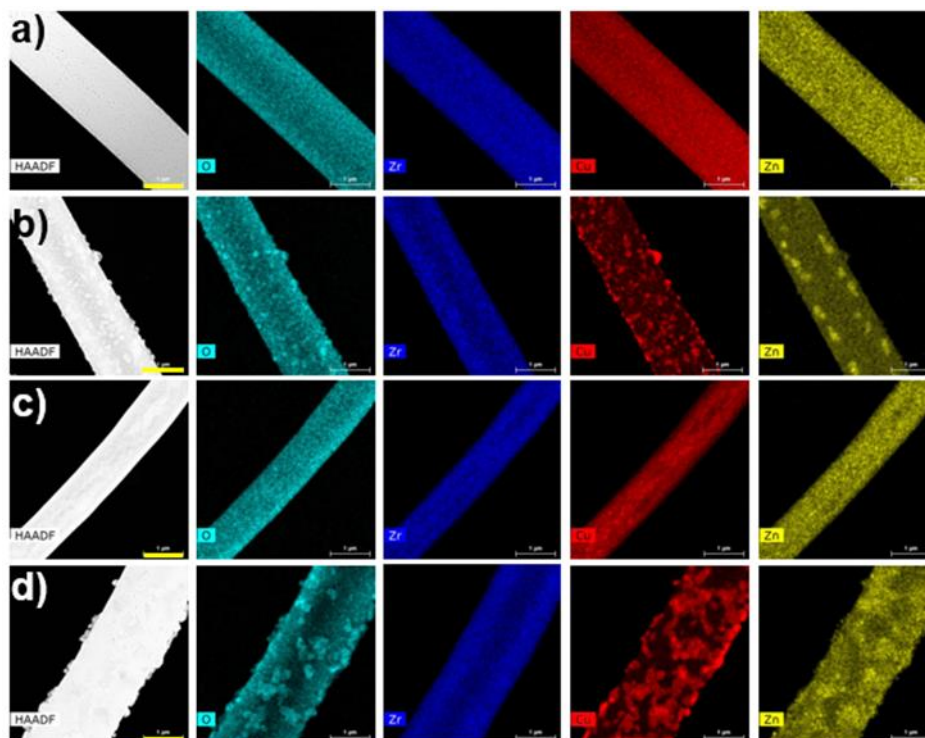
Figure 7.2. HAADF-STEM image, and EDXA elemental mappings of O (greenish-blue), Zr (dark blue), Cu (red) and Zn (yellow), of the fibers **a)** FCZZ25(A), **b)** FCZZ35(A), **c)** FCZZ25(N), and **d)** FCZZ35(N). Bar lengths are 1 µm.

Figure 7.3 presents the N_2 adsorption-desorption isotherms at -196 ºC of the different fibers. All the fibers presented a type IVa isotherm [55], characteristic of a mesoporous solid, adsorbing most of N_2 in the range of high relative pressures. Type H1 hysteresis loop, closing at a relative pressure of 0.8 was observed for the sample FCZZ25(A), which indicated the presence of a narrow range of uniform wide mesopores [55]. When increasing the metal (CuO + ZnO) content, a change in the hysteresis loop from H1 to H5, closing in this case at a relative pressure of 0.4, was appreciated (see FCZZ35(A) in Figure 7.3), indicating the presence of narrower mesopores. It seems that the increased amount of CuO+ZnO loaded in FCZZ35(A) is located on the wider mesopore surface, narrowing the size of these (wider) mesopores (thus, increasing the volume of the narrower mesopores in this sample). FCZZ25(N) and FCZZ35(N) exhibited a type H4 hysteresis loop closing at a relative pressure of 0.4, associated to capillary condensation in mesopores presenting a wide range of

pore sizes. The increase of metal loading in these fibers had also a certain effect on the mesopore size distribution, although it was less pronounced in this case.
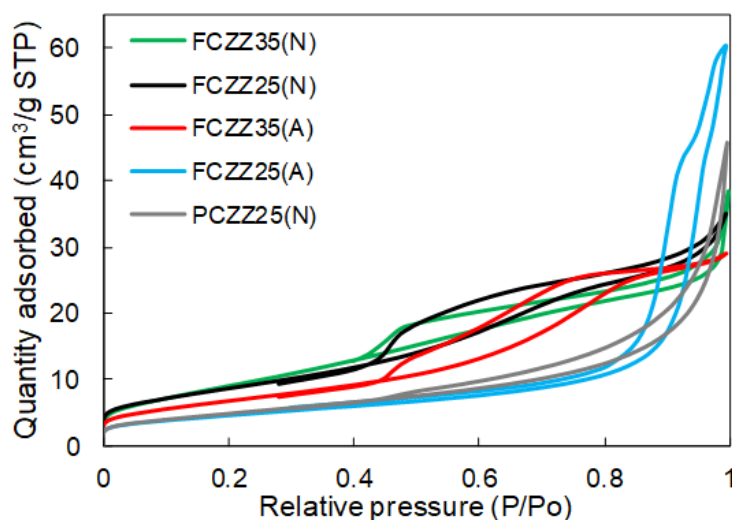
Figure 7.3. N_2 adsorption–desorption isotherms at -196 ºC.

Table 7.1 summarizes the textural parameters calculated from N_2 adsorption-desorption isotherms. All the fibers presented a similar value of the pore volume. However, they showed different specific surface areas, due to their different mesopore size distribution, with higher A_{BET} and A_t for the ones with narrower mesopores. It is noteworthy that the external surface area, A_t, showed very similar values to the ones calculated by the BET equation, A_{BET}, pointing out that these fibers presented mainly a mesoporous texture.

Table 7.1. Different textural parameters, pore volume (V_p), apparent surface area (A_{BET}) and external surface area (A_t), calculated from N_2 adsorption-desorption isotherm.

Sample	V_p (cm^3·g^{-1})	A_{BET} (m^2·g^{-1})	A_t (m^2·g^{-1})
FCZZ25(A)	0.09	17	17
FCZZ35(A)	0.05	25	25
FCZZ25(N)	0.05	32	32
FCZZ35(N)	0.06	35	35
PCZZ25(N)	0.07	18	18

X-ray diffraction patterns of the fibers are shown in Figure 7.4. All the samples presented intense diffraction peaks at $2\theta = 30.2$ º, 35.2 º, 50.6 º and 60.2 º, which correspond to the tetragonal zirconia crystalline phase. The diffraction peaks at $2\theta = 35.6$ º and 38.8 º were identified as CuO crystal phase. It is noteworthy that these peaks intensified and got narrower when increasing the metal content from 25 to 35 %(w/w), evidencing the sintering of the metal. Regarding the ZnO crystal phase, only the diffraction peak at $2\theta = 47.5$ º could be appreciated in the samples FCZZ35(A) and FCZZ35(N). Table 7.2 summarized the mean CuO crystallite size estimated using the Williamson-Hall method. The results showed that the CuO crystallite size greatly increased when passing from 25 to 35 %(w/w) (CuO + ZnO) in the fiber. Regarding the samples FCZZ25(N) and FCZZ25(A), it can be observed that the former showed a much smaller CuO crystallite size than the latter. This fact indicated that the preparation of these fibrillar materials by using Zr acetate and Cu and Zn nitrates as oxide precursors resulted in a higher interaction between the oxides composing the fiber, leading to a better CuO dispersion and preventing its sintering. In this sense, the CuO crystal size here obtained is smaller than that reported for other catalysts calcined at the same temperature (500 ºC) [34] and even at lower temperatures [31,56].
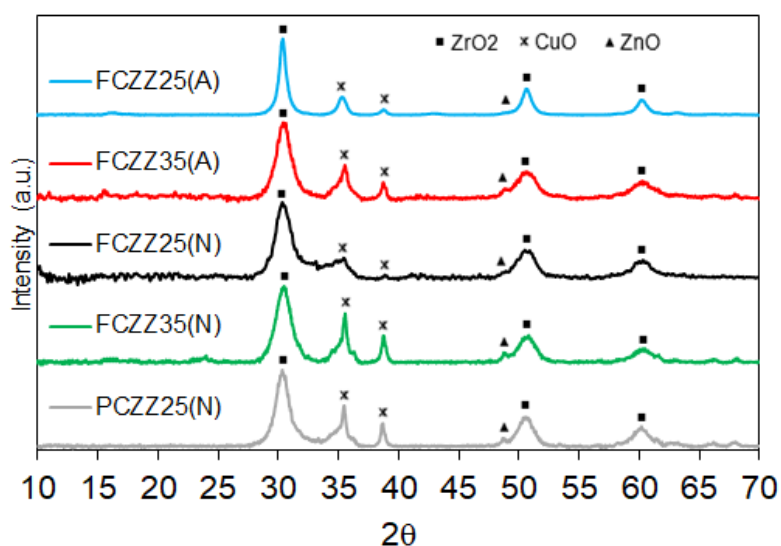
Figure 7.4. XRD pattern of the catalysts.

Table 7.2. CuO particle size ($d_{(CuO)}$), metallic Cu surface area (S_{Cu}) and Cu dispersion (D_{Cu}) for the different catalysts.

Catalyst	D_{Cu} (%) (g/g)	S_{Cu} ($m^2 \cdot g_{Cat}^{-1}$)	$d_{(CuO)}$ (nm)
FCZZ25(A)	2.9	2.8	24.3
FCZZ35(A)	3.2	3.9	52
FCZZ25(N)	9.5	7.9	5.7
FCZZ35(N)	8.2	7.5	46.3
PCZZ25(N)	5.3	4.9	36.4

Figure 7.5 shows the H_2 consumption as a function of temperature obtained from TPR analyses. It has been reported in the literature that ZnO and ZrO_2 are not reduced under the H_2-TPR conditions, therefore, the H_2 consumption observed was only related to the CuO reduction [57]. The temperature at which CuO reduction takes place depends on its particle size (the bigger the CuO particle size, the higher the reduction temperature) [5] and also on the interaction between CuO and other compounds present in the material [34,58]. In this study, CuO reduction occurred at temperatures considerably lower than that reported for CuO-ZnO-Al_2O_3-based catalysts (about 300 ºC) [20,37,59]. This fact can be attributed to a good CuO-ZrO_2 interaction, which has been reported to be favorable for CuO reduction [60]. Attending to the CuO reduction profiles, it can be observed that all the samples presented two overlapping H_2 consumption peaks. A first one at about 170 ºC, which is associated to highly dispersed CuO [61] and a second one at about 190 ºC, related to bulk CuO reduction [62]. The results indicated that the sample FCZZ25(N) presented the highest amount of easily reduced well-dispersed CuO. Moreover, it could be observed that the temperature of the CuO reduction peaks was higher for the samples containing 35 %(w/w) (CuO + ZnO) as compared to the ones containing 25 %(w/w), indicating the presence of bigger CuO particles for the cases of higher metal loading. These results are in good agreement with the ones obtained from TEM-EDXA analyses, where bigger CuO aggregates were appreciated for 35 %(w/w) (CuO + ZnO) loading (see Figure 7.2).
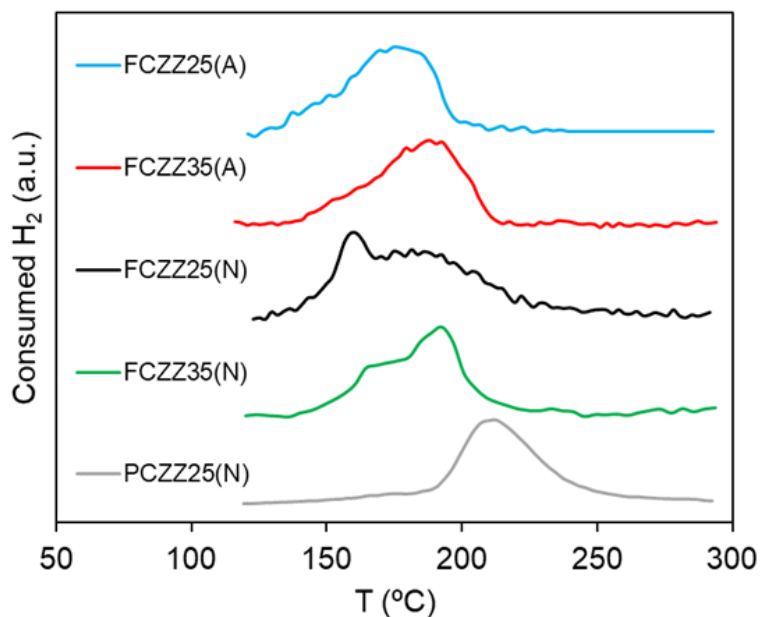
Figure 7.5. H$_2$-TPR profile of the different catalysts

N$_2$O selective chemisorption method was used for the determination of the metallic Cu surface area (S$_{Cu}$) and Cu dispersion (D$_{Cu}$) of the different fibrillar catalysts. Table 7.2 summarizes the surface properties of the metallic phase of the fibers. The results showed much higher values of S$_{Cu}$ and D$_{Cu}$ for FCZZX(N) fibers than for FCZZX(A) ones, which is related to the presence of a higher amount of reducible CuO species in the former fibers. This fact seems to be a consequence of the better interaction between the oxides that compose the fibers prepared by using Zr acetate and Cu and Zn nitrates as oxide precursors. FCZZ25(N) presented higher values of S$_{Cu}$ and D$_{Cu}$ than FCZZ35(N), which can be attributed to the presence of smaller and better-dispersed CuO particles in the sample with lower amount of metal loaded, as already revealed by XRD and TEM-EDXA analyses. Moreover, the ratio of S$_{Cu}$/A$_{BET}$ for FCZZ25(N) indicated that a 25 % of the total surface of the fiber is composed by active Cu, which is very high when compared to other catalysts reported in the literature [5,34,56], highlighting the high metal uniformity and metal Cu dispersion achieved by following the preparation procedure presented in this work.

The fibrillar materials presented here were used as catalysts for methanol synthesis from syngas. In these experiments, a continuous fixed-bed reactor was used. Table 7.3 summarizes the CO conversion and the selectivity to the main products obtained for the prepared fibrillar catalysts as a function of temperature ($H_2/CO = 3$, space velocity of 4800 ml/($g_{cat}\cdot h$), 45 bar and 4 hours on stream). As can be observed, CO conversion increases with temperature, in the temperature range of 250-300 ºC, where a CO conversion close to the equilibrium value (23%) was achieved for the most active samples, FCZZ25(N) and FCZZ35(N). The CO conversion obtained for the different fibrillar catalysts increased in the order FCZZ25(A) < FCZZ35(A) < FCZZ35(N) < FCZZ25(N). When comparing the CO conversion values obtained for the different fibrillar catalysts, it was observed that for the same metal content the fibers prepared using Cu-Zn acetates and Zr propoxide (FCZZ25(A) and FCZZ35(A)) presented lower conversion values than the ones prepared using Cu-Zn nitrates and Zr acetate (FCZZ25(N) and FCZZ35(N)). These results were consistent with the textural parameters calculated from N_2 adsorption-desorption isotherms for the catalysts (Table 7.1), which showed a higher apparent surface area for the fibers prepared using Cu-Zn nitrates and Zr acetate as precursors. In addition, the activity of the fibrillar catalysts was in good agreement with the N_2O chemisorption analyses (See Table 7.2). In this sense, a linear relationship for each of the three reaction temperatures was obtained when plotting the activity of the catalysts (expressed as micromoles of CO converted per gram of catalyst and second) as a function of the Cu surface area (S_{Cu}), as it has been shown in Figure 7.6. This observation is in good agreement with other studies regarding CO/CO_2 hydrogenation to methanol reported in the literature [63,64]. The increase in the S_{Cu} resulted in more dissociatively adsorbed hydrogen, which could be provided by spillover to ZrO or ZrO_2, increasing the activity of the catalyst [42,65]. On the other hand, all the catalysts showed a high selectivity to methanol (higher than 90 %) up to a reaction temperature of 275 ºC (See Table 7.3). Above this temperature, the selectivity to this product slightly dropped due to conversion of some of the formed methanol to DME (Eq. (7.3)), probably on the weak acid site of the ZrO_2 fibers, which have demonstrated some activity for methanol dehydration [48]. Since Cu is also active in the water gas shift reaction [65], water produced due to

the methanol dehydration reaction was removed, producing more H$_2$ and CO$_2$ (Eq. (7.4)).

For comparative purposes, a powder catalyst was prepared keeping the same composition that the one of the fibrillar catalyst that presented the highest CO conversion (FCZZ25(N)). This powder catalyst was prepared following the methodology described in sections 2.1., but skipping the electrospinning process (section 2.1.2), and was denoted as PCZZ25(N). Despite this powder material presented the same composition that the fibrillar one (FCZZ25(N)), the textural and chemical surface properties were different. The N$_2$ adsorption-desorption isotherm obtained for PCZZ25(N) was also included in Figure 7.3. This sample presented a lower N$_2$ uptake as compared to the one of FCZZ25(N), especially in the range of medium-high relative pressure. In addition, the apparent surface area (A$_{BET}$) and external surface area (A$_t$) calculated for PCZZ25(N) showed values 40 % lower than those obtained for the fibrillar catalyst, FCZZ25(N) (see Table 7.1). In the same line, the metallic copper surface area determined by N$_2$O decomposition obtained for PCZZ25(N) showed a similar reduction when it was compared to that for FCZZ25(N) (see Table 7.2). This lower S$_{Cu}$ value was related to the larger CuO particle and crystal sizes observed for the powder catalyst, as revealed by H$_2$-TPR and XRD analyses, respectively (see Figure 7.5 and Table 7.2). These results clearly evidenced that the conformation of the catalyst in a fibrillar morphology at the submicrometric scale by electrospinning was a key aspect for the textural, structural and chemical properties development of these catalytic materials.

The powder material was compacted and sieved to particle size of 100 – 300 μm, to avoid high pressure drops inside the reactor, and used as catalyst for the synthesis of methanol from syngas at the same operation conditions as those used for the fibrillar catalyst conformation. The results showed that the powder catalyst (PCZZ25(N)) presented a 40 % lower CO conversion as compared to that for the fibrillar catalyst (FCZZ25(N)) (see Table 7.3). This CO conversion reduction observed for the powder catalyst is in good agreement with the lower values of the parameters related to the textural, structural and chemical properties of this catalyst if they are compared to the ones for the catalyst with fibrillar morphology, evidencing that this configuration was of great importance

for a higher catalytic efficiency in the methanol synthesis at the studied operation conditions.

Table 7.3. CO conversion and selectivity to main products at different temperatures for the catalyst prepared in this work ($H_2/CO = 3$, space velocity of 4800 ml·g_{cat}^{-1}·h^{-1} and 45 bar).

T (ºC)	Catalyst	X_{CO} (%)	S_{CH3OH} (%)	S_{CO2} (%)	S_{DME} (%)
	FCZZ25(A)	3.5	92.0	5.5	0.8
	FCZZ35(A)	4.9	95.3	2.8	0.9
250	FCZZ25(N)	8.9	92.4	5.2	1.0
	FCZZ35(N)	8.6	94.8	3.2	1.2
	PCZZ25(N)	5.4	93.6	4.0	0.8
	FCZZ25(A)	7.5	90.0	5.7	1.9
	FCZZ35(A)	10.6	91.6	4.6	1.9
275	FCZZ25(N)	18.1	89.5	5.4	2.1
	FCZZ35(N)	17.2	92.3	4.2	2.0
	PCZZ25(N)	10.8	90.7	5.3	1.3
	FCZZ25(A)	11.2	81.1	10.3	3.8
	FCZZ35(A)	14.4	81.8	9.8	3.9
300	FCZZ25(N)	21.6	75.8	12.3	4.9
	FCZZ35(N)	21.2	82.7	9.6	3.9
	PCZZ25(N)	13.2	83.6	8.8	2.4
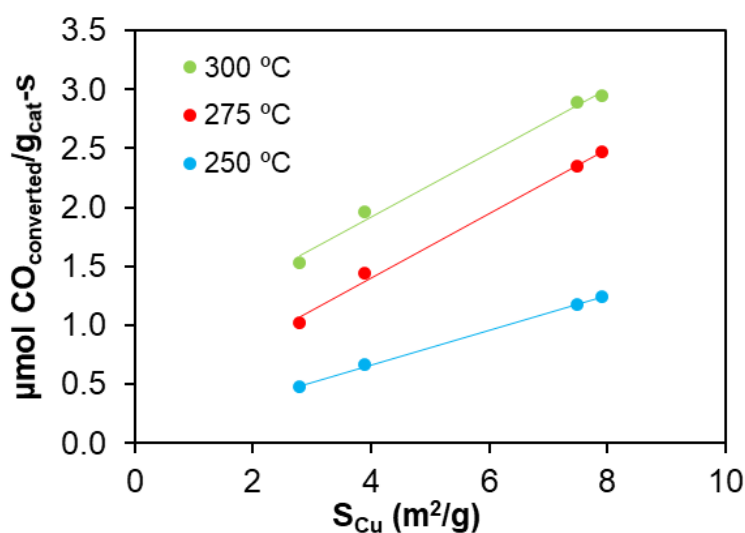
Figure 7.6. Micromoles of CO converted per gram of catalyst and second as a function of the S_{Cu} for the fibrillar catalysts at different reaction temperatures ($H_2/CO = 3$, space velocity of 4800 ml·g_{cat}^{-1}·h^{-1}, 45 bar).

It is worth mentioning that conventional powder catalysts (and especially those of nanometric size) need to be pelletized for their use as catalysts in fixed-bed reactors [63,66] in order to avoid high pressure drops. However, since methanol synthesis is highly exothermic, the use of such pelletized catalysts (larger particle size) would involve, most of the times, intraparticle diffusion limitations [41,42]. In the present study, the spongy-like fibrillar structured materials were directly used as catalysts in a fixed-bed reactor without further modifications, performing very efficiently. So, thanks to their fibrillar conformation, these catalysts could make use of their submicrometric effective dimension, in terms of suppressing intraparticle mass and heat transfer limitations, avoiding, at the same time, problems related to pressure drops in fixed-bed reactors when working with such a reduced particle conformation.

The pressure drop inside the fixed-bed reactor was theoretically calculated for the fibrillar structured catalyst with submicrometric size and for the powder catalyst with the same effective dimension. The porosity for the fibrillar catalytic bed analyzed in the present work (radius of the fibers of 500 nm) showed a value of 0.95, which is in good agreement with the porosity values reported by Jackson and James for different fibrillar materials [67]. This porosity value is very high as compared to the values usually found for packed beds of spheres, which ranges from 0.35 to 0.47 [68].

For the conditions used in this study, the Reynolds number (Re$_{mp}$) for porous media showed a value of $4.81 \cdot 10^{-4}$, indicating a laminar flow regime [69]. Under these conditions, the pressure drop in a packed bed can be calculated by combining the Darcy's Law along with the Kozeny-Carman equation [70,71]. The pressure-drop calculation results showed a value of 0.3 bar/m for the fibrillar packed bed analyzed in the present study. On the other hand, a value of 1650 bar/m was obtained for a packed bed of spherical particles presenting the same dimension than the fibers (r=500 nm), which is more than 5000 times higher than the value calculated for the fibrillar packed bed. These results clearly highlight the advantage of the use of the catalyst in a fibrillar conformation for its application in a fixed bed reactor.

In addition, the catalysts presented in this work exhibits a high flexibility, being it possible to adapt them to a determined reactor shape easily. Furthermore, the fibrillar catalytic beds here presented can be compacted, tuning the bed porosity by this way from 0.99 to 0.92 (see that for FCZZ25(N) in Figure 7.7, as an example). This compacting process has been observed to be reversible, being the original volume of the catalytic bed recovered after removing the compression force.
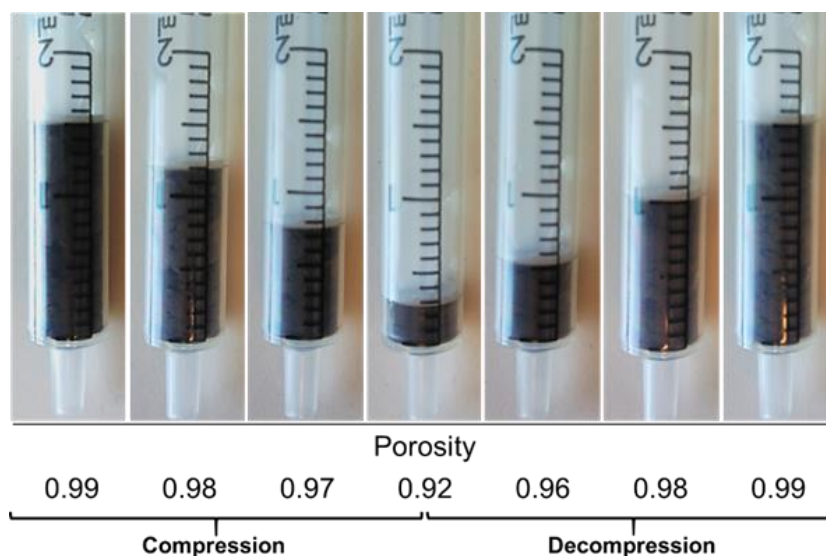
Figure 7.7. Compacting process of catalyst (FCZZ25(N)) bed under different reactor volumes.

7.3.2.- Effect of Zeolite content in the fibrillar catalyst on the methanol dehydration activity.

From the results presented above, it could be concluded that the sample FCZZ25(N) presented the best physicochemical properties and surface characteristic for the metallic phase of the prepared catalysts, with the smallest CuO particle size, which is clearly consistent with its highest catalytic activity for CO hydrogenation. Thus, FCZZ25(N) was chosen as the basis of the metallic function for the preparation of bifunctional fibrillar catalysts. In this sense, different amounts of ZSM-5 zeolite (Zeolyst international, CBV 5524G, Si/Al 50, with a mean crystal size of 120 nm) were added to the Cu-Zn-Zr-based polymeric

solutions and the resulting suspensions were electrospun and calcined, as indicated in sections 7.2.1.2 and 7.2.1.3, to prepare bifunctional catalysts that were used, without further modifications, for the syngas-to-DME process in a continuous fixed-bed pressure reactor. Figure 7.8 shows the CO conversion as a function of the zeolite content for different temperatures (H_2/CO = 3, space velocity of 4800 ml/g_{cat}·h, 45 bar, 4 hours on stream). As can be seen, the CO conversion obtained for these catalysts increased with zeolite content up to an amount of around 10 %(w/w), from which no further increase in CO conversion was observed. It is well-known that in-situ methanol consumption (through dehydration to DME), avoids, to some extent, the methanol synthesis equilibrium constraint and makes it possible to achieve higher conversion of syngas working under the same operating conditions [22,25].
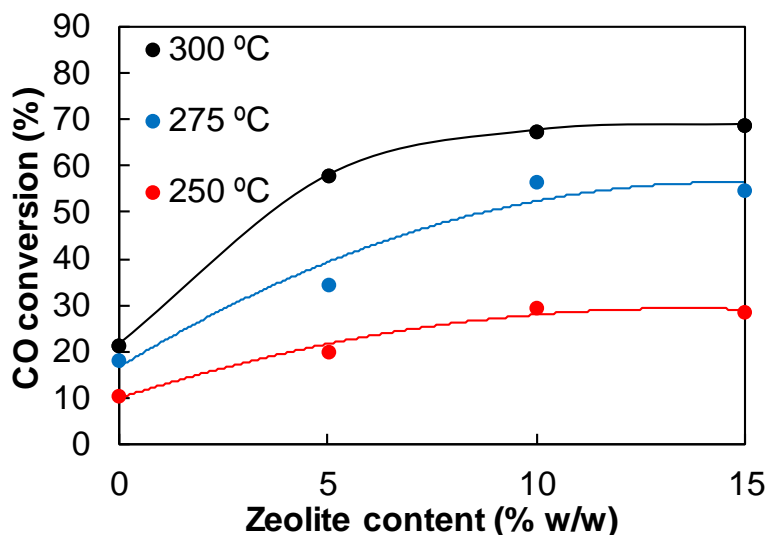
Figure 7.8. CO conversion as a function of zeolite loading for the bifunctional fibrillar catalysts at different temperatures (H_2/CO = 3, space velocity of 4800 ml·g_{cat}^{-1}·h^{-1}, 45 bar, 4 hours on stream).

Figure 7.9 shows the selectivity to the main reaction products as a function of the temperature for the fibrillar catalysts studied. FCZZ25(N), which does not contain any (zeolite) acid phase in its composition, showed a high selectivity to methanol (higher than 90 %) up to 275 ºC. Above this temperature, the selectivity to this product dropped, due mainly to the formation of CO_2 through the water gas

shift (Eq. (7.4)) reaction. A negligible amount of DME is formed at 300° C as a consequence of a very little dehydration of methanol on some weak acid sites of the ZrO_2 fibers [48]. When analyzing the amount of zeolite in the catalysts (FCZZ25(N)-YZ), it was observed that the FCZZ25(N)-5Z sample, containing a 5 %(w/w) of zeolite in its composition, showed lower and higher selectivity to DME and to methanol, respectively, as compared to the ones obtained for FCZZ25(N)-10Z and FCZZ25(N)-15Z, which exhibited a similar product distribution. These differences in product selectivity indicated that a zeolite content of 5 %(w/w) did not provide enough acid phase for further converting most of the produced methanol to DME and thus the product distribution of the overall process was controlled by the methanol dehydration step (Eq. (7.3)). On the other hand, as both FCZZ25(N)-10Z and FCZZ25(N)-15Z catalysts yielded almost no methanol as product, it could be stated that a zeolite content of 10 %(w/w) was enough for converting all the methanol produced in the process, with a very high value of selectivity to DME (63.3%), being, in this case, the product distribution of the process controlled by the methanol synthesis on the Cu active phase (Eqs. (7.1) and (7.2)).
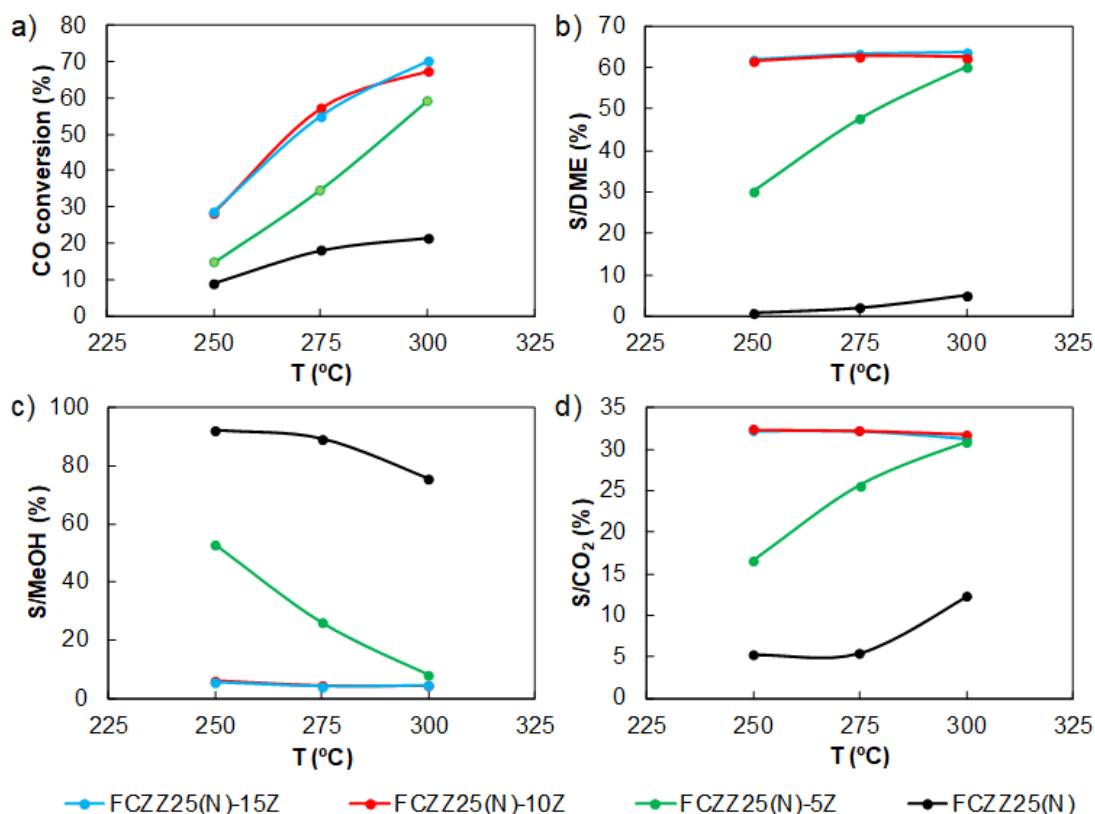
Figure 7.9. a) CO conversion and selectivity to **b)** DME, **c)** Methanol, **d)** CO_2 as a function of temperature for the bifunctional fibrillar catalysts (H₂/CO = 3, space velocity of 4800 ml·g_{cat}^{-1}·h^{-1}, 45 bar, 4 hours on stream).

According to the above results, it could be stated that the FCZZ25(N)-10Z bifunctional catalyst was the best in terms of DME productivity per acid phase mass. This fibrillar bifunctional catalyst was further studied and characterized. The morphology of the FCZZ25(N)-10Z bifunctional catalyst was analyzed by SEM and TEM and results are shown in Figures 7.10 and 7.11, respectively. As in the case of the samples that did not contain any zeolite, this material also consisted in a non-woven fabric of highly homogeneous fibers, presenting a high aspect (length to diameter) ratio and the absence of fused zones. The average diameter calculated for these fibers was 1.5 µm. However, and in contrast to the totally smooth surface exhibited by FCZZ25(N), this sample presented a rougher and more irregular surface. As can be observed in the selected TEM micrographs shown in Figure 7.11 for the FCZZ25(N)-10Z bifunctional catalyst, the fibers presented a smooth surface (very similar to the one of sample FCZZ25(N)) with attached particle aggregates of a mean size of 300 nm. A fairly good distribution

was observed for these particle aggregates along the surface of the fibers, which is a consequence of the high control that the electrospinning technique brings over the distribution of particles in fibrillar materials [47].
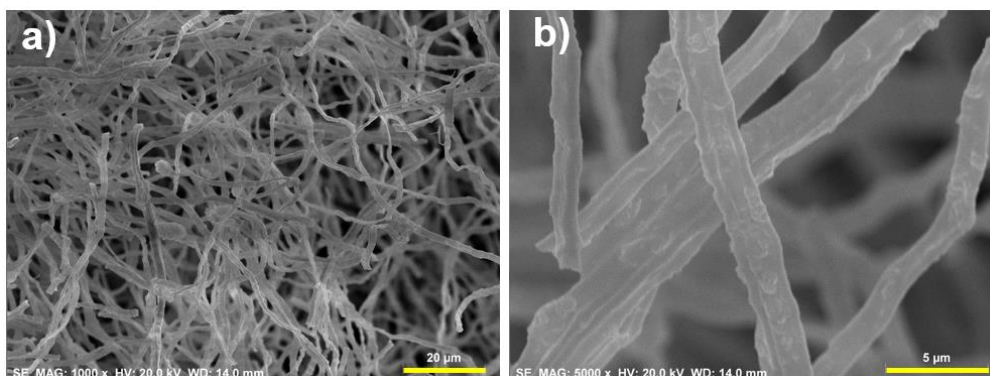
Figure 7.10. Scanning electron micrographs of the bifunctional catalyst FCZZ25(N)-10Z. Bar lengths are a) 20 µm and b) 5 µm.
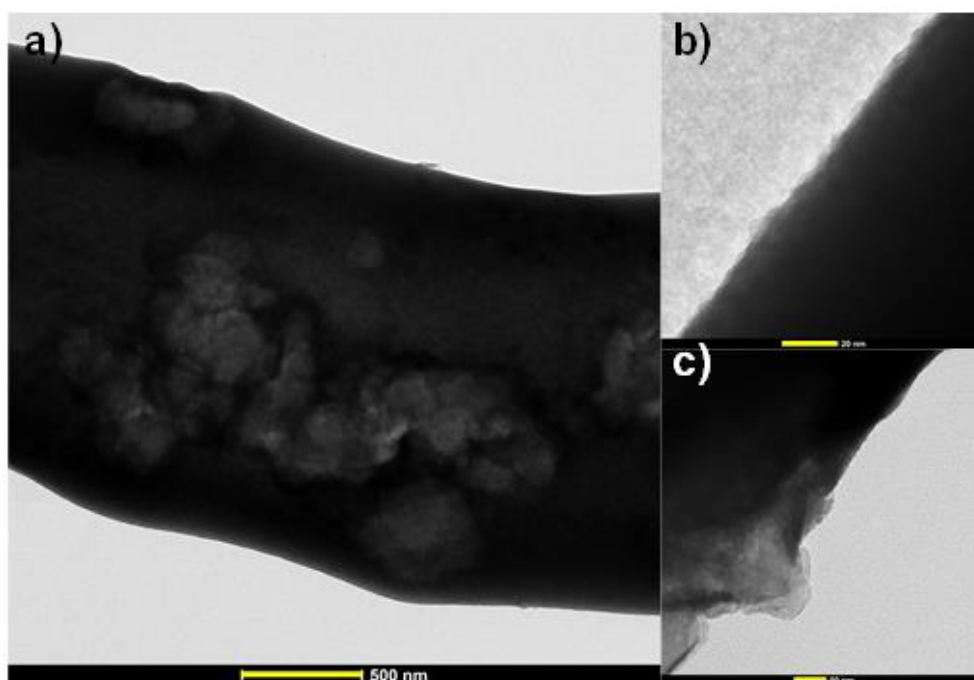
Figure 7.11. Transmission electron micrographs of the bifunctional catalyst FCZZ25(N)-10Z. Bar lengths are a) 500 nm, b) 20 nm and b) 50 nm.

The chemical composition of the FCZZ25(N)-10Z bifunctional fibrillar catalyst was analyzed by transmission electron microscopy energy-dispersive X-ray spectroscopy (TEM-EDXA) and the results are included in Figure 7.12. This

Figure shows that the fiber presented a smooth region with a uniform distribution for Zr, Cu and Zn, as in the case of the sample FCZZ25(N). In contrast, Si was the main element present in the particles aggregations observed on the surface of the fibers, indicating, thus, that these aggregates were composed by zeolite particles, as it has been also reported in the literature for SiO$_2$ [72] and polystyrene [73] nanoparticles. The average size (obtained from TEM analyses) for the zeolite particles forming the aggregates was of 120 nm.
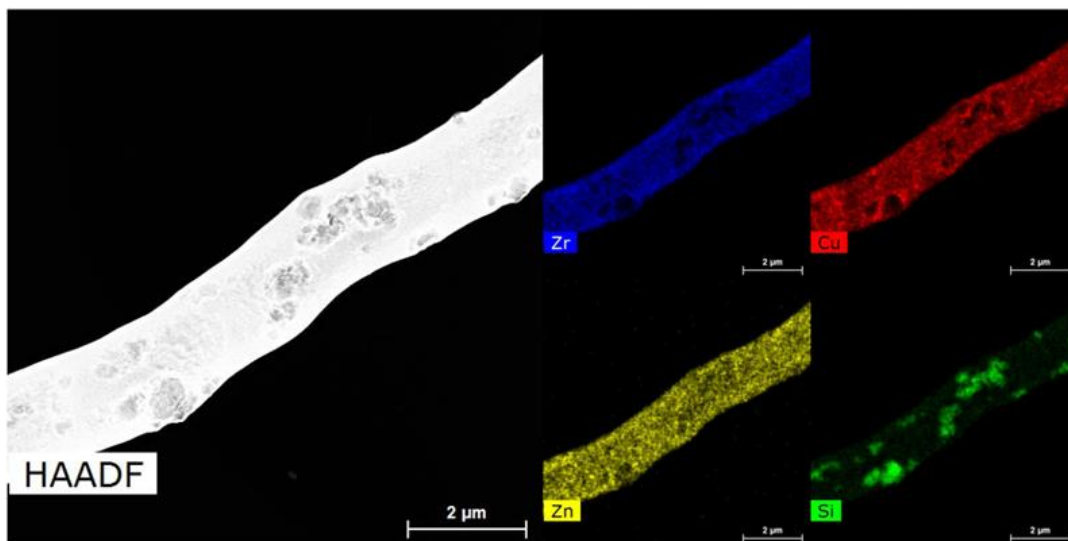
Figure 7.12. HAADF-STEM image, and EDXA elemental mappings of Zr (blue), Cu (red), Zn (yellow) and Si (green) of FCZZ25(N)-10Z.

Figure 7.13 shows the XRD pattern of the bifunctional catalyst, which further confirmed the presence of CuO (2θ = 38.8 º), ZrO$_2$ (2θ = 30.2 º, 35.2 º, 50.6 º and 60.2 º) and zeolite (ZSM-5) (2θ = 7.9 º, 8.9 º, 20.9 º and 23.9 º) crystalline phases. The mean crystallite size value obtained for the ZSM-5 zeolite and CuO in the fibers were estimated as 60 and 7 nm, respectively, by applying the Williamson-Hall method [52].
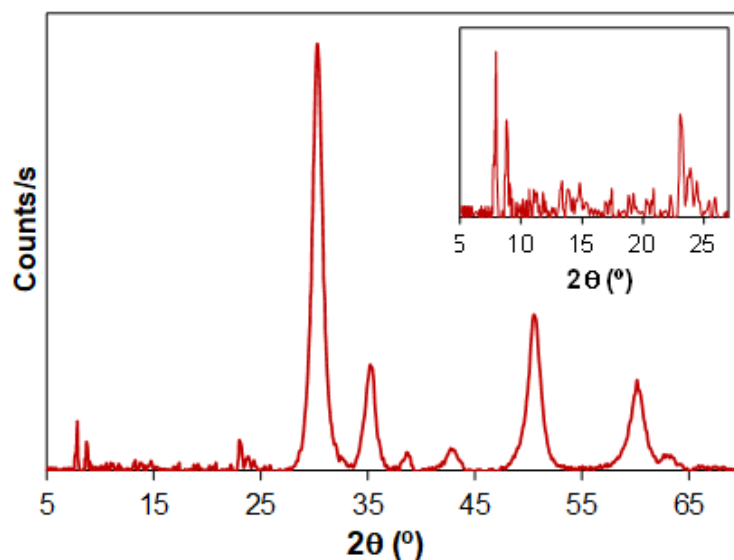
Figure 7.13. XRD pattern of the FCZZ25(N)-10Z bifunctional fibrillar catalyst.

The textural and surface properties for the FCZZ25(N)-10Z bifunctional catalyst were also analyzed. The calculated apparent surface area (A_{BET}) for this fibrillar material showed a value of 67 m^2/g, which is considerably higher than the one obtained for the sample that did not contain any zeolite (see FCZZ25(N) in Table 7.1). This increase in the A_{BET} value was associated to the presence of zeolite nanoparticles, which possesses a well-defined porous texture [74], and it is consistent with the amount of zeolite (10% (w/w)) added to this sample (the apparent surface area for the ZSM-5 zeolite was of 442 m^2/g). On the other hand, H_2-TPR analysis showed that the reduction of the CuO species in FCZZ25(N)-10Z occurred in the same temperature range than the one obtained for the FCZZ25(N) catalyst (120-250 °C), which contained only the metallic phase. The Cu metallic surface area (S_{Cu}) and Cu dispersion (D_{Cu}) values determined by N_2O chemisorption method were 7.7 $m^2 \cdot g_{Cat}^{-1}$ and 9.5 %, respectively, which were almost the same values than the ones calculated for FCZZ25(N) (See Table 7.2).

Attending to the above results, it could be concluded that the metallic function properties of the fibrillar catalyst were not significantly affected by the presence of the zeolite acid phase.

The surface acidity of the FCZZ25(N)-10Z bifunctional fibrillar catalyst was evaluated by temperature programmed desorption of ammonia (NH_3-TPD). In order to study the acidity of each individual phase present on the FCZZ25(N)-10Z

bifunctional catalyst, the acidity of a zirconia fiber sample (FCZZ0(N)), a zirconia-zeolite fiber sample containing the same amount of zeolite that the one of the bifunctional catalyst (FCZZ0(N)-10Z), and a fibrillar catalyst sample (FCZZ25(N)) containing only the metallic phase for the synthesis of methanol, similar to the one of the bifunctional catalyst, were also analyzed. Table 7.4 summarizes the total amount of ammonia desorbed during TPD for each of the aforementioned samples, obtained by integration of the area under NH$_3$-TPD curves. Zirconia fibers, FCZZ0(N), desorbed a very low amount of ammonia during TPD, evidencing that this material presented a low acid character. Once the zeolite was added to the zirconia fibers, the acidity of the material remarkably increased due to the presence of the acid sites of the zeolite (see FCZZ0(N)-10Z in Table 7.4). When analyzing the Cu/Zn containing fibers (FCZZ25(N) and FCZZ25(N)-10Z), a much greater value of desorbed ammonia was obtained, as compared to the ones obtained for the samples that did not contain CuO+ZnO. These data seem to indicate that the presence of Cu/Zn species on the fibers resulted in the generation of a considerable amount of acid sites on the catalysts. In this line, several studies dealing with the preparation of bifunctional catalyst have also reported an increase in the total acidity determined by NH$_3$-TPD, due to presence of Cu/Zn species on the bifunctional catalyst [5,31,32,38,75,76].

Table 7.4. Total acidity determined by NH$_3$-TPD and DME productivity in methanol dehydration (P$_{MeOH}$ = 0.10 atm, W/F$_{MeOH}$ = 0.02 g$_{Cat}$·s·µmol$_{MeOH}$$^{-1}$).

Catalyst	Acidity (µmol$_{NH3}$/g$_{Cat}$)	DME productivity (µmol·g$_{Cat}$$^{-1}$·s^{-1})		
		200 ºC	250 ºC	300 ºC
FCZZ0(N)	30	-	-	-
FCZZ0(N)-10Z	150	1.5	7.5	15.8
FCZZ25(N)	220	-	-	-
FCZZ25(N)-10Z	670	0.9	3.4	4.2

However, the total acidity values obtained for the Cu/Zn-containing catalysts from NH$_3$-TPD analyses may be misleading when considering the catalytic results here obtained. In this sense, the active phase for the synthesis of methanol in FCZZ25(N) presented a much higher number of acid sites than even the one obtained for the acid phase of FCZZ0(N)-10Z, those corresponding to the ZSM-5 zeolite, as observed from NH$_3$-TPD analyses. However, it should

be pointed out that FCZZ25(N) itself did not yield DME in an appreciable extent (S_{DME} < 2.5 % at 275 ºC, see Table 7.3). In this line, Garcia-Trenco et al. [77] reported that the acid sites of the HZSM-5 zeolite are negatively affected by the presence of the active phase for the synthesis of methanol in bifunctional catalysts, reducing the methanol dehydration activity of the catalyst. Therefore, in any case, the acidity and the dehydration activity of FCZZ25(N)-10Z bifunctional catalyst should have been lower than the one of the isolated active phase for the dehydration of methanol, such in FCZZ0(N)-10Z. DME productivity values for the methanol dehydration on FCZZ0(N)-10Z and FCZZ25(N)-10Z have been also included in Table 7.4. As can be seen, the results of these experiments further confirmed the reduction of the dehydration activity of the acid phase when the metallic phase components were present in the catalyst, which seem to be against the results obtained from NH_3-TPD analyses. These results clearly suggest the existence of ammonia adsorption centers on the metallic component of the bifunctional catalysts, which were, at least, not active enough for promoting methanol dehydration.

Regarding this issue, it is well-known that copper-based catalysts are also active for the low temperature selective ammonia oxidation to N_2. In this sense, there are several studies dealing with the characterization of Cu-supported catalysts [78–80]. Chmielarz et al [78] proved that ammonia chemisorption sites were mainly located on the transition metal species present on the support. Moreover, Gang et al. [80] reported that copper lattice oxygen reacts with NH_3 to produce N_2 under NH_3-TPD conditions. In agreement with the aforementioned studies, the generation of nitrogen during the NH_3-TPD analyses for the Cu/Zn containing catalysts (FCZZ25(N) and FCZZ25(N)-10Z) here analyzed was confirmed by MS-spectroscopy, supporting the fact that adsorption of NH_3 on the Cu sites of the catalysts and further reaction to N_2 took place under the operation conditions used in these analyses.

The above results confirmed that the acidity measurements determined by NH_3-TPD are not suitable for evaluating the dehydration activity of this type bifunctional catalysts. Therefore, we state that when analyzing the acidity of this type bifunctional catalysts, more reliable results are obtained by comparing the acidity of the isolated active phases (the ones for methanol formation and

dehydration), as it was done in most of the studies dealing with the preparation of bifunctional catalysts by physical mixing [23,81,82]. In addition, given that detrimental interactions between the acid and the metallic phases emerge when preparing bifunctional catalyst [77], especially for supported catalysts, we also suggest carrying out a methanol dehydration experiment for the assessment of these negative interactions and to compare the dehydration capability of bifunctional catalysts.

The direct synthesis of DME from syngas was further studied for the bifunctional fibrillar catalyst FCZZ25(N)-10N. Table 7.5 presents the CO conversion and selectivity to the main reaction products obtained for FCZZ25(N)-10N catalyst at different temperatures and H$_2$/CO ratios. As it can be observed, CO conversion increased with H$_2$/CO ratio for all the temperatures studied, given that, under the conditions here analyzed, the overall syngas-to-DME process is kinetically controlled by the methanol synthesis reaction, which is favored by a H$_2$-rich environment [4,83]. On the other hand, it has been reported that methanol dehydration is faster in a CO-rich environment, since water vapor generated by the methanol dehydration (Eq. (7.4)) is removed through the water gas shift reaction (Eq. (7.3)), yielding H$_2$ and CO$_2$ [83]. As a result of the higher methanol dehydration rate and the higher water gas shift activity under CO-rich reaction media, the selectivity to methanol decreased while increasing the one towards CO$_2$, when lowering the H$_2$/CO ratio. The selectivity to DME was also affected by changing the H$_2$/CO ratio. A slight decrease in DME was observed when lowering the H$_2$/CO ratio from 3 to 1. However, when considering the selectivity to the reaction products in the organic phase, the selectivity to DME increased from 91.7 to 95.7 % when lowering the H$_2$/CO ratio from 3 to 1. Therefore, the change in the DME selectivity was related to the higher CO$_2$ production occurring at lower H$_2$/CO ratios.

Table 7.5. CO conversion and selectivity to the main reaction products for the direct synthesis of DME from syngas on FCZZ25(N)-10Z at different temperatures and H_2/CO ratios (space velocity of 4800 ml·g_{cat}^{-1}·h^{-1}, 45 bar and 4 hours on stream).

T (ºC)	H_2/CO ratio	X_{CO} (%)	S_{DME} (%)	S_{CH3OH} (%)	S_{CO2} (%)
	1	10.9	57.6	8.6	33.7
250	2	20.1	59.1	8.1	32.7
	3	29.4	60.1	8.3	31.5
	1	22.4	59.8	4.3	35.5
275	2	42.2	61.0	4.6	34.1
	3	57.7	62.7	5.5	31.7
	1	39.8	60.0	2.2	36.9
300	2	60.2	61.2	3.8	34.4
	3	68.0	63.8	5.1	30.6

It is also worth mentioning that the fibrillar bifunctional catalyst in the submicrometric scale here presented showed an enhanced contact between the two active phases (metallic and acid) involved in the direct DME synthesis from syngas, favoring the reaction tandem of methanol formation and dehydration to DME. A representation of the reaction sequence involved in the syngas to DME process on a section of the fibrillar bifunctional catalytic bed here presented is depicted in Figure 7.14.
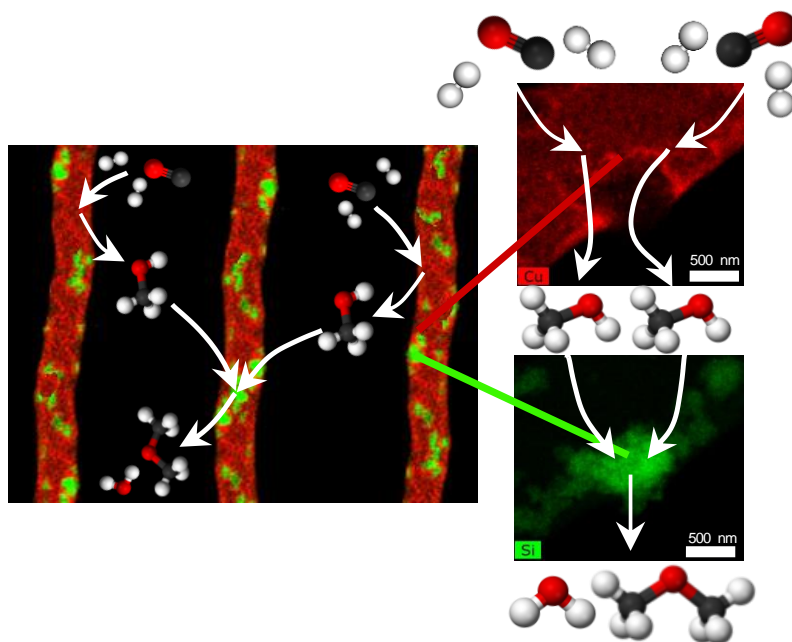
Figure 7.14. Representation of the reaction sequence involved in the syngas to DME process on a section of the fibrillar bifunctional catalytic bed.

In this sense, the catalyst presented in this study showed a fairly good catalytic behavior when it was compared with other advanced catalysts reported in the literature. In this sense, Khoshbin et al. [84] reported the use of CuO–ZnO–Al$_2$O$_3$ nanocatalyst supported over HZSM-5 for this reaction, obtaining CO conversion values ranging from 15 to 39 % at 300 ºC, H$_2$/CO = 2, space velocity of 600 mL/(g$_{cat}$·h) and 40 bar, which are considerably lower than those obtained for the fibrillar catalyst analyzed in the present study. Wang et al.[85] reported the use of core-shell catalysts for this reaction, obtaining a CO conversion values ranging from 28 to 71.1 % and selectivity to DME values ranging from 51.6 to 61.9 % at 260 ºC, H$_2$/CO = 2, space velocity of 1500 mL/(g$_{cat}$·h) and 50 bar. These CO conversion values are slightly higher than the one obtained in the present work at the same temperature. However, it has to be noted that the operating conditions used in the present study were less favorable (reaction pressure 5 bar lower and space velocity more than 3 times higher).

Figure 7.15 shows the Arrhenius plots for the synthesis of DME from syngas on FCZZ25(N)-10Z for different H$_2$/CO ratios, assuming a pseudo-first order reaction model with respect to CO. The values of the activation energy

obtained ranged from 75 to 80 kJ/mol, which are in good agreement with the ones reported in the literature for other catalysts [21,86,87].
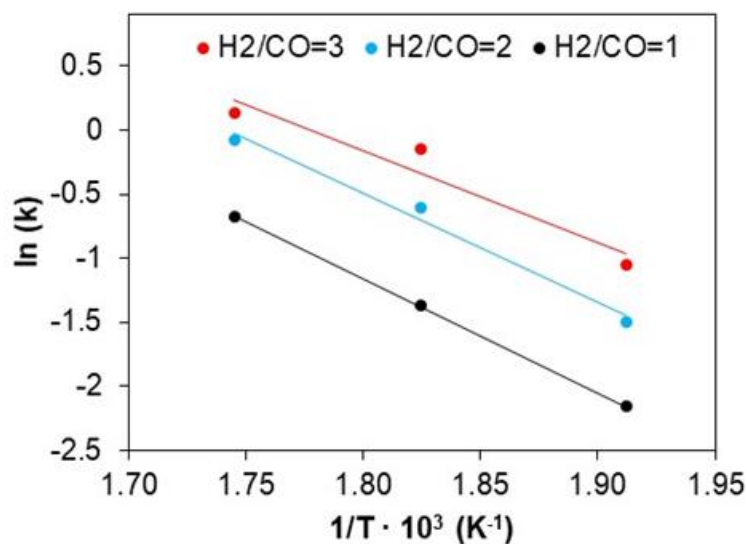
Figure 7.15. Arrhenius plot for the direct DME synthesis from syngas for FCZZ25(N)-10 Z, at 45 bar and different H$_2$/CO ratios.

7.4.-Conclusions

A simple and straightforward methodology for the preparation of CuO/ZnO/ZrO$_2$-ZSM-5 fibrillar bifunctional catalysts by using the electrospinning technique has been described in the present work. The fibrillar bifunctional materials were used as catalysts for the direct DME synthesis from syngas and the catalytic activity was well correlated with the textural, structural and surface chemistry of the bifunctional fibrillary catalysts studied.

A comparison between the fibrillar catalysts here presented and a conventional powder catalyst was carried out. The conformation of the catalyst in a fibrillar morphology was a key factor for the textural, structural and chemical properties development of these catalytic systems and, thus, for their catalytic efficiency.

SEM and TEM images showed fibers presenting a high aspect ratio and mean diameters of 1.5 μm, uniform CuO particles smaller than 10 nm and the

presence of zeolite aggregates attached to the surface of the CuO/ZnO/ZrO$_2$ fibers, with mean size of 300 nm. A fairly good dispersion was observed for these particle aggregates along the surface of the fibers, promoting an enhanced contact between the two active phases involved in the syngas-to-DME process.

The acidity measurements determined by NH$_3$-TPD seem not to be suitable for evaluating the dehydration activity of these bifunctional catalysts. We conclude that when analyzing the acidity of this type of bifunctional catalysts, more reliable results are obtained by comparing the acidity of the isolated active phases (the ones for methanol formation and dehydration). In addition, given that detrimental interactions between the acid and the metallic phases emerge when preparing bifunctional catalyst, we also suggest carrying out a methanol (or other alcohol) dehydration experiment, for the assessment of these negative interactions and to compare the dehydration capability of bifunctional catalysts.

The fibrillar structured bifunctional materials were directly used as catalysts in a continuous fixed-bed reactor. The enhanced contact between the two active phases on the surface of the fibrillar catalyst favored the reaction tandem of methanol formation and dehydration to DME, giving rise to high CO conversion values and selectivity to DME higher than 63% (95 % when considering only the products in the organic phase).

In addition, it is worth highlighting that the fibrillar structured catalysts made use of the submicrometric effective dimension of the two active phases (radius of the fibers lower than 1 µm, size of zeolite aggregates lower than 300 nm), in terms of enhancing intraparticle mass and heat transfer, avoiding, at the same time, the problems related to pressure drops of fixed-bed reactors working with such a reduced particle size. In this sense, the values obtained for the pressure drop calculated for the fibrillar catalytic bed of the reactor reported in the present study was 5000 times smaller than that calculated for a packed bed reactor of spherical particles presenting the same dimension.

.

7.5.-References

[1]   K. Saravanan, H. Ham, N. Tsubaki, J.W. Bae, Recent progress for direct synthesis of dimethyl ether from syngas on the heterogeneous bifunctional hybrid catalysts, Appl. Catal. B Environ. 217 (2017) 494–522. doi:10.1016/J.APCATB.2017.05.085.

[2]   G.A. Olah, A. Goeppert, G.K.S. Prakash, Beyond oil and gas : the methanol economy, Wiley-VCH, 2009.

[3]   M.C. Gutiérrez, J.M. Rosas, M.A. Rodríguez-Cano, I. López-Luque, J. Rodríguez-Mirasol, T. Cordero, Strategic situation, design and simulation of a biorefinery in Andalusia, Energy Convers. Manag. 182 (2019) 201–214. doi:10.1016/j.enconman.2018.12.038.

[4]   W. Lu, L. Teng, W. Xiao, Simulation and experiment study of dimethyl ether synthesis from syngas in a fluidized-bed reactor, Chem. Eng. Sci. 59 (2004) 5455–5464. doi:10.1016/j.ces.2004.07.031.

[5]   Y. Hua, X. Guo, D. Mao, G. Lu, G.L. Rempel, F.T.T. Ng, Single-step synthesis of dimethyl ether from biomass-derived syngas over CuO-ZnO-MOx(M = Zr, Al, Cr, Ti)/HZSM-5 hybrid catalyst: Effects of MOx, Appl. Catal. A Gen. 540 (2017) 68–74. doi:10.1016/j.apcata.2017.04.015.

[6]   T.H. Fleisch, A. Basu, M.J. Gradassi, J.G. Masin, Dimethyl ether: A fuel for the 21st century, Stud. Surf. Sci. Catal. 107 (1997) 117–125. doi:10.1016/S0167-2991(97)80323-0.

[7]   S.C. Sorenson, Dimethyl Ether in Diesel Engines : Progress and Perspectives, J. Eng. Gas Turbines Power. 123 (2001) 652–658. doi:10.1115/1.1370373.

[8]   C. Arcoumanis, C. Bae, R. Crookes, E. Kinoshita, The potential of di-methyl ether (DME) as an alternative fuel for compression-ignition engines : A review, Fuel. 87 (2008) 1014–1030. doi:10.1016/j.fuel.2007.06.007.

[9] Z. Azizi, M. Rezaeimanesh, T. Tohidian, M.R. Rahimpour, Dimethyl ether: A review of technologies and production challenges, Chem. Eng. Process. Process Intensif. 82 (2014) 150–172. doi:10.1016/j.cep.2014.06.007.

[10] M. Yoon, S. Hyun, B. Woo, C. Sik, Combustion and emission characteristics of DME as an alternative fuel for compression ignition engines with a high pressure injection system, Fuel. 87 (2008) 2779–2786. doi:10.1016/j.fuel.2008.01.032.

[11] T.A. Semelsberger, R.L. Borup, H.L. Greene, Dimethyl ether (DME) as an alternative fuel, J. Power Sources. 156 (2006) 497–511. doi:10.1016/j.jpowsour.2005.05.082.

[12] C. Baltes, S. Vukojević, F. Schüth, Correlations between synthesis, precursor, and catalyst structure and activity of a large set of CuO/ZnO/Al2O3 catalysts for methanol synthesis, J. Catal. 258 (2008) 334–344. doi:10.1016/J.JCAT.2008.07.004.

[13] J.D. Grunwaldt, A.M. Molenbroek, N.Y. Topsoe, H. Topsoe, B.S. Clausen, In situ investigations of structural changes in Cu/ZnO catalysts, J. Catal. 194 (2000) 452–460. doi:DOI 10.1006/jcat.2000.2930.

[14] G.C. Chinchen, P.J. Denny, J.R. Jennings, M.S. Spencer, K.C. Waugh, Synthesis of Methanol. Part 1. Catalysts and Kinetics, Appl. Catal. 36 (1988) 1–65. doi:10.1016/S0166-9834(00)80103-7.

[15] E. Catizzone, S. Van Daele, M. Bianco, A. Di Michele, A. Aloise, M. Migliori, V. Valtchev, G. Giordano, Catalytic application of ferrierite nanocrystals in vapour-phase dehydration of methanol to dimethyl ether, Appl. Catal. B Environ. 243 (2019) 273–282. doi:10.1016/j.apcatb.2018.10.060.

[16] M. Xu, J.H. Lunsford, D.W. Goodman, A. Bhattacharyya, Synthesis of dimethyl ether (DME) from methanol over solid-acid catalysts, Appl. Catal. A Gen. 149 (1997) 289–301. doi:10.1016/S0926-860X(96)00275-X.

[17] F. Yaripour, F. Baghaei, I. Schmidt, J. Perregaard, Catalytic dehydration of methanol to dimethyl ether (DME) over solid-acid catalysts, Catal. Commun. 6 (2005) 147–152. doi:10.1016/J.CATCOM.2004.11.012.

[18] G. Bercic, J. Levec, Catalytic dehydration of methanol to dimethyl ether. Kinetic investigation and reactor simulation., Ind. Eng. Chem. Res. 32 (1993) 2478–2484. doi:10.1021/ie00023a006.

[19] M. Sánchez-Contador, A. Ateka, M. Ibáñez, J. Bilbao, A.T. Aguayo, Influence of the operating conditions on the behavior and deactivation of a CuO-ZnO-ZrO 2 @SAPO-11 core-shell-like catalyst in the direct synthesis of DME, Renew. Energy. (2019). doi:10.1016/j.renene.2019.01.093.

[20] A. Ateka, I. Sierra, J. Ereña, J. Bilbao, A.T. Aguayo, Performance of CuO-ZnO-ZrO$_2$ and CuO-ZnO-MnO as metallic functions and SAPO-18 as acid function of the catalyst for the synthesis of DME co-feeding CO$_2$, Fuel Process. Technol. 152 (2016) 34–45. doi:10.1016/j.fuproc.2016.05.041.

[21] F. Dadgar, R. Myrstad, P. Pfeifer, A. Holmen, H.J. Venvik, Direct dimethyl ether synthesis from synthesis gas: The influence of methanol dehydration on methanol synthesis reaction, Catal. Today. 270 (2016) 76–84. doi:10.1016/j.cattod.2015.09.024.

[22] A.T. Aguayo, J. Ereña, D. Mier, J.M. Arandes, M. Olazar, J. Bilbao, Kinetic Modeling of Dimethyl Ether Synthesis in a Single Step on a CuO−ZnO−Al$_2$O$_3$/γ-Al$_2$O$_3$ Catalyst, Ind. Eng. Chem. Res. 46 (2007) 5522–5530. doi:10.1021/IE070269S.

[23] A. García-Trenco, A. Martínez, Direct synthesis of DME from syngas on hybrid CuZnAl/ZSM-5 catalysts: New insights into the role of zeolite acidity, Appl. Catal. A Gen. 411–412 (2012) 170–179. doi:10.1016/j.apcata.2011.10.036.

[24] J. Ereña, R. Garoña, J.M. Arandes, A.T. Aguayo, J. Bilbao, Effect of operating conditions on the synthesis of dimethyl ether over a CuO-ZnO-Al$_2$O$_3$/NaHZSM-5 bifunctional catalyst, Catal. Today. 107–108 (2005) 467–473. doi:10.1016/j.cattod.2005.07.116.

[25]   W.-J. Shen, K.-W. Jun, H.-S. Choi, K.-W. Lee, Thermodynamic investigation of methanol and dimethyl ether synthesis from CO$_2$ Hydrogenation, Korean J. Chem. Eng. 17 (2000) 210–216. doi:10.1007/BF02707145.

[26]   Q. Ge, Y. Huang, F. Qiu, S. Li, Bifunctional catalysts for conversion of synthesis gas to dimethyl ether, Appl. Catal. A Gen. 167 (1998) 23–30.

[27]   M. Stiefel, R. Ahmad, U. Arnold, M. Döring, Direct synthesis of dimethyl ether from carbon-monoxide-rich synthesis gas: Influence of dehydration catalysts and operating conditions, Fuel Process. Technol. 92 (2011) 1466–1474. doi:10.1016/J.FUPROC.2011.03.007.

[28]   D. Mao, W. Yang, J. Xia, B. Zhang, Q. Song, Q. Chen, Highly effective hybrid catalyst for the direct synthesis of dimethyl ether from syngas with magnesium oxide-modified HZSM-5 as a dehydration component, J. Catal. 230 (2005) 140–149. doi:10.1016/J.JCAT.2004.12.007.

[29]   G. Bonura, M. Cordaro, L. Spadaro, C. Cannilla, F. Arena, F. Frusteri, Hybrid Cu–ZnO–ZrO$_2$/H-ZSM5 system for the direct synthesis of DME by CO$_2$ hydrogenation, Appl. Catal. B Environ. 140–141 (2013) 16–24. doi:10.1016/J.APCATB.2013.03.048.

[30]   J. Sun, G. Yang, Y. Yoneyama, N. Tsubaki, Catalysis Chemistry of Dimethyl Ether Synthesis, ACS Catal. 4 (2014) 3346–3356. doi:10.1021/cs500967j.

[31]   P.S.S. Prasad, J.W. Bae, S. Kang, Y. Lee, K. Jun, Single-step synthesis of DME from syngas on Cu – ZnO – Al$_2$O$_3$/zeolite bifunctional catalysts : The superiority of ferrierite over the other zeolites, Fuel Process. Technol. 89 (2008) 1281–1286. doi:10.1016/j.fuproc.2008.07.014.

[32]   S.-H. Kang, J.W. Bae, H.-S. Kim, G.M. Dhar, K.-W. Jun, Enhanced catalytic performance for dimethyl ether synthesis from syngas with the addition of Zr or Ga on a Cu−ZnO−Al$_2$O$_3$/γ-Al$_2$O$_3$ bifunctional catalyst, Energy & Fuels. 24 (2010) 804–810. doi:10.1021/ef901133z.

[33]   R. Ahmad, D. Schrempp, S. Behrens, J. Sauer, M. Döring, U. Arnold, Zeolite-based bifunctional catalysts for the single step synthesis of dimethyl ether from CO-rich synthesis gas, Fuel Process. Technol. 121 (2014) 38–46. doi:10.1016/J.FUPROC.2014.01.006.

[34]   G.R. Moradi, S. Nosrati, F. Yaripor, Effect of the hybrid catalysts preparation method upon direct synthesis of dimethyl ether from synthesis gas, Catal. Commun. 8 (2007) 598–606. doi:10.1016/J.CATCOM.2006.08.023.

[35]   M. Gentzen, W. Habicht, D.E. Doronkin, J.-D. Grunwaldt, J. Sauer, S. Behrens, Bifunctional hybrid catalysts derived from Cu/Zn-based nanoparticles for single-step dimethyl ether synthesis, Catal. Sci. Technol. 6 (2016) 1054–1063. doi:10.1039/C5CY01043H.

[36]   C. Zeng, J. Sun, G. Yang, I. Ooki, K. Hayashi, Y. Yoneyama, A. Taguchi, T. Abe, N. Tsubaki, Highly selective and multifunctional Cu/ZnO/Zeolite catalyst for one-step dimethyl ether synthesis: Preparing catalyst by bimetallic physical sputtering, Fuel. 112 (2013) 140–144. doi:10.1016/J.FUEL.2013.05.026.

[37]   S.-C. Baek, S.-H. Kang, J.W. Bae, Y.-J. Lee, D.-H. Lee, K.-Y. Lee, Effect of copper precursors to the activity for dimethyl ether synthesis from syngas over Cu-ZnO/γ-Al$_2$O$_3$ bifunctional catalysts, Energy & Fuels. 25 (2011) 2438–2443. doi:10.1021/ef200504p.

[38]   J.W. Jung, Y.J. Lee, S.H. Um, P.J. Yoo, D.H. Lee, K.-W. Jun, J.W. Bae, Effect of copper surface area and acidic sites to intrinsic catalytic activity for dimethyl ether synthesis from biomass-derived syngas, Appl. Catal. B Environ. 126 (2012) 1–8. doi:10.1016/J.APCATB.2012.06.026.

[39]   K. Klier, Methanol Synthesis, Adv. Catal. 31 (1982) 243–313. doi:10.1016/S0360-0564(08)60455-1.

[40]   J.C.J. Bart, R.P.A. Sneeden, Copper-zinc oxide-alumina methanol catalysts revisited, Catal. Today. 2 (1987) 1–124. doi:10.1016/0920-5861(87)80001-9.

[41]   G.H. Graaf, H. Scholtens, E.J. Stamhuis, A.A.C.M. Beenackers, Intra-particle diffusion limitations in low-pressure methanol synthesis, Chem. Eng. Sci. 45 (1990) 773–783. doi:10.1016/0009-2509(90)85001-T.

[42]   G.H. Graaf, E.J. Stamhuis, A.A.C.M. Beenackers, Kinetics of low-pressure methanol synthesis, Chem. Eng. Sci. 43 (1988) 3185–3195. doi:10.1016/0009-2509(88)85127-3.

[43]   G. Larsen, R. Velarde-Ortiz, K. Minchow, A. Barrero, I.G. Loscertales, A Method for Making Inorganic and Hybrid (Organic/Inorganic) Fibers and Vesicles with Diameters in the Submicrometer and Micrometer Range via Sol−Gel Chemistry and Electrically Forced Liquid Jets, J. Am. Chem. Soc. 125 (2003) 1154–1155. doi:10.1021/JA028983I.

[44]   R. Ruiz-Rosas, J. Bedia, M. Lallave, I.G. Loscertales, A. Barrero, J. Rodríguez-Mirasol, T. Cordero, The production of submicron diameter carbon fibers by the electrospinning of lignin, Carbon N. Y. 48 (2010) 696–705. doi:10.1016/J.CARBON.2009.10.014.

[45]   I.G. Loscertales, A. Barrero, M. Márquez, R. Spretz, R. Velarde-Ortiz, G. Larsen, Electrically Forced Coaxial Nanojets for One-Step Hollow Nanofiber Design, J. Am. Chem. Soc. 126 (2004) 5376–5377. doi:10.1021/JA049443J.

[46]   K. Huang, X. Chu, W. Feng, C. Zhou, W. Si, X. Wu, L. Yuan, S. Feng, Catalytic behavior of electrospinning synthesized La$_{0.75}$Sr$_{0.25}$MnO$_3$ nanofibers in the oxidation of CO and CH$_4$, Chem. Eng. J. 244 (2014) 27–32. doi:10.1016/J.CEJ.2014.01.056.

[47]   R. Ruiz-Rosas, J.M. Rosas, I.G. Loscertales, J. Rodríguez-Mirasol, T. Cordero, Electrospinning of silica sub-microtubes mats with platinum nanoparticles for NO catalytic reduction, Appl. Catal. B Environ. 156–157 (2014) 15–24. doi:10.1016/J.APCATB.2014.02.047.

[48]   R. Ruiz-Rosas, J. Bedia, J.M. Rosas, M. Lallave, I.G. Loscertales, J. Rodríguez-Mirasol, T. Cordero, Methanol decomposition on electrospun

zirconia nanofibers, Catal. Today. 187 (2012) 77–87. doi:10.1016/j.cattod.2011.10.031.

[49] M. Lallave, J. Bedia, R. Ruiz-Rosas, J. Rodríguez-Mirasol, T. Cordero, J.C. Otero, M. Marquez, A. Barrero, I.G. Loscertales, Filled and Hollow Carbon Nanofibers by Coaxial Electrospinning of Alcell Lignin without Binder Polymers, Adv. Mater. 19 (2007) 4292–4296. doi:10.1002/adma.200700963.

[50] S. Brunauer, P.H. Emmett, E. Teller, Adsorption of Gases in Multimolecular Layers, J. Am. Chem. Soc. 60 (1938) 309–319. doi:10.1021/ja01269a023.

[51] S. Lowell, J.E. Shields, J.E. Morral, Powder Surface Area and Porosity, 2nd Edition, 1985. doi:10.1115/1.3225796.

[52] A. Khorsand Zak, W.H. Abd. Majid, M.E. Abrishami, R. Yousefi, X-ray analysis of ZnO nanoparticles by Williamson–Hall and size–strain plot methods, Solid State Sci. 13 (2011) 251–256. doi:10.1016/J.SOLIDSTATESCIENCES.2010.11.024.

[53] G.C. Chinchen, C.M. Hay, H.D. Vandervell, K.C. Waugh, The measurement of copper surface areas by reactive frontal chromatography, J. Catal. 103 (1987) 79–86. doi:10.1016/0021-9517(87)90094-7.

[54] M. Sánchez-Contador, A. Ateka, P. Rodriguez-Vega, J. Bilbao, A.T. Aguayo, Optimization of the Zr Content in the CuO-ZnO-ZrO$_2$/SAPO-11 Catalyst for the Selective Hydrogenation of CO+CO$_2$ Mixtures in the Direct Synthesis of Dimethyl Ether, Ind. Eng. Chem. Res. 57 (2018) 1169–1178. doi:10.1021/acs.iecr.7b04345.

[55] M. Thommes, K. Kaneko, A. V. Neimark, J.P. Olivier, F. Rodriguez-Reinoso, J. Rouquerol, K.S.W. Sing, Physisorption of gases, with special reference to the evaluation of surface area and pore size distribution (IUPAC Technical Report), Pure Appl. Chem. 87 (2015). doi:10.1515/pac-2014-1117.

[56] J.W. Bae, S.-H. Kang, Y.-J. Lee, K.-W. Jun, Synthesis of DME from syngas on the bifunctional Cu–ZnO–Al$_2$O$_3$/Zr-modified ferrierite: Effect of Zr content, Appl. Catal. B Environ. 90 (2009) 426–435. doi:10.1016/J.APCATB.2009.04.002.

[57] T. Witoon, J. Chalorngtham, P. Dumrongbunditkul, M. Chareonpanich, J. Limtrakul, CO$_2$ hydrogenation to methanol over Cu/ZrO$_2$ catalysts: Effects of zirconia phases, Chem. Eng. J. 293 (2016) 327–336. doi:10.1016/j.cej.2016.02.069.

[58] C. Liu, X. Guo, Q. Guo, D. Mao, J. Yu, G. Lu, Methanol synthesis from CO$_2$ hydrogenation over copper catalysts supported on MgO-modified TiO$_2$, J. Mol. Catal. A Chem. 425 (2016) 86–93. doi:10.1016/J.MOLCATA.2016.09.032.

[59] S. Asthana, C. Samanta, A. Bhaumik, B. Banerjee, R.K. Voolapalli, B. Saha, Direct synthesis of dimethyl ether from syngas over Cu-based catalysts: Enhanced selectivity in the presence of MgO, J. Catal. 334 (2016) 89–101. doi:10.1016/J.JCAT.2015.10.020.

[60] J. Agrell, H. Birgersson, M. Boutonnet, I. Melián-Cabrera, R.M. Navarro, J.L.G. Fierro, Production of hydrogen from methanol over Cu/ZnO catalysts promoted by ZrO$_2$ and Al$_2$O$_3$, J. Catal. 219 (2003) 389–403. doi:10.1016/S0021-9517(03)00221-5.

[61] X. Guo, D. Mao, G. Lu, S. Wang, G. Wu, Glycine–nitrate combustion synthesis of CuO–ZnO–ZrO$_2$ catalysts for methanol synthesis from CO$_2$ hydrogenation, J. Catal. 271 (2010) 178–185. doi:10.1016/J.JCAT.2010.01.009.

[62] G. Avgouropoulos, T. Ioannides, H. Matralis, Influence of the preparation method on the performance of CuO–CeO$_2$ catalysts for the selective oxidation of CO, Appl. Catal. B Environ. 56 (2005) 87–93. doi:10.1016/J.APCATB.2004.07.017.

[63] X. Dong, F. Li, N. Zhao, F. Xiao, J. Wang, Y. Tan, CO$_2$ hydrogenation to methanol over Cu/ZnO/ZrO$_2$ catalysts prepared by precipitation-reduction

method, Appl. Catal. B Environ. 191 (2016) 8–17. doi:10.1016/j.apcatb.2016.03.014.

[64]   G.C. Chinchen, K.C. Waugh, D.A. Whan, The activity and state of the copper surface in methanol synthesis catalysts, Appl. Catal. 25 (1986) 101–107. doi:10.1016/S0166-9834(00)81226-9.

[65]   I.A. Fisher, A.T. Bell, In Situ Infrared Study of Methanol Synthesis from H_2/CO over Cu/SiO_2 and Cu/ZrO_2/SiO_2, J. Catal. 178 (1998) 153–173. doi:10.1006/JCAT.1998.2134.

[66]   G. Bonura, M. Cordaro, C. Cannilla, F. Arena, F. Frusteri, The changing nature of the active site of Cu-Zn-Zr catalysts for the CO_2 hydrogenation reaction to methanol, Appl. Catal. B Environ. 152–153 (2014) 152–161. doi:10.1016/J.APCATB.2014.01.035.

[67]   G.W. Jackson, D.F. James, The permeability of fibrous porous media, Can. J. Chem. Eng. 64 (1986) 364–374. doi:10.1002/cjce.5450640302.

[68]   O. Levenspiel, Engineering Flow and Heat Exchange, Springer US, Boston, MA, 2014. doi:10.1007/978-1-4899-7454-9.

[69]   D. Seguin, A. Montillet, J. Comiti, Experimental characterisation of flow regimes in various porous media—I: Limit of laminar flow regime, Chem. Eng. Sci. 53 (1998) 3751–3761. doi:10.1016/S0009-2509(98)00175-4.

[70]   S. Zhu, R.H. Pelton, K. Collver, Mechanistic modelling of fluid permeation through compressible fiber beds, Chem. Eng. Sci. 50 (1995) 3557–3572. doi:10.1016/0009-2509(95)00205-J.

[71]   E. Mauret, M. Renaud, Transport phenomena in multi-particle systems—I. Limits of applicability of capillary model in high voidage beds-application to fixed beds of fibers and fluidized beds of spheres, Chem. Eng. Sci. 52 (1997) 1807–1817. doi:10.1016/S0009-2509(96)00499-X.

[72]   Y. Jin, D. Yang, D. Kang, X. Jiang, Fabrication of Necklace-like Structures via Electrospinning, Langmuir. 26 (2010) 1186–1190. doi:10.1021/la902313t.

[73]   S. Jiang, W. He, K. Landfester, D. Crespy, S.E. Mylon, The structure of fibers produced by colloid-electrospinning depends on the aggregation state of particles in the electrospinning feed, Polymer (Guildf). 127 (2017) 101–105. doi:10.1016/J.POLYMER.2017.08.061.

[74]   A. Corma, From microporous to mesoporous molecular sieve materials and their use in catalysis, Chem. Rev. 97 (1997) 2373–2420. doi:10.1021/CR960406N.

[75]   J.H. Flores, M.I. Pais da Silva, Acid properties of the hybrid catalyst CuO–ZnO or CuO–ZnO–Al2O3/H-ferrierite: An infrared study, Colloids Surfaces A Physicochem. Eng. Asp. 322 (2008) 113–123. doi:10.1016/J.COLSURFA.2008.02.033.

[76]   S.-H. Kang, J.W. Bae, K.-W. Jun, H.S. Potdar, Dimethyl ether synthesis from syngas over the composite catalysts of Cu–ZnO–Al2O3/Zr-modified zeolites, Catal. Commun. 9 (2008) 2035–2039. doi:10.1016/J.CATCOM.2008.03.046.

[77]   A. García-Trenco, A. Vidal-Moya, A. Martínez, Study of the interaction between components in hybrid CuZnAl/HZSM-5 catalysts and its impact in the syngas-to-DME reaction, Catal. Today. 179 (2012) 43–51. doi:10.1016/J.CATTOD.2011.06.034.

[78]   L. Chmielarz, P. Kuśtrowski, M. Drozdek, R. Dziembaj, P. Cool, E.F. Vansant, Selective catalytic oxidation of ammonia into nitrogen over PCH modified with copper and iron species, Catal. Today. 114 (2006) 319–325. doi:10.1016/J.CATTOD.2006.01.020.

[79]   M. Jabłońska, R. Palkovits, Copper based catalysts for the selective ammonia oxidation into nitrogen and water vapour—Recent trends and open challenges, Appl. Catal. B Environ. 181 (2016) 332–351. doi:10.1016/J.APCATB.2015.07.017.

[80]   L. Gang, J. van Grondelle, B.G. Anderson, R.A. van Santen, Selective Low Temperature NH3 Oxidation to N2 on Copper-Based Catalysts, J. Catal. 186 (1999) 100–109. doi:10.1006/JCAT.1999.2524.

[81] D. Jin, B. Zhu, Z. Hou, J. Fei, H. Lou, X. Zheng, Dimethyl ether synthesis via methanol and syngas over rare earth metals modified zeolite Y and dual Cu–Mn–Zn catalysts, Fuel. 86 (2007) 2707–2713. doi:10.1016/J.FUEL.2007.03.011.

[82] J.-H. Kim, M.J. Park, S.J. Kim, O.-S. Joo, K.-D. Jung, DME synthesis from synthesis gas on the admixed catalysts of $Cu/ZnO/Al_2O_3$ and ZSM-5, Appl. Catal. A Gen. 264 (2004) 37–41. doi:10.1016/J.APCATA.2003.12.058.

[83] J. Ereña, I. Sierra, A.T. Aguayo, A. Ateka, M. Olazar, J. Bilbao, Kinetic modelling of dimethyl ether synthesis from (H_2 + CO_2) by considering catalyst deactivation, Chem. Eng. J. 174 (2011) 660–667. doi:10.1016/J.CEJ.2011.09.067.

[84] R. Khoshbin, M. Haghighi, P. Margan, Combustion dispersion of CuO–ZnO–Al_2O_3 nanocatalyst over HZSM-5 used in DME production as a green fuel: Effect of citric acid to nitrate ratio on catalyst properties and performance, Energy Convers. Manag. 120 (2016) 1–12. doi:10.1016/J.ENCONMAN.2016.04.076.

[85] Y. Wang, W. Wang, Y. Chen, J. Ma, R. Li, Synthesis of dimethyl ether from syngas over core–shell structure catalyst CuO–ZnO–Al_2O_3@SiO_2–Al_2O_3, Chem. Eng. J. 250 (2014) 248–256. doi:10.1016/j.cej.2014.04.018.

[86] J. Yoshihara, C.T. Campbell, Methanol Synthesis and Reverse Water–Gas Shift Kinetics over Cu(110) Model Catalysts: Structural Sensitivity, J. Catal. 161 (1996) 776–782. doi:10.1006/JCAT.1996.0240.

[87] J. Yoshihara, S.C. Parker, A. Schafer, C.T. Campbell, Methanol synthesis and reverse water-gas shift kinetics over clean polycrystalline copper, Catal. Letters. 31 (1995) 313–324. doi:10.1007/BF00808595.

General conclusions and future work

Two different alternative catalysts for the direct synthesis of DME from syngas has prepared and studied. On the one hand, activated carbon-based catalysts, presenting a granular morphology were prepared and, on the other hand, fibrillary structured inorganic catalysts were prepared by using the electrospinning technique.

For the carbon-based catalysts two kinds of activated carbons that were prepared by chemical (with phosphoric acid) and physical (by CO_2 partial gasification) activation of olive stone, an agri-food industry waste, were studied and used as catalyst support. The presence of chemically stable phosphorus surface groups, mainly in the form of $C-O-PO_3$ groups, on the activated carbon prepared via chemical activation with phosphoric acid, seemed to have great relevance in the catalytic performance of these carbon materials. When preparing acid catalysts, by Zr loading on the activated carbons, these phosphorus complexes were of great importance. These groups acted as anchor sites, forming zirconium phosphate species, which were determined to be responsible for the selective methanol dehydration to DME. However, the presence of these phosphorus groups had a negative effect when preparing the methanol synthesis catalysts, by Cu-Zn loading on the activated carbons, due to the formation of Cu phosphate species, which were not active for the methanol synthesis reaction. The physical mixing of the methanol synthesis and methanol dehydration catalysts resulted in the preparation of carbon-based catalytic beds, performed very efficient in the direct DME synthesis from syngas.

Regarding the preparation fibrillary structured inorganic catalysts, the use of the electrospinning technique has been highlighted as a straightforward solution to prepare submicrometric $CuO/ZnO/ZrO_2$-ZSM-5 bifunctional fibrillary catalysts, in flexible non-woven mats, in one step. The fibrillar nanostructured catalyst loading in the fixed-bed reactor resulted in the obtention of a spongy-like

catalytic bed, which presented an enhanced contact, in the submicrometric scale, between the two active phases involved in the syngas to DME process. This catalytic bed worked very efficient in the direct DME synthesis from syngas in terms of intraparticle mass and heat transfer, avoiding, at the same time, the problems related to pressure drops of fixed-bed reactors working with such a reduced particle size. In this sense, the value obtained from drop calculations for fibrillar catalytic bed reported in the present study was 10000 times smaller than the calculated for a packed bed of spherical particles presenting the same dimension.

But there is still more to do.

- The acid carbon-based catalyst has been optimized in terms of metal loading. However, the metal content for methanol synthesis catalyst has not been optimized. In addition, some characterization analyses are to do for this Cu-Zn loaded carbon-based catalyst, especially those related to CuO crystal size and Cu dispersion.
- Given that deactivation is a common problem in the direct DME synthesis from syngas, and it is a matter of concern for the economic viability of the process, the bifunctional catalysts and catalytic beds are to be studied in a long-term stability.
- The different bifunctional catalysts/catalytic beds have been studied for CO hydrogenation. However, the co-feeding of CO_2 and the direct CO_2 hydrogenation is still to do.
- The direct production of light hydrocarbons from syngas, via DME synthesis is also to studied.

Figure Captions

Scheme Captions

Table Captions

UNIVERSIDAD
DE MÁLAGA

Summary

Objectives and scope of this Thesis

This Thesis is motivated by the awareness that fossil fuels will finally come to an end. It could be said that we currently are in a transition period, moving from a petroleum oil-based economy to a more sustainable scenario, in which fuel will be produced via syngas-to-chemical processes, such as the syngas to dimethyl ether (DME) process. In this line, the main purpose of this Thesis is the preparation of alternative efficient catalysts for the direct DME synthesis from syngas.

This Thesis is divided into 7 chapters. Chapter 1 is a general introduction, covering the current state of art of the matter studied in this thesis. The experimental procedures followed in this Thesis are reported in Chapter 2. Chapters 3-7 conform the Results and Discussion block of this Thesis. The results of this Thesis are divided in two main parts, which are related to the two different methodologies followed for the preparation of the catalysts. On the one hand, in Chapters 3-5, the use of activated carbons as catalysts and catalyst supports was investigated. For this aim, two kind of activated carbons were prepared and loaded with different metal salts in order to incorporate the active phases needed for the chemical reactions studied. On the other hand, in Chapters 6 and 7, the preparation of inorganic-based fibrillar structured catalysts was addressed by using the electrospinning technique.

Introduction

From the beginning, human social development has been closely related to energy consumption. The way energy is obtained changes with the passing of the years, and alternative renewable technologies will be needed in order to meet the demands of a growing society.

The world population has grown drastically over the last decades, and recent estimations indicate that this trend will continue. In addition, current societies are prone to a continuous technological development, giving rise to a situation in which a huge amount of resource and energy will be necessary for satisfying people's needs in the near future. Nowadays, most of the energy demand is satisfied by using fossil fuels (carbon, natural gas and petroleum oil). There is no doubt that the fossil fuel reserves will come to an end, and although they will not be exhausted from one day to the next, the supply and demand will provoke a far more spectacular rise in prices than might be expected. In this scenario, synthetic routes for fuel production, by using alternative natural resources, will be more and more needed in order to meet the increasing world demand.

Synthetic oil production routes are feasible. These processes use synthesis gas (a mixture of carbon monoxide and hydrogen) as raw material. The synthesis gas can be produced by partial oxidation or reforming of natural gas or by gasification of coal or biomass. In this line, biomass represents a renewable carbon source, which would lead to a considerable reduction of greenhouse gas emissions in these processes, promoting the transition to an energy system that reduces dependence on fossil fuels in a scenario that contemplates, on the one hand, the scarcity of fossil fuels, and on the other hand the growth of global demand and the impact of emissions on the environment.

Among the synthetic routes for fuel production, syngas-to-methanol and the derived dimethyl ether (DME) process is receiving a great deal of attention. This process allows for operating under different H_2/CO ratios and, moreover, the co-feeding of CO_2 to this process is feasible.

Thanks to its physical and chemical properties, similar to liquified petroleum gases (LPG) and conventional diesel, plus the clean combustion achieved when used as fuel, DME is considered as one of the most promising alternatives to petroleum derived fuel, and thus, its production is the object of much research.

DME can be produced by two alternative processes; a two-step catalytic process (so-called indirect process), which involves a first stage for methanol

synthesis from syngas on (Eq. (1) and (2)) Cu-based catalysts and a second stage for the selective dehydration of methanol to DME (Eq. (3)) on a solid acid catalyst; and a one-step process (so-called direct process), in which synthesis gas is fed to a single reactor containing a bifunctional catalyst, where both methanol synthesis, in parallel with the water gas shift reaction (WGSR) (Eq. (4)), and the selective methanol dehydration take place.
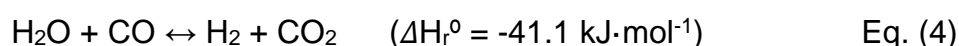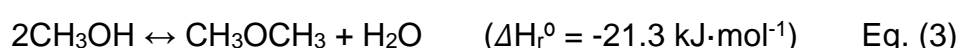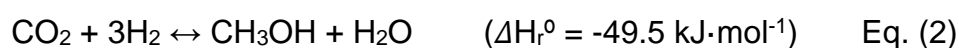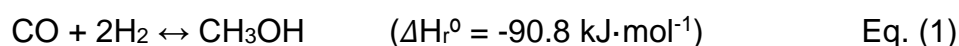
$$CO + 2H_2 \leftrightarrow CH_3OH \qquad (\Delta H_r^0 = -90.8 \ kJ \cdot mol^{-1}) \qquad \text{Eq. (1)}$$

$$CO_2 + 3H_2 \leftrightarrow CH_3OH + H_2O \qquad (\Delta H_r^0 = -49.5 \ kJ \cdot mol^{-1}) \qquad \text{Eq. (2)}$$

$$2CH_3OH \leftrightarrow CH_3OCH_3 + H_2O \qquad (\Delta H_r^0 = -21.3 \ kJ \cdot mol^{-1}) \qquad \text{Eq. (3)}$$

$$H_2O + CO \leftrightarrow H_2 + CO_2 \qquad (\Delta H_r^0 = -41.1 \ kJ \cdot mol^{-1}) \qquad \text{Eq. (4)}$$

Nowadays, DME is mostly produced by the so-called indirect process, using synthesis gas (H_2 + CO/CO_2) as raw material. However, the prospects for the development of a DME-based economy depends on the feasibility of the direct DME synthesis route. The main reason for using the direct route instead of the indirect one relies on the thermodynamic limitations affecting the latter. Chemical reactions involved in methanol synthesis (Eq. (1) and (2)) are reversible and, thus, they are limited by thermodynamic equilibrium, which is a function of the temperature, pressure and the synthesis gas composition. This thermodynamic limitation results in a low synthesis gas conversion per-pass, increasing the operating costs related to methanol separation and synthesis gas recirculation. The use of the direct DME synthesis route allows for in-situ consuming the generated methanol, via dehydration to DME, reducing the equilibrium constrains affecting the methanol synthesis by this way. This thermodynamic advantage permits to work at lower pressure and/or higher temperature achieving a higher synthesis gas conversion per pass. In addition, water generated in the methanol dehydration reaction (Eq. (3)), can be removed from the reaction media by means of the WGSR (Eq. (4)), yielding H_2 and favoring the methanol dehydration reaction. This feature is of high interest when using a CO-enriched synthesis gas, such as the obtained via biomass gasification.

Catalysts used in the direct DME synthesis must present two well-defined catalytic active phases, one accounting for methanol synthesis and the other for

methanol dehydration. The preparation of bifunctional catalysts for this process is usually accomplished by physical mixing of their individual components. As an alternative to these physical mixtures, the use of supported catalysts, in which the solid acid acts as support for the metallic phase, has also been studied, being the tandem process from synthesis gas to DME achieved on the surface of one particle of the catalyst. In the last years, the use of bifunctional capsule catalysts, co-called core-shell catalysts, for the syngas-to-DME process has been reported.

The prospects and demand of DME present a considerable industrial and market potential for both electric energy generation and for being used as domestic fuel. In fact, there is a great development regarding DME production industries all around the world. However, despite the progress achieved to date, there are still pending issues, most of them related to the catalysts used in the process.

Experimental

Chapter 2 presents the general experimental methodology followed in this Thesis. It describes the most relevant aspects dealing with the preparation and characterization of the investigated materials and with the catalytic experiments and the experimental set up used to evaluate the catalysts.

In this Thesis, two different methodologies have been followed for preparing catalysts. On the one hand, activated carbon-based catalysts, presenting a granular morphology, were prepared by chemical and physical activation of a lignocellulosic waste followed by the impregnation with different metal salts. On the other hand, fibrillary structured inorganic catalysts were prepared by using the electrospinning technique.

The porous texture of the prepared catalysts was characterized by N_2 adsorption–desorption at -196 ºC and by CO_2 adsorption at 0 ºC. The surface morphology of the samples was studied by scanning and transmission electron microscopy. The surface chemistry of the samples was characterized by X-ray photoelectron spectroscopy (XPS), temperature programmed desorption (TPD). X-ray diffraction was used for crystal phases identification. The total acidity and acid strength distribution of the prepared catalysts was determined by

temperature programmed desorption of ammonia (NH_3-TPD). The Cu dispersion and the Cu metallic surface area of the bifunctional catalysts were determined by N_2O selective chemisorption. The reducibility of the metallic species presented on the samples was addressed by temperature programmed reduction (H_2-TPR).

Gas phase methanol dehydration experiments were carried at atmospheric pressure in a fixed-bed microreactor (i.d. 4 mm) place inside a vertical furnace with temperature control.

The methanol synthesis and the direct dimethyl ether synthesis from syngas experiments were carried out in a PID Eng. & Tech. Microactivity equipment, which is provided with a stainless steel fixed-bed reactor and allows for operating at high temperature and pressures.

Results and Discussion.

Part 1: Activated carbon as catalysts for DME synthesis.

Activated carbons used as catalysts and catalyst supports have received much attention in the recent decades owing to some great advantages, such as its high specific surface area, high thermal and chemical stability, and the possibility to modify its surface chemistry, tuning its acidity that way. These materials can be obtained from several kinds of lignocellulosic waste, producing economic as well as environmental advantages. However, despite its potential, the use of activated carbons as catalysts for methanol dehydration has scarcely been studied so far. Regarding this issue, it has been pointed out that non-oxidized carbons are unreactive in the methanol decomposition reaction, observing certain activity only after oxidizing its surface. In this sense, some attempts have been made in order to modify the carbon surface by oxidation with chemical reagents, such as O_2, $(NH_4)_2S_2O_8$, H_2SO_4 and HNO_3. However, the acid groups created by these means have a low to moderate thermal stability, resulting in a fast deactivation when the reaction temperature is increased.

Our research group has reported several works on the preparation and characterization of biomass waste-derived activated carbons by chemical

activation with phosphoric acid. The activation with phosphoric acid leads to the preparation of carbon materials presenting oxygen-phosphorus surface groups that show a high thermal and chemical stability, remaining over the carbon surface after the washing step. These surface phosphorus groups provide the activated carbon a surface acidity and a high oxidation resistance, making them suitable for applications in catalysis, such as alcohol dehydration reactions. In this line, methanol dehydration has been achieved on these materials, obtaining a selectivity towards DME higher than 95 %, when air is used as a reaction atmosphere. However, when they are applied as catalysts in a non-oxidizing atmosphere, they suffer from fast deactivation due to coke deposition, exhibiting only a residual methanol conversion lower than 10%. Therefore, these materials cannot be applied to industrial DME production routes, that is, indirect as well as direct DME synthesis processes.

Chapter 3

Chapter 3, entitled "Methanol dehydration to dimethyl ether on Zr-loaded P-containing mesoporous activated carbon catalysts", addresses the preparation and characterization of activated carbon catalysts for the efficient methanol dehydration to DME. In this work, two kinds of activated carbons were prepared by chemical (with phosphoric acid) and physical (by CO_2 partial gasification) activation of olive stone, an agri-food industry waste, and afterwards, they were loaded with different amounts of Zr (0 – 7.5 (w/w)).

The prepared activated carbons presented similar BET surface areas. The chemically activated carbon prepared presented a well-developed porous texture and a high apparent surface area (1260 m^2/g). The physically activated carbon presented a specific surface area very similar to that obtained for the chemically activated carbon (1130 m^2/g). However, this carbon showed a narrower microporosity, as compared to the chemically activated carbon. Once loaded with Zr, the activated carbon catalysts showed a slight decrease, in general, in the textural parameters compared to the ones of the parent activated carbons.

Both activated carbons, were mainly composed by carbon and oxygen. However, the chemically activated carbon also presented a low but still significant surface concentration of phosphorus, which was attributed to the activation step.

The presence of chemically stable phosphorus surface species, mainly in form of C-O-PO$_3$ groups, on the activated carbon prepared via chemical activation with phosphoric acid seems to have a great relevance in the catalytic performance of these carbon materials for methanol dehydration. XPS analysis revealed that zirconium bonded these phosphorus complexes during the metal loading, resulting in the formation of zirconium phosphate species on the activated carbon surface.

The catalytic results showed that the physically activated carbon, which did not contain P surface groups, did not show any catalytic activity. After Zr loading, it showed some initial activity, but this decreased with time on stream, evidencing a deactivation process. The phosphorus-containing activated carbon presented a high initial methanol conversion. However, the conversion dropped in the first reaction minutes, evidencing a deactivation process. Once loaded with zirconium, the resulting material presented a relatively high catalytic activity and steady-state methanol conversion was observed, without deactivation. The catalytic performance was improved with the amount of zirconium added to the activated carbon until a fixed loading amount (of around 5 % (w/w)), from which, no further increasing in the steady-state methanol conversion was observed. The catalytic activity of these materials was attributed to the presence of well dispersed surface zirconium phosphate species, whose formation was limited by the amount of phosphorus present on the carbon surface of the chemically activated carbon.

Zr-loaded phosphorus-containing activated carbons exhibited methanol conversion values close to thermodynamic equilibrium, keeping a selectivity towards DME higher than 95% in the whole range of temperatures used in the industrial DME synthesis (250-400 ºC). The stability results showed that once the materials achieved the steady-state methanol conversion, it remained unaltered for more than 72 hours.

The presence of water vapor in the reaction gas on the catalytic dehydration of methanol was also studied. The results showed that the methanol conversion decreased when increasing the water vapor partial pressure. However, the methanol conversion was not affected with time-on-stream at a

constant water vapor partial pressure. Moreover, the methanol conversion was restored to the value obtained in absence on water once removing the water vapor from the feed, evidencing that the effect of water on the catalytic performance was reversible. The selectivity towards DME was not affected by the presence of water vapor in the feed, with a value higher than 95% observed for all the water vapor pressures studied.

Chapter 4

Chapter 4, entitled "On the kinetics of methanol dehydration to dimethyl ether on Zr-loaded P-containing mesoporous activated carbon catalyst", presents a kinetic study of methanol dehydration to DME on the activated carbon catalyst that exhibited the best catalytic performance in Chapter 3.

As aforementioned, the catalytic activity of the various carbon materials prepared in this Chapter 3 showed remarkable differences. These differences could be related to the surface chemistry of these catalysts. The chemically activated carbon showed only phosphorus species, presenting C-O-P and P-OH bonds as in $C-O-PO_3$ surface groups, which can act as moderate and strong acid sites, respectively, for methanol dehydration. However, a fast deactivation due to coke formation was observed for this catalyst. The Zr-loaded physically activated carbon (not containing P) presented ZrO_2 and oxygen-carbon groups on its surface. This material presented a low activity for methanol dehydration, which was a consequence of the low thermal stability of the oxygenated surface groups and to the low catalytic activity that ZrO_2 exhibits. The Zr-loaded chemically activated carbon contained phosphorus and zirconium chemical surface species, mainly in form of zirconium phosphate, and was the only catalyst prepared in this work exhibiting appreciable methanol conversion at steady-state conditions. Therefore, the presence of this chemical species bonded to the carbon surface seemed to be responsible for the steady-state methanol conversion presented by this catalyst.

Methanol dehydration to DME using zirconium phosphates as catalysts has been reported in the literature, considering the P-OH and P-O-P surface species as active sites for this reaction. According to this study, only phosphorus species are responsible for the methanol dehydration activity of these materials,

and thus, the chemically activated carbon presented in this study, which exhibited phosphorus surface complexes, should have efficiently catalyzed the reaction. However, after a fast deactivation process, this material only showed a residual activity, indicating that neither P-OH nor C-O-P sites are capable of achieving a significant steady-state methanol conversion. On the opposite, as mentioned above, the activated carbon containing zirconium phosphate surface species, did present high steady-state methanol conversion values. Thus, it seems that the active site for this reaction have to consider the presence of both P and Zr.

A kinetic study considering the Zr-O-P groups as the active sites for the reaction was carried out for the selective methanol dehydration to DME on the Zr-loaded P-containing activated carbon and the corresponding kinetic and thermodynamic parameters were obtained. The reaction was performed in a fixed-bed reactor in the temperature range of 250-400 ºC. Since selectivity to DME was higher than 97% for all the conditions studied, the mechanisms proposed in this work only considered the formation of DME as reaction product. Three different reaction mechanisms were studied. The model that best reproduced the experimental data was a modified Langmuir-Hinshelwood mechanism. This mechanism accounts for a first methanol adsorption on the Zr-O-P active site, which cleavages yielding a methoxy group bonded to the phosphorus and a vicinal -OH bonded to the zirconium (Step 1). Subsequently, a second methanol molecule adsorbs on the generated vicinal Zr-OH (Step 2). Then adsorbed methanol reacts with the previously formed methoxy group yielding DME and H_2O, which remains adsorbed on the active site (Step 3). Finally, H_2O is desorbed, being the Zr-O-P group regenerated (Step 4). This model reproduced the experimental data with a high accuracy at the operation conditions studied. The activation energy for the DME production was calculated and a value of 70 kJ mol^{-1} was obtained.

Chapter 5

Chapter 5, entitled "Biomass-derived activated carbon catalysts for the direct dimethyl ether synthesis from syngas", is focused on the direct synthesis of DME from syngas using activated carbons-based catalysts.

The catalysts used for the direct DME synthesis route are composed of two active phases, one accounting for the methanol synthesis (methanol synthesis catalyst) and another one for the methanol dehydration (methanol dehydration catalyst). The preparation of catalysts for this process is usually accomplished by physical mixing of their individual aforementioned catalysts, yielding bifunctional catalytic beds by this way.

In this study, two kinds of activated carbons, prepared by physical (by CO_2 partial gasification) and chemical (with phosphoric acid) activation of olive stones, were used as supports for the preparation of the catalysts. The main difference between them was the presence of chemically stable phosphorus surface groups, mainly in form of $C-O-PO_3$ groups, on the activated carbon prepared via chemical activation with phosphoric acid. These activated carbons were loaded with Cu, Zn and Zr salts to prepare the biomass-derived catalysts used in this work. The preparation of bifunctional catalytic beds was carried out by physical mixing of the corresponding methanol synthesis and methanol dehydration catalysts, by using different acid/metallic mass ratios.

As for the methanol dehydration catalyst, a 5 %(w/w) Zr-loaded chemically activated carbon was used. As described in Chapters 3 and 4, the addition of Zr to the chemically activated carbon resulted in the formation of zirconium phosphate species on the carbon surface, which were capable of promoting the selective methanol dehydration to DME.

As for methanol synthesis component, the two activated carbons and the methanol dehydration catalyst were loaded with Cu-Zn (Cu and Zn loading of 10.5 and 5.5 %(w/w), respectively). The presence of phosphorus groups on the surface of the activated carbons had a great relevance on the catalytic performance of the materials. The results showed strong interactions between the metallic phase and the phosphate surface groups due to the formation Cu phosphate species, which were not active for the methanol synthesis reaction. On the contrary, the physically activated carbon, not containing phosphorus, exhibited a fairly good catalytic behavior, and thus, it was chosen to be used as the methanol synthesis catalyst for the preparation of bifunctional catalytic beds. The preparation of catalysts presenting both methanol synthesis and dehydration

active phases on the same carbon surface was attempted by using the methanol dehydration catalyst as support of the metallic phase. However, the detrimental interaction between Cu and the phosphate species made this preparation strategy unfeasible.

The physical mixing of the methanol synthesis and methanol dehydration catalysts resulted in the preparation of carbon-based catalytic beds, which avoided the metallic-acid detrimental interaction. The study of the different acid/metallic catalyst mass ratios showed that a value of 2 provided the catalytic bed with enough acid sites for making the overall syngas to DME process kinetically controlled by the methanol synthesis reaction.

In the light of the catalytic results, it can be concluded that the direct DME synthesis from syngas can be efficiently carried out by using carbon-based catalysts. In this sense, the metallic function showed a good catalytic behavior for CO hydrogenation, and on the other hand, the acid function exhibited suitable catalytic behavior in the selective methanol dehydration to DME under the syngas to DME reaction conditions.

Part 2: Fibrillar structured bifunctional catalysts for DME synthesis.

The preparation of catalysts for the direct DME synthesis is usually accomplished by physical mixing of the individual catalysts. Although this preparation procedure is simple and easy to scale-up, the catalysts prepared by this procedure present too great a distance between the two active sites involved in the syngas-to-DME process, thus lowering the performance of the catalyst.

An alternative to these physical mixtures is the use of supported catalysts, in which the solid acid acts as support for the metallic phase. By this way, the tandem process from synthesis gas to DME is achieved on the surface of one particle of the bifunctional catalyst. However, these catalysts lack uniformity for the metallic phase given that this phase is randomly distributed on the support, forming aggregates that can sinterize in the catalyst calcination stage. Furthermore, metal deposition on the support results in a strong metal-support interaction, resulting in problems for the reducibility of the metallic phase, and thus, partially deactivating the catalyst.

In addition, the use of bifunctional capsule catalysts, co-called core-shell catalysts, has been also proposed for direct synthesis of DME. In these catalysts, the metallic component is conforming the core of the catalyst and it is confined by a lower thickness acid phase. Although these catalysts have demonstrated a higher efficiency as compare to the ones prepared by physical mixing, they present some drawbacks. On the one hand, the preparation of these catalysts involves complex methodologies and, on the other hand, a granulation stage at some point of their preparation procedure is required for their application in a fixed-bed reactor. This granulation stage, needed for avoiding the pressure drops inside the reactor, limits the size of the core-shell material.

In contrast to these catalyst preparation methodologies, Electrospinning is a simple and straightforward technique that has been used to obtain carbon and polymer fibers in the submicron and nanoscale. In this process, a viscous polymer solution, held by its surface tension at the end of a capillary tube, is subjected to a high voltage electric field, inducing the ejection of a charged liquid jet. Due to the electrostatic repulsions between the surface charges, an unstable whipping of the jet occurs in the space between the capillary tip and the collector electrodes, provoking the solvent evaporation and leading to the deposition of polymer fibers on the collector.

The use of fibrillar structured bifunctional catalysts in the submicrometric scale could be very efficient for the direct production of DME from syngas in fixed-bed reactors, in terms of intraparticle mass and heat transfer, avoiding, at the same time, the problems related to pressure drops when working with such a reduced particle size in this type of reactor.

Chapter 6

Chapter 6, entitled "On the one step preparation of core-shell CuO/ZnO/ZrO$_2$-ZSM-5 fibrillar bifunctional catalysts by electrospinning for the efficient direct synthesis of dimethyl ether from syngas" reports a straightforward method for the one-step preparation of nanostructured zirconia-zeolite fibrillar materials in the form of core-shell like structures, by using the electrospinning technique, and the use of these materials as efficient catalysts for methanol

282

dehydration to dimethyl ether and for the direct synthesis of dimethyl ether from syngas.

In this study, different amounts of ZSM-5 zeolite were added to a PVP-zirconium acetate solution. These polymeric suspensions were electrospun and calcined in a muffle furnace at 500 ºC. SEM and TEM images showed fibers with a high aspect ratio, and mean sizes of 275 nm, and the presence of uniformly separated zeolite aggregates. Analyzing in detail these zeolite aggregates, it could be observed that the zeolite particles assembling seemed to occur, surrounding the zirconium oxide nanofiber, creating local core-shell like structures with sizes ranging from 350 to 550 nm. X-ray diffraction (XRD) analyses further confirmed the presence of both the zirconia and ZSM-5 zeolite crystal phases.

The increase of the zeolite concentration in the electrospinning solution resulted in a higher proportion of the local zirconia-zeolite core-shell like structures, with the corresponding reduction of the length of the fiber between two of these zirconia-zeolite core-shell like structures. Moreover, it was observed that the local zirconia-zeolite core-shell like structures started to join for zeolite loadings higher than 20 %(w/w), where these zeolite aggregates structures were closer and closer, forming core-shell like fibers.

N_2 adsorption-desorption studies showed no loss of textural properties in the zeolite as a consequence of the preparation process. In a similar way, NH_3-TPD highlighted that the acid sites of the parent zeolite and their acid strength distribution remained unaltered when preparing the fibrillar materials.

These ZrO_2-Zeolite fibrillar materials were directly used as catalysts for methanol dehydration in a fixed-bed reactor. The results showed that the possibility of obtaining homogeneously separated nanometric zeolite particle aggregates along the zirconia fibers in a nanostructured catalytic system, allowed controlling the catalytic active sites density inside a fixed-bed reactor, avoiding the generation of hotspots, without the need of adding a further phase in the reactor. By this way, very high methanol conversion and selectivity to DME values were obtained.

The addition of copper and zinc salts to the electrospinning solution resulted in the preparation of fibrillar bifunctional catalysts presenting the same core-shell like structures. TEM-EDXA analyses showed a high dispersion of Cu-Zn along the zirconia fiber surface. Besides, analyzing in depth the core-shell like regions of the material, it could be observed that these elements were clearly laid on the surface of the core, while the zeolite particles were allocated surrounding (covering) the copper core, acting as a shell.

These CuO/ZnO/ZrO$_2$-ZSM-5 fibrillar bifunctional materials were directly used as catalysts for the direct DME synthesis from syngas in a fixed-bed reactor, obtaining by this way spongy-like catalytic beds, which presented an enhanced contact, in the submicrometric scale, between the two active phases involved in the syngas to DME process. This catalytic bed worked very efficient in the direct DME synthesis from syngas, avoiding the problems related to pressure drops of fixed-bed reactors working with such a reduced particle size. The pressure drop inside the fixed-bed reactor was theoretically calculated and compared to the value obtained for a conventional particle packed bed. The results obtained from pressure drop calculation showed a value more than 10000 times smaller for the fibrillar packed bed as compared to the value calculated for a packed bed of particles presenting the same particle dimension.

<u>Chapter 7</u>

Chapter 7, entitled "ZSM-5-decorated CuO/ZnO/ZrO$_2$ fibers as efficient bifunctional catalysts for the direct synthesis of DME from syngas" addresses the preparation, characterization and application of one-dimensional structured bifunctional catalyst, presenting two well-defined catalytic phases, metallic and acid. In this chapter, use of electrospinning technique has been highlighted as a straightforward solution to prepare bifunctional fibrillary catalysts in one step. A detailed parametric study of the direct synthesis of DME from syngas on these bifunctional fibrillar catalysts has been carried out in a continuous fixed-bed reactor.

The experimental procedure carried out for the preparation of the fibrillar materials involved three stages; the preparation of a polymer-based solutions,

the electrospinning of the resulting solution and the calcination of the fibrillar materials at 500 ºC for 4 h.

Two different polymeric solutions, based on different oxide precursors, were used for the preparation of the fibrillar materials. On the one hand, polymeric solutions based on zirconium (IV) propoxide (70 wt % in 1-propanol), polyvinylpyrrolidone (PVP), 1-propanol, zinc acetate and copper acetate were prepared. On the other hand, a polymeric solution based on zirconium acetate (16 %(w/w) in acetic acid), polyvinylpyrrolidone (PVP) and 1-propanol was prepared. In this case, copper nitrate trihydrate and zinc nitrate hexahydrate were used as CuO and ZnO precursors. For both polymeric solutions, Cu and Zn precursors were added in appropriate amount to obtain a final CuO+ZnO concentration of 25 and 35 %(w/w), keeping a molar Cu/Zn ratio of 2, in the final calcined fiber.

SEM micrographs of the samples showed that these mats consisted in a non-woven fabric of fibers. All the prepared materials showed a high aspect (length to diameter) ratio and the absence of fused zones, and presented diameters ranging from 0.7 to 1.7 µm. TEM-EDXA analyses showed that the fibers containing a 25 %(w/w) of CuO+ZnO presented a uniform distribution of all the elements composing the fibrillar materials, whereas, non-uniform Cu and Zn elemental distributions, evidencing the presence of CuO and ZnO aggregates, were observed for the fibers containing a 35 %(w/w) of CuO+ZnO.

The samples were characterized by N_2 adsorption-desorption, H_2-TPR, XRD and N_2O selective chemisorption. The results showed that the fibers containing a 25 %(w/w) of CuO+ZnO, prepared by using zirconium acetate and copper and zinc nitrates, presented the smallest CuO particle size and the best metallic surface properties of the prepared catalysts.

The fibrillar materials were used as catalysts for methanol synthesis from syngas. In these experiments, a high pressure fixed-bed reactor was used. The catalytic activity obtained for the different catalysts was correlated with the textural, structural and surface chemistry of the fibrillar catalysts studied.

In agreement with that observed for the characterization results, the sample containing a 25 %(w/w) of CuO+ZnO, prepared by using Zirconium acetate and copper and zinc nitrates, was the best in terms of CO conversion and methanol yield, and thus, it was chosen as the metallic function for the preparation of bifunctional fibrillar catalysts.

For comparative purposes, a powder catalyst was prepared keeping the same composition of the best catalyst obtained. This material was pelletized and used as catalyst in the same conditions than the fibers were tested. The results showed that this material presented a much lower CO conversion as compared to the fibrillar one, highlighting that the structuration of the catalyst to a fibrillar morphology in the submicrometric scale was a key step for the efficient performance of the catalyst.

For the preparation of the bifunctional catalysts, different amounts of ZSM-5 zeolite (Zeolyst international, CBV 5524G, Si/Al 50, with mean crystal size of 120 nm) were also added to the Cu-Zn-Zr-based polymeric solution, to obtain a final fiber with a zeolite mass concentration ranging from 5 to 15 %(w/w). The resulting suspensions were electrospun and calcined at 500 ºC in air for 4 h.

TEM-EDXA analyses showed that the fiber surface presented smooth surface regions, as for the sample not containing zeolite, being these regions composed by uniform particles smaller than 10 nm, and on the other hand, the presence of particle aggregates, with a mean size of 300 nm, attached to the surface of the fibers, were also appreciated. A fairly good distribution was observed for these particle aggregates along the surface of the fibers, which is a consequence of the huge flexibility and control that electrospinning brings over the distribution of particles in fibrillar materials

The fibrillar structured bifunctional materials were directly used as catalysts for the syngas to DME process in a continuous fixed-bed reactor. The enhanced contact between the two active phases of the fibrillar catalyst favored the reaction tandem of methanol formation and dehydration to DME, giving rise to high CO conversion values and a selectivity to DME higher than 63% (95 % when considering only the products in the organic phase).

In addition, it is worth highlighting that the fibrillar structured catalysts made use of the submicrometric effective dimension of the two active phases (radius of the fibers lower than 1 µm, size of zeolite aggregates lower than 300 nm), in terms of enhancing intraparticle mass and heat transfer, avoiding, at the same time, the problems related to pressure drops of fixed-bed reactors working with such a reduced particle size. In this sense, the value obtained from drop calculations for fibrillar catalytic bed reported in the present study was 5000 times smaller than the calculated for a packed bed of spherical particles presenting the same dimension.

Resumen

Objetivos y alcance de esta Tesis Doctoral

Esta tesis está motivada por la concienciación de que los combustibles fósiles finalmente se agotarán. Se podría decir que actualmente estamos en un período de transición, pasando de una economía energética basada en el petróleo hacia un sistema energético más sostenible, en la cual, los combustibles necesarios se producirán a través de procesos químicos catalíticos utilizando gas de síntesis como materia prima, tales como el proceso de síntesis directa de dimetiléter (DME). En este contexto, el principal objetivo de esta Tesis Doctoral es la preparación de catalizadores alternativos eficientes para el proceso de síntesis directa de DME.

Esta tesis está dividida en 7 capítulos. El capítulo 1 es una introducción general, en ella se introduce el tema y se repasa el estado actual del arte, así como los antecedentes bibliográficos. El capítulo 2 se centra en los procedimientos experimentales seguidos en el desarrollo de esta Tesis Doctoral. Los capítulos 3-7 constituyen el bloque de Resultados y Discusión de la Tesis. Los resultados de esta Tesis Doctoral se han dividido en dos partes, relacionados con la estrategia seguida para la preparación de catalizadores. En los capítulos 3-5 se estudió el uso de carbones activados como catalizadores y soporte de catalizadores. Para ello, se prepararon dos tipos de carbones activados sobre los que se depositaron diferentes sales metálicas, obteniendo así las fases activas necesarias para catalizar las reacciones químicas estudiadas. Por otro lado, en los capítulos 6 y 7 se aborda la preparación de catalizadores inorgánicos fibrilares usando la técnica del Electrohilado.

Introducción

Desde el principio de la humanidad, el desarrollo social ha estado muy relacionado con el consumo de energía. La forma de obtener la energía cambia con el paso de los años, y de acuerdo con las estimaciones actuales, en un futuro próximo serán necesarias nuevas formas de obtener energía a partir de recursos renovables para satisfacer la demanda de la sociedad.
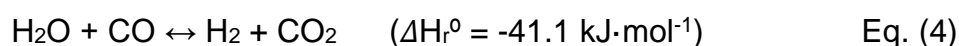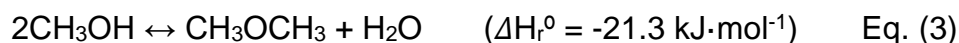
La población mundial ha crecido notablemente en las últimas décadas y las recientes estimaciones indican que esta tendencia continuará. Además, las sociedades actuales están en continuo desarrollo tecnológico, lo que dará lugar a una situación en la que se necesitarán grandes cantidades de recursos para satisfacer la creciente demanda. Actualmente, la mayor parte de la energía se obtiene a partir de combustibles fósiles (carbón, gas natural y petróleo). En este punto cabe señalar que no hay ninguna duda de que las reservas de combustibles fósiles se agotarán, y aunque este agotamiento no ocurrirá de un día para otro, la oferta y la demanda provocarán que el precio de estos recursos se dispare, alcanzando valores muy elevados. En este escenario, es cada vez más necesario el desarrollo de rutas sintéticas de producción de combustibles a partir de recursos naturales alternativos y renovables.

Los procesos químicos que permiten la producción de combustibles sintéticos son viables técnicamente. Estos procesos utilizan gas de síntesis (una mezcla de monóxido de carbono e hidrógeno) como materia prima. El gas de síntesis necesario puede producirse mediante la oxidación parcial o reformado del gas natural, o mediante la gasificación de carbón o biomasa. En este contexto, la biomasa representa una fuente de carbono renovable, cuyo uso conllevaría una reducción de las emisiones de gases invernadero, promoviendo una transición hacia un sistema energético con una menor dependencia de los combustibles fósiles.

Entre las diferentes rutas sintéticas para la producción de combustibles que se conocen, el proceso de síntesis de metanol/DME está recibiendo una gran atención, ya que este proceso permite una cierta flexibilidad a la hora de operar con gas de síntesis con diferentes relaciones H_2/CO e incluso permite la alimentación simultánea de CO_2 al reactor.

El DME está considerado como una de las alternativas a los combustibles derivados del petróleo más prometedoras. Este compuesto presenta propiedades físicas y químicas similares a las de los gases licuados del petróleo (GLP) y al diésel de refinería. Además, su uso como combustible ha demostrado una baja emisión de partículas y de contaminantes atmosféricos. Dadas estas ventajas, su producción está siendo objeto de muchas investigaciones.

Se pueden diferenciar dos métodos de obtención de DME; un proceso catalítico de dos etapas (proceso indirecto), que consta de un primer reactor donde lleva a cabo la síntesis de metanol a partir de gas de síntesis (Eq. (1) y (2)) utilizando un catalizador de cobre y un segundo reactor donde se deshidrata el metanol a DME (Eq. (3)) sobre un catalizador ácido; y un proceso de una sola etapa (proceso directo), en el cual el gas de síntesis se alimenta a un único reactor que contiene un catalizador bifuncional, donde ambas reacciones, la síntesis y la deshidratación de metanol (Eq. (1)-(3)), en paralelo con la reacción de water gas shift (Eq. (4)), tienen lugar.

$$CO + 2H_2 \leftrightarrow CH_3OH \qquad (\Delta H_r^0 = -90.8 \text{ kJ·mol}^{-1}) \qquad \text{Eq. (1)}$$

$$CO_2 + 3H_2 \leftrightarrow CH_3OH + H_2O \qquad (\Delta H_r^0 = -49.5 \text{ kJ·mol}^{-1}) \qquad \text{Eq. (2)}$$

$$2CH_3OH \leftrightarrow CH_3OCH_3 + H_2O \qquad (\Delta H_r^0 = -21.3 \text{ kJ·mol}^{-1}) \qquad \text{Eq. (3)}$$

$$H_2O + CO \leftrightarrow H_2 + CO_2 \qquad (\Delta H_r^0 = -41.1 \text{ kJ·mol}^{-1}) \qquad \text{Eq. (4)}$$
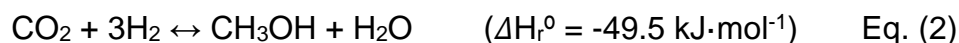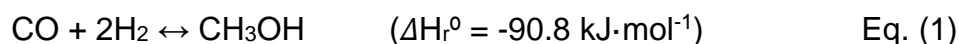
Actualmente la producción de DME se lleva a cabo mediante el proceso indirecto, usando gas de síntesis (H_2 + CO/CO_2) como materia prima. Sin embargo, las previsiones para el desarrollo de una economía basada en el DME se basan en la viabilidad del proceso de síntesis directa de DME. La principal razón para la sustitución del método de síntesis indirecto por el directo reside en las ventajas termodinámicas que ofrece este último. Las reacciones involucradas en la síntesis de metanol (Eq. (1) y (2)) son reversibles y fuertemente exotérmicas y, por lo tanto, están fuertemente limitadas por el equilibrio termodinámico, que es una función de la temperatura, la presión y la composición del gas de síntesis. Esta limitación termodinámica tiene como resultado una baja conversión de gas de síntesis por paso, aumentando los costes de operación relacionados con la separación del metanol y recirculación del gas de síntesis.

El método de síntesis directa, el cual integra la etapa de deshidratación de metanol en el mismo reactor donde se da la síntesis de metanol, permite el consumo in situ del metanol generado (deshidratándolo a DME). De este modo, las limitaciones termodinámicas que afectan a la síntesis de metanol son reducidas en gran medida, siendo posible trabajar a mayor temperatura y/o menor presión, obteniéndose mayores conversiones de gas de síntesis. Además, el agua generada en la reacción de deshidratación de metanol (Eq. (3)) es eliminada del medio de reacción a través de la reacción de water gas shift (WGSR) ((Eq. (4)), produciendo H_2 y favoreciendo la reacción de deshidratación. Esta característica del proceso es muy interesante, especialmente, cuando se utiliza un gas de síntesis con una baja relación H_2/CO, como es el caso del gas de síntesis obtenido a partir de la gasificación de la biomasa.

Los catalizadores utilizados en la síntesis directa de DME deben presentar dos fases catalíticas activas, una sobre la que se llevará a cabo la síntesis de metanol y otra sobre la que transcurrirá la reacción de deshidratación del metanol. La preparación de los catalizadores bifuncionales necesarios para este proceso se suele llevar a cabo mediante la mezcla física de ambas fases catalíticas. Como alternativa a estas mezclas físicas, se ha estudiado la preparación de catalizadores soportados, en los que un catalizador sólido ácido actúa como soporte de la fase metálica, consiguiéndose, de este modo, que el proceso se dé enteramente sobre la superficie de una partícula de catalizador. En los últimos años, se ha propuesto también el uso de catalizadores tipo core-shell para este proceso.

De acuerdo con las previsiones de demanda, el DME presenta un elevado potencial de mercado, tanto para uso para la generación eléctrica, como para ser usado como combustible doméstico. En este sentido, las industrias dedicadas a la producción de DME están experimentando un gran desarrollo en todo el mundo. Sin embargo, a pesar del desarrollo alcanzado actualmente, existen problemas sin resolver, la mayoría de ellos relacionados con los catalizadores utilizados en el proceso.

Experimental

El capítulo 2 presenta la metodología experimental utilizada para la realización de esta Tesis Doctoral. En esta sección se describen los aspectos mas relevantes relacionados con la preparación y la caracterización de los catalizadores utilizados, así como los sistemas de reacción utilizados.

La preparación de catalizadores se ha llevado a cabo siguiendo dos metodologías diferentes. Por un lado, se han preparado catalizadores de base carbonosa con morfología granular. Para ello se prepararon dos tipos de carbones activados (mediante activación química con ácido fosfórico y mediante gasificación parcial con CO_2, respectivamente), los cuales se impregnaron con diferentes sales metálicas. Por otro lado, se han preparado catalizadores de base inorgánica con morfología fibrilar, utilizando la técnica del Electrohilado.

La textura porosa de los catalizadores se estudió mediante adsorción-desorción de N_2 a -196 ºC y mediante adsorción de CO_2 a 0 ºC. La morfología superficial de las muestras se analizó por microscopía electrónica de barrido y de transmisión. La química superficial de las muestras se caracterizó mediante espectroscopia fotoelectrónica de rayos X (XPS), desorción a temperatura programada (TPD). La técnica de difracción de rayos X se usó para la identificación de las fases cristalinas. La acidez total y la distribución de fuerza ácida de los catalizadores se determinó por desorción térmica programada de amoniaco (NH_3-TPD). La dispersión de cobre y la superficie metálica de cobre de los catalizadores se analizó mediante la técnica de quimisorción de N_2O. La reducibilidad de las especies metálicas presentes en las muestras se estudió mediante reducción a temperatura programada con H_2 (H_2-TPR).

Los experimentos de deshidratación de metanol se llevaron a cabo en un microrreactor de lecho fijo (d.i. 4mm) situado en un horno vertical con control de temperatura.

Los experimentos de síntesis de metanol y de síntesis directa de DME a partir de gas de síntesis se llevaron a cabo en un equipo PID Eng. & Tech. Microactivity, el cual está equipado con un reactor de lecho fijo de acero y permite operar a alta temperatura y presión.

Resultados y discusión

<u>Parte 1: Catalizadores de base carbonosa para la síntesis de DME.</u>

El uso de carbón activado como catalizador y soporte de catalizadores ha recibido mucha atención en las últimas décadas debido a sus destacables propiedades, tales como su alta superficie específica, su estabilidad térmica y química, y la posibilidad de modificarle su química y su acidez superficial. Estos materiales pueden ser obtenidos a partir de diferentes tipos de residuos lignocelulósicos, produciendo beneficios económicos y medioambientales. Sin embargo, a pesar de su gran potencial, el uso de carbones activados como catalizadores para la reacción de deshidratación de metanol ha sido muy poco estudiado hasta el momento. Es conocido que la superficie los carbones activados no presenta actividad catalítica en esta reacción, solo observándose cierta actividad tras haber sido sometida a un tratamiento de oxidación. En este sentido, en la bibliografía se pueden encontrar algunos trabajos en los que se lleva a cabo la oxidación de carbones activados utilizando diferentes agentes oxidantes, tales como O_2, $(NH_4)_2S_2O_8$, H_2SO_4 y HNO_3, con el fin de generar grupos ácidos superficiales. Sin embargo, los grupos ácidos superficiales generados mediante esos tratamientos presentan un baja/moderada estabilidad térmica, lo cual se traduce en una rápida desactivación del catalizador al elevar la temperatura del reactor.

Nuestro grupo de investigación a publicado varios trabajos relacionados con la preparación y caracterización de carbones activados mediante activación química de residuos biomásicos con ácido fosfórico. El proceso de activación química con ácido fosfórico da como resultado materiales carbonosos con grupos de fósforo-oxigeno superficiales, los cuales presentan una elevada estabilidad térmica y química, enlazados químicamente a la superficie de los carbones activados. Estos grupos de fósforo superficiales confieren al carbón activado una alta acidez superficial y resistencia a la oxidación, convirtiendo estos materiales en buenos candidatos para ser usados como catalizadores en reacciones químicas como la deshidratación de alcoholes. En este contexto, utilizando estos materiales como catalizadores, se ha logrado la deshidratación de metanol de forma selectiva hacia DME utilizando una atmósfera de reacción

oxidante. Sin embargo, estos catalizadores carbonosos se desactivan fuertemente cuando se utilizan en un ambiente de reacción no oxidante, mostrando solo una conversión de metanol residual inferior al 10 %. Por lo tanto, esos materiales no pueden ser usados como catalizadores en los procesos de síntesis de DME industriales.

<u>Capítulo 3</u>

En el capítulo 3, titulado "Methanol dehydration to dimethyl ether on Zr-loaded P-containing mesoporous activated carbon catalysts" se estudia la preparación y caracterización de catalizadores de base carbonosa y su uso como catalizadores eficientes en la reacción de deshidratación de metanol para producir DME. En este trabajo se prepararon dos carbones activados mediante activación química con ácido fosfórico y mediante activación física de huesos de aceituna, un residuo de la industria agroalimentaria, y posteriormente se impregnaron con diferentes cantidades de Zr (0 – 7.5 (m/m)).

Los carbones activados preparados en este trabajo presentaron superficies específicas similares. El carbón activado preparado mediante activación química ácido fosfórico presentó un desarrollo poroso elevado y una alta superficie específica (A_{BET} = 1260 m^2/g). El carbón obtenido por activación física presentó un área específica muy similar al preparado por activación química (A_{BET} = 1130 m^2/g), sin embargo, este carbón mostró una estructura porosa mas estrecha. Una vez cargados con Zr, los carbones activados mostraron un ligero descenso en los parámetros texturales, al compararlos con los carbones de partida.

Los análisis por XPS mostraron que la superficie de ambos carbones estaba formada, principalmente, por carbono y oxígeno. Sin embargo, el carbón obtenido por activación química también presentó una cantidad significativa de fosforo en su superficie, el cual se atribuyó al proceso de activación. La presencia de especies de fósforo superficiales, principalmente en forma de grupos C-O-PO_3, en los carbones obtenidos por activación química tuvo una gran relevancia en el comportamiento catalítico de estos materiales. Los análisis por XPS mostraron que el Zr se enlazó a esos grupos de fósforo, dando como resultado

la formación de especies de fosfato de zirconio sobre la superficie del carbón activado.

Los resultados catalíticos mostraron que el carbón obtenido por activación física, el cual no contenía P, no presentó actividad catalítica para la deshidratación de metanol. Tras ser cargado con Zr, éste mostró una cierta actividad inicial, sin embargo, esta fue disminuyendo con el tiempo en reacción debido a un proceso de desactivación. El carbón obtenido por activación química con ácido fosfórico, el cual presenta grupos de P superficiales, mostró una elevada conversión inicial, sin embargo, esta cayó en los primeros minutos de reacción, mostrando una fuerte desactivación. Una vez cargado con Zr, el material carbonoso mostro una actividad catalítica relativamente alta, observándose una conversión de metanol estable, sin que se apreciasen procesos de desactivación. La actividad catalítica de estos materiales de base carbonosa aumentó con la carga de Zr hasta una carga del 5 %(m/m), a partir de la cual no se obtuvieron mejoras en la conversión de metanol observada. La actividad catalítica de estos materiales se atribuyó a la presencia de especies de fosfato de zirconio muy bien dispersas, cuya formación estuvo limitada por la cantidad de fósforo presente en la superficie del carbón activo obtenido por activación química.

Los catalizadores de base carbonosa que contenía P y Zr mostraron conversiones de metanol cercanas al equilibrio termodinámico, manteniendo selectividades hacia DME mayores del 95 % en todo el rango de temperaturas estudiado (250 – 400 ºC). Los experimentos de estabilidad mostraron que, una vez alcanzada la conversión de metanol de estado estacionario, esta se mantuvo por mas de 72 horas.

La presencia de vapor de agua en la corriente de entrada al reactor también fue estudiada. Los resultados mostraron que la conversión de metanol disminuyó al aumentar la presión parcial de agua en la corriente de entrada al reactor. Sin embargo, la conversión de metanol no se vio modificada por el tiempo en reacción para una presión parcial de agua constante. Además, la conversión de metanol volvió al valor obtenido en ausencia de agua cuando esta se eliminó de la corriente de entrada del reactor, mostrando que el efecto del

agua en la actividad catalítica era un efecto reversible. La selectividad hacia DME no se vio afectada por la presencia de vapor de agua, obteniéndose un valor mayor del 95 % para todas las presiones parciales estudiadas.

Capítulo 4

El capítulo 4, titulado "On the kinetics of methanol dehydration to dimethyl ether on Zr-loaded P-containing mesoporous activated carbon catalyst", presenta un estudio cinético de la deshidratación selectiva de metanol hacia DME sobre el catalizador de base carbonosa que mejor rendimiento catalítico mostró en el capítulo 3.

Como se mencionó anteriormente, los catalizadores de base carbonosa preparados en el capítulo 3 mostraron actividades catalíticas significativamente diferentes. Estas diferencias se relacionaron con la química superficial de esos catalizadores. El carbón obtenido por activación química presentó grupos de fósforo superficiales, principalmente en forma de $C-O-PO_3$, que contienen enlaces tipo C-O-P y P-OH, los cuales pueden actuar como centros ácidos de carácter moderado y fuerte, respectivamente, y ser activos para la reacción de deshidratación de metanol. Sin embargo, tras un proceso de desactivación por deposición de coque, estos catalizadores se desactivaron. El carbón activado por activación física (el cual no contiene fósforo) y cargado con zirconio presentó ZrO_2 y grupos de oxígeno-carbón en su superficie. Este material presentó una baja actividad para la deshidratación de metanol, pudiéndose atribuir a la baja estabilidad térmica de los grupos oxígeno-carbón superficiales y a la baja actividad catalítica que el ZrO_2 presenta. El carbón activado químicamente y cargado con zirconio mostró especies de fosforo y zirconio superficiales, en forma de fosfatos de zirconio, y fue el único de los catalizadores preparados en este estudio que fue capaz de mantener una conversión de metanol apreciable en estado estacionario. A la vista de esos resultados, se concluyó con que la presencia de estas especies de fosfato de zirconio superficiales fueron las responsables de catalizar la reacción de deshidratación de metanol.

La reacción de deshidratación de metanol usando fosfatos de zirconio como catalizadores se ha reportado en la bibliografía, considerando los grupos P-OH y P-O-P como las especies acticas para esta reacción. De acuerdo con

ese estudio, solo las especies de fósforo serían las responsables de catalizar la reacción y, por lo tanto, el carbón preparado por activación química presentado en este estudio, el cual presentó complejos de fósforo superficiales, debería haber catalizado la reacción de una forma eficiente. Sin embargo, tras un proceso de desactivación, este material solo mostró una conversión residual, indicando que ni los centros P-OH ni los C-O-P son los centros activos de esta reacción. Por el contrario, el carbón activado que presentó especies de fosfato de zirconio si que demostró catalizar la reacción de deshidratación de metanol, logrando una conversión elevada en estado estacionario. Estos resultados sugirieron que el centro activo del catalizador debe de considerar la presencia de P y Zr.

Una vez establecida la especie activa donde se da la reacción, se llevó a cabo un estudio cinético de la reacción de deshidratación de metanol considerando los grupos superficiales Zr-O-P como los centros activos de la reacción. Asimismo, una vez determinado el mecanismo de reacción, se obtuvieron los correspondientes parámetros cinéticos y termodinámicos del proceso. Los experimentos catalíticos se llevaron a cabo en un reactor de lecho fijo en el rango de temperaturas 250 – 400 ºC. Puesto que la selectividad hacia DME fue de más del 97 % en las condiciones analizadas, los mecanismos de reacción propuestos consideraron el DME como único producto.

En este trabajo se propusieron tres mecanismos de reacción. El modelo que mejor reprodujo los datos experimentales fue un mecanismo tipo Langmuir-Hinshelwood modificado. En este mecanismo, una molécula de metanol es adsorbida sobre un centro Zr-O-P, el cual se rompe, dando lugar a la formación de un grupo metoxi unido al fósforo y un Zr-OH vecinal (Etapa 1). A continuación, una segunda molécula de metanol se adsorbe sobre el Zr-OH generado (Etapa 2). Una vez adsorbida, la molécula de metanol reacciona con el grupo metoxi formado previamente dando lugar a la formación de DME y agua, la cual permanece adsorbida sobre el centro activo (Etapa 3). Finalmente, el agua se desorbe del centro activo, regenerando el centro Zr-O-P (Etapa 4). Este modelo reprodujo los datos experimentales con una gran precisión. La energía de activación para la producción de DME fue calculada, obteniéndose un valor de 70 kJ·mol^{-1}.

Capítulo 5

En el capítulo 5, titulado "Biomass-derived activated carbon catalysts direct dimethyl ether synthesis from syngas" se estudia la síntesis directa de DME, a partir de gas de síntesis, usando catalizadores de base carbonosa.

Los catalizadores usados para la reacción de síntesis directa de DME están formados por dos fases activas, una sobre la que tiene lugar la reacción de síntesis de metanol (catalizador para la síntesis de metanol) y otra sobre la que ocurre la deshidratación de metanol (catalizador para la deshidratación de metanol). La preparación de los catalizadores se suele llevar a cabo mediante la mezcla física de los catalizadores individuales, dando como resultado lechos catalíticos bifuncionales.

Para este estudio se prepararon dos tipos de carbones activados, mediante activación química con acido fosfórico y mediante gasificación parcial con CO_2 de hueso de aceituna. La principal diferencia entre ambos carbones fue la presencia de especies de fósforo químicamente estables, en forma de grupos $C-O-PO_3$, sobre la superficie del carbón activado químicamente con ácido fosfórico. Sobre estos carbones activados se depositaron sales de Cu, Zn y Zr, preparando, de ese modo, catalizadores a partir de residuos lignocelulósicos. Para la preparación de los lechos catalíticos bifuncionales se llevaron a cabo mezclas físicas de los correspondientes catalizadores de síntesis de metanol y de deshidratación de metanol, estudiándose diferentes relaciones másicas entre ellos.

Como catalizador para la deshidratación de metanol, en este estudio se utilizó un carbón preparado por activación química con ácido fosfórico cargado con un 5 % (m/m) de zirconio. Tal como se expuso en los capítulos 3 y 4, este catalizador presentó especies de fosfato de zirconio sobre su superficie, las cuales demostraron ser capaces de llevar a cabo la deshidratación de metanol hacia DME de forma muy selectiva.

Como catalizador para la síntesis de metanol, los dos carbones activados, así como el catalizador deshidratación de metanol, fueron cargados con Cu y Zn (10.5 y 5.5 (m/m), respectivamente). La presencia de grupos superficiales de

fósforo sobre la superficie del carbón activado demostró tener una gran relevancia en la actividad catalítica de los materiales. Los resultados mostraron fuertes interacciones entre la fase metálica y los grupos fosfato superficiales, observándose la formación de fosfatos de cobre. Estas especies de fosfato de cobre demostraron ser inactivas en la reacción de síntesis de metanol. Por el contrario, el carbón obtenido por activación física, que no contenía fósforo, mostró un buen comportamiento catalítico y, por lo tanto, fue elegido como catalizador para la síntesis de metanol en la preparación de lechos catalíticos bifuncionales.

En este trabajo se intentó la preparación de catalizadores bifuncionales, en los que ambas fases catalíticas están sobre la misma partícula de catalizador, utilizando el catalizador de deshidratación de metanol como soporte de la fase metálica. Los resultados mostraron que las interacciones entre el P y el Cu hicieron esta vía de preparación de catalizadores ineficaz.

La mezcla física de los catalizadores de síntesis y de deshidratación de metanol dio lugar a la preparación de lechos catalíticos bifuncionales, evitando las interacciones negativas entre la fase metálica y la ácida. El estudio de las diferentes relaciones másicas entre ambos catalizadores mostró que un valor de m(catalizador ácido)/m(catalizador metálico) de 2 proporcionaba al lecho catalítico suficientes sitios ácidos para hacer que el proceso de síntesis directa de DME estuviera controlado por la reacción de síntesis de metanol.

A la vista de todos los resultados mostrados, se pudo concluir que la reacción de síntesis directa de DME a partir de gas de síntesis puede ser llevada a cabo de forma eficiente utilizando catalizadores de base carbonosa. En este sentido, el catalizador de síntesis de metanol mostró un buen comportamiento catalítico para la hidrogenación de CO y, por otro lado, el catalizador de deshidratación de metanol mostró un comportamiento catalítico adecuado en la reacción de deshidratación de metanol en las condiciones de síntesis directa de DME.

<u>Parte 2: Catalizadores fibrilares para la síntesis de DME.</u>

Como se comentó anteriormente, los catalizadores para llevar a cabo la síntesis directa de DME se suelen preparar mediante mezcla física de los catalizadores individuales. Aunque este método de preparación es simple y permite un fácil escalado, los catalizadores preparados presentan una gran distancia entre los dos sitios activos involucrados en el proceso de síntesis directa de DME, lo que hace que se reduzca su eficiencia.

Una alternativa a estas mezclas físicas es el uso de catalizadores soportados. En estos catalizadores, un sólido ácido actúa como soporte de la fase metálica. De este modo, el tándem de reacciones involucradas en el proceso de síntesis directa de DME se da en la superficie de una partícula de catalizador. Sin embargo, este tipo de catalizadores soportados presenta muy a menudo falta de uniformidad de la fase metálica, ya que esta queda distribuida de forma aleatoria sobre el soporte, formando agregados que a veces sinterizan después del proceso de calcinación a elevadas temperaturas. Además, la fase activa metálica suele interaccionar fuertemente con el soporte ácido, dificultando la reducción de los óxidos metálicos o desactivando parcialmente el catalizador.

Además de estos tipos de catalizadores, recientemente han propuesto catalizadores estructurados tipo core-shell, en los que el núcleo estaría compuesto por la fase metálica, el cual quedaría rodeado perfectamente por una capa de catalizador ácido. Aunque estos catalizadores bifuncionales han demostrado una alta eficiencia, comparados con los catalizadores preparados por mezclas físicas, presentan ciertas desventajas. Por un lado, la preparación de estos materiales requiere procesos de síntesis complejos y, por otro lado, para su aplicación en un reactor de lecho fijo es imprescindible que estos sean peletizados para evitar problemas de pérdida de carga en el reactor, lo que limita la dimensión de estos materiales core-shell.

A diferencia de las metodologías experimentales usadas para preparar los catalizadores anteriormente mencionados, el Electrohilado constituye una vía directa y simple que permite la obtención de fibras, poliméricas y de carbono, en la escala nanométrica y submicrométrica. En el proceso de Electrohilado, una disolución polimérica viscosa se hace fluir a través de un capilar, sobre el

---

que se aplica un campo eléctrico de elevado potencial. La aplicación de esta diferencia de potencial induce la eyección de un chorro de fluido cargado. Durante el tiempo de vuelo (tiempo que tarda el chorro de fluido en alcanzar el colector), las repulsiones electrostáticas entre las cargas superficiales generadas provocan la aparición de inestabilidades como el "whipping", o latigueo, que provocan la evaporación del disolvente y estrechan el filamento polimérico resultante, permitiendo la deposición de las fibras en el colector.

El uso de catalizadores bifuncionales sumicrométricos con morfología fibrilar sería muy interesante para llevar a cabo la síntesis directa de DME en un reactor de lecho fijo, ya que se evitarían las limitaciones de transferencia de masa y energía, evitando al mismo tiempo los problemas de pérdida de carga derivados de usar un tamaño de partícula tan reducido.

 Capítulo 6

El capítulo 6, titulado "On the one step preparation of core-shell CuO/ZnO/ZrO$_2$-ZSM-5 fibrillar bifunctional catalysts by electrospinning for the efficient direct synthesis of dimethyl ether from syngas" aborda la preparación de materiales fibrilares de ZrO$_2$-zeolita nanoestructurados en forma de estructuras tipo "core-shell", de una forma simple y directa, mediante el uso de la técnica del Electrohilado, y su uso como catalizadores en la reacción de deshidratación de metanol a dimetiléter y para la síntesis directa de dimetiléter a partir de syngas, mostrando una gran eficiencia.

En este estudio se prepararon diferentes suspensiones de zeolita ZSM-5, para ello se adicionaron diferentes cantidades de zeolita a una disolución de PVP-acetato de zirconio. Las suspensiones preparadas se electrohilaron y los materiales resultantes se calcinaron en una mufla a 500 ºC. Las imágenes obtenidas por TEM y SEM mostraron que los materiales estaban compuestos por fibras con un tamaño medio de 275 nm. Asimismo, se observó la presencia de agregados de zeolita, con un tamaño medio de 400 nm, los cuales aparecían uniformemente separados a lo largo de las fibras. Cuando se analizaron en detalle esos agregados de zeolita, se pudo observar que las partículas de zeolita (con un tamaño medio de 120 nm) se habían agregado rodeando al núcleo de óxido de circonio, dando lugar a la formación de

estructuras tipo "core-shell" de tamaños entre 350 y 550 nm. Los análisis por XRD confirmaron la presencia de las fases cristalinas ZSM-5 y óxido de zirconio.

El aumento de la concentración de zeolita en las suspensiones poliméricas se tradujo en una mayor proporción de estructuras tipo "core-shell" en las fibras, produciéndose un acortamiento en la distancia que aparece entre estas estructuras. Además, se observó que, para cargas de zeolita en la fibra final calcinada superiores al 20 %(m/m), esas estructuras tipo "core-shell" locales se empezaron a unir, formando fibras con morfología tipo "core-shell".

Los estudios texturales realizados mediante adsorción-desorción de N_2 mostraron que la textura porosa de la zeolita no se ve afectada por el proceso de preparación del material estructurado. Del mismo modo, se comprobó, mediante NH_3-TPD, que la acidez de la zeolita también permaneció inalterada tras el proceso de preparación.

Estos materiales fibrilares de ZrO_2-Zeolita se utilizaron directamente como catalizadores para la reacción de deshidratación de metanol en un reactor de lecho fijo. Los resultados mostraron que la posibilidad de obtener esas nanoestructuras de zeolita homogéneamente separadas permite controlar la densidad de centros ácidos en el lecho catalítico, evitando la presencia de puntos calientes en el reactor sin necesidad de adicionar una fase extra al reactor. En este sentido, estos materiales funcionaron de forma muy eficiente, obteniéndose conversiones de metanol y una selectividad hacia DME muy elevadas.

La adición de sales de cobre y cinc a las suspensiones poliméricas permitió la preparación de catalizadores bifuncionales con morfología fibrilar, los cuales presentaban las mismas estructuras tipo "core-shell". Los análisis por TEM-EDXA mostraron una alta dispersión de Cu y Zn en la superficie de las fibras. Además, analizando las regiones tipo "core-shell", se pudo observar que esos elementos estaban principalmente en el núcleo, mientras que las partículas de zeolita estaban situadas rodeando (cubriendo) el núcleo metálico, actuando como una envoltura.

Estos materiales fibrilares bifuncionales se usaron directamente como catalizadores para la síntesis directa de DME a partir de gas de síntesis en un reactor de lecho fijo. El empaquetamiento de estos materiales dio lugar a la obtención de lechos empacados tipo esponja, lo cuales mostraron un muy buen contacto, en la escala submicrométrica, entre las dos fases activas involucradas en el proceso de síntesis directa de DME. Estos lechos catalíticos mostraron una gran eficiencia en la reacción objeto de estudio, evitando los problemas relacionados con la perdida carga derivados del uso de un tamaño de partícula submicrométrico en un reactor de lecho fijo. Los resultados obtenidos del cálculo de pérdidas de carga en el reactor de lecho fijo mostraron que ésta fue 10000 veces mas pequeña para el caso de un lecho empacado de fibras que para un lecho empacado de partículas presentando la misma dimensión.

Capítulo 7

En el capítulo 7, titulado "ZSM-5-decorated $CuO/ZnO/ZrO_2$ fibers as efficient bifunctional catalysts for the direct synthesis of DME from syngas" se aborda la preparación, caracterización y aplicación de catalizadores fibrilares bifuncionales. En este sentido, la técnica del electrohilado se presenta como una solución para la preparación, en una sola etapa, de catalizadores fibrilares bifuncionales. Además, en este capítulo se llevó a cabo un estudio paramétrico de la síntesis directa de DME en un reactor de lecho fijo.

El procedimiento experimental seguido para la preparación de los materiales fibrilares consta de tres etapas; la preparación de una disolución polimérica, el Electrohilado de esa disolución y la calcinación (500 ºC, 4 h) de las fibras resultantes.

En este estudio se usaron dos disoluciones poliméricas diferentes. Por un lado, se prepararon disoluciones basadas en propóxido de zirconio, polivinilpirrolidona (PVP), propanol, acetato de cinc y acetato de cobre. Por otro lado, se prepararon disoluciones basadas en acetato de zirconio, polivinilpirrolidona (PVP), propanol, nitrato de cinc y nitrato de cobre. Las cantidades de precursores de Cu y Zn se añadieron en las proporciones

adecuadas para alcanzar una cantidad final de CuO+ZnO de 25 y 35 %(m/m), manteniendo una relación molar Cu/Zn de 2, en la fibra final calcinada.

Las imágenes obtenidas por microscopia electrónica de barrido mostraron que lo materiales presentaban morfología fibrilar, con diámetros entre 0.7 y 1.7 μm. Los análisis por TEM-EDXA mostraron que las fibras con un contenido en CuO+ZnO del 25 %(m/m) presentaron una distribución uniforme de Cu y Zn, mientras que cuando el contenido de CuO+ZnO se elevó hasta el 35 %(m/m) se observó la presencia de agregados de CuO y ZnO.

Las fibras preparadas se caracterizaron mediante adsorción-desorción de N$_2$, H$_2$-TPR, XRD y quimisorción de N$_2$O. Los resultados mostraron que las fibras que contenían un 25 %(m/m) de CuO+ZnO, preparadas usando acetato de zirconio y nitratos de cobre y cinc, presentaron el menor tamaño de partícula de CuO y la mayor superficie de cobre metálico.

Estos materiales fibrilares se usaron como catalizadores para la síntesis de metanol a partir de gas de síntesis en un reactor de lecho fijo. La actividad catalítica obtenida con los diferentes catalizadores se correlacionó con las propiedades texturales, estructurales y de química superficial de los catalizadores fibrilares. La muestra que contenía un 25 %(m/m) de CuO+ZnO, preparadas usando acetato de zirconio y nitratos de cobre y cinc, presentó la mayor conversión de gas de síntesis y el mayor rendimiento hacia metanol. Esta composición y formulación se utilizó como base para la preparación de los catalizadores bifuncionales.

A modo de comparación, se preparó un catalizador con morfología granular con la misma composición del mejor catalizador fibrilar. Este material se peletizó y se usó como catalizador en las mismas condiciones que los materiales fibrilares. Los resultados mostraron que este catalizador presentó una conversión de gas de síntesis mucho mas baja que el catalizador fibrilar, señalando que la estructuración del catalizador en morfología fibrilar, en la escala submicrométrica, fue un paso clave para el funcionamiento eficiente del catalizador.

Para la preparación de los catalizadores bifuncionales se añadieron diferentes cantidades de zeolita ZSM-5 a las disoluciones poliméricas de Cu-Zn-Zr. De este modo, se obtuvieron materiales con una concentración másica de zeolita entre el 5 y el 15 %(m/m) en la fibra final calcinada. Las suspensiones generadas se eletrohilaron y se calcinaron a 500 ºC en aire durante 4 horas.

Los análisis por TEM-EDXA mostraron que la superficie de las fibras resultantes estaba compuesta principalmente por zonas lisas, iguales que las fibras que no contenían zeolita, compuestas por partículas uniformes de un tamaño menor de 10 nm y, por otro lado, se observó la presencia de agregados, de un tamaño medio de 300 nm, de partículas de zeolita. Se pudo observar una buena distribución de esos agregados de zeolita a lo largo de la superficie de las fibras. Esto se atribuyó a la gran capacidad de dispersión que tiene la técnica del Electrohilado para distribuir uniformemente partículas en fibras.

Los materiales fibrilares bifuncionales se utilizaron directamente como catalizadores en síntesis directa de DME en un reactor de lecho fijo. El buen contacto existente entre las dos fases catalíticas involucradas en el proceso favoreció el tándem de reacciones de formación y deshidratación de metanol, dando lugar a valores de conversión de gas de síntesis elevados y selectividades hacia DME de más del 63 % (95 % si solo se consideran los productos en la fase orgánica).

Además, es importante destacar que estos catalizadores fibrilares presentaron una dimensión efectiva submicrométrica (radio menor de 1 μm, tamaño de agregados de zeolita menor de 300 nm), lo que conlleva la ausencia de problemas de difusión térmicos y másicos. Además, la morfología fibrilar de estos materiales evitó los problemas relacionados con la pérdida de carga en el reactor derivados de usar ese tamaño de partícula. En este sentido, el valor obtenido para el cálculo de pérdida de carga usando estos materiales fibrilares fue 5000 veces mas pequeño que el calculado para el uso de un lecho de partículas esféricas con la misma dimensión efectiva.

Acknowledgments

Con esta memoria finalizo mi etapa como investigador predoctoral. Han sido cinco años de esfuerzo y trabajo, pero también de buenos momentos y experiencias inolvidables. Por todo ello, quiero dar las gracias a todos los que han hecho posible que hoy esté donde estoy.

A Dios por estar siempre a mi lado.

A mis directores, el Dr. Tomás Cordero y el Dr. José Rodríguez Mirasol, por confiar en mi desde el primer momento, por compartir conmigo vuestros amplios conocimientos y por cada uno de vuestros consejos durante estos años.

A los doctores del grupo de investigación, Nani, Ramiro y Fran, a vosotros también os debo mucho de mi conocimiento adquirido durante estos años de Tesis. Gracias por mantener el laboratorio siempre a punto y estar siempre dispuestos a ayudar.

A mis compañeros de tesis, Elisa, Paul, Juanjo, Imane, Javi, Miguel y Miguel Ángel. Gracias a vosotros, el trabajo en el laboratorio ha ido acompañado de una buena dosis de buen humor y alegría. Siempre dispuestos a escuchar, ayudar y, por supuesto, tomar un café.

A todos los que han pasado por el laboratorio durante estos años, Tomás, Mari Carmen, Raúl, Mpho, Rafael, Lourdes, Eli, Olaya, Hugo, Merdah, Heresh, José Berruezo, Iván, Alicia, Jaime, Tatiana, Jose Luis, Cintia y Sandra por los buenos momentos.

To Dr. Freek Kapteijn for giving me the opportunity to learn and work with you during my research stay. You gave me a warm home when I was abroad. I want to thank also Dr. María José Valero for taking care of me and treating me as your little brother when I was abroad.

A los técnicos del SCAI, María Dolores, Goyo, Adolfo, Valle y Laura, por vuestra amabilidad, disponibilidad y profesionalidad.

A mi mujer, Deborah, por tu amor y alegría, por escucharme y comprenderme en todo momento, por animarme cada día a seguir adelante con mis proyectos y, sobre todo, por tu paciencia conmigo durante estos años. Y a mi hijo, José, porque sin saberlo él, me ha dado muchísima alegría estos últimos meses.

A mis padres, Juan Antonio y María Carmen por todo el cariño que me habéis dado durante toda mi vida, por haberme apoyado y haber confiado en mí siempre.

A mis hermanas, Laura y María, por vuestras muestras de cariño y la alegría que me habéis transmitido desde que nacisteis.

José Palomo Jiménez

Málaga, noviembre de 2019

Journals

This work is a compendium of the following publications:

-**J. Palomo**, J. Rodríguez-Mirasol, T. Cordero, Methanol Dehydration to Dimethyl Ether on Zr-Loaded P-Containing Mesoporous Activated Carbon Catalysts, Materials 2019, 12, 2204. doi:10.3390/ma12132204.

-**J. Palomo**, M.A. Rodríguez-Cano, J. Rodríguez-Mirasol, T. Cordero, On the kinetics of methanol dehydration to dimethyl ether on Zr-loaded P-containing mesoporous activated carbon catalyst, Chemical Engineering Journal 378 (2019) 122198. doi.org/10.1016/j.cej.2019.122198

-**J. Palomo**, M.A. Rodríguez-Cano, J.Berruezo-García, J. Rodríguez-Mirasol, T. Cordero, On the one step preparation of core-shell $CuO/ZnO/ZrO_2$-ZSM-5 fibrillar bifunctional catalysts by electrospinning for the efficient direct synthesis of dimethyl ether from syngas. Submitted to Chemical Engineering Journal.

-**J. Palomo**, M.A. Rodríguez-Cano, J. Rodríguez-Mirasol, T. Cordero, ZSM-5-decorated $CuO/ZnO/ZrO_2$ fibers as efficient bifunctional catalysts for the direct synthesis of DME from syngas. Submitted to Applied Catalysis B: Environmental.

Others publication by the author:

-T. Cordero-Lanzac, J.M. Rosas, F.J. García-Mateos, J.J. Ternero-Hidalgo, **J. Palomo**, J. Rodríguez-Mirasol, T. Cordero, Role of different nitrogen functionalities on the electrochemical performance of activated carbons, Carbon. 126 (2018) 65–76. doi:10.1016/j.carbon.2017.09.092.

-**J. Palomo**, J.J. Ternero-Hidalgo, J.M. Rosas, J. Rodríguez-Mirasol, T. Cordero, Selective nitrogen functionalization of phosphorus-containing activated carbons, Fuel Process. Technol. (2017). doi:10.1016/j.fuproc.2016.10.006.

-J.J. Ternero-Hidalgo, J.M. Rosas, **J. Palomo**, M.J. Valero-Romero, J. Rodríguez-Mirasol, T. Cordero, Functionalization of activated carbons by HNO3 treatment: Influence of phosphorus surface groups, Carbon. 101 (2016) 409–419. doi:10.1016/j.carbon.2016.02.015.

Congress contributions

This work has also generated the following congress contributions:

-**José Palomo**, Miguel A. Rodríguez-Cano, José Rodríguez-Mirasol, Tomás Cordero. Biomass-derived activated carbon catalysts for the one-step dimethyl ether synthesis from syngas. The World Conference on Carbon 2019. Lexington, Estados Unidos (2019).

-**José Palomo**, Miguel A. Rodríguez-Cano, José Rodríguez-Mirasol, Tomás Cordero. Electrospun $CuO/ZnO/ZrO_2$-ZSM-5 fibrillar bifunctional catalysts for the direct DME synthesis. ANQUE-ICCE-CIBIQ 2019. Santander, España (2019).

-M. J. Valero-Romero, **José Palomo**, Miguel A. Rodríguez-Cano, José Rodríguez-Mirasol, Tomás Cordero. Reaction scheme and kinetic study for methanol dehydration to dimethyl ether on a P-containing mesoporous acid carbon catalyst. ANQUE-ICCE-CIBIQ 2019. Santander, España (2019).

-**José Palomo**, Miguel A. Rodríguez-Cano, José Rodríguez-Mirasol, Tomás Cordero. Kinetic study of methanol dehydration to DME on Zr-loaded P-containing mesoporous activated carbon catalyst. ANQUE-ICCE-CIBIQ 2019. Santander, España (2019).

-**José Palomo**, Miguel A. Rodríguez-Cano, José Rodríguez-Mirasol, Tomás Cordero. On the kinetics of methanol dehydration over ZrO_2

supported-carbon-derived catalysts. XXIV Encontro Luso-Galego de Química. Oporto, Portugal (2018).

-**José Palomo**, Miguel A. Rodríguez-Cano, Juana M. Rosas, José Rodríguez-Mirasol, Tomás Cordero. Kinetic study of methanol dehydration over ZrO_2 supported-activated carbons. The World Conference on Carbon 2018. Madrid, Spain (2018).

-**José Palomo**, Juana M. Rosas, José Rodríguez-Mirasol, Tomás Cordero. Preparación de carbones activos dopados con ZrO_2 para su aplicación en la deshidratación de metanol. XIV Reunión del Grupo Español del Carbón. Málaga, Spain (2017).

-Juan J. Ternero-Hidalgo, **José Palomo**, Juana M. Rosas, José Rodríguez-Mirasol, Tomás Cordero. Preparación de carbones activos de alto desarrollo poroso por activación química con H_2SO_4 y H_3PO_4. XIV Reunión del Grupo Español del Carbón. Málaga, Spain (2017).

-**José Palomo**, Juana M. Rosas, José Rodríguez-Mirasol, Tomás Cordero. Deshidratación de metanol sobre carbones activados dopados con ZrO_2. Reunión de la Sociedad Española de Catálisis. SECAT'17. Oviedo, Spain (2017).

-**José Palomo**, Juana M. Rosas, José Rodríguez-Mirasol, Tomás Cordero. Methanol dehydration over ZrO_2 supported-activated carbons. 6th EuCheMS Chemistry Congress. Sevilla, Spain (2016).

-Juan J. Ternero-Hidalgo, **José Palomo**, Juana M. Rosas, José Rodríguez-Mirasol, Tomás Cordero. Selective nitrogen functionalization of P-containing carbons. The World Conference on Carbon 2016. Pennsylvania, Estados Unidos (2016).

-**J. Palomo**, J.J. Ternero-Hidalgo, J.M. Rosas, J. Rodríguez-Mirasol, T. Cordero. Funcionalización superficial de carbones activos con grupos nitrogenados mediante reacciones de oxidación/reducción. XIII Reunión del Grupo Español del Carbón. Alicante, Spain (2015).

-J.J. Ternero-Hidalgo, **J. Palomo**, J.M. Rosas, J. Rodríguez-Mirasol, T. Cordero. Influencia de la presencia de compuestos superficiales de p sobre la funcionalización de carbones activos con HNO_3. XIII Reunión del Grupo Español del Carbón. Alicante, Spain (2015).

Predoctoral research internships

Department of Chemical Engineering, Catalysis Engineering Section. Faculty of Applied Sciences. Delft Universisity of Technology.

Supervisor: Professor Freek Kapteijn

Period: From 15h of September to 14th of December 2017

Topic: *Fisher-Tropsch process.*

Programa de Doctorado:
Química y Tecnologías Químicas. Materiales y Nanotecnología.
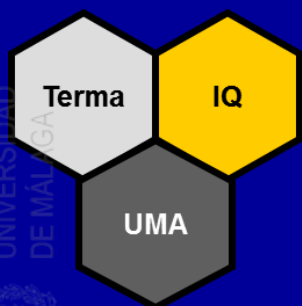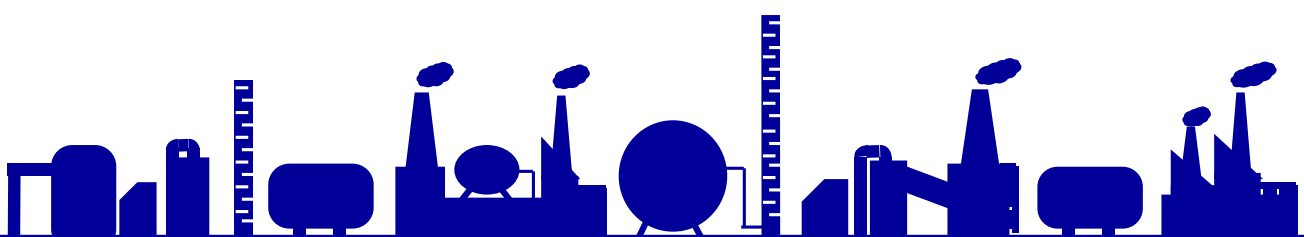
Tecnología de Residuos y Medioambiente
Universidad de Málaga